THÈSE POUR OBTENIR LE GRADE DE DOCTEUR DE L'UNIVERSITÉ DE MONTPELLIER

En Ecologie et Biodiversité

École doctorale GAIA

Institut de Recherche pour le Développement
Unité mixte de recherche AMAP

Contributions of multi-temporal airborne LiDAR data to mapping carbon stocks and fluxes in tropical forests.

Présentée par Claudia Milena HUERTAS GARCIA
Le 04 juillet 2022

Sous la direction de Grégoire Vincent et Raphaël Pélissier

Devant le jury composé de

M. David Coomes, Professeur des universités, University of Cambridge	Rapporteur / Examinateur
M. Jérôme Chave, Directeur de recherche, CNRS	Rapporteur / Examinateur
Mme. Sylvie Durrieu, Chargé de recherche, INRAE	Examinatrice
Mme. Adeline Fayolle, Maître de conférences, Gembloux Agro-Bio Tech	Examinatrice
M. Grégoire Vincent, Directeur de recherche, IRD-Montpellier	Directeur de thèse
M. Raphaël Pélissier, Co-directeur de recherche, IRD-Montpellier	Co-directeur de thèse
M. Jérôme Chave, Directeur de recherche, CNRS	Président du jury

UNIVERSITÉ DE MONTPELLIER

Foreword

This doctoral thesis is the result of four years of work carried out between the Université de Montpellier (via the Doctoral School ED GAIA), the UMR AMAP research unit (*botAnique et Modélisation de l'Architecture des Plantes et des végétations*) in Montpellier (France) and the IRD institute (*Institut de recherche pour le développement*). The *Ministère de l'Enseignement supérieur et de la Recherche*, MESR (in the context of the MOPGA "Make our planet great again" doctoral program- mopga-pdh-0000000035) and the IRD co-funded this thesis. The data used in this thesis were collected by the UMR AMAP laboratory and collaborating institutions through various research projects.

Conceptual figure of this thesis
created by Johanna Marcela GARCIA SANABRIA (2021)

Contributions of multi-temporal airborne LiDAR data to mapping carbon stocks and fluxes in tropical forests.

1. Table of contents

1. Table of contents 3

2. Acknowledgments 7

3. Abstract (English) 9

4. Resumé (French) 11

5. Resumen (Español) 13

6. Version abrégée en français (10 pages minimum) 17

7. List of abbreviations and acronyms 26

8. General introduction 27

8.1. Carbon cycle, forests and climate change 27

8.2. LiDAR contributions to reducing uncertainties in carbon stocks and fluxes in tropical forests 29

8.2.1. To provide access to 3D knowledge in tropical forest ecology and silviculture. 30

8.2.2. ALS Operations 32

8.3. The general context of the thesis and questions 33

8.3.1. Research Questions 35

8.3.2. Q1. Efflux modeling (Detection of mortality with LiDAR) 35

8.3.5. Manuscript structure 37

9. Materials and methods: Site and LiDAR data characteristics 38

9.1. Context and characteristics Paracou 38

9.1.1. Site with long term data (dynamic over 30 to 35 years) 38

9.2. Specifications and parameters of the LiDAR acquisition at Paracou 42

10. CHAPTER 1. Mapping tree mortality rate in a tropical moist forest using multi-temporal LiDAR 46

10.1. Introduction 47

10.2. Methodology 49

10.2.1. Study site and forest inventory data 49

10.2.2. ALS data and processing 52

10.2.3. Gap Dynamics Index 53
10.2.4. Tree mortality and gap dynamics models....54
10.3. Results 55
10.3.1. Comparison of gap dynamics and mortality rates within plots 55
10.3.2. Mortality and gap dynamics determinants....56
10.3.3. Temporal changes in mortality detection with ALS....58
10.4. Discussion 59
10.4.1. Gap dynamics is strongly related to BA loss rate across all forest types 59
10.4.2. Spatial and temporal variation in mortality rates....60
10.4.3. Limitations in the current study 60
10.4.4. Future research directions 61
10.5. Conclusions 62
11. CHAPTER 2: Reducing bias and uncertainty in plot-level AGB by combining ground inventories and ALS. 64
11.1. Introduction....65
11.2. Methodology & Materials 67
11.2.1. Study site....67
11.2.2. LiDAR data 68
11.3. Height modeling (see Figure 15)....69
11.3.1. Manual-based stem crown matching (Dataset 1) 69
11.3.2. Automatic stem-crown matching using Canopy Constructor (Dataset 2)....70
11.3.3. Stem height modeling 72
11.3.7. Impacts on AGB 74
11.4. Results 74
11.4.1. Prediction of individual tree heights 74
11.4.2. Comparison of species-specific allometries obtained from direct adjustment vs. using CC adjusted Heights....76
11.4.3. AGB error at plot level 77
11.4.4. Exploring the effects of hydromorphological units, previous logging and structural characteristics of the plot (BA, QMD) on allometry. 78

11.5. Discussion 79
11.5.1. Impact of censorship of small diameter stems 80
11.5.2. Habitat-specific effect on H-DBH allometry 80
11.5.3. Interspecies variability 80
11.5.4. Local canopy height as a covariate in H-DBH allometries 81
11.5.5. Covariation of DBH-height and forest structural characteristics. 81
11.5.6. Critical evaluation of the CC approach 81
11.5.7. Potential and perspectives of ALS 82
11.6. Conclusions 82
12. CHAPTER 3. Can multitemporal airborne LiDAR data predict primary productivity in dense tropical forests? 84
12.1. Introduction 84
12.2. Materials and Methods 86
12.2.1. Inventory data and forest characteristics 86
12.2.2. BA and AGB calculations 87
12.2.3. BA and AGB influxes 88
12.2.4. Airborne LiDAR data 89
12.2.5. LiDAR data processing and uncertainty analysis 89
12.3. Results 91
12.3.1. Canopy Height gain prediction of AGWNPP and BA increments plots. 91
12.3.2. Stability of predictions over time 93
12.3.3. Median canopy height gain at the landscape level. 94
12.4. Discussion 96
12.4.1. Choice of indicator 96
12.4.2. Model accuracy and performance 96
12.4.3. General decrease in AGWNPP during 2013-2019 97
12.4.4. Source of the spatial bias detected in model prediction 98
12.5. Conclusions 101
13. Synthesis and perspectives 103

13.1. Synthesis 103
13.1.1. Strength of this study 104
13.1.2. Sources of uncertainty 106
13.1.3. Future work 107
14. References 109
15. Appendix 137
16. List of figures and tables 151

2. Acknowledgments

I would like to thank all those who with their readings, observations and comments, have continuously improved this document and the articles written.

In these pages, I will undoubtedly forget many people who contributed to my completion of this process, apologies in advance to them; just to name those who have accompanied me in these last three years would be unfair to all those who have been by my side along the way. I want to thank those who have collaborated from very early on in this academic path. My first teacher Claudia Azucena whose learning I would understand over time implied the wisdom of defeats and failures in the learning process. I thank my biology teacher Martha Cote for introducing me to this fantastic world of plants and Millan, who rudely told me that physics was not my field. I thank my Colombian colleagues: Marcela Quiñonez, Carlos Jaramillo, Mauricio Diaz Granados, Santiago Palacios, René Lopez, Andrés Avella, Amarfi Fajardo, William Ariza and Brigitte Baptiste, for their unceasing motivation to bet on research for the love of forests in a country where things are not easy. I thank my school friends Isa and Ednus, who did not doubt until the end that I would complete this process. To my friends from the University, Miriam, Mery, Silvia, Anita, Fabio, Laura, Nicolas, and others, for the good times spent in the forest. To my Colombian coworkers for their passion, dedication and support, and my colleagues at UMR AMAP who welcomed me with my strange accent, showing me the rigor, the disciplined and well-done work, and the delights of French food. To my colleagues Sue, Anthony, Mélaine, James, Fabian, Camille Girard-Tercieux and Maximilien for their collaboration and being a great help in various processes of my thesis. To Valérie Roinel and Nathalie Hodebert for all her administrative help; to the staff of the cantine of CIRAD for all their kindness and good dishes that allowed me to have a great time eating throughout my stay.

To my supervisors, Raphaël, Daniel and Grégorie, for their support, all their teachings and for convincing me to follow this path I sometimes doubted. To Greg for his persistent presence, good heart, and role as an incredible mentor who with a lot of determination and patience set out to teach me his vast knowledge in ecology and remote sensing. Finally, after so much effort, I can say that we did it.

To my closest group of friends, who have been the standard and the support, who have filled me with their love, hugs and constant presence, total thanks I will always give to Antoine, JuanDa, Vivi, Johanna, Andrés, Titouan, Maïri, Camille Salmon, Mathilde, Dim, Nata, Iréne and Estefania. To my friends of pétanque, who made me feel at home through good matches and good stories, to my meditation circle in Madrid and my master Dokusho, Daizan and Maria Elena by inspiration to find my own way (the one that murmurs the blood). To my family for

understanding this quite complex challenge far from them, for all the moments that I could not be close to, but they tried to make me feel close to home (I'll be back soon). To my cousins and Isabel, Alejandra, Sofia, and Mrs. Astrid for helping me take care of my mom in my absence. To my Nanita for being the engine to continue every day and filling me with an armor of love proof against everything. And especially to you, Mimi, that little girl with many fears, precautions that have shown to bring out an inner strength greater than herself, do not forget the process and keep humility and especially kindness.

And final thanks to the origin of all this, *La selva* and the forests “*de la tierra del olvido*” I never thought that a trip to the rainforest at the age of fourteen would generate so many changes in my life. I owe you the knowledge of other languages, the constant amazement of the simple events of existence, the mirror of life's learning on a daily scale and my fierce objective to defend your territory so that we all can see the beauty that is behind you, one day I promised to defend you, and I hope to keep that promise.

Infinite thanks to all from the bottomland of my heart. *Gracias totales*

3. Abstract (English)

Keywords: LiDAR, tropical forest, flux, mortality, productivity and allometry.

Current climate change affects tropical forests functioning and might jeopardize their role as a global carbon sink. Accurately documenting forest carbon fluxes at a meaningful scale is therefore a pressing challenge. Airborne LiDAR (ALS), which can provide a fine-grained description of canopy structure and dynamics has great potential. This thesis explores the capabilities and limitations of airborne multitemporal LiDAR to map patterns of C fluxes over space and time to reduce uncertainty in models of carbon stocks and fluxes in tropical forests. We relied on a combination of repeated ALS overflights extending over ten years and a large network of plots totaling more than 1.2 km^2 of field inventories conducted at the Permanent Research Station of Paracou (French Guiana).

The first chapter (**Q1. Efflux Modeling Mortality**) addresses the possibility of developing reliable estimates of biomass, basal area and stem number loss (efflux) from observed changes in canopy height with repeated ALS overflights and further assesses whether gap dynamics show persistent over time. Absolute basal area loss rate was linearly correlated to gap dynamics at the plot level (R^2=0.60) and more strongly so when the analysis was restricted to undisturbed forests (R^2 =0.72). The rate of basal area loss was better predicted from gap dynamics than the rate of stem loss. At the landscape scale, LiDAR data revealed that spatial patterns of gap creation were related to local topography and canopy height, where high canopy forests and bottomlands had higher mortality rates. It is concluded that gap dynamics allow tracking the change in forest carbon fluxes, complementing the monitoring of net carbon change derived from static carbon estimates.

The second chapter (**Q2. Allometry and carbon stock**) quantifies the reduction of error in plot-level AGB estimates achieved using locally adjusted height-diameter allometries. Tree height data were obtained either from individually segmented crown in the LiDAR point cloud or from an individual-based forest model (Canopy Constructor) globally adjusted to the Canopy height model. Bayesian multilevel modeling approach incorporated local canopy height and species identity as co-variates. The quadratic error in predicting mean height was reduced by a factor of four by replacing the best universal alternative allometry with the locally derived ALS allometric H-DBH relationship, where nearly half of the reduction in quadratic error was due to reduced bias. A universal model (not adjusted for site-specific H-DBH allometry) underestimated AGB by 12-13 % at the site level. The inclusion of species identity and canopy height was a considerable improvement, dramatically reducing the uncertainty in H prediction.

The third chapter (**Q3. Influx modeling Productivity**) examines whether the canopy height gain derived from ALS can be used to map Aboveground Woody Net Primary Productivity (AGWNPP). The model predicted AGWNPP across the entire range of plots at the spatial resolution of 125m with an R^2 of 0.75 and a relative RMSE of 11%. Applying the method to the landscape scale, the maps revealed a spurious spatial pattern of productivity with higher values in seasonally flooded areas. Critically reviewing the model development procedure allowed to identify possible shortcomings. While a final unbiased AGWNPP model was not tested, this analysis also provided an opportunity to critically examine the overall relevance of the exercise. We conclude that measuring change in net carbon change (rather than developing a model of raw carbon influx) might be a more promising avenue, likely to provide more robust and more spatially accurate results than a net primary productivity model.

In the last chapter, we synthesize the conclusions of the articles, following with a critical reflection on the work done and discussing the potential of LiDAR in ecology and conservation.

4. Resumé (French)

Mots clés : LiDAR, forêt tropicale, flux, mortalité, productivité et allométrie.

Le changement climatique affecte le fonctionnement des forêts tropicales et met en péril leur rôle de puits de carbone (C). Documenter avec précision les flux de carbone forestiers à une échelle significative est un défi pressant. Le LiDAR aéroporté (ALS) fournit une description fine de la structure et de la dynamique de la canopée. Cette thèse explore les capacités du LiDAR multi-temporel à cartographier les flux de C et leur évolution dans le temps afin de réduire l'incertitude des modèles de stocks et de flux de C dans les forêts tropicales. Nous nous appuyons sur la combinaison de survols ALS répétés s'étendant sur 10 ans d'une part et sur un grand réseau de parcelles totalisant plus de 1,2 km^2 d'inventaires sur le terrain réalisés à la station de recherche de Paracou (Guyane française).

Le premier chapitre (**Q1. Modélisation de l'efflux Mortalité**) traite de la possibilité de développer des estimations fiables de la perte en biomasse, en surface terrière et en nombre de tiges à partir des changements de hauteur de la canopée. En outre on cherche à évaluer si les patrons spatiaux de dynamique des trouées se perpétuent entre périodes d'observations successives. La corrélation entre la surface terrière perdue et la surface de trouées nouvellement formées est significative (R^2=0.60) et particulièrement élevée pour les forêts non exploitées (R^2=0.72). Le taux de perte de surface terrière est mieux prédit que le taux de mortalité. À l'échelle du paysage, l'ALS révèle une organisation spatiale des trouées liée à la fois à la topographie locale et au type de forêt (hauteur de la canopée). Les forêts hautes d'une part et les forêts de bas-fond d'autre part présentent des taux de mortalité plus élevés que la moyenne.

Le deuxième chapitre (**Q2. Allométrie et stock de carbone**) quantifie la réduction de l'erreur dans les estimations de l'AGB obtenue en utilisant des allométries hauteur-diamètre ajustées localement. La fusion entre les données de hauteur de l'ALS et les données d'inventaire au sol se fait soit par segmentation de couronnes individuelles, soit en en utilisant une méthode globale qui, par itérations successives, minimise l'écart entre le Modèle Numérique de Canopée issu de l'ALS et le modèle de canopée dérivé de l'application de relations allométriques aux données d'inventaires. Un modèle hiérarchique bayésien est utilisé pour ajuster la hauteur des arbres en fonction de l'espèce et de la hauteur locale de la canopée. L'erreur quadratique sur la hauteur est réduite d'un facteur 4 en remplaçant la meilleure allométrie universelle par l'allométrie locale. Près de la moitié de la réduction de l'erreur quadratique est due à la réduction du biais. Le modèle allométrique universel sous-estime l'AGB de 12 à 13 % au niveau du site selon les parcelles. L'inclusion de l'identité des espèces

et de la hauteur de la canopée réduit fortement l'incertitude sur la hauteur et supprime les biais observés par type de forêt.

Le troisième chapitre (**Q3. Modélisation de l'afflux Productivité**) examine si la médiane des accroissements en hauteur de la canopée est un bon prédicteur de la productivité primaire nette ligneuse épigée (AGWNPP). Le modèle prédit l'AGWNPP sur l'ensemble des parcelles à la résolution spatiale de 125 m avec un R^2 de 0,75 et un RMSE relatif de 11%. Les cartes à l'échelle du paysage ont révélé une structuration spatiale inattendue de la productivité, avec des valeurs plus élevées dans les zones saisonnièrement inondées. L'examen critique de la procédure de développement du modèle a permis d'identifier certains problèmes et de réexaminer la pertinence générale de l'entreprise. La mesure du changement net de C (plutôt que la caractérisation du flux entrant de C) est sans doute à privilégier car elle est susceptible de donner des résultats plus robustes et spatialement non biaisés.

Enfin, une brève synthèse est proposée dans un dernier chapitre.

5. Resumen (Español)

Palabras clave: LiDAR, bosque tropical, flujos, mortalidad, productividad y alometría.

El cambio climático actual afecta al funcionamiento de los bosques tropicales y podría poner en peligro su papel como sumidero global de carbono. Por lo tanto, documentar con precisión los flujos de carbono de los bosques a una escala significativa es un reto apremiante. El LiDAR aerotransportado (ALS), que puede proporcionar una descripción de escala fina de la estructura y la dinámica del dosel, tiene un gran potencial. Esta tesis explora las capacidades y limitaciones del LiDAR multitemporal aerotransportado para cartografiar los patrones de los flujos de C en el espacio y el tiempo con el fin de reducir la incertidumbre en los modelos de las reservas y flujos de carbono en los bosques tropicales. Nos basamos en una combinación de sobrevuelos repetidos de ALS que se extienden durante diez años y una gran red de parcelas que suman más de 1.2 km^2 de inventarios de campo realizados en la Estación Permanente de Investigación de Paracou (Guayana Francesa).

El primer capítulo (**P1. Mortalidad por modelización de efluentes**) aborda la posibilidad de desarrollar estimaciones fiables de la pérdida de biomasa, área basal y número de tallos (flujos salientes) a partir de los cambios observados en la altura del dosel con repetidos sobrevuelos de ALS y evalúa además si la dinámica de los claros muestra persistencia en el tiempo. La tasa de pérdida de área basal absoluta se correlacionó linealmente con la dinámica de los claros a nivel de parcela (R^2=0.60) y con mayor intensidad cuando el análisis se restringió a los bosques no perturbados (R^2 =0.72). La tasa de pérdida de área basal se predijo mejor a partir de la dinámica de claros que la tasa de pérdida de tallos. A escala del paisaje, los datos LiDAR revelaron que los patrones espaciales de creación de claros estaban relacionados con la topografía local y la altura del dosel, donde los bosques de dosel alto y las zonas de fondo tenían mayores tasas de mortalidad. Se concluye que la dinámica de los claros permite rastrear el cambio en los flujos de carbono forestal, complementando el seguimiento del cambio neto de carbono derivado de las estimaciones estáticas de carbono.

El segundo capítulo (**P2. Alometría y reservas de carbono**) cuantifica la reducción del error en las estimaciones de AGB a nivel de parcela conseguida utilizando alometrías altura-diámetro ajustadas localmente. Los datos de altura de los árboles se obtuvieron a partir de las copas segmentadas individualmente en la nube de puntos LiDAR o del modelo forestal basado en el individuo (*Canopy Constructor*) ajustado globalmente al modelo de altura del dosel. El enfoque de modelado multinivel bayesiano incorporó la altura local del dosel y la identidad de las especies como covariables. El error cuadrático en la predicción de la altura media se redujo en un factor de cuatro al sustituir la mejor alometría alternativa universal por

la relación alométrica H-DBH derivada localmente de ALS, donde casi la mitad de la reducción del error cuadrático se debió a la reducción del sesgo. Un modelo universal (no ajustado a la alometría H-DBH específica del lugar) subestimó el AGB en un 12-13 % a nivel de lugar. La inclusión de la identidad de las especies y la altura del dosel supuso una mejora considerable, reduciendo drásticamente la incertidumbre en la predicción de H.

El tercer capítulo (**P3. Modelización de la productividad- Influjos**) examina si la ganancia de altura del dosel derivada del ALS puede utilizarse para cartografiar la productividad primaria neta leñosa sobre el suelo (AGWNPP). El modelo predijo la AGWNPP en toda la gama de parcelas a una resolución espacial de 125m con un R^2 de 0.75 y un RMSE relativo del 11%. Aplicando el método a la escala del paisaje, los mapas revelaron un patrón espacial erróneo de productividad con valores más altos en las zonas estacionalmente inundadas. La revisión crítica del procedimiento de desarrollo del modelo permitió identificar posibles deficiencias. Aunque no se probó un modelo final AGWNPP insesgado, este análisis también brindó la oportunidad de examinar críticamente la relevancia general del ejercicio. Llegando a la conclusión de que la medición del cambio en el carbono neto (en lugar de desarrollar un modelo de afluencia de carbono en bruto) podría ser una vía más prometedora, que probablemente proporcionaría resultados más sólidos y espacialmente más precisos que un modelo de productividad primaria neta.

En el último capítulo, sintetizamos las conclusiones de los artículos, siguiendo con una reflexión crítica sobre el trabajo realizado y discutiendo el potencial del LiDAR en ecología y conservación.

A mi madre, a mi Nanita, a Yoshi, a Camo.

Algún día volveré a ti, volveré con las botas embarradas por otras tierras, con pasos que han conocido nuevas cadencias y experiencias, con las ideas revolucionadas y con las manos listas para escribir en palabras en otras lenguas. Volveré a ti, como vuelve una hija que busca su esencia, que dejó un equipaje muy denso que cargaba, lleno de heridas y limitaciones auto impuestas, y con un espacio cuál búsqueda incesante hacia algo etéreo. Algún día volveré a ti, para que, entre susurros, cantos de guacharos y lluvias torrenciales, me cobijes bajo la Ceiba, y con tu profunda paciencia y amor de madre me enseñes más de lo que yo puedo hablar de ti entre todas estas páginas escritas.

Un jour, je reviendrai vers toi, je reviendrai avec mes bottes boueuses d'autres terres, des pas ayant connu de nouvelles cadences et expériences, avec mes idées révolutionnées et mes mains prêtes à écrire des mots dans d'autres langues. Je reviendrai vers toi, comme une fille qui revient à la recherche de son essence, qui a laissé derrière elle un bagage très dense qu'elle a porté, plein de blessures et de limitations auto-imposées, et avec un espace dans lequel il faut chercher sans cesse vers quelque chose d'éthéré. Un jour, je reviendrai vers toi, pour qu'entre les chuchotements, les chants des oiseaux et les pluies torrentielles, tu m'abrites sous le Ceiba, et avec ta profonde patience et ton amour maternel, tu m'apprennes plus que ce que je peux dire de toi dans toutes ces pages écrites.

6. Version abrégée en français (10 pages minimum)

Introduction

Dans le cadre du changement climatique accéléré lié au changement de composition de l'atmosphère et en particulier son enrichissement en CO_2 (IPCC, 2021), il existe un intérêt politique et scientifique croissant pour l'établissement d'une comptabilité carbone précise et transparente au niveau mondial. Bien que les études sur l'écologie et la végétation se soient multipliées au cours des dernières décennies, des divergences dans l'estimation semi-décennale des flux de CO_2 (jusqu'à 1 Gigatonne C par an) persistent (Friedlingstein et al., 2021). Ces différences pourraient être en partie résolues si les incertitudes dans les estimations des changements causés par les modifications de l'utilisation des terres et des processus naturels de la végétation étaient réduites. Une des clés se trouve dans la compréhension de la dynamique des forêts tropicales, qui sont des éléments importants de ce cycle, stockant 55 % du C (Pan et al., 2011). Malheureusement, ces forêts sont exposées à des pressions anthropiques diverses et intenses, notamment la déforestation et la conversion à l'agriculture et à l'extraction de bois (FAO, 2020; Gibson et al., 2011). Ces pressions directes combinées à l'intensification de phénomènes naturels extrêmes, tels que les périodes de sécheresse et les inondations causées par El Niño-Southern oscillation, ont provoqué de profondes transformations du fonctionnement des forêts comme l'augmentation de la mortalité des arbres (Aleixo et al., 2019; Leitold et al., 2018; van der Laan-Luijkx et al., 2015). Ces changements contribuent à la libération accélérée de CO_2 dans l'atmosphère et génèrent des émissions d'autres gaz à effet de serre, ce qui induit une accélération des taux de renouvellement et, à son tour, la mortalité naturelle des arbres, faisant passer les forêts tropicales du statut de puits de carbone à celui de source de carbone (Phillips et al., 2016), une situation qui pourrait amorcer le point de basculement vers un état sec au cours du 21e siècle (IPCC, 2021).

Afin de comprendre ces scénarios possibles et afin de réduire les incertitudes liées aux valeurs des flux et des stocks de C dans les forêts et surtout dans les écosystèmes tropicaux, il est d'une importance capitale de trouver des méthodes et de s'appuyer sur des technologies qui permettent d'obtenir des données précises et robustes pour effectuer ces analyses. L'un des défis importants de la cartographie du carbone dans les tropiques est le manque d'inventaires forestiers représentatifs, en raison de la difficulté de mesurer ces zones avec les techniques forestières traditionnelles, et également le coût élevé de la collecte des données (Baker et al., 2021). De plus, les réseaux de parcelles actuels sont insuffisants et sont bien souvent restreints à des paysages spécifiques (Marvin et al., 2014). Dans ce contexte, la télédétection joue un rôle essentiel dans la compréhension et l'évaluation des informations forestières au fil

du temps, permettant ainsi une surveillance complète des ressources forestières. Contribuant à cet objectif, le LiDAR aéroporté offre la possibilité de couvrir de manière répétée de grandes zones, même éloignées, qui peuvent être répliquées dans l'espace de manière adéquate à des échelles spatiales pertinentes. Cette technologie, qui appartient à la famille des capteurs de télédétection active, utilise l'énergie laser pour la représentation géométrique du terrain, enregistrant des données topographiques précises et denses en trois dimensions (Collis, 1969; Lefsky et al., 2002; Lohani and Ghosh, 2017). Cette technique topographique a assez tôt été utilisée dans le cadre d'études d'écologie forestière pour l'étude des caractéristiques structurelles, morphologiques et fonctionnelles des forêts, du fait de ses caractéristiques d'exactitude et de précision supérieures à celles des autres méthodes de télédétection ; générant également un bon compromis entre la couverture spatiale et temporelle (Alexander et al., 2017; Lefsky et al., 1998).

Objectifs

Dans le cadre de ce travail de thèse, différentes approches de télédétection LiDAR aéroportées ou ALS (*Airborne Laser Scanning*) sont évaluées pour caractériser la dynamique et la structure des forêts tropicales, avec pour objectif de réduire les incertitudes qui existent actuellement dans l'estimation des stocks de carbone à différentes échelles spatiales en termes de biomasse épigée (AGB), de flux (productivité et perte) et de hauteur moyenne de la forêt. L'objectif est de déterminer les capacités et les limites du LiDAR multitemporel aéroporté par rapport à (i) la détection des changements (**Mortalité (Q1) et Productivité (Q3))** dans les flux de carbone au fil du temps (ii) la réduction de l'incertitude des modèles globaux des stocks et flux de carbone dans les forêts tropicales (**Allométrie et stock de carbone (Q2))** et, enfin (iii) proposer des recommandations pour l'utilisation du LiDAR aéroporté dans l'estimation de la dynamique des flux de carbone dans les forêts tropicales.

Matériel et méthodes

Pour répondre à ces questions, on a eu recours à des acquisition LiDAR aéroporté (ALS) répétées menées à la station expérimentale de Paracou, située dans la partie côtière de la Guyane française (5°18'N - 52°53'). Cette station est l'un des sites de forêt tropicale les plus riches en termes de données de surveillance forestière au niveau du sol. Le faciès dominant est caractéristique des forêts humides de terre ferme et présente une hauteur moyenne de la canopée de 27 m. Un réseau de 16 parcelles permanentes (118,75 ha) y a été établi. Le dispositif comprend des parcelles non perturbées (6 de 6,25 ha et 1 de 25 ha) et des parcelles ayant été assujetties à une exploitation forestière contrôlée entre 1986 et 1988 selon trois modalités (9 parcelles de 6,25 ha) (Gourlet-Fleury et al., 2004). Les parcelles présentent un spectre assez large de structure et de dynamique, résultant à la fois de l'hétérogénéité

environnementale et des différents niveaux de perturbation passée. Dans les parcelles ayant subi les traitements les plus sévères (T2 et T3), la surface terrière est encore 10% plus faible et la densité des tiges est 10% plus élevée que dans les parcelles témoin 35 ans après l'exploitation. À leur tour, les parcelles témoin peuvent être différenciées au regard de la hauteur de la canopée vraisemblablement en lien avec des différences édaphiques (Morneau, 2007; Vincent et al., 2010). Dans toutes les parcelles, les arbres de plus de 10 cm de DHP (diamètre à hauteur de poitrine, mesuré à 130 cm au-dessus du sol ou à 50 cm au-dessus des contreforts) ont été régulièrement cartographiés et recensés depuis 1984 pour certaines d'entre elles et jusqu'à aujourd'hui pour l'ensemble. La fréquence des relevés a varié au fil des ans pour les différentes parcelles. Depuis 1996, les parcelles exploitées sont remesurées tous les deux ans, tandis que les T0 (parcelles témoins) sont remesurées chaque année.

Sur le plan des données LiDAR aéroporté, la station dispose de 15 ans de mesures sur une emprise d'environ 10 km^2, avec des données répétées dans le temps entre 2004 et 2019, toutes réalisées par la société privée ALTOA (< http://www.altoa.org >). Les caractéristiques de ces levés LiDAR ont évolué en même temps que les développements technologiques, il existe donc des différences au niveau des hauteurs de vol (variant de 170 m en 2009 à 800 m en moyenne en 2015 et 2019), des vecteurs utilisés (hélicoptère 2004 et 2009 ou avion 2013, 2015 et 2019), des différences également au niveau de l'angle de balayage, de la fréquence d'émission des impulsions et du mode d'enregistrement des retours (retour unique (2004 et 2009) ou retours multiples).

Modélisation de l'efflux - Mortalité (Q1)

Dans cette section, on utilise le suivi pendant 10 ans de 84 675 tiges provenant de 115 ha de parcelles pour évaluer la capacité du LiDAR aéroporté à cartographier la mortalité des arbres en termes de perte de biomasse, de nombre de tiges et de surface terrière. Le prédicteur retenu est la proportion de surface de canopée affectée par des affaissements. Cette variable est obtenue à partir de modèles de hauteur de canopée dérivés de trois levés LiDAR réalisés sur une période de 10 ans (2009-2015-2019) et couvrant une zone commune de 5,24 km^2.

On cherche à répondre spécifiquement aux questions suivantes :

Q1-1. Quelle est la corrélation entre les taux de perte de tiges et de surface terrière (issus des inventaires de terrain) et la proportion de surface de canopée en affaissement (issue de l'ALS) ?

Q1-2. Comment la mortalité dérivée des relevés au sol varie-t-elle en fonction du régime de drainage local, de l'historique d'exploitation forestière et du faciès forestier ?

Q1-3. Ces mêmes facteurs affectent-ils la dynamique des trouées à l'échelle du paysage ?

Q1-4. L'accélération récente de la mortalité observée dans les parcelles non perturbées est-elle perceptible à l'échelle du paysage à l'aide des données ALS ?

Les inventaires de 2009, 2015 et 2019 (2010, 2015 et 2020 pour P16) ont été utilisés pour la comparaison avec les données ALS. Une standardisation de la densité des impulsions lidar a été effectuée, en la réduisant à 10 impulsions par m^2 (densité de 2009) ainsi qu'une restriction de l'angle de balayage à +/-20 degrés pour augmenter la cohérence entre les données. Pour évaluer la dynamique du changement de la canopée, un modèle numérique canopée (MNC) a été calculé comme la différence entre le modèle numérique de terrain de 2015 (considéré comme le plus précis), et la hauteur maximale des premiers retours (Hmax) dans une grille de cellule de 1 m^2 pour chaque levé LiDAR.

Les nouvelles trouées (événements de perte de hauteur de la canopée) ont été mesurées en calculant la différence des MNC entre la date 1 et la date 2. On a étudié trois périodes : 2009 - 2019 comme période principale, et deux sous-divisions 2009-2015 et 2015-2019. Nous avons adopté l'approche de Leitold et al. (2018) et défini une trouée comme un affaissement d'au moins 4 pixels contigus affectés par une diminution de la hauteur de la canopée d'au moins 3m. Enfin, un indice de dynamique de trouées (GDI) est calculé comme la proportion de pixels en trouée divisé par la période d'observation exprimée en années. On a également défini une variable de hauteur de canopée (HC) comme étant le 90^e percentile des valeurs CHM 2009 par pixel dans un voisinage de 125x125 m.

Pour établir les modèles de mortalité des arbres et de dynamique des peuplements, un modèle linéaire simple a d'abord été utilisé pour comparer les taux de mortalité des tiges et les pertes de surface terrière (BA) estimés par parcelle, avec l'indice de dynamique de trouées GDI (Q1-1). Un modèle GLM avec une fonction de lien logit et une distribution binomiale a été utilisé pour comparer les effets des variables environnementales sur les taux de mortalité mesurés et le GDI (Q1-2 et Q1-3). Les variables environnementales correspondent au type de forêt et à l'habitat. Le type de forêt combine des informations sur l'historique des perturbations (intensité de l'exploitation forestière) et la hauteur de la canopée (HC) qui discrimine les forêts basses non perturbées (SUF) et la forêt haute non perturbée (TUF). Les classes d'habitat correspondent aux quatre catégories de sol hydromorphologiques définies par (Ferry et al., 2010; Morneau, 2007), et identifiées par ces auteurs comme constituant un facteur influent de la variation spatiale des taux de mortalité. L'indice d'humidité topographique (TWI), utilisé dans les études d'hydrologie pour décrire la tendance d'une zone à accumuler l'eau (Mattivi et al., 2019), a été employé pour extrapoler la classification des habitats au niveau du paysage. Toutes les analyses ont été effectuées en R version 3.6.3 et avec LAStools pour le traitement des nuages de points LiDAR.

Les résultats ont montré que la dynamique des trouées (GDI) est fortement liée au taux de perte de BA dans tous les types de forêts. Lorsqu'elle était limitée aux parcelles de forêt non perturbées, la relation entre les taux de mortalité et le GDI est particulièrement forte (R^2 = 0,72 et 0,49 pour la surface terrière absolue et les taux de perte de tiges, respectivement), mais elle diminue de manière significative lorsque les parcelles exploitées sont incluses. La corrélation est généralement plus élevée pour les taux de perte de BA que pour les taux de perte de tiges, car l'ALS est plus sensible à la mort des grands arbres.

Le taux relatif de perte de tiges est cependant mieux prédit que le taux absolu en raison de la covariation de la densité des petites tiges et du taux de mortalité le long du gradient de perturbation (intensité des traitements). L'incapacité à prédire le nombre de tiges perdues par unité de surface est attribuable au fait que de nombreuses petites tiges meurent dans les parcelles exploitées par auto-éclaircie mais sans créer de perturbation notable et canopée et ne sont pas détectées par l'ALS. Par conséquent, la fréquence des trouées ne peut être considérée comme un indicateur robuste des taux de mortalité des tiges dans un paysage qui comprend des peuplements secondarisés présentant une surmortalité des tiges en sous étage.

Les taux relatifs de perte de BA et de tiges prédits par les GLM montrent des modèles similaires de réponse à l'habitat et au type de forêt. On observe des taux de perte de BA et de tiges plus élevés dans la forêt haute (TUF) que dans le faciès dominant (SUF) et qui augmentent le long du gradient d'intensité d'exploitation (T1 à T3). Bien que globalement similaires, certaines divergences notables entre taux de perte de surface terrière et taux de mortalité selon les types forestiers sont apparentes. Ceci reflète de ce que la relation entre les deux variables (BA et tiges) est médiée par la distribution de diamètre des tiges qui varie selon les faciès forestiers. De plus la mortalité différentielle des tiges en fonction du diamètre va également varier selon l'histoire des perturbations passées. Par exemple, les différences entre la perte de tige et la perte de BA prédites par le GDI pour T2 et T3 sont le résultat de la distribution particulière des diamètres dans ces parcelles sévèrement exploitées, qui contiennent une forte abondance de pionniers à courte durée de vie avec une mortalité élevée par auto-éclaircie des petits arbres.

L'analyse à l'échelle du paysage (à l'exclusion des parcelles exploitées) a montré des modèles spatiaux de GDI significativement corrélés au cours des deux périodes successives (r=0,48 résolution de 60 m 2009-2015, 2015-2019). Ces modèles spatiaux persistants de la dynamique de la canopée sont liés aux différences de drainage local (TWI) et de stature forestière (HC).

Une augmentation du taux de mortalité des BA et des tiges entre 2009-2015 et 2015-2019 a été observée, celle-ci étant plus élevée dans les forêts basses (SUF) que dans les forêts hautes (TUF) (+19 % contre +10 %, et +28 % contre +8 %, respectivement pour les BA et les tiges). Ce patron est également observé dans le GDI, avec une légère augmentation (+6 %) du GDI à l'échelle du paysage pendant la deuxième période, bien que plus faible que le changement dans le GDI observé dans les parcelles non perturbées (+9 %).

Allométrie et stock de carbone (Q2)

Plusieurs études ont souligné l'incertitude provenant de l'utilisation d'allométries pantropicales dans les estimations de biomasse, qui ne tiennent pas compte de la variation idiosyncratique du rapport H-DBH d'un site à l'autre (Chave et al., 2014; Feldpausch et al., 2011; Ledo et al., 2016; Rocha de Souza Pereira et al., 2018). Ce problème est particulièrement aigu en forêt tropicale dense, où les mesures de hauteur sur le terrain sont de qualité médiocre en raison notamment de la visibilité réduite (Hunter et al., 2013; Larjavaara and Muller-Landau, 2013; Lima et al., 2021). Dans ce chapitre, nous combinons les données d'inventaire provenant d'un réseau dense de parcelles permanentes à Paracou et les données de l'ALS. À cette fin, nous avons utilisé deux ensembles de données. L'un (Dataset 1) est basé sur 3304 mesures de la hauteur, du diamètre des arbres et de l'identification de l'espèce, obtenues en faisant soigneusement correspondre les hauteurs de couronne dérivées de l'ALS, après vérification de la correspondance houppier-tige sur le terrain. Le jeu de données 2 (Dataset 2) constitue un jeu de données plus important (n=72200). Il a été obtenu par appariement hauteur-diamètre automatique et a permis d'explorer les éventuels facteurs environnementaux affectant les relations H-DBH. Trois périodes 2015, 2016 et 2019 ont été utilisées pour ALS, avec une densité de points moyenne comprise entre 25 et 27 impulsions/m^2.

Plus précisément, nous cherchons à répondre aux questions suivantes : (Q2-1) Dans quelle mesure les allométries dérivées du Dataset 1 et du Dataset 2 permettent-elles de réduire l'incertitude concernant la hauteur des arbres individuels et l'AGB au niveau de la parcelle, (Q2-2) Quelle est l'efficacité de l'appariement automatique par rapport à l'appariement terrain des tiges et des couronnes, (Q2-3) Dans quelle mesure les allométries spécifiques aux espèces dérivées des deux méthodes sont-elles cohérentes, (Q2-4) La grande couverture spatiale du Dataset 2 révèle-t-elle des sources supplémentaires de variation systématique dans les allométries locales ?

Le dataset 1 (n=3304) a été construit en délimitant manuellement les houppiers dans les modèles de hauteur de canopée de 1 m de résolution et dans les images aériennes RVB de 10 cm de résolution. Le 95e percentile des valeurs de hauteur au sein de chaque couronne

extraite du modèle numérique de canopée (MNC) a été utilisé pour calculer la hauteur de chaque couronne segmentée.

Nous avons eu recours à la modélisation bayésienne pour tester différents modèles de complexité croissante (introduction graduelle de co-variables) et différentes formes analytiques de la relation H-DHP. Le premier modèle considéré était une allométrie unique pour l'ensemble du site (Modèle 1). La hauteur de la canopée (LCH) dans un voisinage local a ensuite été ajoutée comme co-variable dans le Modèle 2. Nous avons utilisé la hauteur moyenne de la canopée dans un voisinage circulaire pour caractériser la hauteur de la canopée locale. Un troisième modèle incluait uniquement les espèces (Modèle 2bis). Et en dernier lieu, un modèle complet qui prenait compte les deux co-variables (LCH + espèces) (Modèle 3). Dans les modèles par espèce, les espèces n'ayant qu'un représentant (singleton) ont été regroupées, ce qui s'est avéré efficace pour réduire l'incertitude de la prédiction du modèle. Nous avons considéré trois équations allométriques qui expriment H en fonction du DHP : loi de puissance ($\widehat{H}$=a x DHP^b - Équation 1), Weibull à deux paramètres $\widehat{H}$ = a x (1-exp(-DHP/b)) - Équation 2) et Michaelis Menten ($\widehat{H}$=a x DHP/(b+DHP) - Équation 3) (Molto et al., 2014). Tous les ajustements ont été effectués à l'aide de la bibliothèque brms (paquet R brms version 4.1.0 (Bürkner, 2017) basé sur le logiciel Stan (Gelman et al., 2015). Pour tous les modèles, trois équations ont été testées et appliquées à l'ensemble des observations du dataset 1 (n=3304). Nous avons utilisé à l'indicateur WAIC (*Widely Applicable Information Criterion*) et la racine carrée de l'erreur quadratique moyenne (RMSE) pour évaluer les modèles.

Pour constituer le deuxième jeu de données (Dataset 2) une procédure d'ajustement automatique des hauteurs d'arbres a été appliquée à l'ensemble des données de l''inventaire du CIRAD (16 parcelles, 72200 tiges) en 2016 (2015 pour la parcelle P16). Nous avons pour cela eu recours au modèle Canopy Constructor (CC). La hauteur et la largeur de la couronne de chaque arbre de l'inventaire (~72200 tiges) ont été prédites en fonction d'une allométrie commune déterminée pour le site à partir des données du dataset1, puis en minimisant de manière itérative la différence entre le modèle numérique de canopée (MNC) observé et simulé. Une relation H-DHP universelle pour les forêts pantropicales développée par Chave et al. (2014) a également été utilisée comme modèle de référence pour la comparaison.

Nos résultats montrent que l'utilisation d'équations allométriques H-DHP calibrées localement permet de réduire un biais d'évaluation de la biomasse important à Paracou. Les deux approches testées ont fourni des prédictions similaires et supérieures de 33 à 50 t. ha^{-1} (selon le type de forêt) à celles obtenues en utilisant l'allométrie pantropicale de référence. Le modèle

pantropical a montré un biais notable, en sous-estimant la hauteur moyenne des arbres du dataset 1 de 3,5 m.

La meilleure prédiction (WAIC le plus bas) a été obtenue en combinant l'équation de Michaelis Menten pour décrire la relation H-DHP et le modèle 3 (LHC et identité des espèces en co-variables). Les modèles avec co-variables, utilisées seules ou en association, se sont révélés bien meilleurs (WAIC et RMSE beaucoup plus faibles) que les modèles alternatifs plus simples. Le biais initial observé sur les hauteurs moyennes (de -1,12 m à + 1,07 m selon le type de forêt) est presque entièrement résorbé après l'introduction de LHC ou de LHC et de l'identité des espèces dans le modèle.

L'utilisation d'un modèle allométrique local avec co-variables a permis de prendre en compte efficacement la variation spatiale systématique observée dans les relations H-DHP. L'inclusion de la seule hauteur de la canopée locale sans prise en compte de l'identité des espèces a déjà permis la résorption de ce biais. L'inclusion de l'identité de l'espèce a de plus réduit considérablement l'incertitude de la prédiction de H, et ce quelle que soit la forme de la relation allométrique. L'appariement automatique des tiges et des couronnes par CC génère des échantillons H-DHP très cohérents avec ceux établis par ajustement manuel : les modèles non paramétriques de hauteur en fonction du diamètre sont très proches. Ces modèles révèlent également des différences interspécifiques marquées.

Aucune des deux approches précédentes cependant ne produit des données de hauteur robustes pour les arbres de petit diamètre. En effet ceux-ci atteignent rarement le sommet de la canopée et sont donc rarement visibles dans le Modèle Numérique de Canopée dérivé de l'ALS. Cette incertitude affectant les petites tiges, a réduit la précision des modèles allométriques proposés. Pour augmenter la précision et la robustesse de ces modèles, l'échantillonnage devrait être complété par des tiges plus petites. D'autres capteurs LiDAR tels que TLS pourraient être mobilisés à cette fin.

Modélisation de l'influx - Productivité (Q3)

L'approche développée dans cette section est basée sur un modèle qui relie directement la valeur médiane des accroissements en hauteur de la canopée (calculée à partir des données LiDAR de 2013, 2015 et 2019) à la productivité primaire nette ligneuse épigée (AGWNPP) – ou à l'augmentation de la surface terrière mesurées par l'inventaire sol. Ce modèle, validé à différentes résolutions spatiales (6,25 ha, 1,56 ha et 0,39 ha), capture la croissance la plus active sur les parcelles exploitées et est également applicable aux parcelles non exploitées. Il a ensuite été appliqué à l'échelle du paysage pour cartographier la productivité primaire. Les cartes obtenues ont révélé un patron montrant des zones de plus grande productivité dans les bas-fonds. Ce patron paradoxal (contredisant des observations précédentes réalisées sur le

même site, sur une période différente, et un nombre plus petit de parcelles) nous a amené à réexaminer le protocole expérimental suivi. Les bas-fonds, bien que plus actifs (turnover plus élevé), seraient légèrement moins productifs dans leur ensemble en raison de la combinaison de trois facteurs contrebalançant cette forte dynamique : une densité de tiges plus faible, une densité moyenne de bois plus faible et des arbres moins élancés. La forte dynamique de canopée dans les bas-fonds bien captée par le LiDAR multi-temporel a conduit à une surestimation de la productivité associée. Une des raisons en est que ces bas-fonds sont généralement étroits et intriqués et n'ont de ce ne fait pas été traités séparément dans le modèle liant dynamique de canopée et productivité primaire. Une seconde raison tient au choix de la métrique LiDAR retenue qui n'est sans doute pas judicieux. Pour disposer d'un indicateur peu sensible à la durée de la période d'observation le choix a été fait d'utiliser une statistique d'intensité (la médiane des accroissements de canopée non rapportée à la surface en accroissement, qui pour une même dynamique va évoluer avec la longueur de la période considérée). Ce choix a conduit à ne pas différencier des dynamiques d'accroissement affectant des proportions variables de la surface totale et notamment les forêts post-exploitation et les zones de bas-fond. La cartographie de l'AGWNPP à partir des indices de changement de hauteur de la canopée de l'ALS semble finalement délicate. Les stratégies possibles d'améliorations du modèle initial proposé sont discutées.

7. List of abbreviations and acronyms

AGB: Above-ground biomass
AGWNPP: Above-ground woody net primary productivity
AIC: Akaike Information Criterion
ALS: Airborne LiDAR Scanning
AOL: Airborne Oceanographic Laser
BA: Basal area
CC: Canopy Constructor
CHM: Canopy Height Model
CNES: Centre national d'études spatiales
DBH: Diameter at breast height
DEM: Digital elevation model
DTM: Digital terrain model
EFOS: Emissions from fossil fuel combustion
ER: Evidence ratio
ERDF: European Regional Development Fund
ERTS: Earth Resources Satellite Sensor
ESA: European Space Agency
GDI: Gap dynamics index
GNSS: Global Navigation Satellite System
GPS: Global Positioning System
HC: Canopy height
Hmax: Local maximum height
Hmean: Local mean height
IMU: Inertial measurement unit
LCH: Canopy height in a local neighborhood
LiDAR: LIght Detection And Ranging
LUC: Land-use change emissions
MLS: Mobile Laser Scanning
MNC: Modèle numérique canopée
MPHG: Median positive height gain unnormalized by surface
MSE: Mean squared error
NIR: Near-infrared reflectance
NPP: Net primary productivity
QMD: Quadratic Mean Diameter
REDD+: Reducing Emissions from Deforestation and Forest Degradation
RMSE: Root mean square error
SAR: Synthetic-aperture radar
Stem: Stem loss
SUF: Short Undisturbed Forest
TLS: Terrestrial laser scanning
TUF: Tall Undisturbed Forest
TWI: Topographic Wetness Index
UAV: Unmanned aerial vehicle
WAIC: Widely Applicable Information Criterion

8. General introduction

8.1. Carbon cycle, forests and climate change

Among the dominant issues of the new millennium is the growing scientific and political interest in the global carbon budget, resulting from changes in atmospheric chemistry and their influence on the evolving climate of the terrestrial biosphere. These changes are mainly due to carbon dioxide (CO_2) emissions from fossil fuel combustion (EFOS) and land-use change emissions (LUC), which for the decade 2010-2019 accounted for 9.4 and 1.6 Gt C yr^{-1} (Friedlingstein et al., 2021; Houghton et al., 2012). Both atmospheric CO_2 concentrations and differences between total estimated emissions and changes in the atmosphere, ocean and terrestrial biosphere are considered for closing the global C budget (Friedlingstein et al., 2021). Estimation of the global balance and its components is essential for the prospects of mitigation actions and the implementation of climate stabilization policies in a scenario of accelerating global warming trend, where the four decades have been successively warmer, with the most significant temperature increase occurring between 2003 and 2012 (+0.19°C) (IPCC, 2021).

In general, discrepancies of up to 1 Gt C per year persist in representing semi-decadal variability in CO_2 fluxes. At the terrestrial level, flux estimates require optimization, including variability and trends caused by land-use changes (Friedlingstein et al., 2021) and natural vegetation processes. Forest cover stores about half of the world's forest carbon, with the current stock of C in the world's forests estimated at 44% in soil, 42% in living above-ground biomass, 8% in deadwood, and 5% in the litter. Geographically, tropical forests store 55% of this C (Pan et al., 2011), representing one of the terrestrial ecosystems with the highest carbon dioxide uptake stored in biomass (Marvin et al., 2014). In addition, they incorporate 30% of the terrestrial net primary production (NPP) (Ichii et al., 2005; Marvin et al., 2014), where the Amazon sequesters approximately 25% of annual global terrestrial CO_2 (Brienen et al., 2015; Pan et al., 2011). The average carbon stock for the forests of South America, Africa and Asia is estimated to be about 173 Mg ha^{-1} (Sullivan et al., 2017).

Forests currently cover 31% of the world's land area, with approximately one-third of that area being primary forest (FAO, 2020). However, the perspective is not encouraging, as diverse and intense anthropogenic pressures affect these forests, with an estimated loss of 420 million hectares due to deforestation and conversion to agriculture and timber production (FAO, 2020; Gibson et al., 2011). Emissions due to fires, deforestation and degradation of tropical forests since January 2020 were estimated, at the end of October 2020, at 227 Tg C (313 Tg C on average between 1997 and 2019); where the Amazonian and Southeast Asian forests are the most deforested in the world (Friedlingstein et al., 2021). There is also an indirect impact (degradation) of these increasing human pressures on the resilience of these ecosystems, making them more vulnerable to drought, fire and tree mortality (Malhi et al., 2008). The

apparent change in precipitation during the dry-to-wet season has led to increased tree mortality at the individual level (Aleixo et al., 2019; Leitold et al., 2018; van der Laan-Luijkx et al., 2015). Also, the intensification of extreme events such as dry periods and floods caused by El Niño - Southern Oscillation, landslides and fires directly affect natural forests on a large scale (Allen et al., 2015; Cochrane and Barber, 2009; Gale, 2006; McDowell et al., 2018). Specific studies for the northern Amazon have shown a high probability of increasing these extreme events in the coming decades (Joetzjer et al., 2013). This is due to the increased frequency of windstorms and tornadoes, changing rainfall patterns and increasing temperatures. This trend has significant impacts not only on the global carbon balance (Schuur, 2003) but also contributes to the increase in early successional species (Vincent et al., 2011a) and the dominance of lianas in the canopy (van der Heijden and Phillips, 2008) and invasive species, and redoubling of tree rotation rates (Brienen et al., 2015; Phillips et al., 2008). These accelerated changes lead to profound transformations in forest functioning, contribute to the immediate release of carbon dioxide into the atmosphere, and produce greenhouse gas emissions.

To compensate, afforestation and reforestation and the growth of intact forests have helped mitigate the historical increase in atmospheric CO_2 by storing C in biomass. However, the strength of CO_2 sinks in intact tropical forests is probably declining in both the Amazon (Brienen et al., 2015) and Africa (Hubau et al., 2020). The potential unproven effect of continuous fertilization with atmospheric CO_2 and nitrogen inputs on plant growth (Friedlingstein et al., 2021) could be increasingly outweighed by the impacts of drought and air temperatures on tree survival and mortality (Hubau et al., 2020). African forests seem to have maintained a positive sink force for longer than Amazonian forests. This may be due to their slower dynamics and the long average carbon retention time. Although an increase in forest carbon uptake will eventually lead to an increase in carbon release, the time it takes for the outflow to reach the inflow levels will depend on the residence time of the carbon in the forest. This suggests that forest turnover rates largely determine the evolution of the forest carbon sink in response to climate change (Hubau et al., 2020). Accelerating forest turnover rates through increasing tree mortality rates can shift tropical forests from carbon sinks to carbon sources (Phillips et al., 2016). These changes, affecting intact forests and the continued deforestation of critical ecosystems such as the Amazon, combined with global warming, increase the likelihood of crossing the tipping point into a dry state during the 21st century (IPCC, 2021).

8.2. LiDAR contributions to reducing uncertainties in carbon stocks and fluxes in tropical forests

A fine description of the structure and the dynamics of tropical forests in key landscapes should contribute to a better understanding of the interplay of environmental factors which determine forest growth and resilience (Keeling and Phillips, 2007; Kellner et al., 2011; Taylor et al., 2015) In addition, it will offer the possibility to model habitat disturbances and their effect on biodiversity and ecosystem services (Alexander et al., 2017). This new knowledge will support the management and conservation of these ecosystems (Feldmann et al., 2018).

Therefore, there is a need to generate methods and new tools that allow us to expand forest dynamics and structure studies, generating knowledge to comprehend how these critical ecosystems evolve in climate change. Such studies should ideally have coverage of hundreds to thousands of hectares (to capture natural landscape level complexity) and be replicated across a series of tropical landscapes.

There is also a very practical need to improve national carbon inventories in relation to REDD+ or track pledges made by countries in their National determined Contribution to C emission reduction mechanisms. Significant uncertainties remain in forestry and ecological studies of carbon flux and stock values in tropical forests (Chave et al., 2005; Molto et al., 2013; Pan et al., 2011). One of the significant challenges in carbon mapping in the tropics is the lack of a national scale representative forest inventories, partly due to the difficulty of monitoring natural tropical forests with traditional forestry techniques and the high cost of data collection (Baker et al., 2021). These situations lead to insufficient existing networks of limited area and covering a small range of habitats and landscapes (Baker et al., 2021; Marvin et al., 2014). The diversity and complexity of tropical forests contrast with the limited information available to define possible states and scenarios. In this context, remote sensing plays an essential role in understanding and assessing forest information over time, thus allowing comprehensive monitoring of forest resources.

The use of remote sensing for forest resource assessment provides three levels of information: (i) spatial extent of forest cover; (ii) forest type; and (iii) biophysical and biochemical properties of the vegetation (Boyd and Danson, 2005). Over time, the evaluation of forest information allows for comprehensive monitoring of resources. Since the first international Earth Resources Satellite Sensor (ERTS) launch in 1972, we have advanced our knowledge of these ecosystems' extent, characteristics, and biochemical properties (Boyd and Danson, 2005). In addition, the advancement of new high-resolution active remote sensing technologies, such as light detection and ranging (LiDAR) based sensors, has greatly improved the ability to model stand dynamics and structure. It contributes to understanding the drivers of spatial and

temporal variation in forests, reducing sources of uncertainty in global vegetation models (Lovenduski and Bonan, 2017; Vincent et al., 2014). Progress continues in developing innovative methods based on the fusion of data from active and passive sensors (which, in most cases, include LiDAR). As well as forest-specific satellite monitoring missions, such as the NASA-ISRO NISAR (L- and S-band SAR) or ESA-BIOMASS (P-band SAR) missions (Carreiras et al., 2017; Chave et al., 2020; Duncanson et al., 2020). The main objective of these missions is the measurement of forest biomass, which will allow us to assess terrestrial carbon stocks and fluxes and improve our understanding of the global carbon cycle.

8.2.1. To provide access to 3D knowledge in tropical forest ecology and silviculture.

LiDAR is a resurgent technology that has begun to be exploited in a variety of disciplines, where it has had a positive impact on ecological studies by allowing for better observation of structural, morphological, and functional aspects of the forest in terms of accuracy, precision, and spatial and temporal coverage (Alexander et al., 2017; Lefsky et al., 1998). The LiDAR survey is very qualified in this field because, through the use of a focused laser pulse, it can effectively penetrate the vegetation cover, offering an excellent alternative to obtaining accurate multidimensional (3D) modeling of forest strata (Lefsky et al., 2002), allowing, at a low operational cost, to obtain results on large areas that, possibly in the field and in the traditional way, would require years to be measured.

LiDAR stands for LIght Detection And Ranging radar technology, which describes the active remote sensing technique that uses laser energy for geometric terrain representation, recording accurate and dense topographic data in three dimensions (Collis, 1969; Lefsky et al., 2002; Lohani and Ghosh, 2017). In its general principle, LiDAR measures the distance between the transmitter (sensor or measuring instrument) and the target surface, determining this distance as the time elapsed between the emission of the laser pulse and the arrival at the receiver (the sensor itself) by the reflection of this pulse or the return signal. The distance to and from the target is found as the multiplication of the elapsed time interval by the speed of light. The division of this product in two allows for calculating the distance between the sensor and the target (Bachman, 1979).

The first to use LiDAR was Middleton and Spilhaus (1954), cited by Collis (1969) in a publication on meteorological instruments, where the laser was employed to determine cloud base elevation (ceilometer). Shortly after its development, the use of this device was then amplified to evaluate perceptual dimensions in atmospheric physics and chemistry (ozone observation, stratospheric aerosol layer and air pollution), in meteorology (Collis, 1969) and oceanographic applications (Hickman and Hogg, 1969; Lefsky et al., 1998; Robson et al., 2012). Finally, the technology has leaped the precision measurement of terrestrial objects, with

the landing of GPS (Global Positioning System) and the progress of IMU (Inertial Measurement Unit) technologies. Moreover, laser and computer technology make LiDAR more affordable, less expensive, and accurate (Lohani and Ghosh, 2017). Nowadays, it is used in multiple applications such as (i) flood modeling, (ii) simulation of electromagnetic wave propagation (Lohani and Ghosh, 2017), (iii) coastal habitat determination (Chust et al., 2008), (iv) barometric studies (Irish and White, 1998) (v) rainfall interception (Roth et al., 2007). In addition, (vi) wind speed measurement (Baumgarten, 2010), (vii) snow surface measurements (Deems et al., 2013) and, combined with spectral information from optical sensors (viii), increase the accuracy of classification of land use and occupation (Mesas-Carrascosa et al., 2012).

The notion of using airborne lasers for measurements in ecological and forestry studies emerged with Hickman and Hogg (1969) and the use of the Airborne Oceanographic Laser (AOL), whose primary objective was to determine water depths in the Atlantic Ocean. However, other developments, such as forestry studies, were possible (Lim et al., 2003; Lohani and Ghosh, 2017). From there, LiDAR has contributed to the structural, compositional and functional analysis of vegetation (Alexander et al., 2017). In addition, it has been used in various applications to measure biomass and forest structure. Some authors support the use of this technology, both for direct measurements such as height, crown size and density (number of individuals), as well as for indirect measurements such as above-ground biomass, leaf and basal area and stem volume (Ayrey et al., 2019; Montealegre et al., 2016; Popescu et al., 2003; Shao et al., 2019; Villikka et al., n.d.). In the last decade, it has been used mainly for the quantification of stocks (Asner et al., 2012; Asner and Mascaro, 2014; Dubayah et al., 2010; Marvin et al., 2014), as well as changes expressed as variations in canopy height and gap fractions and their spatial organization (Hunter et al., 2015; Leitold et al., 2018; Senécal et al., 2018).

Since its expansion as a technology, in particular, ALS (*Airborne laser scanning*) has been used in temperate and tropical forests to determine biomass and calculate carbon fluxes, closely linked to initiatives such as REDD (Reducing Emissions from Deforestation and Forest Degradation) (NASA, 2020) to understand climate change. Several authors argue for the need to use this technique in addition to field plots to enhance these estimates (Marvin et al., 2014; Réjou-Méchain et al., 2019). Improvements in nanotechnology have led to improvements in accuracy, cost, and characteristics, for example, recording observations (Gallay, 2013). Early sensors were recording only along a single limited transect. In contrast, newer systems, such as those included in this study, operate in a continuous scan mode, in which the orientation of the laser illumination and the receiver's field of view are directed from side to side by one or more rotating oscillating mirrors, so that the platform moves forward, while the sampled points

are scanned over a wide band or grid-like strip in an image (Lefsky et al., 2002) (Figure 1). Thus, improving capture detail and data resolution. This ability to obtain models of high resolution and precision makes it gradually become a widely used tool in ecological studies, where it is used as a fundamental element or also by allowing to complete and extrapolate of the data obtained in the field and to complement the information with other images obtained by other remote sensors. At this point, in recent years, it has been actively included in projects and missions of space monitoring at the global level, constituting the reference to evaluate and validate the biomass models obtained by spectral images or synthetic aperture radars, as is the case of biomass monitoring missions such as the NASA-ISRO and BIOMASS- SAR mission (Carreiras et al., 2017; Duncanson et al., 2020).

8.2.2. ALS Operations

An airborne LiDAR or ALS system consists of (i) an airborne platform (airplane, helicopter, or satellite) that is used to carry (ii) a LiDAR sensor, which is responsible for generating short-duration laser pulses (on the order of a few nanoseconds), transmitting them to the surface or object of study, and then receiving the return signal as a waveform, measuring the travel time between the pulse and the return; to also capture the type of return (e.g., first return, last return, or multiple returns) and finally to associate each return pulse with the GNSS time and the angle of incidence at which the pulse was transmitted. (iii) A GNSS receiver operates simultaneously or in tandem with a GNSS ground station receiver and observes the aircraft's position at each GNSS scan time (at a frequency of 1 Hz or 2 Hz). iv) An IMU sensor observes the aircraft's accelerations and orientations much higher than GNSS (400 Hz). Finally, v) an onboard computer, which records the various data produced by the sensors using GNSS time, archives the raw data (Lohani and Ghosh, 2017) Figure 1.

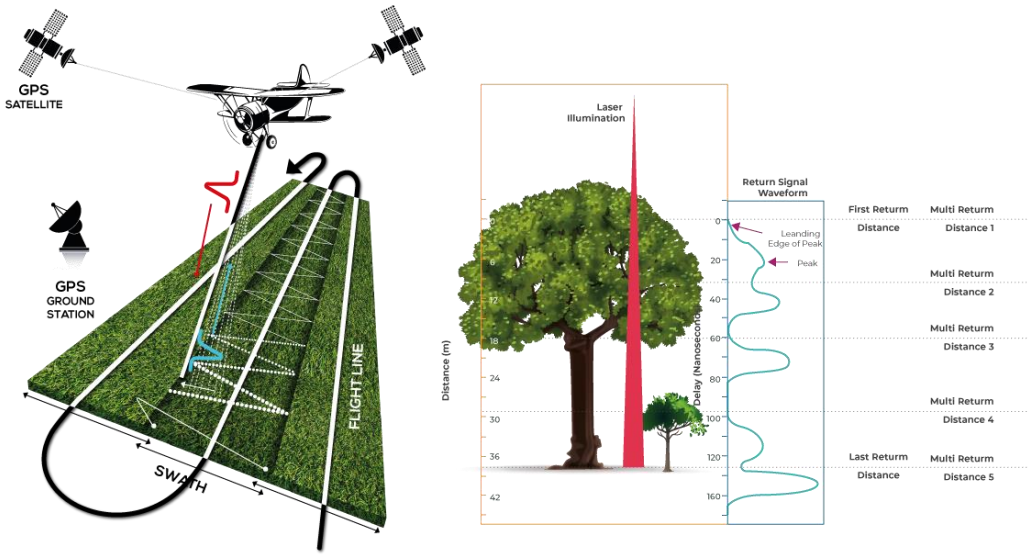

Figure 1. Left. The general principle of an Airborne LiDAR acquisition. Extracted and modified from Presentation of the International Conference on Tropical Silviculture. (Vincent et al., 2011b). Right. Conceptual differences between waveform and discrete return LiDAR recording (Adapted and modified from Lefsky et al.,(2002)).

The ALS operates from aircraft or helicopters at altitudes between 100 and 4000 m from the ground. During the flight, the laser scanner displays object line-of-sight tilt magnitudes relative to the scanner coordinate system, the angle of incidence of the laser beam (Θ), and the intensity of the reflected laser energy. The maximum value of Θ defines the scanner's field of view (FOV) angle. The path of a laser beam within a strip is directed by a rotating or oscillating mirror and by the forward motion of the aircraft (Figure 1). As a result, the footprint drifts across the Earth's surface, creating a semi-regular pattern. The flight altitude and field of view control the width of the swath. The emitted laser energy has narrow beam divergence angles, so the resulting footprints are small and altitude-dependent (NOAA, 2012; Wehr, 2018). The footprint size affects the pulse penetration level into the vegetated areas and the level of detectable detail that can be recorded (Gallay, 2013). The information acquired during the flight provides a dense cloud of point measurements containing the elevation of multiple surfaces illuminated by the laser footprint. Sample densities typically range from 0.1 to 20 points per square meter. This information, when processed, can generate high-resolution digital elevation models (DEMs) (Gallay, 2013; Roussel and Auty, 2020; Wehr, 2018). The laser wavelength is constant, with a narrow bandwidth of two to five nanometers (nm). Currently, ALS systems emit near-infrared light with typical wavelengths of 1064 nm (Gallay, 2013).

8.3. The general context of the thesis and questions

This thesis was carried out within the Joint Research Unit UMR AMAP - botAnique et Modélisation de l'Architecture des Plantes et des végétations within the team belonging to the current theme TETROFOR - Tropical Vegetation by Remote Sensing. This team proposes

innovative remote sensing methods to assess forests' structure, composition, and dynamics by applying technologies such as LiDAR. Several research programs and projects fund the research work and data, including the European Regional Development Fund (ERDF agreement n°2907 of 04/11/08), the CNES convention n°150372/00 2015/2016. STEM-LEAF and BIOMASS projects. TOSCA Continental Surfaces 2013-2015 and the DendroLIDAR project belong to FSFB (MAA) and FEADER Guyane. As well as the "Investissement d'Avenir" program managed by the French National Research Agency [CEBA, ref. ANR-10-LABX-25-01], in collaboration with the University of Cambridge through the NERC grant, who provided the ALS 2019 data [NE/S010750/1].

Furthermore, this work builds on a collaboration with the Guyafor project, which is dedicated to the long-term study of forest dynamics and biodiversity from a network of permanent plots installed in French Guiana, including Paracou (< https://paracou.cirad.fr/ >) and which gave us access to the inventories, which provided the data needed to develop this thesis.

The general framework of the thesis work consists of developing remote sensing approaches with airborne LiDAR to capture the dynamics and structure of tropical forests, allowing to reduce the uncertainties that currently exist in the estimation of carbon stocks at different spatial scales in terms of above-ground biomass (AGB), fluxes (productivity and loss) and mean forest height. This study provides a new perspective on large-scale monitoring and mapping of tropical forests, taking a critical look at innovative ALS-based methods, reducing the costs of field data collection and optimizing sampling efforts. This leveraging capacity of ALS is critical to making rapid progress in understanding alterations caused by climate change, deepening our understanding of the analysis of interactions with environmental factors and, in particular, the drivers of spatial and temporal variation in carbon fluxes.

Our specific objectives are to determine the capabilities and limitations of airborne multi-temporal LiDAR in (i) Detecting changes (mortality and productivity) in carbon flux patterns over time. (ii) reducing uncertainty in global models of carbon stocks and fluxes in tropical forests. We rely on repeated ALS studies conducted at the Paracou Permanent Research Station (French Guiana) to answer these questions.

8.3.1. Research Questions

Three central questions organize my thinking and are presented in the diagram below (Figure 2):

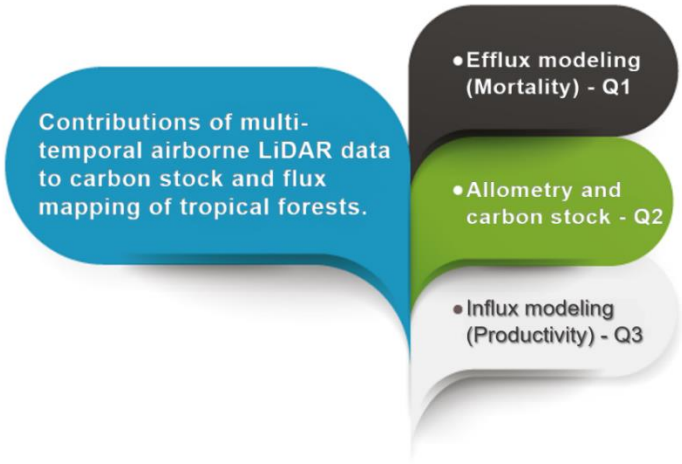

Figure 2. Diagram detailing the organization of research questions that characterize tropical forest carbon fluxes and stocks from LiDAR

8.3.2. Q1. Efflux modeling (Detection of mortality with LiDAR)

Measuring tree mortality rates is crucial to reducing uncertainties in the contribution of tropical forests to the carbon budget. Several studies have shown an increase in mortality in tropical forests in recent decades (Bonal et al., 2008; Brienen et al., 2015; Corlett, 2016; Dalagnol et al., 2021; Leitold et al., 2018). However, uncertainty remains about the overall behavior because most studies are based on small areas (≤1ha) or limited networks of plots. Therefore, technological developments such as LiDAR that promote understanding of abiotic factors at the site scale are relevant, allowing us to identify specific spatial patterns consistent with vulnerable areas, such as areas with greater dynamics over time. In this section of the study, we examine the potential of ALS to map change in forest structure over large areas with high accuracy, thereby contributing to understanding spatial and temporal patterns of mortality at the landscape scale. We seek to identify constraints and generate recommendations for extrapolating this information to larger areas, supporting accurate measurement of the carbon budget, and guiding policy and conservation actions in areas vulnerable to or threatened by climate change.

In this chapter, our research question focuses on whether it is possible to produce reliable estimates of parameters such as biomass, basal area and number of stems loss (Efflux) from the canopy height change observed with ALS data in disturbed and undisturbed tropical

forests. We also ask whether mortality is spatially structured at the landscape scale, whether those patterns are preserved over time and the drivers of those patterns.

Combined inventories on 115 ha of permanent plots in a broad spectrum of undisturbed, selectively logged dense forest structures and dynamics in French Guiana are compared to a measure of gap fraction dynamics obtained from canopy height models derived from three ALS datasets (2009-2015-2019).

8.3.3. Q2/ Allometry and carbon stocks

One of the most significant uncertainties in calculating the global carbon budget is the estimation of tropical forest biomass. Variables such as DBH (diameter at breast height-measured at 130 cm from the ground or 50 cm above the buttresses), wood density, and height are used to estimate the above-ground biomass (AGB) of individual trees, which has led to the development of allometric equations relating these structural attributes to individual AGB (Chave et al., 2009, 2005; Vincent et al., 2014; Xu et al., 2018). One area of future research is to improve the development and application of local allometries (relating measured diameter to estimated stem height) (Chave et al., 2014; Réjou-Méchain et al., 2015) to replace locally biased pan-tropical allometries (Chave et al., 2005; Ledo et al., 2016; Molto et al., 2013). This can be done by coupling LiDAR and terrestrial data at the plot scale.

In this section, our research question is focused on establishing the magnitude of error reduction in plot-level AGB prediction in tropical forests achieved by adjusting local allometries (H-DBH)? Local adjustment of allometries includes the effect of canopy height in a local neighborhood and species identity. We compare two radically different methods to merge ALS data with plot inventory data for establishing those local allometries.

8.3.4. Q3/ Influx modeling (Mapping net primary productivity with LiDAR)

Understanding tropical forest responses to climate variation are challenging due to tropical forests' heterogeneous structure and composition, especially since inferring change from a small number of forest inventory plots is problematic (Goetz et al., 2015). ALS is a powerful technique to explore large areas in a short time frame with high accuracy and efficiency, allowing the observation of forest dynamics at large spatial scales and producing new insights on the interacting factors that affect the dynamics (Zhao et al., 2018). This section focuses on forest growth, complementing the work conducted on the analysis of mortality and forest stock estimates. The ability to map primary productivity in these forests at the landscape scale may help identify the drivers of forest regrowth following logging or clear-cutting (Chave et al., 2020).

This section examines the following research questions: how accurate is the correlation between canopy height increase measured with ALS and above-ground woody net primary productivity (AGWNPP) in the Paracou experimental forest? Can such a relation be used to map productivity over space and time?

We evaluate the ability of repetitive LiDAR to map plot-level net woody above-ground primary productivity (AGWNPP) from ALS data for a range of different spatial and temporal scales. We provide recommendations on what to consider when estimating fluxes in forests with diverse dynamics, as presented in Paracou.

8.3.5. Manuscript structure

This dissertation is presented in the form of journal articles. Chapters 2 through 4 are written as published, submitted, or forthcoming articles. Chapter M&M introduces the study area and the LiDAR data used. Chapter 1 addresses question 1 on mortality detection. Chapter 2 covers Question 2 and error reduction in height and AGB estimates from local allometry (H-DBH) fitting. Chapter 3 is devoted to the aspects to consider when inferring primary productivity from ALS data. Finally, the last chapter synthesizes and summarizes the results obtained, presenting a critical analysis of the perspectives and considerations for future work.

9. Materials and methods: Site and LiDAR data characteristics

9.1. Context and characteristics Paracou

9.1.1. Site with long term data (dynamic over 30 to 35 years)

The studied landscape is located in the coastal part of French Guiana in the county of Sinnamary, where the Paracou experimental research station (5°18'N - 52°53') was set up in the 80s. This station is one of the richest tropical forest sites in terms of the availability of forest monitoring data at ground level (currently 118.75 ha measured, 75ha since 1984). In addition, it has been subject to LiDAR overflights since 2004. Furthermore, Paracou plots capture two undisturbed forest types with different soil-related canopy height characteristics (Morneau, 2007; Vincent et al., 2010). Most importantly, the network of plots includes 56 ha of forest with a history of logging (more than 34 years with different treatment intensities). This allows testing of the accuracy and sensitivity of the models as a function of the degree of disturbance. Understanding the evolution of undisturbed and secondary forests is directly relevant to forest management policies and climate change mitigation interventions (Rutishauser et al., 2015). The affluence of data available at the Paracou site is invaluable to testing the capabilities and assessing the limitations of extrapolating models built from LiDAR data, providing general recommendations and specific processing methodologies.

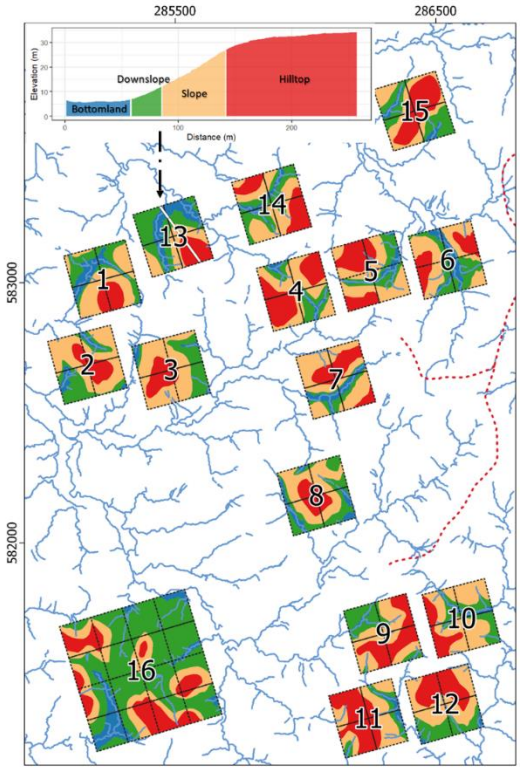

Figure 3. Map of the study area showing the individual plots and sub-plots division (125 X 125 m) considered in the analyses, with the respective habitat units according to Ferry et al. (2010) classification. The top profile corresponds to a trace (white line) on plot P13. The drainages shown are

extracted from the LiDAR terrain model and calculated in GRASS GIS (GRASS Development Team, 2017) using the (r. watershed) function.

The 16 permanent plots (fifteen of 6.25 ha and one of 25 ha, for a total of 118.75 ha) are covered by lowland tropical forest (average canopy height 27 m) and exhibits a broad spectrum of structure and dynamics, resulting from environmental heterogeneity and different levels of past disturbance. Floristically, it is dominated by three botanical families: *Lecythidaceae, Fabaceae* and *Chrysobalanaceae*. The topography is relatively flat, often with steep slopes (varying between 6 and 20%). A dense hydrographic network forms several valleys with a succession of small hills (altitude between 2 m and 40 m). The hydrogeomorphic units (habitats) vary from hilltops (flat tops) to a slope zone (medium to the steep slope, low-intensity flooding), to a low zone (flat to gentle slope, medium intensity flooding), to a lowland (flat and high-intensity flooding) (Ferry et al., 2010; Gourlet-Fleury et al., 2004; Morneau, 2007) - Figure 3. The dominant soils are of the acrisol type, while the strongly hydromorphic soils with permanent water tables are of the haplic gleysol type. (Epron et al., 2006). The soils have a low permeability, which leads to lateral drainage during heavy rainfall (Barthès, 1988; Gourlet-Fleury et al., 2004). The rainfall pattern is characterized by long periods of precipitation (annual average of 2829 mm - Figure 4) interrupted by two dry periods, a short one in March and a long one that begins in mid-August and lasts until mid-November (METEO France, 2020). The climate is described as Af tropical rainforest climate (Köppen classification) with an average annual temperature of 26.7°C and an average maximum temperature of 30.75 from 1980 to 2012 (Figure 4).

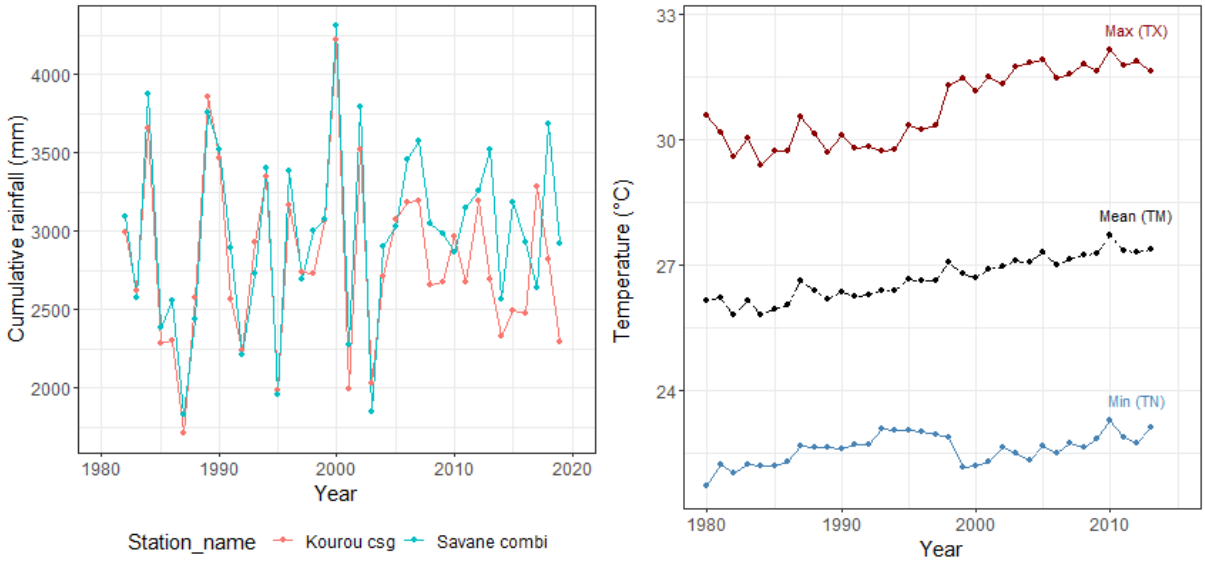

Figure 4. Climatological description of the Paracou site. On the left. Annual rainfall records CSG, Sinnamary, Savane Combi (source MétéoFrance and CNES). Right. Records of average daily mean temperature (TM), minimum temperature (TN) and maximum temperature (TX) at Savane Combi (source MétéoFrance).

The Paracou experimental station project was conceived in 1982 by the Centre de Recherche Agricole pour le Développement (CIRAD). The project's initial objective was to develop guidelines for forest management in the framework of commercial timber exploitation in French Guiana. Between 1986 and 1988, twelve monitoring plots were established, nine of which (81 ha) were subjected to different intensities of logging treatments, as shown in Table 1 (T1 - T3), with T3 being the most intense of the three treatments. Three plots, T0 (P1, P6 and P11), were designated as control plots. Between 1990 and 1992, three new T0 plots of 9 ha (P13, P14 and P15) and one plot of 25 ha (P16) were included. The latter was designed to study the ecology and dynamics of undisturbed ecosystems. Since 1988, no additional logging treatments have been conducted in the area (Gourlet-Fleury et al., 2004). Total biomass loss per treatment (from logging, poisoning and damaged forest) was 12-33% for T1, 33-56% for T2 and 35-56% for T3 (CIRAD, 2016a; Gourlet-Fleury et al., 2004) (Table 1). In the case of the control forests, there was no apparent anthropogenic pressure. However, Schmitt (1984) comments that at that time, balata (*Manilkara bidentata)* collectors passed through the area. Currently, the stands remain structurally distinct. BA ranges from 26 $m^2.ha^{-1}$ to over $30m^2.ha^{-1}$ (Figure 5).

Table 1. Treatments were applied to the Paracou plots. The number of dead individuals in silvicultural treatments includes trees that died after forest treatment (logging, firewood, and thinning) and trees destroyed by forestry work. Adapted from:(CIRAD, 2016b; Gourlet-Fleury et al., 2004)

Intensity	Plots	Applied treatments			Dead trees				Growth in canopy[1] height (m^{-1} ha yr^{-1})
		Wood	Firewood	Thinning out	Cuts	Operation	Poisoned	Forestry	
T0: Control	1,6,11,13,14,15				0	0	0	0	0.15
T1: Low intensity	2,7,9	DBH ≥ 50 or 60 cm			3.3	2.3	0	5.6	0.19
T2: Medium intensity	3,5,10	DBH ≥ 50 or 60 cm		DBH ≥ 40 cm	3.8	2.6	5.2	11.6	0.23
T3: High intensity	4,8,12	DBH ≥ 50 or 60 cm	40 cm ≤ DBH ≤ 50 cm	DBH ≥ 50 cm	6.3	4.2	3.6	14.1	0.24
P16: Control	16 (25 ha)				0	0	0	0	

Undisturbed forests show marked structural differences in canopy height (mean canopy height in 2019 T0=28.2 m, P16=30.3 m), as well as differences in root mean square diameter and stem density (but not basal area) (Figure 5). Plots P1 to P15 are characteristic of lowland “terra

[1] Measured from the 2009 and 2019 canopy models.

firme" forests, with a tabular system incised by streams. In contrast, the forest of plot P16, located in the southwest, is closer to the main river draining the area, closer to the vast floodplain with deeper soils developed on migmatite (Gourlet-Fleury et al., 2004; Morneau, 2007) and probably more shallow water table. As in P13, the more hydromorphic habitat is well represented in this plot, covering 13.7 and 14% of the corresponding area (Figure 3). P16 differs from the rest of the control plots by its lower stem densities and larger mean quadratic diameter (Figure 5).

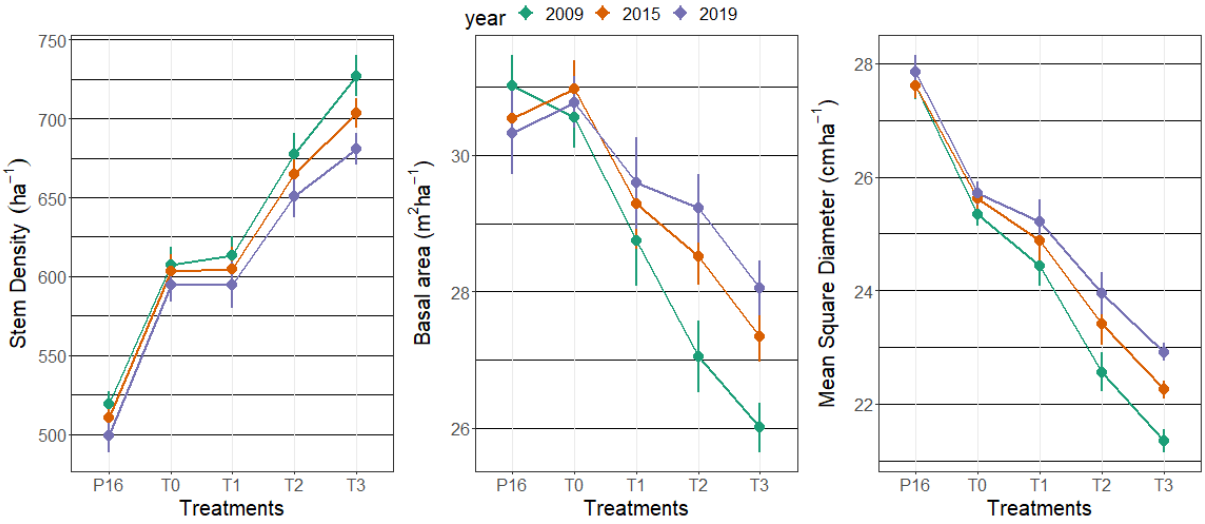

Figure 5. Treatment-estimated mean values of the dendrometric variables: stem density (N in stems. ha^{-1}), basal area (BA in m^2 ha^{-1}), and mean square diameter (in cm). The vertical bars represent the standard deviation of the mean per subplot (125 X 125 m). In the case of plot 16, the inventories correspond to the years 2010, 2015, and 2020.

Trees larger than 10 cm DBH (diameter at breast height - measured at 130 cm from the ground or 50 cm above the buttresses) have been mapped and are regularly measured in the 16 plots, albeit at a different frequency (every year for T0 lots every other for T1-T3 and every five years for P16). The data recorded for each individual are geographic coordinates of the individual, vernacular name, stem circumference measured at 1.3 m, tree status (dead or alive), type of death (including primary tree fall, standing dead, dieback, felled tree), botanical information and general observations (CIRAD, 2016a). All inventory plots are used in the development of the entire study (i.e., 19 * 6.25 = 118.75 ha, 19 plots are considered because P16 is subdivided into four plots). In addition, all available intermediate dates were considered to estimate both the dynamics and the stocks occurring during a given period (detailed later in each chapter). However, the exact dates of the field surveys were not always recorded accurately for each plot, which introduces uncertainty about the actual period, particularly to growth and mortality between surveys.

9.2. Specifications and parameters of the LiDAR acquisition at Paracou

Paracou is one of the few sites in the rainforest with 15 years of repeated airborne LiDAR measurements (~10 km^2). The available data were obtained from 2004 to 2019 by the private company ALTOA (< http://www.altoa.org >), an airborne surveying company based in French Guiana and dedicated to precision measurements using LiDAR technology and aerial photography. (ALTOA, 2018). For our study, we focused specifically on data from 2009, 2013, 2015, and 2019 covering a common area of 5.24 km^2. The selection of years was made for various reasons: the quality or low density in 2004, limited extent (not all plots were covered in 2011), or incomplete field data (not all plots were surveyed in 2016).

The characteristics of the acquisitions differ based on certain factors: vehicle (helicopter or airplane), scan angle, flight altitude, pulse repetition rate, and LiDAR acquisition mode (single (2009) or multiple returns). The 2009 campaign was conducted in a helicopter flying at an altitude between 120 and 220 m above ground level. The other campaigns were conducted in airplanes (BN2 Islander in 2013, CESSNA 207 in 2015 and BN2 Islander in 2019). The onboard systems (whose operation was explained in section 8.2.2) consisted of an altimeter on each aircraft, a laser scanner rangefinder, an inertial control unit (IMU) and a dual-frequency global positioning system (GPS) onboard (ALTOA, 2019, 2013; Geo data, 2016). Both in 2009 and 2015, more than one acquisition was made (three for the former and two for the latter). In 2009 the first acquisition (April) did not meet all desired characteristics, which determined the need for additional flights (Sept-October). The data from the different flights conducted in 2009 were finally combined with increasing the average density of points. In 2015, the flight was repeated due to quality issues affecting the imagery acquired simultaneously. In 2015, two high-density LiDAR acquisitions were made within 15 days. This replicate flight served to explore the structure of error affecting Canopy Height Models and exhibit the impact of phenological change on perceived canopy height. There were differences in flight height across campaigns. Together with LiDAR power and sensitivity, flight height affects the penetration of the laser beam and, therefore, the number of points that reach the ground (Fradette et al., 2019) (See specifications in Table 2)

Table 2. LiDAR acquisition characteristics and parameters, in their raw form and delivered by ALTOA, discriminated for each date for the periods 2009 to 2015. This information was adapted from (ALTOA, 2019; Geo data, 2016; Vincent et al., 2012a, 2012b)

Year	2009 A	2009 B	2009 C	2013	2015 A	2015 B	2019
Date	April 8 - 9	September	October	24 -25 September	05 October	20 October	15 November
Aircraft	Helicopter	Helicopter	Helicopter	Light aircraft	Light aircraft	Light aircraft	Light aircraft
Type and brand of sensor	LMS-280i RIEGL	LMS6Q140i-60	LMS6Q140i-60	LMS-Q560 RIEGL	LMS-Q780 RIEGL (12% power)	LMS-Q780 RIEGL (12% power)	LMS-Q780 RIEGL (25% power)
Flight height (m)	170 120- 220	170 120- 220	170 120- 220	450	800	800	800 600- 900
Flight speed (km/h)	------	------	------	180	180	180	180
Scanner angle	±20° ±15	±30°	±30°	±20°	±°20	±25°	±30°
Line spacing (m)	120 à 220	------	------	147	171	171	103
Average footprint size (cm)	10	45	45	20	20	20	20
LiDAR point density (All returns)	6	4	5.	23	27	38	42
Area covered (km^2)	11.97	2.21	3.04	9.68	10.45	10.45	9.4

The sensors used are RIEGL scanners. The orientation of the laser illumination and the receiver's field of view are directed from side to side by rotating polygonal mirrors. The axis of the mirrors rotates continuously at a fixed speed to provide repetitive unidirectional scans so that as the aircraft moves forward, the sampled points fall in broadband or swath, giving a parallel line scanning pattern whose wavelength region is the near-infrared (NIR), where the reflectance of the vegetation is high (Lefsky et al., 2002; RIEGL, 2004). However, although the wavelength region is in the NIR, there are differences in wavelengths (Table 3). The specific wavelength of the scanner directly influences the object's reflectance. The relative difference in reflectance between soil and vegetation will affect the apparent penetration.

Table 3. Detailed technical specifications of ALS used in the 2009, 2013, and 2015 intakes. Information was adapted from technical reports: (ALTOA, 2019, 2015, 2013; Maltamo, 2014; RIEGL, 2013, 2010, 2004; Shan and Toth, 2009; Smearcheck, 2008; Vincent et al., 2012a)

Type and reference	LMS-280i RIEGL	LMS-Q140i-60 RIEGL	LMS-Q560 RIEGL	LMS-Q780 RIEGL
Wavelength (nm)	PIR[2] 1064	PIR 900	PIR 1550	PIR 1064
Accuracy ([3]mm[4])	±20	±50	±20	±20
Laser beam divergence (mrad)	≤0.5	≤3.0	≤ 0.5	≤ 0.25
Laser pulse repetition rate - PRR (kHz[5])	Up to 24	Up to 30	Up to 240	Up to 400
Range of the scanning angle	45° at 100% of row 60° to 90% of rank	80°	± 22.5° = 45° total (± 30° = 60° total)	± 30° = 60° total
Resolution of the angle measurement	0.0025°	0.036°	0.001°	0.001°
Measurement principle	Last return	Last return	Unlimited (full-wave return)	Unlimited (full-wave return)
Maximum measuring range (m)	850 (ρ ≥ 20%) 1500 ρ ≥ 80%	150 (ρ ≥ 10%) 450 (ρ ≥ 80%)	1120 (ρ ≥ 20%) 1800 (ρ ≥ 60%)	1500 (ρ ≥ 20%) 2400 (ρ ≥ 60%)
Minimum measuring range (m)	30	2	30	50

NB: **ρ** = reflectance of the object, Maximum measuring range given assuming target larger than laser footprint, perpendicular angle of incidence and 40km visibility

The data were published in the planimetric reference system RGFG95/UTM zone 22N (EPSG:32622), and the vertical reference system is IGN-NGG 77. It is important to note that the original planimetric datum for 2009 was WGS 84 (EPSG:4326), while the original datum for the other years is the same as the publication. In addition, for the comparison between periods, a standard density reduction of 10 or 12 pulses per m^2 (2009 or 2013 density) was performed after restricting the scan angle to +/-20 degrees to increase the consistency between the datasets and allow their proper comparison. The specific processing steps applied

[2] Near infrared.

[3] Standard deviation of one sigma at a distance of 250 m under RIEGL test conditions. Precision is the degree to which a measured quantity conforms to its true value. (RIEGL, 2010).

[4] 1σ standard deviation.

[5] The average measurement rate is half the PRR rate within the 45° scan angle range (RIEGL, 2004).

to the point clouds and numerical models that were finally extracted may differ between the studies and are specified in each chapter.

10. CHAPTER 1. Mapping tree mortality rate in a tropical moist forest using multi-temporal LiDAR

This article was accepted on 05 April 2022 and will be published in International Journal of Applied Earth Observation and Geoinformation. (Huertas et al., 2022)

Claudia Huertas[a] (claudia.huertasgarcia@ird.fr), Daniel Sabatier[a] (daniel.sabatier@ird.fr), Géraldine Derroire[b] (geraldine.derroire@cirad.fr), Bruno Ferry[c] (bruno.ferry@agroparistech.fr), Toby. D. Jackson[d] (tj312@cam.ac.uk), Raphaël Pélissier[a] (raphael.pelissier@ird.fr), Grégoire Vincent[a] (gregoire.vincent@ird.fr)

[a] AMAP, Univ Montpellier, CIRAD, CNRS, INRAE, IRD, Montpellier, France.

[b] Centre de Coopération Internationale en Recherche Agronomique pour le Développement (CIRAD), 22 UMR EcoFoG (Agroparistech, CNRS, INRAE, Université des Antilles, Université de Guyane).

[c] UMR SILVA, AgroParisTech, INRAE, 54280 Champenoux, France.

[d] Department of Plant Sciences, University of Cambridge, Downing Street, Cambridge, CB2 3EA.

Highlights

- Airborne LiDAR was used to map tree mortality rate patterns in tropical forest
- Newly formed gap area predicted basal area loss better than stem loss
- Spatial patterns of gap creation were related to local topography and canopy height
- High canopy forests and bottomlands had higher mortality rates

Abstract

Background and Aims: Several studies have shown an increase in tree mortality in intact tropical forests in recent decades. However, most studies are based on networks of field plots whose representativeness is debated. We examine the potential of repeated Airborne LiDAR Scanning data to map forest structure change over large areas with high spatial resolution and to detect tree mortality patterns at landscape level.

Methods: The study site is a complex forested landscape in French Guiana with varied topographic positions, vegetation structures and disturbance history. We computed a Gap Dynamics Index from Canopy Height Models derived from successive LiDAR data sets (2009, 2015 and 2019) that we compared to field-measured mortality rates (in stem number and basal area loss) obtained from regular monitoring of 74 1.56-ha permanent plots.

Results: At the plot level, the relation between gap dynamics and absolute basal area loss rate (combining fallen and standing dead trees) was overall highly significant (R^2=0.60) and

especially tight for the 59 ha of unlogged forest (R^2=0.72). Basal area loss rate was better predicted from gap dynamics than stem loss rate. In particular, in previously logged plots, intense self-thinning of small stems did not translate into detectable gaps, leading to poor predictability of stem mortality by LiDAR in those forests severely disturbed 30 years before. At the landscape scale, LiDAR data revealed spatial patterns of gap creation that persisted over the successive analysis periods. Those spatial patterns were related to local topography and canopy height. High canopy forests and bottomlands were more dynamic, with a higher fraction of canopy affected by gaps per unit time indicating higher basal area loss rates.

Conclusion: Gap detection and mapping via multitemporal LiDAR data is poised to become instrumental in characterizing landscape-scale forest response to current global change. Meaningful comparison of gap dynamics across time and space will, however, depend on consistent LiDAR acquisition characteristics.

Keywords

Mortality, gap dynamics index, basal area loss, stem loss, LiDAR, tropical forest.

10.1. Introduction

Evidence for an accelerating global warming trend is accumulating. Each of the last four decades has been successively warmer, with the most significant increase in temperature between 2003 and 2012 (+0.19 °C) (IPCC, 2021). The Amazon, a region considered the richest in terrestrial species (Barlow et al., 2018) and one of the largest global sinks of terrestrial carbon, sequestering ~25% of annual global CO_2 emissions (Brienen et al., 2015; Pan et al., 2011), is also one of the terrestrial areas most vulnerable to global warming (Laurance and Williamson, 2001; Malhi et al., 2008). In this region, a change in precipitation during the transition from the dry to the wet season has been shown to cause trees to die more frequently (Aleixo et al., 2019). In addition, the intensification of extreme events, such as wind-throw, fires, floods or landslides (Gale, 2006), in synergy with human activities (Cochrane and Barber, 2009), intrinsically affects the intensity and frequency of large-scale mortality (Allen et al., 2015; Leitold et al., 2018; McDowell et al., 2018). Furthermore, over the last decades, change in tree turnover rate has been hypothesized to be a major determinant of the recently documented decline of intact forest C sink (Brienen et al., 2015; Phillips et al., 2008). Therefore, spatial and temporal monitoring of tree mortality rates is of direct relevance to better understand the drivers of mortality and should, in particular, help ascertain if the intact Amazonian forests are still carbon sinks or have become net sources of CO_2 (Brienen et al., 2015; Pan et al., 2011; Vieira et al., 2004).

For decades, these conclusions have been derived from field inventories of networks of permanent field plots (Baker et al., 2021; ForestPlots.net et al., 2021; Malhi et al., 2002). Nevertheless, this approach is limited by inventory plots' representativeness of surrounding landscapes, which is especially critical for the mortality process and impedes drawing robust conclusions by not sufficiently capturing the dynamics of different habitats (Di Vittorio et al., 2014; Marvin et al., 2014). For example, according to a study covering four lowland and six mountain landscapes ranging 500 to 1.200 ha in size (Marvin et al., 2014), at least 100 1-hectare plots per landscape would be needed to optimally measure above-ground carbon density in heterogeneous landscapes with 90% accuracy, so it would be challenging to have robust and realistic global models covering diverse habitats with currently available networks. Thus, a strategy combining repeated, standardized, and adequately replicated measurements at plot scale with remote sensing approaches to extrapolate at landscape-scale should be prioritized in the coming years (Chave et al., 2019; Kellner and Asner, 2009; Phillips et al., 2016; Réjou-Méchain et al., 2019).

A majority of remote sensing studies that quantify the extent, severity and timing of the disturbance events on the C cycle have been conducted at medium to coarse resolution, varying from a few hundred meters to tens of square kilometers (Xiao et al., 2019). This enables the identification of factors captured at the regional level (Asner and Alencar, 2010). However, higher spatial resolution over large geographic areas in the measurement of biomass primary gross or net production and gap dynamics remains a priority. For example, a study of biomass changes in a natural Amazonian Forest with multiple plots and remote sensing data sources found that 98.6% of biomass losses correspond to mortality at a small scale (<0.1 ha) (Espírito-Santo et al., 2015). New remote sensing technologies, such as Airborne LiDAR Scanning (ALS), have great potential here as they can detect a change in canopy structure, which can inform about biomass dynamics (Cao et al., 2016; Dubayah et al., 2010; Meyer et al., 2013; Rex et al., 2020) and tree mortality (Dalagnol et al., 2021; Thomas et al., 2013). Another advantage of ALS over other technologies is that it documents terrain elevation as well as canopy structure. Accurate land surface models provide the ability to represent variables associated with local topography and hydrological networks. These variables often co-vary with the structure and dynamics of tropical forests (Coomes et al., 2019; Detto et al., 2013). They have been shown to predict mortality (Campbell et al., 2020), including drought-vulnerable or drought-resistant areas associated with the concept of refuge (orographic wet spots) (Sousa et al., 2020), waterlogged soil that can produce anoxia (Parent et al., 2008), soil fertility related to topography and nutrient deposition (Allié et al., 2015; de Toledo et al., 2011), and treefall vulnerability due to slopes or slope exposure to wind (Alexander et al., 2018). Other advantages offered by ALS technology are the possibility of repeatedly covering large areas,

even if remote, that are adequately replicated over relevant spatial scales. ALS can monitor large areas quickly, which is crucial for tracking the demography of millions of trees. ALS can provide data to inform models of forest responses to change (Bustamante et al., 2016; Longo et al., 2020).

Studies exploring tropical forest dynamics from ALS mostly rely on a static definition of gaps (Asner et al., 2013; Asner and Mascaro, 2014; Espírito-Santo et al., 2015) but see (Hunter et al., 2015). However, the relation between gap frequency and mortality is indirect and likely to vary with forest structure. In addition, confounding permanent canopy openings (clearings, rocky outcrops, etc.) may further blur the expected relation between gap frequency and tree turnover rate. For instance, (Dalagnol et al., 2021) reported an R^2 of 0.7 for a non-linear logarithmic relationship between static gap fraction (%) and annualized dynamic gap fraction (% yr^{-1}) for 5-ha plot areas over five sites in the Brazilian Amazon, suggesting a considerable distortion between the static and dynamic perception of gaps. Studies relating to gap dynamics measured from repeated remote sensing data and ground measurement of tree mortality remain limited in intact tropical forests.

In this study, we use long-term monitoring of 84,675 stems from 115 ha of permanent forest plots to evaluate the ability of repeated ALS data to monitor tree mortality in a complex forest landscape. Dense forests dominate the landscape, including undisturbed plots and plots recovering from past logging conducted in the mid-80s. In particular, we address the following questions:

1. How tightly correlated are field-observed stem and basal area loss rates with ALS-detected gap dynamics?
2. How does mortality derived from the ground census vary with local drainage regime, past logging history, and local canopy height?
3. Do the same factors affect gap dynamics at landscape scale as captured by repeated ALS data?
4. Is the recent acceleration of mortality observed in undisturbed plots confirmed at the landscape scale using ALS data?

10.2. Methodology

10.2.1. Study site and forest inventory data

The study site is Paracou Experimental Station, located in the coastal part of French Guiana (5°18'N - 52°53'). It is covered by lowland rainforest on acrisol soil type with haplic gleysol type (Epron et al., 2006) in hydromorphic bottomlands with a permanent water table. Rainfall is determined by long periods of precipitation (annual mean of 2829 mm during 1980-2019,

source Météo France) interrupted by a short dry season in March and a long one from mid-August to mid-November. The climate is described as tropical rainy climate Af in (Köppen classification) with a mean annual temperature of 26.7°C.

Paracou Experimental Station benefits from an extensive collection of forest inventory and remote sensing data. A network of 15 6.25-ha plots (Figure 6), submitted to various logging intensities between 1986 and 1988, is surveyed every 1 to 2 years since 1996. Logging intensity has four levels: control plots (unlogged) and plots subjected to silvicultural treatments of increasing intensity (T1 to T3; see Table 4 and (Gourlet-Fleury et al., 2004) for more details). An additional 25-ha unlogged plot established in 1992 is surveyed every five years. In all plots, trees over 10 cm DBH (diameter at breast height, measured at 130 cm above the ground or 50 cm above the buttresses) are regularly measured for girth increment, mortality and recruitment.

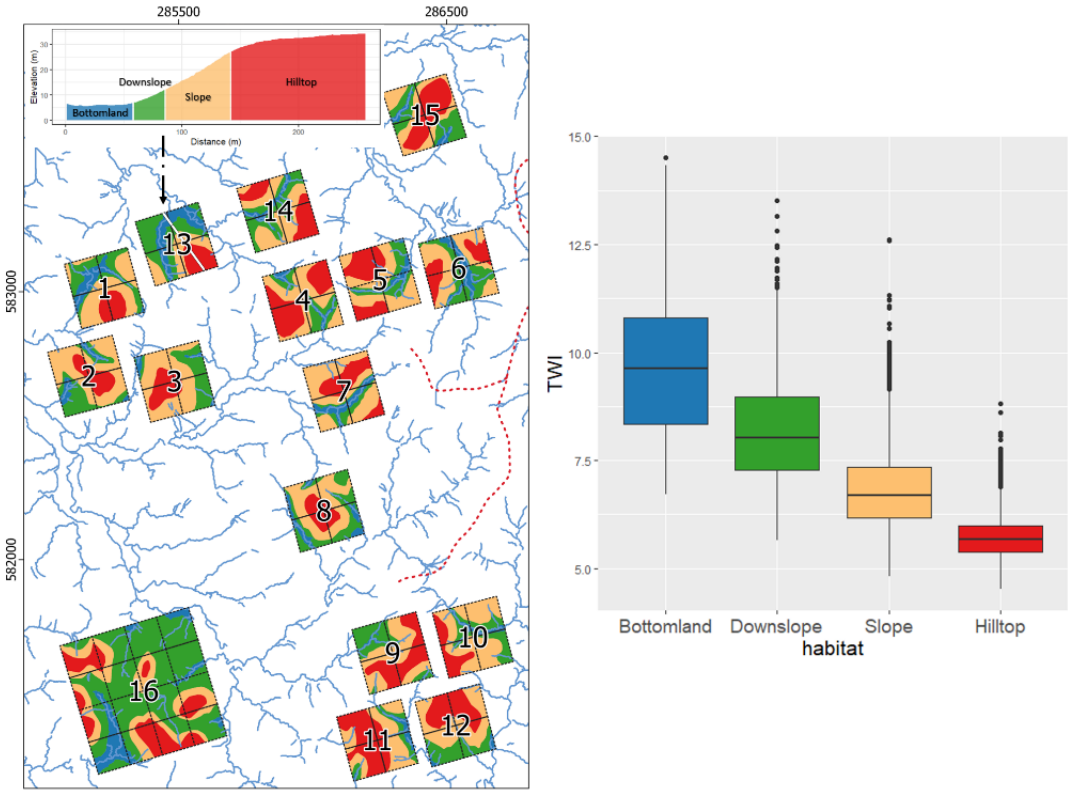

Figure 6. Left. Map of the study area, showing the different plots and the soil hydrological classes (Habitats; see text). Plot numbers refer to Forest type characteristics summarized in Table 4. Right. Boxplot showing the consistency between Habitat classification and Topographic Wetness Index (TWI) computed over the entire landscape based on the digital terrain model derived from Airborne LiDAR Scanning data (see text).

Table 4. Forest Types definition combining silvicultural treatments of increasing intensity (T1 to T3) and canopy height (HC) for undisturbed plots. Plot numbers refer to Fig. 1. Forest stature was defined from the 2009 Canopy Height Model (CHM) derived from Airborne LiDAR Scanning data as the 90th percentile of pixel-wise CHM values in a 125 m radius (see text). Biomass loss corresponds to the total woody biomass loss attributed to silvicultural treatments (see for details Appendix 1 and (Gourlet-Fleury et al., 2004)).

Forest type	Plot number	Plot area	Mean plot-wise canopy height (HC)	Mean Quadratic Diameter (2015)	Sylvicultural treatment	Harvested biomass
Undisturbed plots						
Short undisturbed forest (SUF)	1,6,11,13,14,15	6.25 ha	28.6 m	25.6 cm	None	0
Tall undisturbed forest (TUF)	16	25 ha	30.8 m	27.6 cm	None	0
Logged plots						
Treatment 1 (T1)	2,7,9	6.25 ha	28.5 m	24.8 cm	Timber	12-33%
Treatment 2 (T2)	3,5,10	6.25 ha	26.7 m	23.2 cm	Timber and Thinning	33-56%
Treatment 3 (T3)	4,8,12	6.25 ha	26.1 m	22.2 cm	Timber, Thinning and Fuelwood	35-56%

From these data, tree mortality was estimated per 125 m x 125 m subplots (~1.56 ha), calculated as the basal area (BA) or stems (Stem) loss from a plot during the studied periods. Relative mortality rates were standardized by the number of live stems or the basal area at the beginning of the observation periods. A subplot of 1.56 ha from one logged plot (P3) was excluded as it lacked data in 2015. These simple mortality rate indicators proved to be robust compared to more sophisticated individual-based models (Kohyama et al., 2018); $r = .997$, $p < .001$).

The logged plots show clear successional dynamics illustrated by an increase in basal area and a simultaneous decrease in stem density over the last two decades. The number of stems is higher in the most severe treatments and remains higher than in the control plots in

treatments T2 and T3, 35 years after logging (Figure 7). A higher frequency of small diameter stems and a lower mean wood density are observed with increasing logging intensity (Appendix 6), both patterns being characteristic of post-harvest successional dynamics.

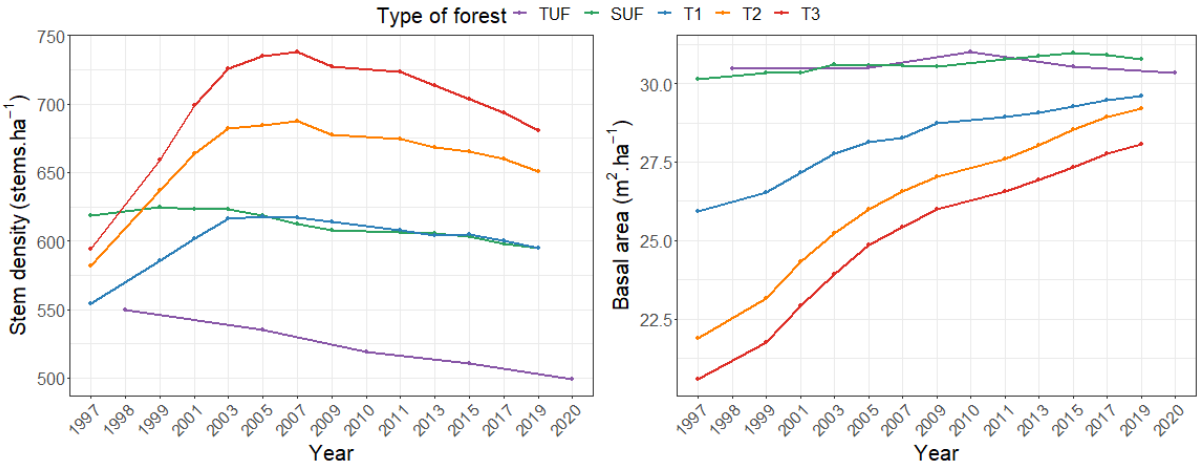

Figure 7. Mean stem density (stems.ha^{-1}, left) and basal area (BA in m^2 .ha^{-1}, right) over 20 years in the different forest types. TUF: Tall Undisturbed Forest; SUF: Short Undisturbed Forest; T1-3: Logged forests of increasing intensity (see ha^{-1} for details).

In the rest of the paper, we used information from the 2009, 2015 and 2019 inventories to compare with the ALS data, except for the 25-ha unlogged plot (P16-Figure 6), where 2010, 2015 and 2020 censuses were used.

10.2.2. ALS data and processing

Data from 2009, 2015 and 2019 (Appendix 2) covering a common area of 5.24 km^2 slightly differed in acquisition characteristics: vehicle (helicopter or airplane), scan angle, flight altitude, pulse rate and LiDAR acquisition mode (single last return in 2009 or multiple returns) - (Appendix 2). In 2009 three different flights were conducted (April, September and October) with two different sensors. The different data sets from 2009 were combined to achieve a relatively high pulse density (10 pulses.m^{-2}). The other two higher density flights (2015 and 2019) were down-sampled to 10 pulses per m^2 after restricting the scan angle to +/-20 degrees to increase consistency with 2009 data. Local maximum return height is known to depend on pulse density (Roussel et al., 2017). We found that resampling was necessary as without pulse density standardization gap dynamics estimate (see below) was biased by 10% (Appendix 9).

All point cloud data was processed using LidR package (version 3.2.1 (Roussel and Auty, 2020) in R, except for denoising, which used lasnoise function in Lastools software (version 210128).

To assess canopy change dynamics, a canopy height model (CHM) was calculated from the standardized ALS data points at each date. The point cloud was first normalized by subtracting

the ground height from the original point cloud measurement. For this purpose, the 2015 digital terrain model calculated with the R package Raster (version 3.4-13 (Hijmans, 2020)) was used for the different dates as it was considered the most accurate (highest density of terrain points). This was equivalent to using differences in the canopy surface model non-normalized by terrain height, since the same terrain model was used for all dates. The height-normalized point clouds were then rasterized with a resolution of 1 m, taking the maximum height of the first returns (Hmax). Hmax was also found to minimize the impact on CHM of leaf density variation (phenology effect), affecting penetration and mean height of returns (Appendix 7 and Appendix 8). We also tested a CHM produced using mean first return height per cell instead of maximum, which proved to be less effective for our analysis.

We also defined a height of canopy variable (HC) as the 90th percentile of pixel-wise CHM 2009 values in a 125x125 m neighborhood. HC should be less sensitive than mean canopy height to gap frequency and to the inclusion of small bottomlands which have a more open canopy (Vincent et al., 2010).

10.2.3. Gap Dynamics Index

Gaps were measured dynamically (canopy height loss events) by calculating the difference of CHM between date 1 and date 2. A gap was defined as contiguous pixels affected by a canopy height decrease between two ALS campaigns, larger than a specified threshold. Contiguity was defined in an eight-pixel direction, i.e., including corner contacts. Different thresholds were tested according to different gap detection methods reported in the literature. The various methods (presented in Appendix 5) were assessed by comparison to ground-based mortality rates. The approach of Leitold et al. (2018), defining a minimum gap size of 4 m^2 and a minimum height loss of 3 m between two ALS surveys, showed the highest correlation with field data ($r = .78$, $p < .001$ with absolute BA loss; $r = .41$, $p < .001$ with relative Stem loss). A binary raster image was obtained from mapping gaps formed between successive ALS campaigns. A gap dynamics index (GDI) was computed at the 125-m subplot level as the ratio of total pixels detected as gaps (according to (Leitold et al., 2018)) to the total subplot area. This GDI was annualized for comparison with ground-based mortality rates.

For the ten years (2009 -2019), the final gap raster was obtained as the combination of gaps newly formed in each of the two intervals 2009-2015 and 2015-2019. Gap opening and closure being a continuous process, the perceived yearly gap fraction will decrease as the time between ALS campaigns increases. For instance, when GDI was estimated directly from the 2009 and 2019 CHMs only, the canopy dynamics was about 20 % lower than estimated per period (2009-2015 and 2015-2019). This bias was more significant in more dynamic plots (Appendix 4).

10.2.4. Tree mortality and gap dynamics models

We used simple linear models to compare mortality rates in Stems and BA estimated at the plot level with GDI (research question 1). To compare the effects of environmental variables on mortality rates and GDI (research questions 2 and 3), which all ranged from 0 to 1, we used generalized linear models (GLM) with a logit link function and a binomial distribution, and homologous independent variables defined at the plot and landscape levels.

At the plot level, stem and BA loss rates were predicted from Habitat and Forest type variables using observation units corresponding to the total area occupied by a habitat class in the 125 x 125 m sampling units. Habitat classes correspond to the four soil hydromorphological categories defined by (Ferry et al., 2010; Morneau, 2007) (Figure 6): hilltop (flat to gentle slope, soil waterlogging very rare), slope (medium to steep slope, low-intensity waterlogging), downslope (flat to gentle slope, medium-intensity waterlogging) and bottomland (flat, high-intensity waterlogging). These units were delineated based on waterlogging and slope angle (a proxy for soil weathering intensity (Pélissier et al., 2002)). Habitat, defined in this way, was previously identified as a significant factor in predicting spatial variation in mortality rates (Ferry et al., 2010). Forest type combines past disturbance history (logging intensity) and canopy height (HC) information. Plot-wise, mean HC was used to separate undisturbed plots as Short undisturbed forest (SUF) and Tall undisturbed forest (TUF) (see Table 4). Not only do these forests differ in canopy height and Height-Diameter allometry (Vincent et al., 2014, 2010) but also in diameter distribution and dynamics (see Figure 7 and Appendix 6). These differences in forest stature are suspected to reflect differences in parent material, TUF developing on migmatitic bedrock (Gourlet-Fleury et al., 2004) that tends to be better drained (Schmitt, 1984).

Disturbed forest areas (logged plots, tracks and camps) were masked at landscape level prior to analysis. The elementary observation considered was the 1-meter pixel GDI value (gap vs. non-gap), with canopy height (HC) and a Topographic Wetness Index (TWI) as independent variables. TWI was used to extrapolate at the landscape level the Habitat classification used at the plot level. TWI is widely used in hydrology studies to describe the tendency of an area to accumulate water (Mattivi et al., 2019). It was computed from the digital terrain model derived from ALS data, using the r.topidx tool in the GRASS GIS (version 7.8.2) software, at a resolution of 60 m, then resampled to 10 m using bilinear interpolation. The consistency of TWI and Habitat assessed at 60 m resolution was good despite some overlap in TWI distribution between bottomland and downslope classes (see boxplot in Figure 6). To limit spatial autocorrelation effects in the GLM fitted at the landscape level to predict GDI, we did not run the model on the entire set of pixels but instead selected a subset of pixels along a 50 x 50 m grid, so that they can be considered as spatially independent. The grid was randomly located,

and the analysis was repeated 100 times. Nested GLMs were ranked using the Akaike Information Criterion (AIC). We also computed the evidence ratio (ER = exp(0.5x∆AIC), which compares the relative likelihood that one model is better than another. All analyses were conducted in R version 3.6.3.

10.3. Results

10.3.1. Comparison of gap dynamics and mortality rates within plots

BA and stem loss rate (both absolute and relative) were compared across undisturbed and logged forests to the GDI estimated from ALS data (Figure 8). BA loss rate was more highly correlated to GDI than stem loss rate. BA relative loss rate was more strongly correlated to GDI than BA absolute loss rate when the analysis was restricted to undisturbed plots (r=.85, p = <0.001 vs. r=.78, p = <0.001). GDI was moderately correlated with relative but not with absolute stem loss rate when disturbed and undisturbed plots were pooled. The relative stem loss rate was better predicted than the absolute rate due to co-variation in small stem density and mortality rate across the disturbance gradient (see Figure 7).

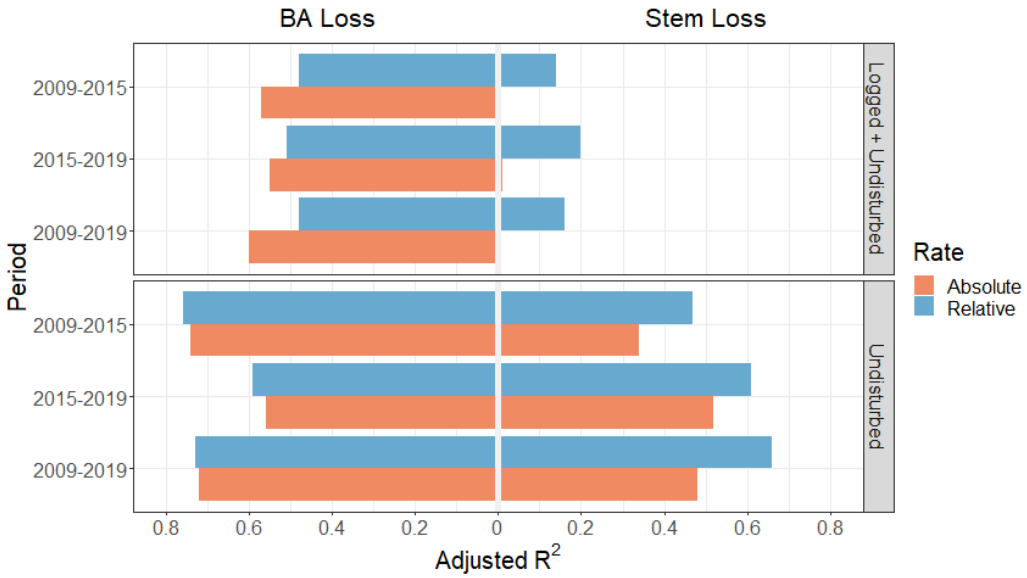

Figure 8. Adjusted R-squared of the linear regression between GDI and BA or stem loss rates according to different periods. Absolute loss rates in red and relative loos rates in blue. Upper graphs include all plots, and lower graphs include only undisturbed plots.

Scatter plot of absolute BA loss rate and GDI per forest type illustrates the sensitivity of the relation to disturbance level. When restricted to unlogged plot (SUF and TUF), the relation was particularly strong (R^2 = 0.72, RSE= 0.0032; Figure 9).

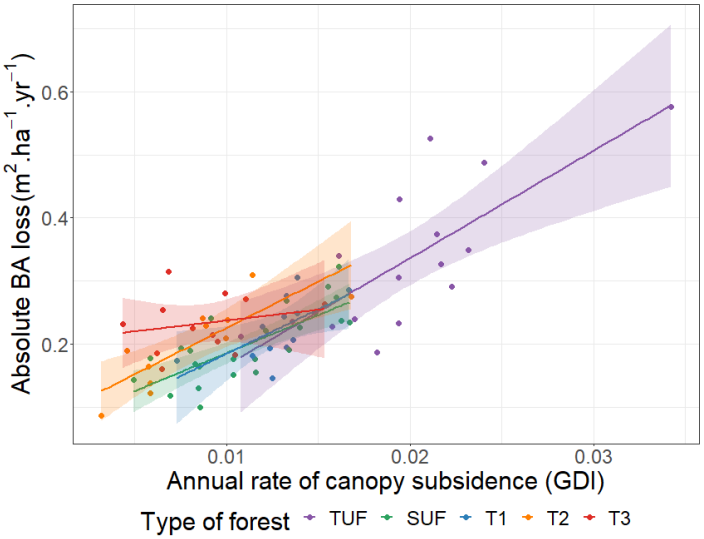

Figure 9. Absolute basal area loss ($m^2.ha^{-1}.yr^{-1}$) versus GDI (annual rate of canopy subsidence) for 2009 -2019 per 125 x 125 m subplot for all types of forests. Regression lines (solid) with a 95% confidence level. TUF: Tall Undisturbed Forest; SUF: Short Undisturbed Forest. T1 to T3: Sylvicultural treatments of increasing intensity (see Table 4 for more details).

10.3.2. Mortality and gap dynamics determinants

Relative BA and stem loss rates predicted from the GLMs show similar response patterns to Habitat and Forest Type (Figure 10). Stem and BA loss rates were predicted to be higher in TUF than SUF and to increase with treatment intensity (T1 to T3). While global responses were similar, there were differences between Forest Types as the relation between both variables (BA and stems) is mediated by stem diameter distribution density which varied across Forest Types (see Quadratic mean diameter in Table 4).

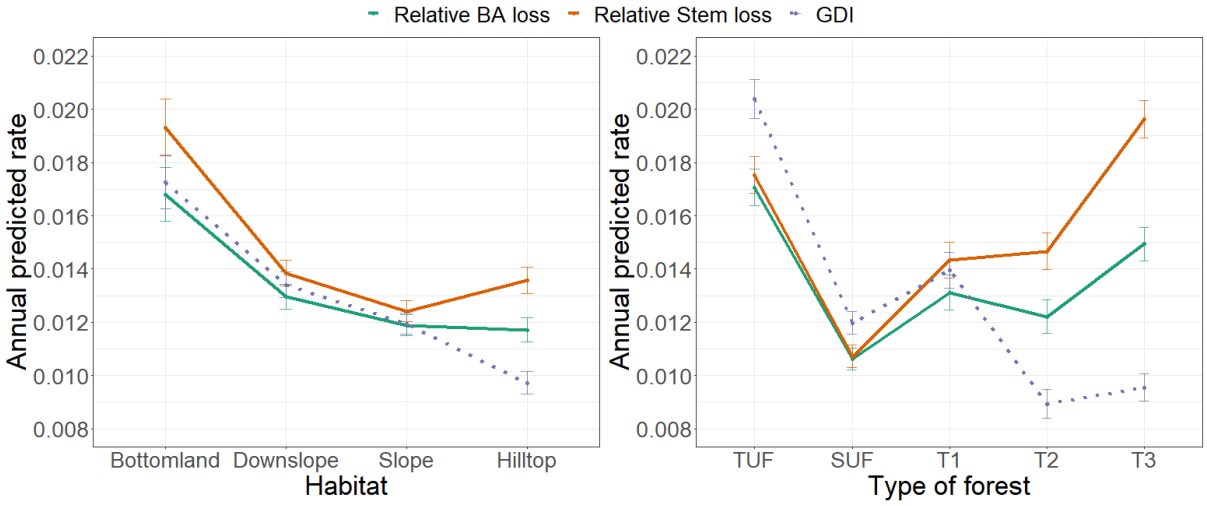

Figure 10. Effect of Habitat and Forest type (TUF = Tall Undisturbed Forest, SUF = Short Undisturbed Forest, T1-T3 = increasing level of logging intensity) on annual basal and stem loss rates predicted for the period 2009-2019 per hectare. Error bars represent 95% confidence limits.

GDI, as predicted from Habitat and Forest Type, matched the patterns modeled from ground data (Figure 10), with the notable exception of a low predicted GDI in highly disturbed plots (T2 and T3) and Hilltop habitat.

Differences between predicted stem loss, BA loss and GDI for T2 and T3 result from the peculiar diameter distribution in these severely logged plots, which contain a high abundance of short-lived pioneers with a high mortality from self-thinning of small trees. This mortality is well captured by stem loss predictions, less so by BA loss predictions and not at all by GDI predictions as it does not leave a canopy gap detectable by ALS.

The slight divergence between predictions for Hilltop class was less expected. It reflects a difference in diameter distribution of dead trees between habitats and notably a reduction in mean quadratic diameter on hilltops (Appendix 10).

At a landscape scale, we compared the GLM predictions of GDI with TWI and HC (Figure 11) effects separately or together, including their interaction. The analysis was repeated 100 times (see M&M). The best model included both predictors without interaction (Table 5).

Table 5. Median values of statistics of nested models of gap dynamic index computed at 1m pixel for 100 random pixel selections.

Model	GDI~TWI+HC	GDI~HC	GDI~TWI	GDI~HC*TWI
Median AIC	1162.74	1174.45	1170.25	1164.37
Median Evidence Ratio	-	299.7	40.3	2.24

As a complement, the spatial cross-correlation between individual 1-m pixel values of TWI and GDI over undisturbed areas (i.e., logged plots, tracks and camp masked) was equal to r=0.35 (P<0.001 - torus translation test; (Harms et al., 2001)). On the other hand, the correlation between HC and GDI was 0.40 (P<0.001 - torus translation test; (Harms et al., 2001)).

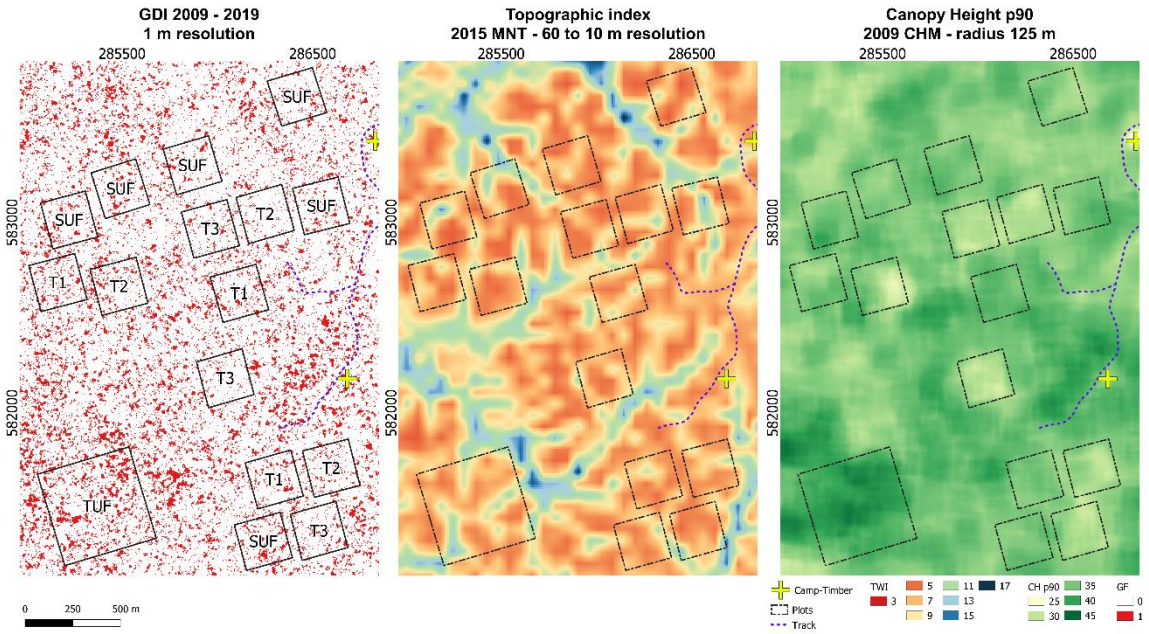

Figure 11. a) GDI per pixel of 1 m. b) TWI (calculated at 60 m, resampled at 10 m. c) and canopy height (HC) taken as the 90th percentile (p90) of 1-m CHM 2009 values in a 125 m radius neighborhood.

10.3.3. Temporal changes in mortality detection with ALS

We tested spatial cross-correlation of GDI overtime at landscape-level and observed a significant correlation between the periods 2009-2015 and 2015-2019 (Figure 12) (r=.50, p = <0.001, torus translation test).

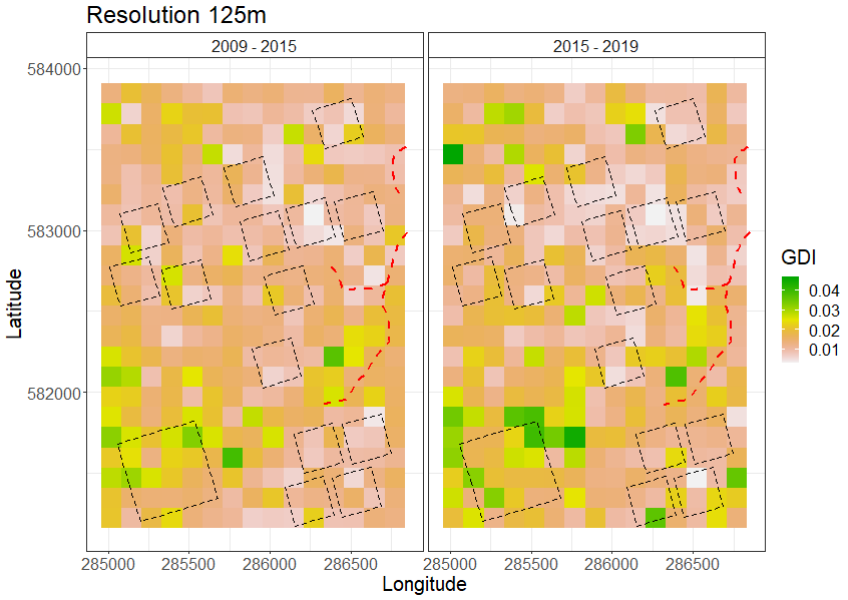

Figure 12. Map of a Gap Dynamics Index derived from repeated Airborne LiDAR Scanning data in two successive periods: 2009-2015 and 2015-2019, showing a persistent spatial pattern.

Mean and median BA and stem absolute loss increased in the undisturbed forest at the 125-m subplot level between 2009-2015 and 2015-2019. Mean change in BA relative loss rate,

stem relative loss rate and GDI were 14%, 12% and 9%, respectively (Figure 13). A Wilcoxon signed-rank test concluded to a significant change over time for BA (Z=268, p=0.028) and stem (Z=238, p=0.011) but not for GDI (Z=340, p=0.177).

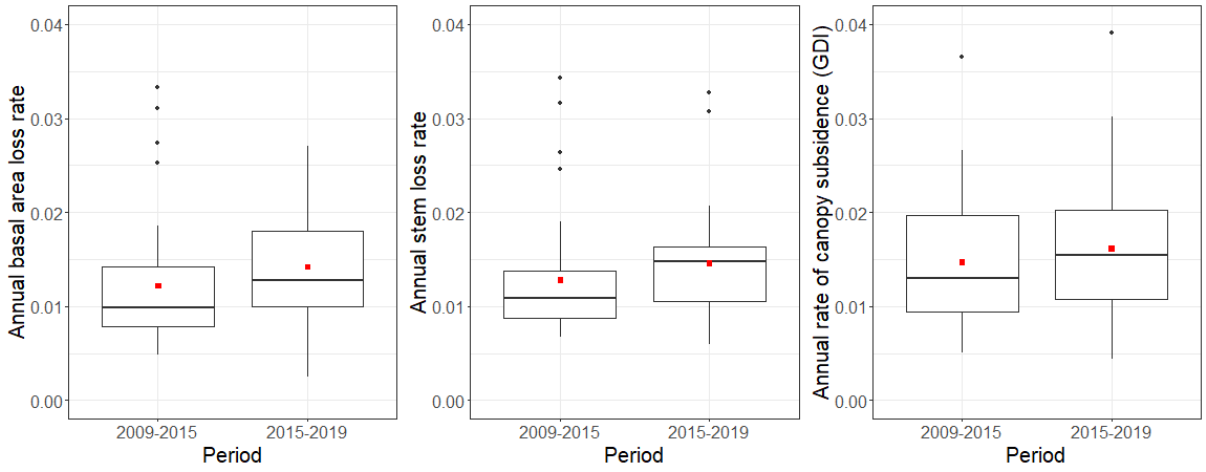

Figure 13. Mortality (BA and stem loss rates) and gap dynamics index GDI (annual rate of canopy subsidence) derived from repeated Airborne LiDAR Scanning data for different study periods (unlogged plots only). The red dots correspond to the mean value.

The increase in BA and stem mortality rate between 2009-2015 and 2015-2019 was higher in short (SUF) than in tall (TUF) forests (+19% vs. +10%, and +28% vs. +8%, respectively for BA and stem).

Masking all field plots and disturbed areas (tracks and camps), we found a slight increase (+6%) in GDI during the second period, albeit lower than the change in GDI observed within undisturbed plots (+9%). Differences between periods were, however, not statistically significant (Wilcoxon's signed-rank test: p=.82).

10.4. Discussion

10.4.1. Gap dynamics is strongly related to BA loss rate across all forest types

We found that gap dynamics *sensu* (Leitold et al., 2018) was generally well correlated to mortality rates at 125 m resolution. The strength of this correlation nonetheless varied with the mortality rates indicators considered: relative or absolute loss rates expressed on a stem or BA basis. When restricted to undisturbed forest plots, the relation between mortality rates and the gap dynamics index (GDI) was high (R^2 = 0.72 and 0.49 for absolute basal area and stem loss rates, respectively), but it decreased significantly when logged plots were included (Figure 8). Correlation was typically higher for relative BA loss rates than relative stem loss rates because ALS is more sensitive to the death of large trees. Failure to predict the number of stems lost per unit area resulted from many more small stems undetected by ALS dying in logged plots (Appendix 6). Conversely, when expressed in terms of basal area loss, the smaller

basal area in logged plots increased the discrepancy between GDI and basal area loss expressed in relative terms.

These results indicate that the canopy height model derived from repeated ALS was not sensitive to subcanopy trees mortality. Hence, gap frequency cannot be considered a robust proxy of stem mortality rates across a landscape including mature stands recovering from recent disturbance with accelerated demographic rates. However, the correlation with basal area loss appears to be much more stable and carbon flux monitoring from repeated ALS remains a valid option.

10.4.2. Spatial and temporal variation in mortality rates

Analysis at the landscape level (excluding logged plots) showed significantly correlated spatial patterns of GDI in two successive periods (r=0.48 60 m resolution 2009-2015, 2015-2019). Those persistent spatial patterns of canopy dynamics were related to differences in local drainage (TWI) and forest stature (HC) (Figure 11) and the effects of these two variables appeared to be additive (Table 5). Similar response patterns of GDI to Habitat and HC were observed at the plot level (Figure 10, undisturbed forest).

Habitat effects on tree mortality had already been documented at the plot scale on this site (Ferry et al., 2010; Morneau, 2007). We extended those results to the tall forest (TUF) and logged forest (Figure 10). Thanks to ALS, mortality patterns in relation to forest height and local drainage were further confirmed to exist at a larger spatial scale (>5 km^2) across undisturbed forest types.

The acceleration in yearly GDI from 2009-2015 to 2015-2019 (+9%) was not as strong as the acceleration in mortality rates observed in ground data (+14% increase in BA loss rate). This may be due to several limitations in the data used here.

10.4.3. Limitations in the current study

The observed relation between basal area loss and GDI may be blurred by the imperfect match between ground inventories' monitoring dates and ALS campaigns. For instance, TUF (plot 16), ground data were collected in 2010 and 2020, while ALS was acquired in 2009 and 2019 and we know from a previous study at the same site (Vincent et al., 2012b) that a 1-yr time lag between ground and ALS data can result in c. 1% uncertainty in LiDAR-derived BA estimations. We decided nevertheless to keep this plot in the present study because its structure and dynamics differed markedly from SUF. This brought more significance to the findings presented by including a more diverse set of forest types.

Another source of temporal mismatch stemmed from the long-time span over which ground censuses extend (it takes up to six months to complete the measurement of all 16 plots) compared to the few hours it takes to complete an ALS overflight covering all plots. To further complicate matters, the exact ground census date was not available for each plot every year. This introduced uncertainty in ground-based estimates of mortality rates.

ALS data used in the present study was not devoid of limitations of their own. Differences in ALS acquisition characteristics between 2009 and subsequent dates other than point density and scan angle could not be mitigated. These included footprint size, penetration and single last vs. multiple return modes (Appendix 2). This may notably have affected the temporal comparison between 2009-2015 and 2015-2019. Therefore, the net effect of the differing LiDAR system characteristics on CHM differences is difficult to assess. Another significant source of uncertainty affecting the 2009 pooled data set may come from mixing data acquired at six-month intervals (in different seasons).

Deriving CHM from the local maximum height (rather than the mean return height, for instance) made the CHM fairly robust to differences in penetration or scanning angle (Appendix 7). It also allowed seasonal leaf loss not to be confused with gap creation (Appendix 8). Conversely, defoliation, which may also be an early sign of tree death, will not be picked up.

ALS may also fail to detect standing dead trees in the upper canopy until they undergo a significant degree of decay which may take months or even years. For example, in Paracou, 48% of the trees dying from 1991 to 2020 in SUF plots have been recorded as dying standing.

False-positive errors may occur as well. Large branch fall, stem breakage without tree death, partial die-back may all generate a local change in CHM that our indicator may pick up while not associated with tree death. Such events are probably frequent and of significant magnitude, as suggested by previous studies (Chambers et al., 2001; Chave et al., 2003; van der Meer and Bongers, 1996).

10.4.4. Future research directions

Detecting the change in canopy structure not affecting the uppermost canopy would have required using the entire point cloud rather than a surface model extracted from the point cloud. At least two different strategies could be considered: individual tree death detection and change in estimated plant area density. However, both strategies suffer from methodological limitations due to the lack of accuracy of 3D information below the canopy, as the ALS signal is rapidly attenuated through the vegetation layers (Vincent et al., 2017). A solution to better describe below canopy structure may be to massively increase sampling density while using an extremely narrow laser beam (low flying UAV LiDAR System for instance). Monitoring tree

death below the canopy would further require detecting, segmenting, and ideally tracking individual tree crowns over time. Individual crown monitoring and frequent overflights would further allow detecting permanently leafless dead crowns, improving detection of trees dying standing. Indeed, leaflessness can readily be detected in high-density point clouds (Appendix 8). While progress is being made in 3D individual tree crown segmentation in ALS point cloud (Aubry-Kientz et al., 2021, 2019), reliable segmentation of non-dominant or non-emergent trees is still a difficult task in dense multi-layered forests since spectral information which is needed to individualize crowns is restricted to the sunlit upper canopy.

10.5. Conclusions

This study demonstrated that multitemporal ALS can produce reliable estimates of relative and absolute basal area loss and stem mortality rates in natural forests and confirmed the ability of ALS to detect previously identified patterns of mortality rates related to local topography and its association with terrain wetness index. Mortality rates expressed as basal area loss rates were generally better predicted than stem mortality loss rates, especially in severely disturbed plots. Gap dynamics can help track change in forest carbon fluxes and should usefully complement carbon net change monitoring derived from static carbon estimates modeled from ALS at different dates. Standardization of ALS acquisition parameters across dates (and sites) is a prerequisite for drawing meaningful comparisons. It is also essential to compare periods of similar duration due to the dynamic nature of gap creation and closure. If such conditions are met, repeated ALS should effectively detect and map possible changes in mortality rates triggered by climatic change.

The fine description of the spatial organization of canopy dynamics may further help identify likely environmental drivers of the variability of forest turnover rates, even if, as evidenced in the present paper, absolute estimations of mortality rates from ALS data are still tainted with uncertainty. In addition, wall-to-wall maps of canopy gap dynamics will inform about the representativeness of existing plots.

Acknowledgments

We gratefully acknowledge funding by "Investissement d'Avenir" programs managed by Agence Nationale de la Recherche [CEBA, ref. ANR-10-LABX-25-01]. Claudia Huertas was supported by a « Make Our Planet Great Again - MOPGA » program doctoral grant co-funded by IRD (the French Research Institute for Sustainable Development). Toby Jackson was supported by NERC grant [NE/S010750/1]. We are also grateful to David Coomes for sharing the 2019 ALS data funded by NERC grant [NE/S010750/1] and to the Centre National d'Etudes Spatiales for co-financing the 2015 ALS campaign.

Author Statement

Claudia Huertas: Conceptualization, Investigation, Formal analysis, Writing - Original Draft

Daniel Sabatier: Conceptualization, Writing - Review & Editing

Géraldine Derroire: Resources, Writing - Review & Editing

Bruno Ferry: Writing - Review & Editing

Toby. D. Jackson: Writing - Review & Editing

Raphaël Pélissier: Writing - Review & Editing

Grégoire Vincent: Conceptualization, Investigation , Writing - Original Draft, Supervision

11. CHAPTER 2: Reducing bias and uncertainty in plot-level AGB by combining ground inventories and ALS.

Claudia Huertas[a] (claudia.huertasgarcia@ird.fr), Fabian-Jörg Fischer[b] (fabian.j.d.fischer@gmx.de), Mélaine Aubry-Kientz[c] (melaine.aubry.kientz@gmail.com), James Balld (ball.jgc@gmail.com), Grégoire Vincent[a] (gregoire.vincent@ird.fr)

[a] AMAP, Univ Montpellier, CIRAD, CNRS, INRAE, IRD, Montpellier, France.

[b] Laboratoire Evolution et Diversité Biologique (EDB - CNRS/Université Toulouse III Paul Sabatier/IRD).

[c] AgroParisTech, UMR EcoFoG (Agroparistech, Inra, Université des Antilles, Université de la Guyane, Cirad), Campus Agronomique, 97310 Kourou, French Guiana.

[d] Department of Plant Sciences, University of Cambridge, Downing Street, Cambridge, CB2 3EA.

Abstract

Accurate carbon stock predictions are vital for climate change projections. However, a considerable deficit of ground-based data exists, particularly in carbon-rich tropical forests. Pantropical allometries for tree dimensions and biomass have reduced bias at the regional level, but there continue to be inconsistencies and biases at the local level due to reference data quality. Height measurements, for example, are often obtained with classical measuring instruments such as clinometers and rangefinders, which have limited accuracy in dense, closed-canopy forests, which, in turn, makes them a limiting factor for mapping carbon at the global scale. The present study seeks to establish the effectiveness of airborne laser scanning data for determining local allometric relationships between tree diameter and tree height, improving the accuracy of estimating individual tree height and above-ground biomass (AGB) at the plot level. We used ground inventory data from an extensive network of permanent sample plots in a dense forest in French Guiana, covering both undisturbed forests across hydrographic gradients and areas selectively cut in the past, and combined these data with data obtained from airborne laser scanning (ALS). We established allometric height-diameter (H-DBH) models, using both a Bayesian multilevel modeling approach and an individual-based forest model (Canopy Constructor) (Fischer et al., (2020))). Combining ALS and inventory data significantly reduces height prediction and AGB uncertainty. The quadratic error in mean height prediction is reduced by a factor of four by replacing the best universal pantropical allometry with a locally derived allometric H-DBH relationship. Both modeling's approaches provided similar AGB predictions of 33 to 50 $t.ha^{-1}$ (depending on forest type) higher than those obtained

by the reference pantropical allometry. In the local models, the inclusion of species identity and canopy height was a considerable improvement, significantly reducing the uncertainty of the prediction of H.

11.1. Introduction

Land uptake through vegetation growth is the main carbon sink on Earth, contributing to fixing an estimated 3.4 Gt of C per year^{-1} from the atmosphere (Friedlingstein et al., 2021). However, the uncertainty affecting this estimation is high (Brienen et al., 2015; Lovenduski and Bonan, 2017). Various international efforts have been initiated recently to develop space-based missions dedicated to AGB monitoring, which should reduce the large uncertainties on carbon stocks and fluxes on the global scale. Among the most prominent are GEDI, NASA-ISRO (NISAR) (Duncanson et al., 2020) and the European Space Agency (ESA) BIOMASS (Carreiras et al., 2017). While the availability of dedicated global remote sensing products has increased and will continue to increase, ground truth reference data is becoming the limiting factor in mapping carbon on a global scale (Duncanson et al., 2019; NASA, 2020). There is a particularly blatant deficit of accurate ground data in the tropics, where forest inventories cover only a tiny fraction of the total area of natural forests (Chave et al., 2019). The problem is not only the scarcity of data but also the quality. Indeed, estimating plot-level AGB from forest inventories (which typically include tree diameter and tree species identity) faces specific challenges in hyper-diverse, dense tropical forests, as was previously noted (Duncanson et al., 2021; Marvin et al., 2014; Réjou-Méchain et al., 2019). We briefly review those specificities in the next paragraph.

Monitoring AGB from plot inventory data typically involves the use of allometric models to infer individual tree above-ground biomass (AGB) from tree dimensions (height and diameter) and wood density (Chave et al., 2009, 2005; Vincent et al., 2014; Xu et al., 2018). Due to the extremely high species diversity in tropical forests and the paucity of available data, non-species-specific pantropical allometries have been built and are applied across the tropics (Chave et al., 2014; Duncanson et al., 2022; Feldpausch et al., 2011). Various studies have highlighted the uncertainty stemming from using pantropical allometries in biomass estimates, which neglect site-to-site idiosyncratic variation in the H-DBH relationship (Feldpausch et al., 2011). Even if bioclimatic factors are considered covariates in pantropical models, they only cover coarse spatial scales and cannot account for within- or between-site variation below that scale. The latter may arise from differences in local fertility, disturbance history (Ferry et al., 2010; Rutishauser et al., 2016), or floristic composition. The extreme floristic richness of tropical forests has precluded the development of species-specific allometries, a difficulty compounded by the fact that tree height estimation with field instruments (hypsometers and

laser meters) is ineffective in tall dense forests. In such environments, field measurements of tree height result in data of questionable quality (Hunter et al., 2013; Larjavaara and Muller-Landau, 2013; Lima et al., 2021). In addition, the high cost of field data collection constrains the sampling effort (Colgan et al., 2013; Sullivan et al., 2018), further reducing the accuracy of local allometries.

LiDAR (Light Detection and Ranging) technology offers the opportunity to improve the accuracy of individual tree height estimates. Airborne laser scanning (ALS) and terrestrial laser scanning (TLS) have demonstrated their potential for the 3D structural characterization of forests, offering the possibility to collect detailed measurements of the vertical structure of the forest canopy (Dassot et al., 2011; Vincent et al., 2010). TLS has the potential to accurately measure the AGB of individual trees (Momo Takoudjou et al., 2018), provided that the understory and neighboring trees are cleared prior to scanning. However, its applicability for estimating AGB at the plot level in dense forests has not yet been established (Gonzalez de Tanago et al., 2018; Wilkes et al., 2017).

ALS, on the other hand, which does not directly measure wood volume, provides accurate canopy height models at a much larger scale in a much shorter time. Therefore, ALS is often used to upscale plot data to a larger scale. To this end, a statistical model must be developed that relates the metrics extracted from the canopy height model and the plot based AGB estimates. However, ALS-derived data can also improve the accuracy of plot-level AGB estimates derived from inventories (e.g., (Fischer et al., 2020)). ALS provides information on individual tree heights, which can be matched to ground inventory data. In this way, pantropical or site-specific allometric relationships can be refined by including species identity or relevant local environmental factors. For instance, tree slenderness was previously reported to vary with local canopy height (Vincent et al., 2012a). Through the Digital Terrain Model, it procures, ALS also provides the opportunity to explore how tree height varies along topographic and hydrographic gradients. Local terrain features may indeed influence local forest structure (Coomes et al., 2019; Detto et al., 2013), which has been found to affect allometries (Molto et al., 2013).

The present study merges ground inventory data from a dense network of permanent sample plots in a site in French Guiana and ALS data in two different ways. The first approach relies on 3304 tree height and tree diameter measurements obtained by carefully matching ALS-derived crown heights and ground-based DBH measurements from plot inventory. We tested a nested Bayesian modeling framework of H-DBH allometry. We first considered unique allometry for the entire site (i.e., common allometry adjusted to all individuals), then allometry that included the canopy height in a local neighborhood as a covariate, and finally, a full model

that also considered species identity. In the second approach, the so-called Canopy Constructor (Fischer et al., 2020), height and crown width were predicted for every tree in the inventory (~72200 stems) by proceeding from site-wide allometry and then iteratively minimizing the difference between the observed Canopy Height Model (CHM) and the simulated CHM.

In this study, we address the following questions:

To what extent can allometries derived from dataset 1 (manual matching, 3304 stems) and dataset 2 (automatic matching, 72200 stems) reduce uncertainty on individual tree height and plot-level AGB?

- How efficient is the automatic matching of stem and crowns compared to field matching?

- How consistent are species-specific allometries derived from the two methods?

- Does the large spatial coverage of dataset 2 reveal additional sources of systematic variation in local allometries?

11.2. Methodology & Materials

11.2.1. Study site

The study was conducted at the Paracou experimental station (5° 18'N - 52° 53'W) in French Guiana. This lowland rainforest is dominated by the tree *families Lecythidaceae, Fabaceae* and *Chrysobalanaceae*; 700 species are registered, 18% of which are species with a unique observation. The climate is affected by the Intertropical Convergence Zone, with an average annual temperature of 26 °C and a pluviometry determined by long periods of precipitation (annual average of 2829 mm during 1980-2019, source Météo France) interrupted by a short dry season in March and a long one from mid-August to mid-November. A slightly undulating topography characterizes the site. A dense hydrographic network forms seasonally flooded bottomlands and a succession of small hills with often steep slopes and flat tops (Schmitt, 1984). The dominant soil type is shallow ferralitic, typical of the eroded soil covers occurring in northern French Guiana (Guitet et al., 2015; Sabatier et al., 1997): while deeper, well-drained Ferrallitic soils occur in some interfluves, low-permeability acrisols are found on slopes up to the hilltop and plateau, leading to shallow drainage during more intense rainfall (Barthès, 1988; Gourlet-Fleury et al., 2004).

For the site, four hydromorphological units have been defined by Ferry et al. (2010) and Morneau (2007). These units were delimited according to waterlogging and slope angle for the 16 CIRAD plots (Figure 14, white dashed line): hilltop (flat to gentle slope, low soil

waterlogging), slope (medium to a steep slope, low intensity waterlogging), downslope (flat to gentle slope, medium intensity waterlogging) and bottomland (flat, high intensity waterlogging).

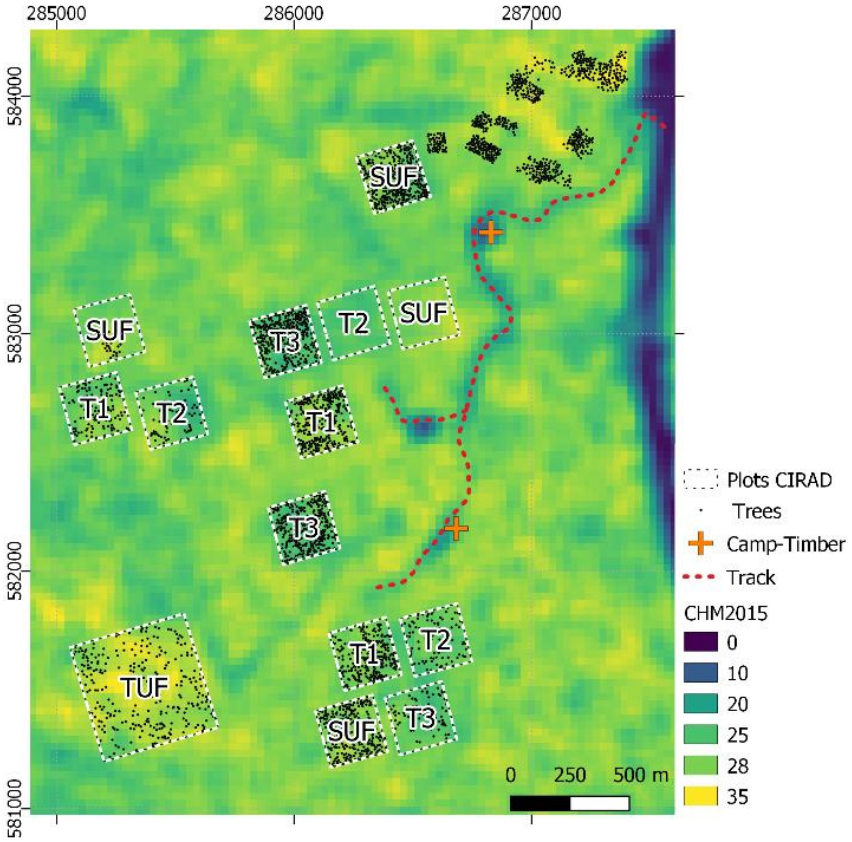

Figure 14. Distribution of the trees segmented and sampled for the allometric models (n=3304). The background represents the canopy height smoothed in 2015 with a resolution of 30 m. The individuals are located inside the permanent CIRAD plots (dotted white line) and outside (the northeast of the images).

Nine plots of 6.25ha were logged between 1986 and 1988 following three silvicultural treatment modalities (increasing intensity from T1 to T3 - Figure 14 and Appendix 11). In the CIRAD plots, a distinction is made between the control plots (T0) of 6.25 ha and plot 16 (P16) of 25 ha since these correspond to higher forests (mean canopy height T0=28.2 m vs. P16=30.3 m). Therefore, these forests will be called (TUF) Tall undisturbed forests, while the control 6.25 plots will be referred to as Short undisturbed forests (SUF) (Figure 14).

Species names in the field database were homogenized using the library "Leipzig Catalogue of Vascular Plants" (LCVP) in R - (Freiberg et al., 2020), and the wood density (WD) extracted from the global wood density database - WD in g/cm^3 per species.

11.2.2. LiDAR data

Three CHMs were used corresponding to different ALS acquisitions (2015, 2016 (model used for the automatic stem-crown matching) and 2019). The LiDAR scans were acquired by the private company Altoa (http://www.altoa.fr/) with an LMS-Q780 RIEGL LiDAR; the average

altitude of the flights was 800 m, the scan angle ± 20° and the mean footprint size at the ground level of 20 cm, the two acquisitions differed slightly in the average point density which was 25 pulses/m^2 for 2015 and 2016 and 27 pulses/m^2 for 2019.

The point cloud data were processed with Lastools software (version 210128) and the LidR package (version 3.2.1 (Roussel and Auty, 2020). To homogenize density between campaigns, a down-sampling process was performed at 25 pulses per m^2. Finally, a one-meter canopy surface model of the area was produced for each date. The ground points of each campaign were used to produce a digital terrain model per date. The points altitude was converted to the height above ground by subtracting the corresponding terrain height. A Canopy Height Model (CHM) was finally obtained by taking the maximum first return height per 1-m square cell.

11.3. Height modeling (see Figure 15)

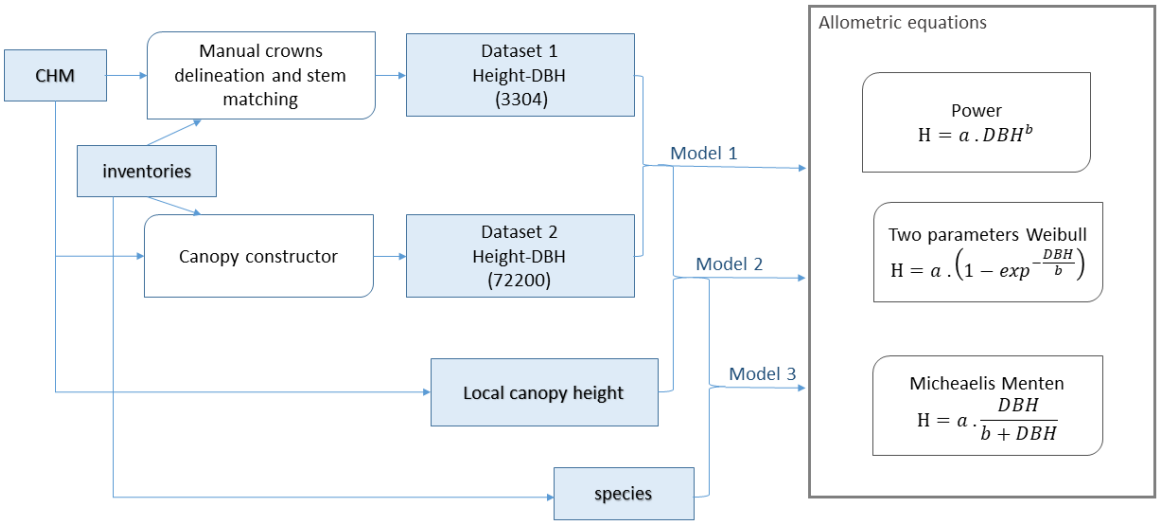

Figure 15. Schematic diagram showing the processes for modeling the heights, including the procedure of the two Datasets used and the allometric equations.

11.3.1. Manual-based stem crown matching (Dataset 1)

In total, 3372 trees were considered (median DBH 42 cm). Of these, 3304 were used for local allometries (Figure 14 and see Appendix 11), excluding outliers by quantile regression. Observations were considered outliers if they fell outside the median +/- 5 times the Inter Quartile Range rule for the entire population. In addition, for sufficiently abundant species (n>=10), observations outside the median +/- 3 times the Inter Quartile Range were excluded).

Crowns were manually delineated on the 1m-resolution canopy height maps and coincident 10cm-resolution RGB airborne imagery. Next, the matching of the crowns with the inventories

and databases was carried out, taking into account the location and diameter of the stem of each tree. Each crown segment was then checked and possibly adjusted in the field. Finally, the "diameter at breast height" (DBH, measured at 130 cm from the ground or 50 cm above the buttresses) and the botanical tree identification were retrieved from the inventory database.

Height was calculated for each segmented crown (each segment was a simple polygon spatial file). The 95th percentile of the height values within each delimited crown was extracted from the canopy height model (CHM). The 95th percentile (H_p95) was preferred to the maximum height to minimize the impact of possible segmentation errors, including high pixels from a higher neighboring crown. The slope between H_p95 and maximum height was 0.99 (robust linear regression, no intercept). Therefore, using the 95th percentile did not generate a significant bias in tree height.

In addition, for a subset of 21 trees, we compared tree height estimates obtained from Terrestrial laser scanning (TLS) and ALS (Bossoukpe, 2020). We found that both methods produced consistent results (R^2=0.96, Appendix 17), and no bias was detected.

11.3.2. Automatic stem-crown matching using Canopy Constructor (Dataset 2)

A larger dataset (n=72200) was created, for which stems and crowns were matched using a simulation approach (Figure 15). The Canopy Constructor (CC) is an individual-based forest model (code available here: https://github.com/fischer-fjd/CanopyConstructor) that uses a combination of field inventories and airborne laser scanning (ALS) to reconstruct 3D canopies tree by tree. At its core is an algorithm that creates an optimal and spatially explicit fit of the canopy height model obtained from ALS. The algorithm uses field-measured tree diameters and stand-level allometric relationships between tree dimensions to make an initial guess with respect to individual tree properties, with deviations from the mean randomly distributed in space. Random deviations are initially swapped between trees to optimize the reconstruction spatially until improvements become negligible (Fischer et al., 2020). The resulting 3D reconstructions can infer tree-level biometric properties, map fine-scale forest structures such as spatial distributions in above-ground biomass or analyze large-scale patterns such as gap size-frequency distributions (Jucker, 2022). If the model is run with many different parameter combinations, it can also be used to infer the stand-level allometric structure in the first place and thus can initialize dynamic forest models (Fischer et al., 2020). However, in our case, as mean allometry had already been inferred, we only used the core procedure, i.e., creating a spatially explicit representation of the canopy.

For this task, we added a few improvements to the model code. Briefly, improvements encompass the following changes: 1. "Mirror trees": trees at plot edges and corners, whose

crowns reach beyond the simulated area, are mirrored back into the simulated forest at another plot edge or corner with a similar canopy height structure. This removes edge effects and their substantial impact on canopy structure (Knapp et al., 2021; Mascaro et al., 2011) and allows the utilization of the Canopy Constructor down to 0.25 ha plots without bias. 2. Species-level allometries: species identity is considered in the fitting procedure so that crown swapping concomitantly optimizes canopy fit and improves the allometric relationships for height-diameter and crown radius-diameter at the species level. This is done by fitting allometric relationships for each species, updating them after every crown swap and accepting the fit only when the overall error of the species-specific models decreases compared to the previous configuration. 3. Empirical parameterization of crown shapes: crown shapes resemble more closely empirically delineated crowns and can now be parameterized as a distribution over height layers within the crown. 4. Speed and flexibility improvements: a faster, more flexible procedure has been implemented to preserve the underlying allometric structure without requiring the binning into diameter classes.

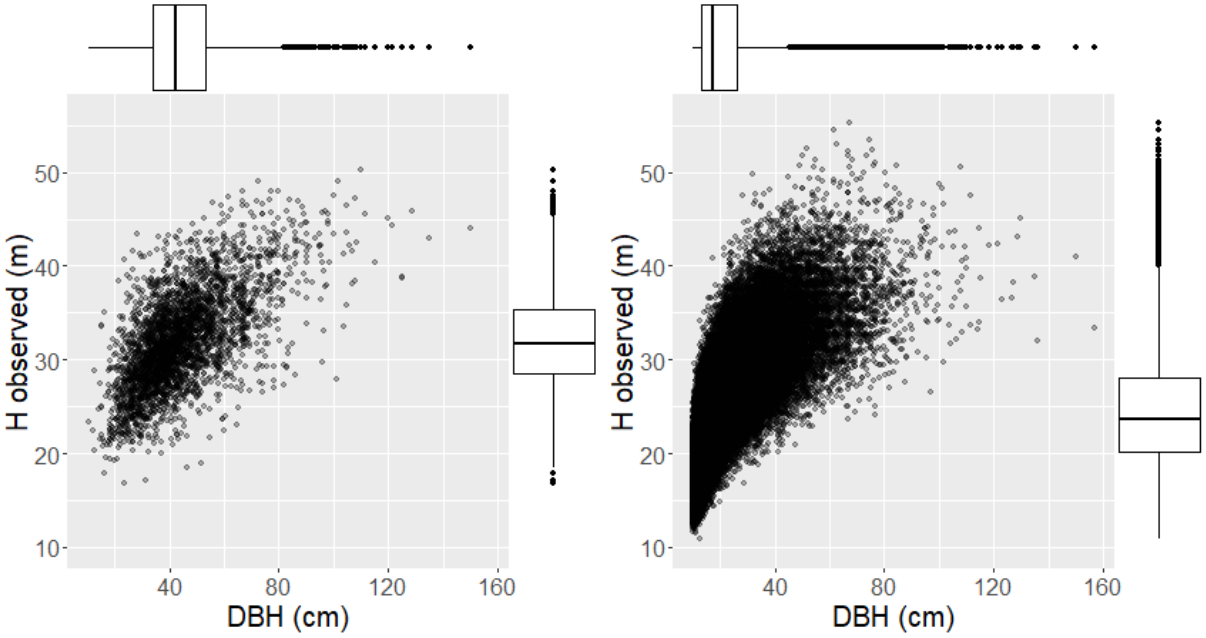

Figure 16. (a) Scatterplot of the trees presented in Figure 14 in X the diameters and in Y the heights measured with the ALS (dataset 1). The marginal distribution shows the boxplot of the two variables for the population. (b). Scatterplots of trees from the global fit of CC predictions to the CIRAD database for individuals with DBH>=10 cm diameters are extracted from permanent plot monitoring and height predicted with the CC modeling (dataset 2). The marginal distribution shows the boxplot of the two variables for the population.

11.3.3. Stem height modeling

11.3.4. 1/ Manual/Field-based crowns

For the manual/field-based data, we considered three allometric equations expressing H as a function of DBH: power law (PW) ($\widehat{H}$=a x DBH^b - Equation 1), two-parameter Weibull (W2) $\widehat{H}$ = a x (1-exp(-DBH/b Equation 2) and Michaelis Menten (MM) ($\widehat{H}$=a x DBH/(b+DBH) - Equation 3) (Molto et al., 2014) (Figure 15).

Different models were tested (i.e., considering different predictors/modifiers of the allometric equations). For all models, the three equations were tested and applied to the entire set of ground validated height-DBH observations (n=3304). Weakly informative priors were used for both parameters (gamma distribution with parameters (1.5, 0.01))

Model 1 used unique allometry for all trees.

Model 2 included canopy height in a local neighborhood (LCH) as a covariate affecting parameter **a** in all three equations (see Appendix 12). A previous study conducted on the same site (Vincent et al., 2012) reported that stem slenderness increased with local canopy height (LCH), probably in response to local fertility differences. We used median canopy height in a circular buffer to characterize local canopy height. In a preliminary analysis, we tested various neighborhood sizes ranging from 30 to 60 m radius. The smallest radius was selected based on the smallest Akaike Information Criterion value of the allometric model. In this exploration of the neighborhood size effect, pixels from the target tree crown were systematically excluded from the local canopy height calculations, avoiding a circular relationship with the height variable in the model. We used the median local height rather than the mean to be less sensitive to possible canopy gaps close to our target tree. Indeed, we intended to capture an index of spatial variability of canopy stature robust to transient changes that would not necessarily represent longer-term differences. For the estimation of LCH, we used the canopy model of 2015.

Model 3 also included species identity, which affected all three candidate equations' **a** and **b** parameters (cf. Figure 15). Singletons (species with a unique observation that represented about 6% of all dataset 1) were pooled into one singleton-species class. This pooling of the rarest species proved effective in reducing model prediction uncertainty. Grouping of singletons was also applied in model 2bis.

Model 2bis, which included species as a random effect but excluded LCH, was also considered for comparison.

All adjustments were performed using a Bayesian multilevel modeling framework. We used the library brms (brms R package version 4.1.0 (Bürkner, 2017) based on Stan software (Gelman et al., 2015). Models and parameterization are provided in Appendix 12 (The code is accessible on GitHub at this link, and the code of the final full model is provided in Appendix 25). The allometric equation was selected on the best fit criterion of the most complete model. Models 1 to 3 (using the previously selected allometric equation) were then fitted to dataset 2, restricted to stems with DBH≥ 20cm. Residuals were mapped and analyzed for systematic deviations from the expected mean 0 by forest type, hydromorphological unit, or in relation to plot structure

11.3.5. 2/ Automatic stem- crowns matching

We used two types of height-diameter allometries as input for the simulation model – a 2-parameter Michaelis Menten function and a power law with a multiplicative error structure. Similarly, we tested two types of crown radius-diameter allometries, both power laws, but one based on the exact area of the empirically derived crown shapes and the second one based on the area of their convex hulls. Due to idealized, symmetric crown shapes in the Canopy Constructor, we hypothesized the latter to give a more adequate representation of the canopy than the irregular and sometimes porous raw crown shapes. We ran five simulations for each height and crown radius allometry to account for uncertainty, based on five random draws from the respective *brms* posteriors. This resulted in a total of 20 simulations. The correlations between residuals from the height allometries and residuals from the crown radius allometries were propagated to the Canopy Constructor simulations by drawing residuals from a multivariate distribution with covariation between height and crown radius residuals.

This approach was applied to the CIRAD inventory data (16 plots, 72200 stems) in 2016 (2015 for plot P16) using LiDAR from the same year. The diameter distribution of this data set was characterized by the abundance of small stems (median DBH 17.35 cm, Figure 16b). Acknowledging that smaller stems were poorly adjusted from ALS data, we restricted this analysis to a subset of trees based on their diameter, keeping only trees with at least 20 cm DBH. This provided a ~ten times larger data set (28845 vs. 3034) than dataset 1 and a much broader spatial coverage.

11.3.6. 3/ Comparison

A universal H-DBH relationship for pantropical forests developed by Chave et al. (2014), which we will refer to as Model 0, was used as the reference model for comparison. We compared the allometric models, defining the residuals as the difference between the observed data and the predicted values of the model and evaluating in terms of mean squared error (MSE = Σ (y_i

- $\hat{y}_i)2/n$, y_i is the observed value; $\hat{y}_i$ is the corresponding predicted value; n = the number of observations) and the variance (of the difference between the observed and predicted values), in terms as well of the root mean squared variance of the residuals (RMSE) and BIAS as the mean of the residuals. And for Bayesian models, we calculate the Widely Applicable Information Criterion (WAIC) based on the posterior probability calculated with the loo library in R (Yao et al., 2017)

11.3.7. Impacts on AGB

Predictions of AGB per plot using the various allometric models were calculated for 76 1.56 ha (all CIRAD plots, DBH>=10 cm, n=72200 - Figure 16b). We also used the pantropical equation proposed by (Chave et al., 2014) to calculate individual tree AGB, except for palms, for which we used the specific allometry for the genus Euterpe presented by (Réjou-Méchain et al., 2015) based on the work of (Miranda et al., 2012) and the generic allometry for all other genera of *Arecaceae* (Sullivan et al., 2020).

11.4. Results

11.4.1. Prediction of individual tree heights

The power-law model form was often the best model in terms of fit quality (Appendix 12) (especially for the simplest model types 1 and 2. However, the differences in quality were generally marginal compared to the next best model, and it predicted unrealistically high trees in the 10-15 cm DBH size class (Appendix 24). It was not penalized because of the low number of observations in that DBH range in our field-checked training set.

The best combination (lowest WAIC) was achieved using equation MM and model three. Differences in performance due to adding or removing a predictor were typically larger than differences observed by interchanging allometric equations (Appendix 12).

Models with additional covariates vastly outperformed simpler models (much lower WAIC and RMSE). This was the case whether the covariates (LHC and species identity) were considered alone or together. The best model (model 3) included both covariates (Table 6).

Table 6. Local allometric equations fitted to predict mean height (H; in m) as DBH function (in cm). Results for each of the models and functions are presented in Appendix 12. Data input corresponds to Dataset 1

	Predictors	WAIC	RMSE	N
model 1 - MM	-----	18574.06	4.02	3304
model 2 - MM	Local canopy height (LHC)	17781.97	3.56	3304
model 2b - MM	Species	17485.29	3.26	3304
model 3 - MM	Local canopy height + species	16627.92	2.78	3304

The pantropical model showed a notable bias, underestimating the mean tree height by 3.5 m (Table 7). As a result, the Mean Squared Error (MSE) in predicted height was reduced by a factor of four when replacing the best universal allometric H-DBH (model 0) with a locally derived relationship. More than half of the quadratic reduction in error was due to the reduction in bias (i.e., it would not decrease with increasing sample size).

We also compared the predictions of CC for a subset of trees in dataset1, which were located in CIRAD plots (n=2568). RMSE of CC predictions was slightly larger than model 3 - MM and presented a moderate negative bias of -0.5 m (Table 7). This bias seemed to affect trees across all plots (Figure 17). MSE was reduced by a factor of 3 compared to the MSE of the pan-tropical model.

Table 7. Table of individual tree height estimation error for the different models, including the pantropical, model 3 (reference model) and CC simulation. The data used here correspond to the 16 CIRAD plots in 2015. * single arbitrarily chosen simulation output

Model		**Individual tree height**			
		mse	bias	var	rmse
model 0	Pantropical	26.53	3.5065	14.24	5.15
model 3 - MM	Local reference	5.91	0.0599	5.91	2.43
model CC*	Canopy Constructor	8.72	-0.5156	8.46	2.95

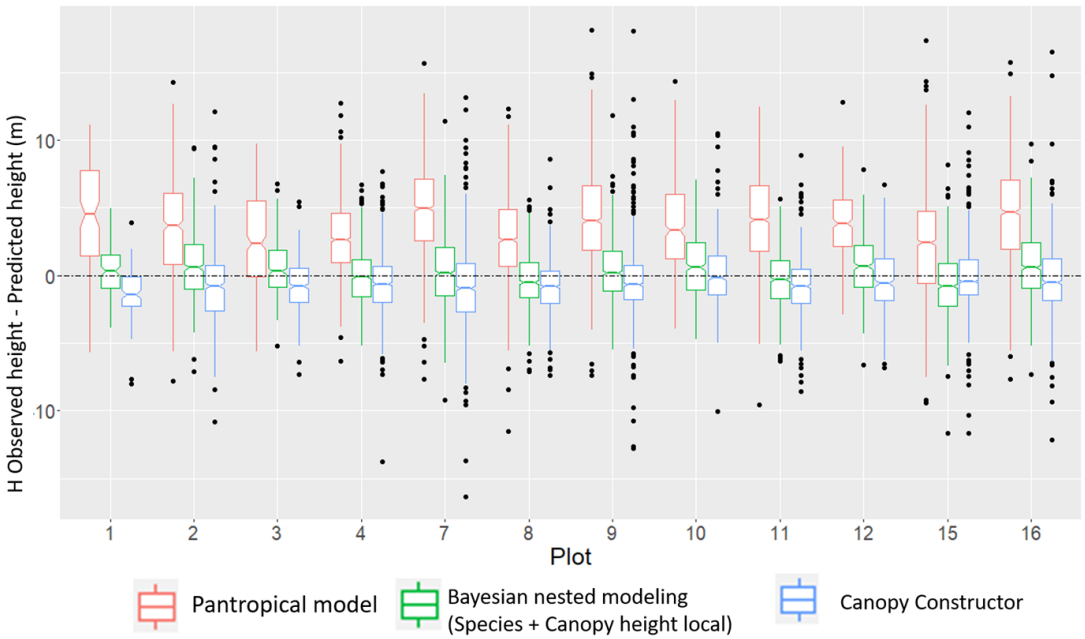

Figure 17. Boxplot of individual tree height estimation error in meters per plot using Chave's pantropical equation, reference model and the canopy constructor predictions. The dotted line represents the 0 error.

11.4.2. Comparison of species-specific allometries obtained from direct adjustment vs. using CC adjusted Heights

CC height estimates were slightly biased and noisier than direct height estimates (Table 7). However, the overall patterns matched well with predictions from the field-based model (Figure 17). There was a good correspondence between species-specific allometries inferred via simulation and those derived from manually delineated crowns, both visually (Figure 18) through formal tests.

A visually examining a gam predicted height fitted to both data sets indicates a highly consistent ranking of species smoothed height at a given diameter (Figure 18). This lends credit to using CC-derived species-specific allometric patterns for trees above 20cm DBH.

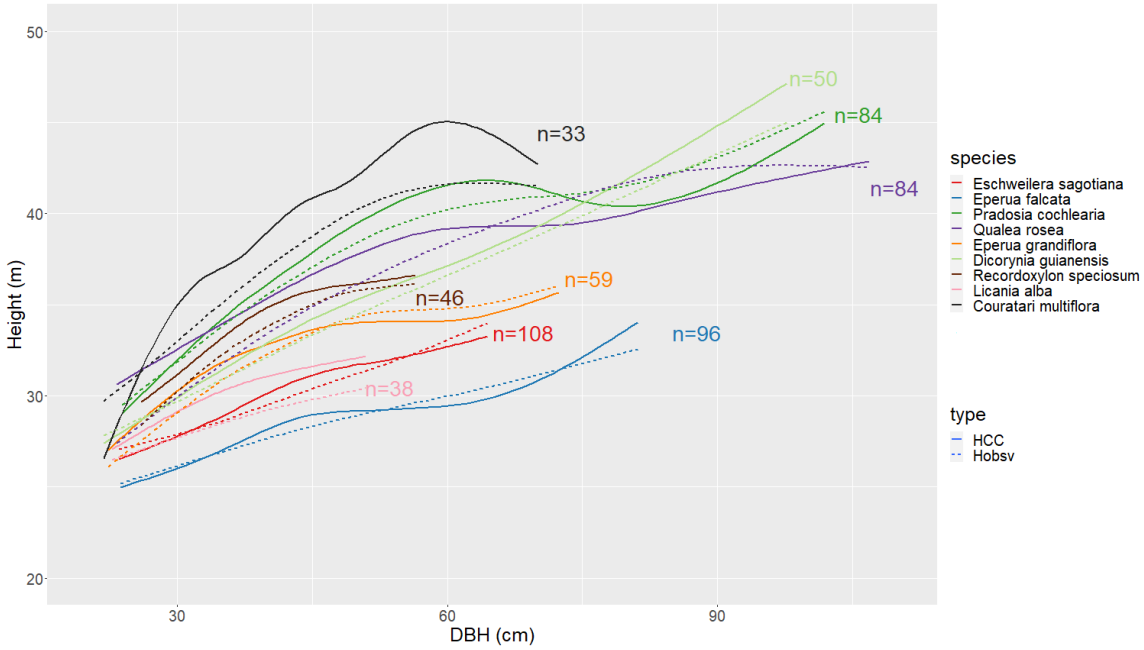

Figure 18. Curves of the H-DBH relationships of the value simulated by CC ($\widehat{H}_{CC}$) and the observed value (Dataset 1), for the most abundant species (n>=30), in solid line the curve (gam method) of the CC model, in dashed line the curve of the data observed in the field. The analysis is limited to individuals over 20 cm DBH, excluding intensely logged plots (T1 and T2).

Figure 19 reports the H-DBH relations of a subset of abundant species. For each of those species, hundreds of observations were pooled. It can be seen that species have highly variable heights for a given diameter (more than 11m or 27% difference at 50cm DBH, for instance; compare *Couratari multiflora* and *Eperua falcata*). It can also be seen that some H-DBH lines cross over, suggesting indeed that species allometries differ not only in scale but also in shape.

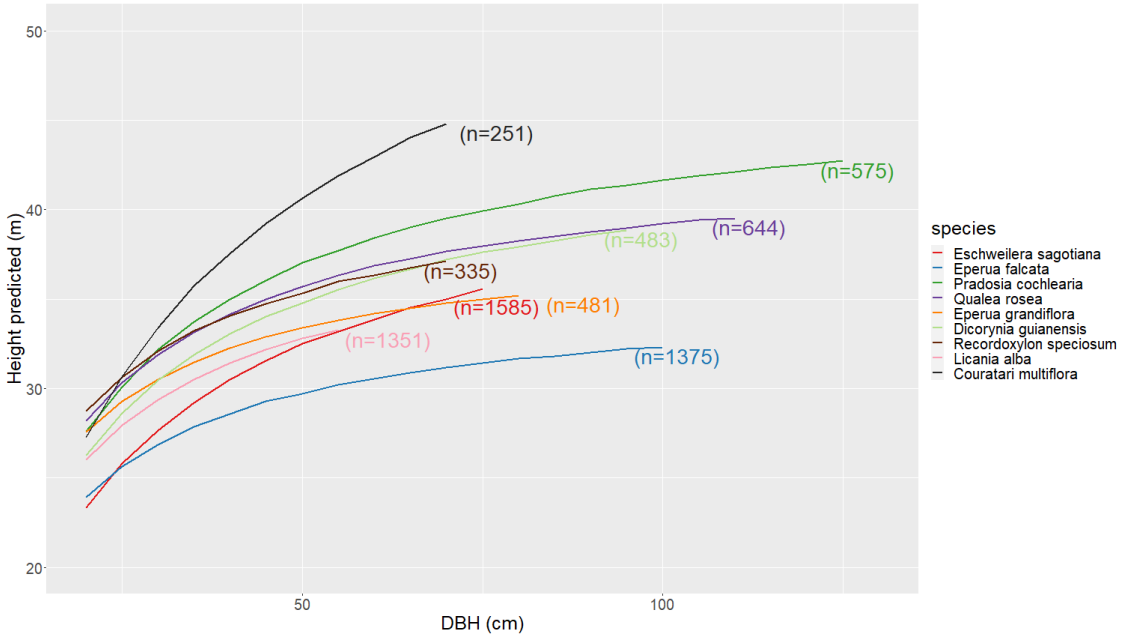

Figure 19. Curves of the H-DBH relationships were obtained from the prediction of the 3-MM model, taking as reference the extracted heights adjusted by CC of the trees with DBH ≥ 20 cm (Dataset 2).

11.4.3. AGB error at plot level

The pantropical model (compared to the local fit reference model 3 - MM) underestimated plot-level AGB (Figure 20) by 33 to 50 t/ha or 12 to 13% (Table 8). Plot level AGB estimates produced using CC predictions, on the other hand, were highly consistent with the reference model (NRMSD= 2%, Figure 20). Estimates per forest type were within a 1% difference.

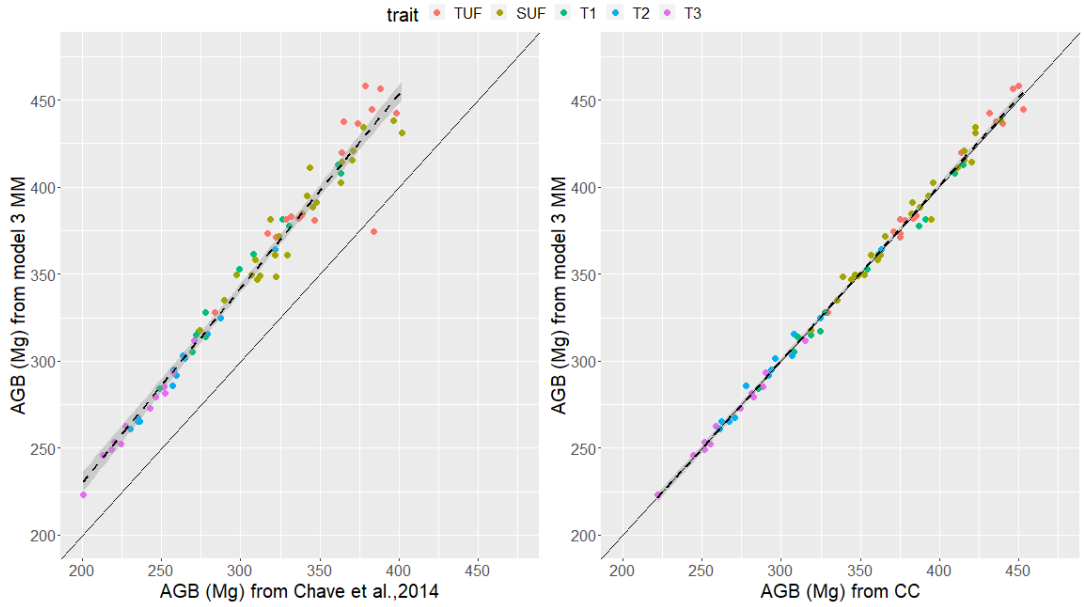

Figure 20. Estimates of above-ground biomass in Mg.ha^{-1} per plot of 1.56 ha. The colors indicate the different treatments. Right comparison between the reference model (model 3) and the pantropical model. The comparison between the local and CC models is on the left. We consider the CC estimates as a reference (Dataset 2).

Table 8. Above-ground biomass per treatment (AGB in Mg.ha^{-1}) is calculated as the mean per plot of 1.56 ha. (Number of trees=72200)

	TUF	SUF	T1	T2	T3
Pantropical model	353	337	301	260	235
Model reference (Model 3)	403	382	347	295	268
Canopy constructor	402	380	350	294	268

11.4.4. Exploring the effects of hydromorphological units, previous logging and structural characteristics of the plot (BA, QMD) on allometry.

We selected the CC-adjusted heights of trees with DBH > 20cm (n=28845). We fitted two sets of models (MM1-3, PW 1-3) using the equations which performed best in the analysis of dataset1 (Appendix 12). We excluded small stems from the analysis recognizing that they were poorly adjusted as they were mostly lying below the canopy surface model. We also ran the same analysis by selecting only stems whose crowns were deemed visible from above (visibility >25%, n=29965) and found similar results, so we only present results obtained applying a DBH cut-off point (Appendix 18 and Appendix 19).

The moderate bias (+0.65 m MM) affecting tree height in bottomlands after fitting a single allometric model (MM1 or PW1) disappeared or was much reduced after introducing species identity or LHC as covariates (Figure 21 and Appendix 18). The initially strong bias (from -1.12 m to + 1.07 m) affecting tree heights across forest types was almost completely resorbed after introducing LHC or LHC and species identity in the model (Figure 21 and Appendix 20). A moderate overestimation bias (of +0.37 m) persisted in Tall forests (TUF) for the full model MM-3.

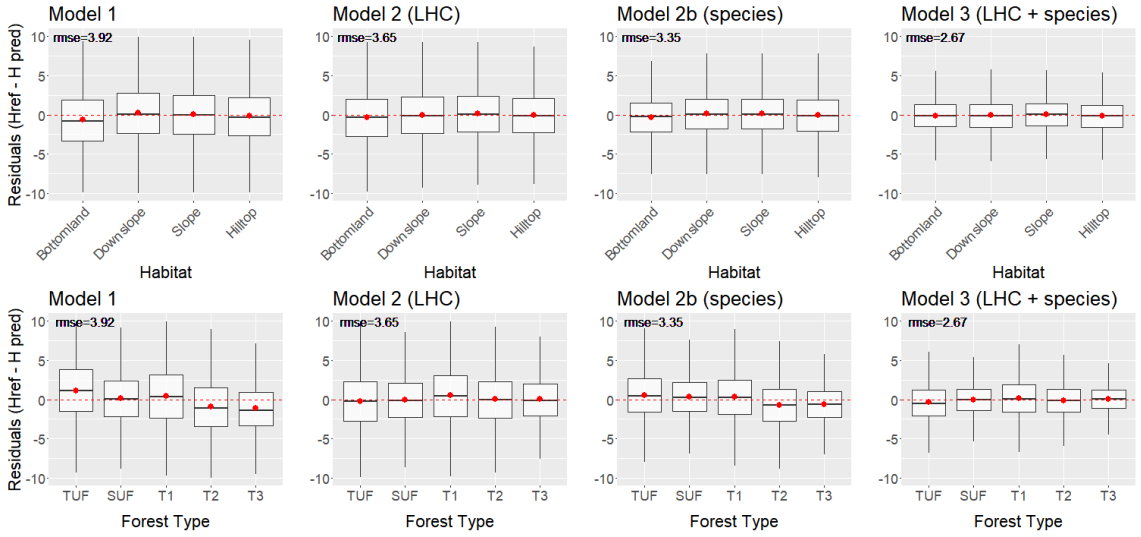

Figure 21. Residuals of models MM equation compared in the top section with the habitat units and in the bottom section with the different treatments (T1-T3) and plots of unlogged low forest (SUF) and unlogged high forest (TUF).

Table 9 Models MM1 and MM2b (as well as PW1 and PW2b) showed a significant correlation. Large BA plots tended to have either higher than expected trees (model 1) or lower than expected trees (model 2b, which included only a species effect). Model 2 (which included the local canopy height effect only) showed the lowest - marginally significant - correlation between plot structural variables and mean residuals. Model 3 (complete model) showed a slight negative correlation, i.e., a tendency for overestimating highly stocked or high QMD plots (Table 9 and Appendix 22).

Table 9. Pearson correlation test between model residues and the structure variables (basal area and quadratic diameter) for plots of 125 m X 125 m and the residuals of models 1 to 3 of the power and MM equations. Total observations 76

cor	p_value	equation	model	variable
0.49	0.00001	power	model1	BA
-0.24	0.03437	power	model2	BA
0.53	<0.00001	power	model2b	BA
-0.31	0.00562	power	model3	BA
0.50	<0.00001	MM	model1	BA
-0.26	0.02256	MM	model2	BA
0.59	<0.00001	MM	model2b	BA
-0.33	0.00364	MM	model3	BA
0.63	<0.00001	power	model1	QMD
-0.22	0.05758	power	model2	QMD
0.64	<0.00001	power	model2b	QMD
-0.31	0.00611	power	model3	QMD
0.65	<0.00001	MM	model1	QMD
-0.21	0.07016	MM	model2	QMD
0.68	<0.00001	MM	model2b	QMD
-0.30	0.00753	MM	model3	QMD

We also analyzed bias per habitat or forest type after fitting models MM1 to MM2 to the entire set of trees in the CIRAD database (n=72200) but analyzing the residuals for the trees above 20cm DBH (n=28819) (Appendix 20). The RMSE and BIAS of the different models were much higher than when the model was adjusted to a subset of trees with DBH≥20cm).

11.5. Discussion

We evaluated two ways of combining ALS data and ground inventories to improve the allometric model of stem height (inferred from ALS) as DBH function (from ground inventory) and the consequent change in AGB estimation at the plot level. The two approaches provided similar predictions, 33 to 50 $t.ha^{-1}$ (depending on forest type) higher than those obtained using a reference pantropical allometry. Local allometries (MM3 and CC) effectively accounted for

systematic spatial variation and species specificity in the observed allometry and reduced overall RMSE in tree height used in AGB allometries. The inclusion of local canopy height significantly improved the site model whether species identity was included or not (MM2vsMM1 and MM3vsMM2b, respectively, Figure 21).

11.5.1. Impact of censorship of small diameter stems

Both data sets yielded uncertain height predictions for small-diameter trees, which seldom reached the upper canopy and were rarely visible in the ALS-derived CHM.

We assumed that local canopy height would affect all trees (both upper canopy and subcanopy trees alike, cf model 2 and 3). Experimental evidence shows that even shade specialist species respond to crowding/light availability by altering their H-DBH relations (Harja et al., 2012). Still, the magnitude of this response could be lower for subcanopy species than upper canopy species. TLS, which can provide accurate tree height estimates of subcanopy trees, could be used to explore this point further (Seidel et al., 2021).

11.5.2. Habitat-specific effect on H-DBH allometry

The effect of habitat on the H-DBH ratio in Paracou was previously analyzed, focusing on a much more restricted area by Ferry et al. (2010). Their Figure 8 (e) reported a trend for trees to show decreasing slenderness from bottomland to lower slope to upper slope (the latter not different for hilltop). We did not find that trend to hold at a large scale. However, we did find that trees were, on average more stunted in bottomlands; this effect disappeared when species identity or local canopy height was taken into account (Figure 21)

11.5.3. Interspecies variability

Individual tree crown delineation and field matching and automatic stem and crown matching via CC yielded similar species-specific H-DBH relationships on a common subset of stems (Figure 18). This is an important finding as it indicates that CC global fitting strategy can yield abundant H-DBH data, which, once coupled with taxonomic information from plot inventories, provides a way to effectively capture species specificity in allometric models. Including species identity yielded considerable improvement through a significant reduction in H prediction uncertainty irrespective of the form of the allometric relation (Table 6 & Figure 21). This large across-species variability in allometric relation is also well visible in Figure 19.

Nonetheless, a single mathematical formulation for H-DBH might not be adequate for all species (Burt et al., 2020). An improved allometric model could consider a mathematical formulation conditional to species identity. The choice of the best mathematical formulation will also be more robust once smaller stems are included in the calibration data set.

11.5.4. Local canopy height as a covariate in H-DBH allometries

Canopy height in the local neighborhood of a tree was previously correlated with tree slenderness (higher H for a given DBH) at the species and the community levels (Vincent et al., 2012a). Rutishauser (2016), also working in Paracou but using a different data set, reported that logging negatively affected tree slenderness. Here we found that a site adjusted allometry not including local canopy height as a covariate resulted in overestimating heights in the two most intensively logged treatments (Figure 21). However, once local canopy height (which was lower in logged over plots) was considered, this bias disappeared.

Hence, a simple and easy to compute indicator removed bias in H-DBH, whether it originated from past logging or natural difference in local canopy height. The next step will be to explore if this easy-to-compute indicator performs equally well across more sites covering an even broader range of forest types.

11.5.5. Covariation of DBH-height and forest structural characteristics.

Co-variation between forest structural characteristics and tree allometries in tropical forests has been reported in various studies (Banin et al., 2012; Feldpausch et al., 2011; Molto et al., 2014). In many other forest types, both planted and naturally occurring, stem density and/or stocking affected H-DBH relationships (Vanclay and Henry, 1988; Wang et al., 1998; Zeide and Vanderschaaf, 2002). Our results (Table 9) suggest a slight negative correlation between predicted height and BA and QMD. This correlation was twice as large when considering unique allometry for the site (MM1).

It was previously found that local canopy height and plot structure covary at the site. (Vincent et al., 2010). This relation is likely to be functional and might hold across many forests. However, to our knowledge, a comprehensive conceptual model relating forest structure, canopy height, and tree slenderness in natural multispecies forests is still lacking. Spatially explicit 3D simulation models (Maréchaux and Chave, 2017; Vincent and Harja Asmara, 2008) may help clarify assumptions in this respect.

11.5.6. Critical evaluation of the CC approach

The CC predictions, which had slightly higher RMSE when compared to the calibration data used for adjusting the allometric model (Table 7), also showed a small bias (-0.5m).

Tested against dataset1, canopy constructor estimates proved to be slightly lower for short trees (H <27.5 m) and slightly higher for tall trees (H >35 m) (Appendix 14).

Applying allometric equations to CC estimates (MM3 fitted on dataset2) or using CC height estimates directly produced consistent overall H-DBH mean trends (Appendix 15).

The output of the CC model was also found to be largely insensitive to the mathematical form of the initial allometry model (MM or PW), data not shown.

11.5.7. Potential and perspectives of ALS

To minimize bias in biomass assessment protocols in tropical forests, it is commonly recognized that it is necessary to use locally calibrated allometric H-DBH equations (NASA, 2020). However, the commonest protocol relies on pantropical relations due to a lack of height data. Local tree height measurements from clinometer or rangefinders may be used to adjust models to the sites. However, the high level of error bearing on such local height measurements, which is expected to be significantly larger than the error in the data used to build the biomass allometric models, seriously questions the actual improvement in accuracy that can be achieved in this way (Burt et al., 2020). Furthermore, site effects are estimated irrespective of species identity. Other studies have found little evidence supporting taxon-specific allometric models as opposed to general allometric models (Fayolle et al., 2013). The latter study considered tree height and AGB measurement by destructively sampling 138 trees ranging from 5.30 to 192.50 cm in DBH and extending across 47 taxa. The high variability in size, the high number of taxa, and the low number of individuals probably limited the statistical power of a test designed to detect a species effect. Until recently, there was little alternative but to hope that the known-to-exist biases would not severely undermine the predictions made by models fitted using data plagued with uncertainty (e.g., Duncanson et al., (2020)). Unfortunately, our results do not support such wishful thinking.

This study showed that combining ALS and inventory data could significantly reduce the height and AGB prediction uncertainty. To complement tree height sampling from the ALS and include smaller stems not correctly captured, TLS may be the best alternative (Dassot et al., 2011).

11.6. Conclusions

The combination of ALS and inventory data proved effective in reducing the uncertainty in predicting height (H-DBH) and consequently AGB in a dense tropical forest. Automatic field-based stem-crown matching produced results that compared well to field-based matching. Predictions of individual tree heights were similar and predictions of plot-level AGB estimates were very consistent. In both cases, AGB predictions were higher than those obtained by the reference pantropical allometry, the difference ranging from 33 to 50 $t.ha^{-1}$ depending on forest type. The quadratic error of height was reduced by a factor of 4 when replacing the pantropical allometry with the optimal local model. The optimal model included local canopy height in individual tree neighborhoods and species identity as covariates in height prediction. Automatic stem-crown matching produced by the Canopy Constructor allowed to massively increase the

sample size per species, using the model data (Canopy Constructor) not only in the initialization but also in the evaluation phase. The current most important limitation to the wide development of species-specific allometries from the combination of ALS data and field inventory is the sampling bias toward larger trees. It is recommended to include smaller stems in the calibration dataset, using other technologies such as TLS, which may be the best currently available alternative.

Author Statement

Claudia Huertas: Conceptualization, Investigation, Formal analysis, Writing - Original Draft.
Fabian-Jörg Fischer: Conceptualization, Methodology, Formal analysis, Writing - Review & Editing.
Mélaine Aubry-Kientz: Methodology, Conceptualization, Writing - Review & Editing.
James Ball: Resources, Validation.
Grégoire Vincent: Conceptualization, Investigation, Writing - Original Draft, Supervision.

12. CHAPTER 3. Can multitemporal airborne LiDAR data predict primary productivity in dense tropical forests?

Claudia Huertas[a] (claudia.huertasgarcia@ird.fr), Daniel Sabatier[a] (daniel.sabatier@ird.fr), Géraldine Derroire[b] (geraldine.derroire@cirad.fr), Raphaël Pélissier[a] (raphael.pelissier@ird.fr), Grégoire Vincent[a] (gregoire.vincent@ird.fr)

[a] AMAP, Univ Montpellier, CIRAD, CNRS, INRAE, IRD, Montpellier, France.

[b] Centre de Coopération Internationale en Recherche Agronomique pour le Développement (CIRAD), UMR EcoFoG (Agroparistech, CNRS, INRAE, Université des Antilles, Université de Guyane).

Abstract

The factors influencing net primary productivity in tropical forests are not well understood. Accurate landscape-scale maps of forest productivity overlaid with maps of environmental factors would provide clues as to which environmental drivers predominantly determine observed productivity patterns. We modeled Above-ground woody net primary productivity (AGWNPP) from repeated plot and LiDAR data for different time periods. Our study is based on six years of tree stem circumference records from a 93.75 ha plot network, including undisturbed and selectively logged forests in French Guiana. Three LiDAR overflights were conducted during the same period. The LiDAR-derived mean canopy height gain at 1 m resolution correlated with AGWNPP (and basal area increment) at the plot level, provided that pulse density was regularized across dates before analysis. Plot-level AGWNP predictions over six years showed an accuracy of 11% (relative RMSE) for 1.56 ha sampling plots and 6% for 6.25 ha sampling plots. The results were consistent regardless of the length of the period considered between two LiDAR acquisitions (here from 2 to 6 years). Landscape-level AGWNPP derived from LiDAR data showed a pattern related to past logging intensity and Topographic Wetness Index. Previous productivity studies contradict the predicted spatial pattern of higher productivity in the bottomlands, and we explore the reasons for this discrepancy.

Keywords: Above-ground woody net primary productivity, basal area gain, growth, canopy height change, LiDAR, tropical forest.

12.1. Introduction

Rainforests provide an essential role in regulating terrestrial climate and heat and energy exchanges with the atmosphere. (Bonan, 2008; Shao et al., 2019). They stock about half of the world's forest carbon (Pan et al., 2011), constitute approximately 20% of terrestrial carbon

pools and 30% of terrestrial net primary production (NPP) (Ichii et al., 2005; Marvin et al., 2014). The growth of intact forests has contributed to forestation and reforestation to mitigate the historical increase in atmospheric CO2 by enhancing C storage in biomass (Brienen et al., 2015). However, the CO2 sink force of intact tropical forests appears to be declining in both the Amazon and African regions (Hubau et al., 2020), possibly due to the impacts of rising drought and air temperatures, affecting the growth and mortality of trees (Hubau et al., 2020). African forests appear to have maintained a favorable sink strength longer than Amazonian forests, potentially due to slower dynamics and a longer mean residence time of the associated carbon (Hubau et al., 2020). An increase in C uptake by the forest will increase C release after a given time; that period will depend on the mean residence time. This suggests that forest turnover rates may control the evolution of the forest carbon sink in response to climate change, and in turn, climate change could modify the mean residence time. Increased forest turnover rates due to increased mortality could eventually convert tropical forests from sinks to sources of C (Phillips et al., 2016). Unpredictability regarding the evolution of the C storage capacity of intact rainforests is related to both the uncertainty in the evolution of climate change and the limited understanding of the environmental drivers of carbon storage and turnover (Fatichi et al., 2019; Keeling and Phillips, 2007; Kellner et al., 2011; Taylor et al., 2015). The ability to map forest turnover at the landscape scale would provide information on the drivers of primary productivity and their relationship to carbon fluxes and stocks and be instrumental for parameterizing and testing dynamic vegetation models (Frolking et al., 2009).

Net Primary Productivity of an ecosystem is the net carbon input obtained after deducting the carbon loss through plant respiration. Below ground Net Primary Productivity (root growth) is rarely measured and is considered proportional to above-ground Net Primary Productivity. Above-ground NPP can be disaggregated into four main components: The two most important are long-term above-ground biomass increments inferred from measured stem diameter and leaf turnover estimated from litterfall monitoring (Clark et al., 2001a). A synthesis of field data from tropical forests (Clark et al., 2001b) indicates that litterfall C flux in tropical forests is approximately twice as large as the estimated increase in woody biomass. In the same study, the importance of two other components (losses to consumers and volatile organic compounds) was sometimes assessed, and their contribution was much lower.

Although the guidelines on how primary productivity can be estimated from plot-level measurements are well established, scaling up estimates to the landscape or regional level can be challenging, as the representativeness of forest plot networks may be questionable (Fisher et al., 2008; Marvin et al., 2014). A crucial concern is the limited extent of current plot networks (in aggregate, they may cover less than 0.01% of tropical forests worldwide) and their limited ability to cover an extensive range of environmental gradients. Additionally, their

installation and measurement are complicated in tropical forests, where access is complicated (Salovaara et al., 2005). Consequently, plot selection favors easily accessible sites or less disturbed areas, as pointed out by (Malhi et al., 2002), referring to the "majestic forest bias," where forest monitoring favors mature forests on sites without gaps.

Several authors have advocated the need to take advantage of remote sensing technologies to complement field plots and improve biomass estimates (Marvin et al., 2014; Réjou-Méchain et al., 2019); similar arguments also apply to vegetation dynamics studies. Airborne laser scanners (LiDAR) are particularly relevant to studying intermediate-scale vegetation dynamics. LiDAR can map the forest canopy rapidly with great detail and efficiency, also covering large areas (landscape scale) (Zhao et al., 2018). LiDAR point clouds describe the forest canopy in 3D, thus providing a continuous estimate of canopy height, a key parameter for carbon stock estimation. Although many studies have used the potential of LiDAR to quantify carbon stocks (Dubayah et al., 2010; Marvin et al., 2014; Rocha de Souza Pereira et al., 2018; Vincent et al., 2014), less effort has been invested in identifying a reliable indicator of canopy dynamics derived from LiDAR as a proxy to characterize gross AGB fluxes (as opposed to net fluxes that equate to stock change).

This paper explores how multitemporal LiDAR can fill these gaps between plot and landscape estimates of tropical forest primary productivity. We test the extent to which the Above Ground Woody Net Primary Net Productivity (AGWNPP) of a forest stand is correlated with the rate of canopy height gain once areas of canopy subsidence are excluded. We use LiDAR-measured canopy height to predict two indicators of forest growth, AGWNPP and basal area increment (BA) of surviving trees, assessed from periodic field inventories in lowland rainforest. The plots' network includes undisturbed, selectively logged forest stands covering 93.75 ha in total. The present analysis covers six years and uses three LiDAR overflights conducted in 2013, 2015 and 2019.

12.2. Materials and Methods

12.2.1. Inventory data and forest characteristics

The study site is the experimental station of Paracou (5° 18'N - 52° 53'W) in French Guiana. This lowland tropical rainforest (average canopy height of 27 m). A gently undulating topography characterizes the site, and a dense hydrographic network forms seasonally flooded bottomlands and a succession of small hills with often steep slopes and flat tops (Schmitt, 1984). The dominant soil type is shallow ferralitic, typical to the eroded soil covers occurring in northern French Guiana (Guitet et al., 2016; Sabatier et al., 1997). Deeper, well-drained ferralsols occur in some interfluves. Low permeability acrisols are found on slopes up to the

top of the hill and plateau, which leads to superficial drainage during the most torrential rains (Barthès, 1991; Gourlet-Fleury et al., 2004).

The current network of plots, established in the 1980s, consists of 15 plots of 6.25 ha. Six plots were designated as control plots (T0). Nine fields were subjected to different silvicultural treatment intensities (T1 - T3) from 1986 to 1988. Since then, no additional logging has been conducted in the area. The total loss of AGB following silvicultural treatment (through logging, poison-girdling and damages by forest works) was 12-33% for T1, 33-56% for T2 and 35-56% for T3 (Gourlet-Fleury et al., 2004). In the 15 plots, trees above 10 cm DBH (Diameter at breast height – measured at 130 cm above the ground or 50 cm above buttresses) have been mapped and regularly re-censused from 1984 to the present. Monitoring frequency has varied over the years for different plots. Since 1996 logged-over plots have been censused every other year, while T0 (control plots) are censused every year. All analyses were conducted for three nested plot sizes 250 x 250 m (6.25 ha), 125 x 125 m (1.56 ha), and 62.5 x 62.5 m (0.39 ha).

12.2.2. BA and AGB calculations

Stem cross-section (BA) in square meters and tree height (H) in meters were computed from individual stem girth records for each census year. H was calculated from the DBH using a local allometric formula developed specifically for the site (Vincent et al., 2014). The wood density (WD) values were drawn from the global wood density database (WD) in $g.cm^{-3}$ (Chave et al., 2009) for each species or higher level of botanical identification when species could not be ascertained. Finally, AGB in Mg was computed using the pantropical equation proposed in (Chave et al., 2014), except for palm, for which we used the specific allometry for genus *Euterpe* presented by (Réjou-Méchain et al., 2015) based on the work of (Miranda et al., 2012), and generic allometry for all other genera of *Arecaceae* (Sullivan et al., 2020). Figure 22 shows the convergent evolution of AGB and stems density across treatments over the 2013-2019 period extending from c. 24 to 30 years after silvicultural treatments. A decreasing trend in stem density affected all plots, including the undisturbed control plots (T0), where the AGB increase seemed to plateau around 2015.

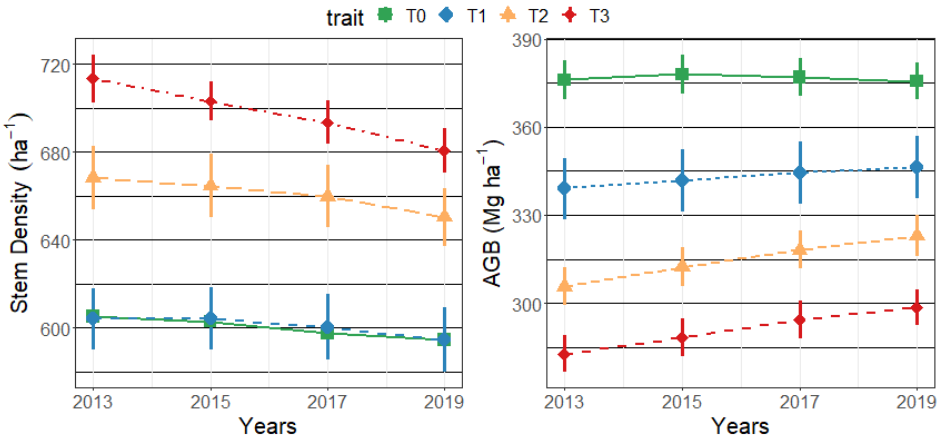

Figure 22. Mean stem density (stems.ha^{-1}, left) and above-ground biomass per treatment (AGB in Mg.ha^{-1}, right) per treatment; vertical bars represent +/- the standard error of the mean per plot of 1.56 ha.

12.2.3. BA and AGB influxes

We calculated increments in AGB and BA for the different plot sizes (6.25 ha, 1.56 ha, 0.39 ha) based on individual tree records following the guidelines in (Clark et al., 2001a). AGB increment, hereafter referred to as AGWNPP, was calculated as the sum of AGB growth of surviving trees and AGB ingrowth (of newly recruited stems, i.e., those passing the 10 cm DBH threshold) each census interval. The sum of AGB growth and AGB ingrowth equals AGWNPP. The same procedure was used to compute BA increment.

All rates were annualized by dividing by observation period (in years) and normalized per ha. Since nine plots (T1-T3) were measured every other year only, a correction was made for trees being recruited between successive censuses by attributing their appearance date to the middle of the census interval. Hence the growth period of a tree recruited within a two-year interval was considered equal to one year. Similarly, dead trees were systematically considered to have died at the census interval midpoint. AGWNPP contribution of trees dying within an interval was estimated by considering they had a growth rate equal to the surviving trees' AGB (or BA) growth rate. Accounting for the growth of trees between their last census and estimated death date amounted to an increase in estimated AGWNPP of less than 0.9%.

Ground inventory data showed that over the six years from 2013 to 2019, the AGWNPP decreased both in control and logged over plots (Figure 23).

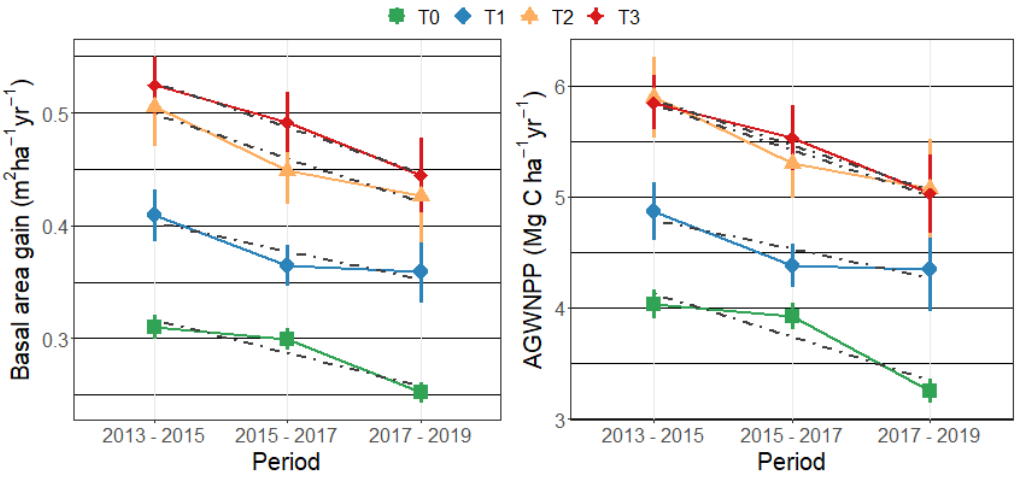

Figure 23. Mean AGWNPP over the six years for plots of 1.56 ha. The dotted line shows the trend as a simple linear regression. The vertical bars represent +/- the standard error of the plot mean.

12.2.4. Airborne LiDAR data

The airborne laser scanning data was collected by a private company Altoa (<http://www.altoa.org>). Acquisition characteristics have changed over time: type of sensor, flight line height and final pulse density (Table 10).

Table 10. Characteristics of LiDAR acquisitions for the different overflights.

Acquisition time	September 2013	October 2015	November 2019
Sensor model	LMS-Q560 RIEGL	LMS-Q780 RIEGL	LMS-Q780 RIEGL
Laser beam divergence (mrad)	≤ 0.5	≤ 0.25	≤ 0.25
Average point density (pulses m^{-2})	12	12 (25*)	12 (27*)
Maximum scan angle	20°	20°	20°
Average flying altitude (m)	450	800	800
Mean footprint size (cm)	22.5	20	20

*Initial pulse density (before thinning)

12.2.5. LiDAR data processing and uncertainty analysis

Our objective was to predict the positive component of forest change in woody biomass (or basal area) from repeat LiDAR overflights, as opposed to the net change in standing biomass or stocking. Therefore, we focused on positive height increments (gains) alone. Gains were annualized to allow comparison between periods of different lengths. We did not standardize height gain by area of observation to avoid introducing a bias with different lengths of period of observation. Indeed, for any given forested area and monitoring period, some parts of the canopy will show an increase in height while other parts will be affected by a decrease in height due to tree or branch fall. The balance between both movements (low intensity, continuous

diffuse growth vs. occasional localized gap creations) will depend on the time interval between successive LiDAR campaigns. The longer the period, the smaller the area not affected by gaps. For instance, by applying the gap definition suggested in (Leitold et al., 2018), i.e., areas affected by a drop in canopy height of at least 3m in amplitude and 4m^2 in extent, we found that gaps affected 2.6%, 5.0% and 7.5% of the total area in 2013-2015, 2015-2019, and 2013-2019 respectively.

We first computed a canopy height model (CHM) from LiDAR data points at each date. CHM was derived using a standard procedure (Vincent et al., 2012b). First, LiDAR points were rasterized at 1 m resolution, taking the maximum height of first returns using the lidR R package (Roussel and Auty, 2020). The same digital terrain model (DTM) based on 2015 overflight was then subtracted from the three canopy surface rasters to produce CHMs. The DTM was obtained by interpolating ground points using Lastools software (version 190927, Rapid Lasso©); the ground points were filtered using TerraScan (Terrasolid ©) software. We chose to use the maximum height per cell (rather than mean height) to minimize the impact of the leaf density variation, which affects penetration and hence mean return height. Maximum height is less sensitive to foliage density, provided that the pulse density is sufficient (Appendix 8). Haphazard patterns of leaf exchange in the hyper-diverse moist tropical forest (Loubry, 1994) may constitute a potentially important source of noise.

To compute the change in canopy height between two dates, we subtracted CHM of date 1 from CHM of date 2. However, change over time in acquisition characteristics may have introduced undesired differences between CHMs computed at different dates. In addition, CHMs will carry some uncertainty due to the sampling nature of LiDAR sensing. This error will depend on various sampling characteristics, particularly the return pulse density (Roussel et al., 2017). Increasing density will asymptotically increase the recorded maximum height. To avoid systematic bias, we resampled all data sets to a standard density of 12 pulses per m^2.

We used the highest density point clouds from 2015 and 2019 to evaluate the uncertainty bearing on height gain. We compared height gain estimates for a range of cell sizes encompassing the field plot sizes (Table 11). Height gains were computed from CHMs derived from point clouds thinned down to 12 pulses per m^2. Thinning was done after randomly splitting the full point cloud into two halves, and the resulting point clouds were used as pseudo-replicates.

Root Mean Squared Deviation between height gains provided an estimate of the uncertainty. This should be considered as a lower bound to the true uncertainty since by randomly subsampling a dense point cloud, we partially preserved the spatial structure of the initial sampling pattern. This is illustrated by the highly significant ($P < 0.001$) Pearson correlation in

pulse count per m^2 across sub-samples (r=0.5 in 2015 r=0.46 in 2019). Therefore, part of the errors induced by the initially imbalanced local pulse density between dates will be common to both sub-samples and remain undetected.

Table 11. Relative Root Mean Squared Deviation in canopy height gain predictors for different spatial scales estimated from split sub-sampling (period 2015-2019).

Cell size	50m	62.5m	100m	125m	250m
Median positive height gain	3.32%	2.63%	1.66%	1.29%	0.72%
Mean positive height gain	5.61%	4.63%	2.76%	2.22%	1.04%

We considered mean and median canopy height change as candidate predictors of BA increment or AGWNPP. Median height gain was less variable (lower RMSD) than the mean height gain (Table 11) and was therefore preferred.

12.3. Results

12.3.1. Canopy Height gain prediction of AGWNPP and BA increments plots.

Median Canopy Height increase was tightly correlated to AGWNPP and BA increment over the 2013-2019 period (Table 12). Model performance improved with larger plot size: multiplying the plot area by four typically reduced RMSE by slightly less than 2 (Table 12).

Table 12. Adjusted R-squared (R^2), root mean square error (RMSE) and relative root mean square error (rRMSE), calculated as the ratio of RMSE over the mean of the values of the dependent variable, fit statistics of the linear regression between the median canopy height increase versus AGWNPP and Basal Area increment per plot between 2013 - 2019. RMSE is expressed in the following units: (AGWNPP) $Mg.ha^{-1}.yr^{-1}$, (BA) $m^2.ha^{-1}.yr^{-1}$

	62.5 x 62.5 m			**125 x 125 m**			**250 x 250 m**		
	R^2	**RMSE**	**rRMSE**	**R^2**	**RMSE**	**rRMSE**	**R^2**	**RMSE**	**rRMSE**
AGWNPP	0.48	0.85	20.0%	0.75	0.48	11.2%	0.90	0.27	6.4%
BA increment	0.63	0.07	19.6%	0.85	0.01	11.0%	0.93	0.02	6.7%

The model parameters (slope and intercept) were unchanged when the spatial resolution was increased from 250 m to 125 m. However, for 62.5m plots, the estimated slope was about 12% lower than 250 m (Table 13 and Figure 24).

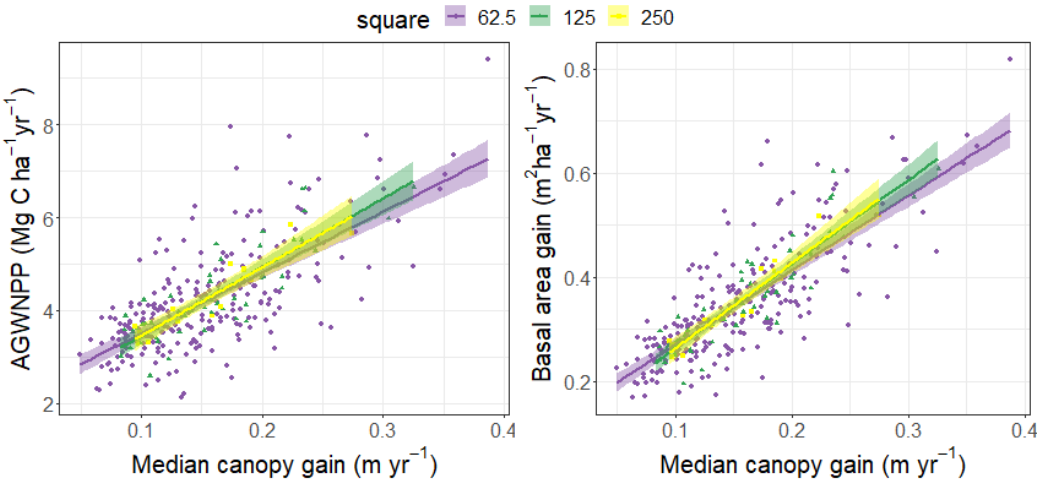

Figure 24. AGWNPP (Left) and BA gain (Right) regression for the different plot sizes (0.39, 1.56 and 6.25 ha) over the period 2013 -2019. The solid lines correspond to the regression line, and the filling shows the confidence interval.

Table 13. Effect of spatial resolution on intercept and slope model parameters for the 2013-2019 analysis period. The estimated value of interception and slope. The 95% confidence interval is presented between parentheses; the intervals were calculated using the bias-corrected and accelerated (BCa) bootstrap percentile method based on 1000 replications.

	62.5 x 62.5 m		**125 x 125 m**		**250 x 250 m**	
	Slope	Intercept	Slope	Intercept	Slope	Intercept
AGWNPP	12.74 [10.94:14.81]	1.89 [1.54:2.20]	15.02 [12.54:17.67]	1.51 [1.07:1.90]	14.88 [12.22:18.65]	1.54 [0.92:2.01]
BA	1.41 [1.26:1.56]	0.09 [0.07:0.12]	1.64 [1.47:1.87]	0.05 [0.01:0.08]	1.65 [1.44:2.02]	0.05 [-0.01:0.09]

A common model relating median canopy height gain to BA increment or AGWNPP seemed appropriate for all stand types (silvicultural treatments and control plots), as shown in Figure 25. ANCOVA conducted for 125x125m plots detected no interaction with stand type for AGWNPP (P=0.19) or BA (P=0.16). We tested for spatial correlation in the residuals between neighboring 125 m subplots within larger plots using Moran statistics using the SDEP package in R (Bivand et al., 2008) and found none (BA: P=0.35 AGWNPP, P=0.16). We also successfully tested the normality of the residuals using the Shapiro-Wilk statistics.

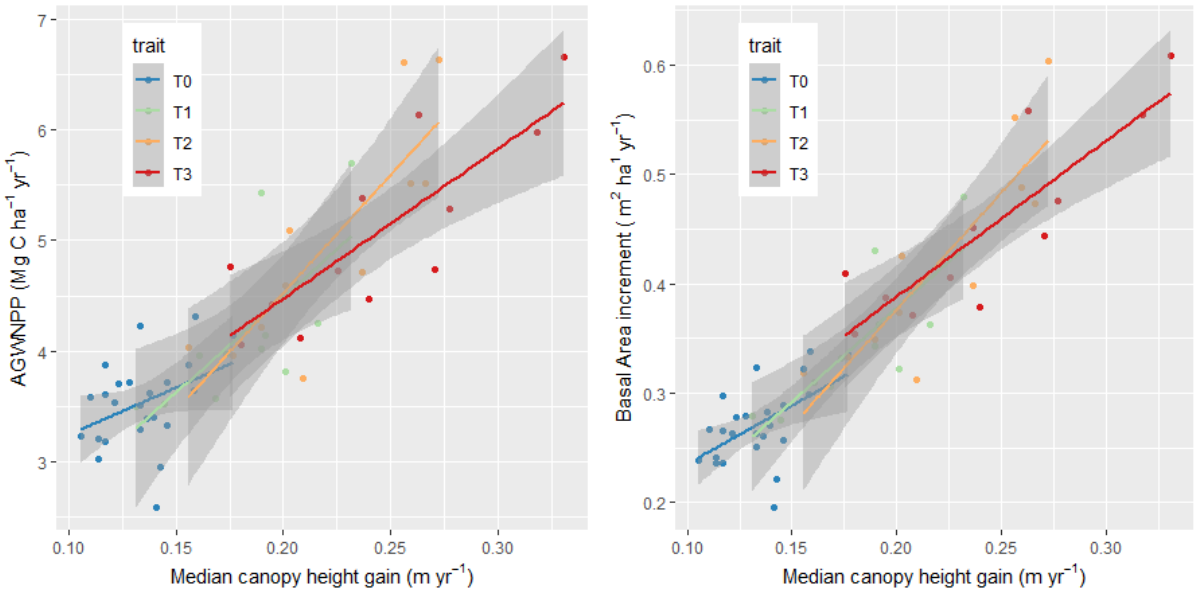

Figure 25 Left - AGWNPP regression model. Right – Basal area model for the period 2013 -2019. Each point represents one 125 x 125 m plot. Different forest types are color-coded (T0: undisturbed forests, T1 to T3: logged over plots ordered by increasing disturbance). The solid lines correspond to the regression line and 0.95 confidence interval in shaded tones.

12.3.2. Stability of predictions over time

Regression slopes for both response variables (BA gain and AGWNPP) varied little between the different periods considered. Intercepts differences were larger than slopes both for AGWNPP and BA (Table 14 and Figure 26) but did not appear to be statistically significant (Table 14).

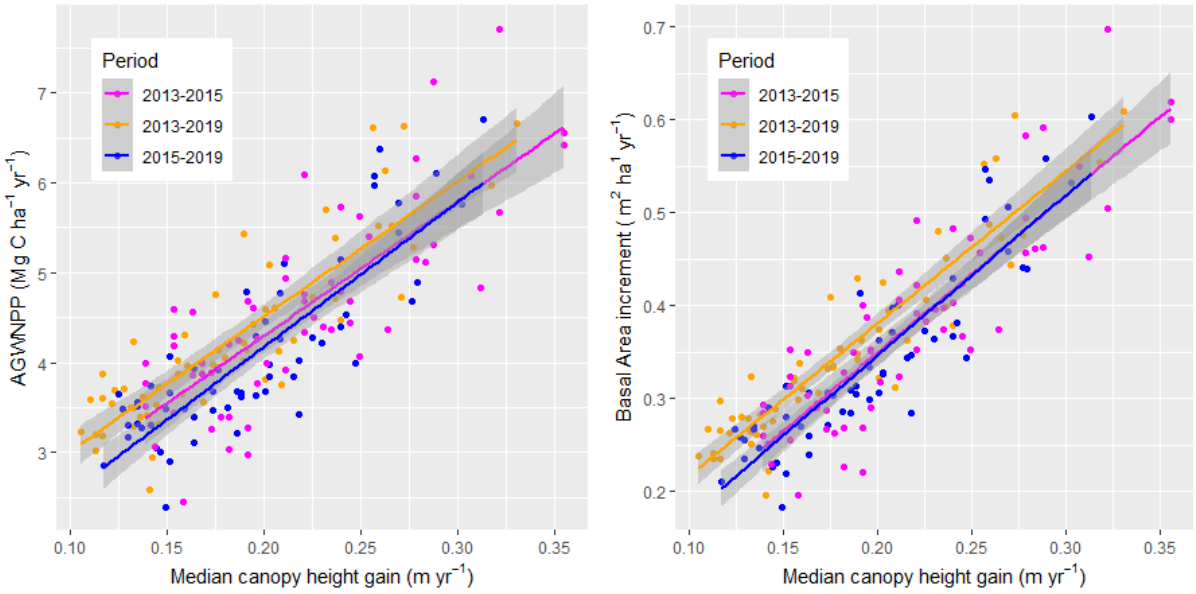

Figure 26 Linear regression of canopy height gain and AGWNPP (Left) or Basal area gain (Right) for different time intervals (color-coded). Each point represents one 125 x 125 m plot.

The intercept was systematically more significant (in relative terms) for AGWNPP than for BA increment. For instance, it was around 30% and 10% of the mean for the 2013-2019 period. This might reflect the non-linear relation between BA increments and AGWNPP. Indeed, higher increments were associated with a lower wood density at the plot level, as shown by the strong negative correlation between AGWNPP and the 2019 community weighted mean wood density (r=-0.82, P <0.001, n=59, 1.56 ha plots).

Table 14. Impact of period length on the prediction of AGWNPP and BA increase (T0, T1, T2, T3) Estimated intercept and slope value. A 95% confidence interval is given in brackets; the intervals are calculated using the bias-corrected and accelerated bootstrap percentile (BCa) based on 1000 replications.

	2013-2015		**2015-2019**		**2013-2019**	
	Slope	Intercept	Slope	Intercept	Slope	Intercept
AGWNPP	14.98 [12.12:18.58]	1.30 [0.54:1.91]	16.12 [13.39:19.19]	0.95 [0.38:1.46]	15.02 [12.64:17.58]	1.51 [1.09:1.92]
BA	1.69 [1.46:2.01]	0.01 [-0.06:0.06]	1.73 [1.47:1.94]	0.00 [-0.04:0.05]	1.64 [1.45:1.85]	0.05 [0.02:0.08]

12.3.3. Median canopy height gain at the landscape level.

Figure 27 shows a side-by-side view of Canopy height gain and the Topographic Wetness Index (TWI). TWI is derived from the terrain model; it is an index widely used in hydrology studies to describe a cell's tendency to accumulate water (Mattivi et al., 2019). This study used the tool r.topidx present in GRASS GIS 7.8.2 software. We computed TWI and Median canopy height gain at the common resolution of 60m.

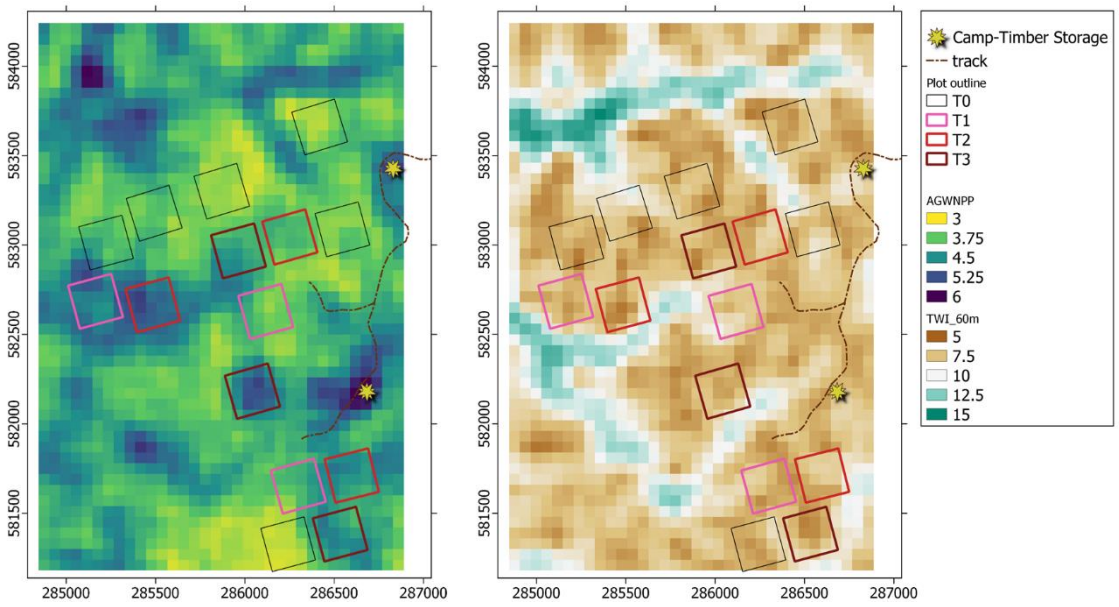

Figure 27 Left: AGWNPP (Mg C.ha^{-1}.yr^{-1}) prediction map calculated from the canopy gain map from 2015 to 2019 at the grid cell size of 60m; the shapefile of the plots is overlaid with the treatment label. Right: TWI for a resolution of 60 m. The two maps were smoothed with a 3x3 kernel–centered mean filter

When the canopy height gain indicator is used, patterns of higher intensity in severely logged plots are observed (Figure 27 left). Also visible, especially in the northern zone, is the close coincidence between patterns produced by valley bottoms (high TWI). The landscape-scale Pearson correlation between TWI and Median canopy height gain was calculated after excluding disturbed areas (logged over plots and tracks) at a grid cell size of 60 m (n=1641) and was equal to 0.56. A torus translation test (Harms et al., 2001) was used to confirm the significance of the association (P<0.001). Along the track, yellow cross symbols mark areas of high growth intensity corresponding to a former timber storage area (south) and the campground (north). Figure 28 shows the mean canopy height gain distribution in various forest classes from canopy dynamics. It confirms that growth intensity increased with silvicultural treatment intensity, while control plots appeared significantly less productive for both analysis periods (2013-2015 and 2015-2019). We also observed that the control plots (T0) significantly statistically grew less (18% on mean) than the undisturbed forest outside of plots (Other). This may reflect the "majestic forest bias," i.e., permanent plots could have been located to avoid large tracts of seasonally flooded areas. The decline in productivity recorded at the plot level (Figure 23) is also found at the level of the entire forest landscape. A similar pattern was observed in the case of BA.

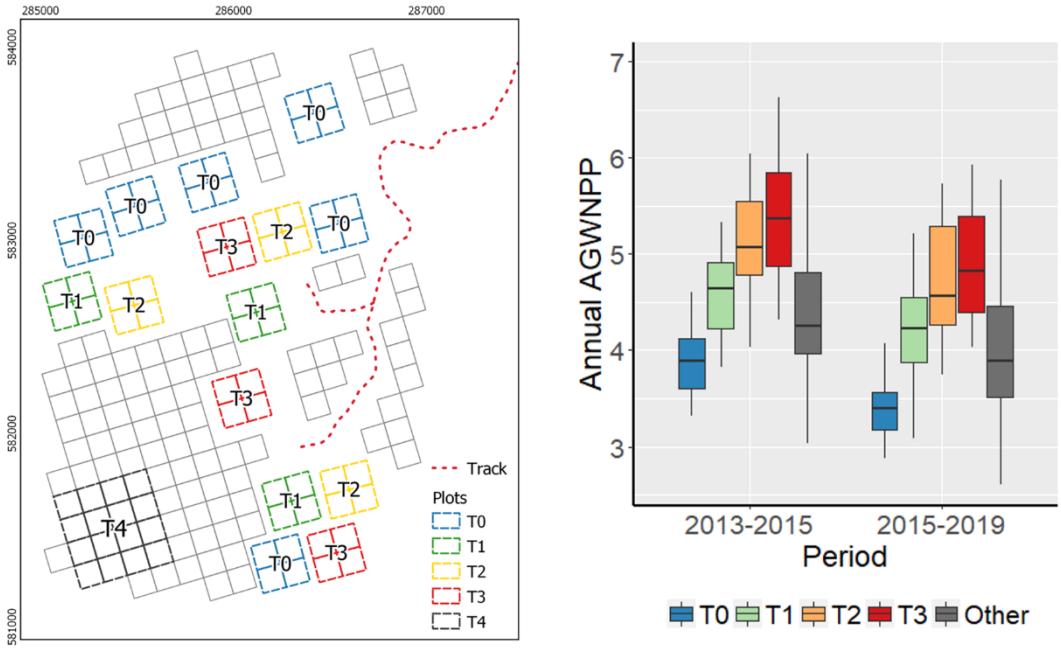

Figure 28 Left: the map with the representation of the landscape grid of 125x125m cells. Right: the boxplots of the median canopy gain for the years 2013 - 2019 per cell. The control and treatment plots are in different colors and the landscape areas outside the T0-T3 plots are gray. Right: boxplot showing the general decrease in AGWNPP over time.

12.4. Discussion

12.4.1. Choice of indicator

While much work has been devoted to predicting AGB from single-pass LiDAR, detecting growth patterns from repeat LiDAR overflights has received less attention. Our objective was not to derive stock changes from estimates at two successive dates, as previously attempted (Dalponte et al., 2019; Réjou-Méchain et al., 2015; Zhao et al., 2018). Instead, our prime interest was to develop a reliable and straightforward Above Ground Woody NPP indicator in tropical forests applicable at the landscape scale. A few studies have addressed monitoring growth (and mortality) at the individual tree scale using Airborne LiDAR (Duncanson and Dubayah, 2018; Zhao et al., 2018). However, the individual tree approach still faces the substantial limitation of not recovering reliable information for the entire population of stems in a stand, which is particularly challenging in dense multi-story vegetation (Aubry-Kientz et al., 2021).

Canopy Height Model at each date was computed from a point cloud down sampled to the minimum pulse density data in our time series to avoid systematic bias in height change estimate. Thinning is akin to discarding information and may be particularly ineffective if sampling is strongly unbalanced. For any given study, choosing the different types of error to favor may have to be pondered against the objective considered. If spatially contrasting the canopy height gain in a particular site is the primary purpose, then degrading the higher density data set may prove counter-effective, as it will only blur the spatial pattern of interest. If comparing periods (or different campaigns in different areas) is the primary purpose, then data sets standardized in terms of sampling intensity should probably be preferred to avoid bias in height differences. We do not recommend using CHM based on mean first return height (instead of maximum return height) because of its sensitivity to changes in foliage density (Appendix 8).

12.4.2. Model accuracy and performance

Despite the wide range of structure and dynamics encountered at our study site and potential uncertainties affecting the dependent variables, remarkably accurate predictions of cumulative AGWNPP and BA ingrowth were achieved (up to 0.90-0.93 R^2 and less than 7% RSME at 6.25 ha plot for a six-year observation period: Table 12).

The simple linear regression model was consistent across plot sizes. The smallest plots (62.5 x 62.5 m) showed a slightly lower slope and higher intercept. This probably reflects a regression dilution bias (Frost and Thompson, 2000). While the true uncertainty bearing on the predictor remains unknown, there is no doubt that the canopy height change estimate in small

plots was less reliable than in larger plots (Table 11). Not surprisingly, models goodness of fit increased with a coarser resolution. An increase in sampling variance was largely responsible for the decrease in the goodness of fit between LiDAR and ground data observed on smaller plots. When the plot area was increased by a factor of 16, the RMSE was divided by a factor of about 3 (Table 12 and Figure 24). This reduction in RMSE was less than the decrease in the standard error of the mean expected by increasing the sample size by a factor of 16, which would be 4 ($sqrt(16)$). Since no spatial correlation was detected at 125x125m (which could have explained a lower than expected decrease in error while aggregating subplots), it is likely that the observed pattern indicated the presence of a systematic error component (bias) in the model. Similarly, when comparing different observation periods, we found that the regression model had to be adjusted (Figure 26). This could be a consequence of the few months a single census of such a large plot network will take to be completed. The necessarily lengthy ground census will never exactly match LiDAR acquisition dates. Hence, while the predictive power model is high, it appears that calibration per period (and to a lesser extent per prediction resolution) is preferable.

Recalibration of the model for each LiDAR new overflight may anyway prove necessary in case of change in LiDAR data characteristics. While pulse density can be homogenized, other characteristics may differ and introduce more discrepancies that are challenging to address. These include a difference in laser footprint size and laser penetration (Gaveau and Hill, 2003) or spatial sampling evenness. The accuracy of LiDAR point clouds alignment, especially between different dates, may also prove limiting. Achieving a fine co-alignment of strips in a dense forest where matching surfaces/common objects are often missing remains a delicate step unless simultaneous photography is available (Bretar et al., 2004).

12.4.3. General decrease in AGWNPP during 2013-2019

The forest stands studied here covered a wide range of structures and dynamics resulting from environmental heterogeneity and different past disturbance levels (see Figure 22). All stands (logged over plots and control plots) shared the same decreasing trend (Figure 23). A decrease in AGWNPP of logged plots c. 24-30 years after silvicultural operations was expected. Logging has released resources (space, nutrients, and water), and the ensuing reduced competition initially favored forest growth. Competition gradually increased following forest regrowth, thereby reducing the forest growth rate. The decrease observed in the unlogged forest cannot be explained in the same way. However, the reduction in AGWNPP of control plots is mirrored by a slow and steady decrease in stem density (Figure 23), a thinning process expected in a transition to mature forest. The observed plateau in AGWNPP may be a turning point and shortly be followed by a decrease in AGB stocks. How representative of the larger forested

area were the control plots? The landscape analysis (Figure 27) suggests that the level of AGWNPP observed in plots may not represent the landscape level (which was about 18% higher, but see 7.16 below). Nonetheless, the decreasing trend in AGWNPP was consistent between control plots and the rest of the undisturbed forested areas at the site.

Our observations are in line with earlier findings reported in (Brienen et al., 2015). The latter study analyzed an extensive network of permanent plots over the Amazon (including the control plots of the present study in preceding years) and found that growth rates had been declining steadily over the 1990-2010 period while mortality kept increasing, leading to a substantial decrease in net biomass increase (C sink force) of the Amazon Forest.

Wall-to-wall mapping of the net primary productivity at landscape to regional scale provides an opportunity to pin down the drivers of the observed patterns of primary productivity. Indeed, landscape-scale maps of AGWNPP provide estimates of C influx over larger areas than ever before and open a new avenue for exploring causes of spatial variation in tropical forest growth. Correlation with environmental factors (temperature, precipitation, soil type, topography, etc.) may help identify drivers controlling the AGWNPP. Multi-temporal LiDAR also allows monitoring forest recovery following logging/clear-cutting and possibly identifying sites' lower/higher recovery rates. Ecological processes underpinning the reported contrasting recovery rates in the tropics remain unclear (Chave et al., 2020). Once such differences between sites have been established and characterized, they can more effectively be related to environmental factors and structural and functional composition contrasts.

This study also revealed a strong negative correlation between community weighted mean wood density and mean canopy height gain at 1.56 ha plot size (r=-0.82). Several studies have reported the dependency between wood density and forest dynamics. At the individual tree level (Chao et al., 2008), wood density was a good predictor of mortality risk in Amazon forests. At stand level (Nascimento et al., 2005) reported that wood density was negatively associated with mortality, recruitment, and growth rates in Amazon forests, a result found by (Osunkoya et al., 2007) in Borneo. Spatial variation in wood density remains a significant source of uncertainty in forest carbon mapping (Réjou-Méchain et al., 2019). The strong relationship between canopy dynamics and community weighted wood density should improve AGB stock estimates from LiDAR overflights by resolving the spatial variation in wood density.

12.4.4. Source of the spatial bias detected in model prediction

Our map (Figure 27) showed a coincident pattern between TWI and AGWNPP. The likelihood of this positive relation was supported by statistical tests. The inferred landscape-scale pattern revealing increased productivity in areas of high waterlogging frequency is however in contradiction with observations made at the plot level reported in (Ferry et al., 2010). They

found that bottomland and downslopes areas were 10% less productive than hilltops and upper slopes. Despite their high turnover rate, the productivity of bottomlands was lower (Table 15) due to the combination of three factors that compensated for this strong dynamic: lower stem density, lower average wood density and less slender trees. We did not use a specific allometric equation for bottomlands in the present study (although results from the previous chapter strongly support the assumption that differences in allometry should be taken into account). We did not find a significant difference in productivity at the plot level between hydromorphological classes in undisturbed forests (Table 15). A lower stem density (Appendix 3 or Vincent et al. (2010)) and a lower community weighted mean wood density (Appendix 6) counterbalanced the higher dynamics in the bottomlands (Table 15). In case a specific H-DBH allometric model was considered for bottomlands, such as in Ferry et al. (2010), bottomlands appeared to be less productive than undisturbed forests. Both analyses point towards a spatial bias affecting the final productivity map derived from ALS.

Table 15. Total annualized AGWNPP by habitat unit and forest type, calculated using 2013-2019 data.

Habitat	AGWNPP ($Mg\ C.ha^{-1}.yr^{-1}$)			
	SUF (T0)	**T1**	**T2**	**T3**
Bottomland	3.87	3.93	4.06	4.58
Downslope	3.59	5.29	4.39	5.42
Slope	3.80	4.51	5.16	5.29
Hilltop	3.97	4.32	5.39	6.11

Potential sources of errors are now reviewed, and possible improvements are suggested for future work. Possible model misspecification can be traced back to three shortcomings: missing covariate, improper spatial unit definition, and inadequate LiDAR metric).

Figure 25 and the associated analysis of covariance led us to conclude that a single common model relating AGWNPP, and canopy height gain would be valid at 125mx125m irrespective of forest past disturbance intensity. However, we did not examine whether the model may need to be adapted to bottomlands or more generally, to the prevailing local drainage regime. Bottomlands have higher turnover rates and lower AGB stocks (see Chapter 2). Due to their high canopy turnover rates, the canopy height gain is important, and this is picked up by repeat ALS. However, the lower biomass per unit area will downplay this effect on productivity. Our model failed to capture the pattern specific to bottomlands constituted by high canopy dynamics and moderate productivity because of the specific spatial arrangement of the

drainage pattern. Plots are crisscrossed by a network of narrow gullies, which intersected many 62.5x62.5 m subplots but to a variable extent. Therefore, any specific relation between canopy height gain and net woody primary productivity remained undetected given our experimental design. Another limitation of our model may come from the LiDAR-derived metric used to capture canopy height gain and used as a proxy for productivity. The LiDAR metric used (Median positive height gain hereafter MPHG) was used without normalization by area of observation to allow comparison of periods of different lengths. This implicitly assumed that" height growth intensity" would reflect productivity irrespective of forest structure or imbalance between growth and mortality. The metric might be improved in a heterogeneous landscape by weighting MPHG value by the relative area of the growing canopy (MPHG * growing area/observation area). This would amount to equating AGWNPP with the gross increase in canopy volume per observation area. Alternatively, the "potential area" of growth might be considered for normalizing MPHG. This normalizing factor would be computed as the proportion of area not affected by gaps, i.e., MPHG * (1-GapDynamicIndex). This would capture the difference between dynamic canopies in bottomlands (where gaps are frequent) and dynamic canopies in plots recovering from past disturbances where gaps are rare (Chapter 1). Training data might have been stratified by drainage class to detect this shortcoming. There is, however, a chance that this would not work well given the limited spatial extent and low compactness of those hydromorphological classes within the permanent sample plots. As shown in Figure 27, large flat bottomlands exist in the landscape, but they were carefully avoided when delineating the permanent sample plots and are not present in the training data. The noise level in the canopy height gain at the 62.5m subplot resolution was sufficient to create a dilution bias in the regression model (Figure 24). By dissecting training samples into contorted shapes with a high border-to-area ratio, the noise level is likely to increase significantly, and the model's accuracy may degrade further. Another option would therefore be to use the local drainage information as an additional predictor in a multiple regression approach where productivity would explicitly depend on TWI and Median Positive Height Gain.

There may also be no robust direct approach to AGWNPP mapping from repeat ALS. It might be necessary to uncouple the estimation of AGB and estimation of canopy dynamics to map AGWNPP better. Estimation of AGB from LiDAR coverage will also suffer from potential sampling biases such as those discussed in the previous paragraph. However, LiDAR metrics observed at one point in time will be more accurate than estimates of canopy height change. Hence the lower noise in the predictors may render a stratification approach by drainage class effective for AGB prediction even if it is not for AGWNPP.

12.5. Conclusions

The median positive change in canopy height calculated from repeated LiDAR data after regularizing pulse density between dates was used to predict AGWNPP in linear regression. Predictions of basal area increment and AGWNPP at the plot level were consistent over a wide range of spatial resolutions (from 0.39 to 6.25 ha). Model prediction accuracy increased with lower spatial resolution.

Plot-level AGWNPP calculations demonstrated a decreasing trend over time, consistent with the declining C sink strength of the Amazon previously reported.

A straightforward and robust approach to mapping AGWNPP from multi-temporal ALS coverage may not exist. Decoupling the AGB estimate on the one hand and the canopy dynamics on the other may provide a more effective way of investigating drivers of forest C flows than a direct mapping of C influx and efflux.

In any case, the drainage regime that affects both C stocks and flow rates should be considered an explicit predictor in the models, taking advantage of the fact that it is readily accessible from ALS data.

Finally, the strong negative correlation which was found to exist between plot-level mean wood density and median canopy height increase indicates that multitemporal LiDAR can help reduce uncertainty in LiDAR-derived AGB at a large scale by providing maps of community weighted mean wood density. Somewhat unexpectedly, LiDAR can provide information on wood density which remains a major source of uncertainty in spatial C maps.

Acknowledgments

We gratefully acknowledge funding by "Investissement d'Avenir" programs managed by Agence Nationale de la Recherche [CEBA, ref. ANR-10-LABX-25-01] and a BGF grant from the French Ministry of Ecology (MEDDE) support the DynForDiv project. In addition, Claudia Huertas was supported by a « Make Our Planet Great Again - MOPGA » program doctoral grant co-funded by IRD (the French research Institute for sustainable Development). We are also grateful to David Coomes for sharing the 2019 LiDAR data funded by NERC grant [NE/S010750/1] and to the Centre National d'Etudes Spatiales for co-financing the 2015 LiDAR campaign.

Author Contributions

CH and GV conceived the study and wrote up the article. CH, GV and DS analyzed the data. GD participated in managing and providing plot-network inventory data. RP and GD provided critical feedback and helped shape the analyses and the manuscript.

Data sharing

Canopy Height Models (2013, 2015, 2019), Digital Terrain Model (2015) and BA and AGB increment data per 62.5m subplots are available for download from the following repository (https://dataverse.ird.fr/) [to be uploaded after paper acceptance].

13. Synthesis and perspectives

13.1. Synthesis

Overall, the results and analyses we present throughout the document constitute a solid demonstration that repeated ALS can play an essential role in monitoring changes in forest carbon stock and flux estimates. We highlight the importance of research, implementation and monitoring at sites such as Paracou, which are valuable both because of the diverse tropical forest landscape, showing different topographic units, vegetation structures and disturbance history, as well as the quality and quantity of its datasets which classify it as a supersite (NASA, 2020), Our first chapter **(Q1. Efflux Modeling - Mortality),** led us to examine the potential of repeated ALS to map changes in forest structure over large areas to detect landscape-level mortality patterns. A measure of canopy gap dynamics (GDI) was derived from Canopy Height Models from successive dates (2009, 2015 and 2019). It was compared to measured mortality rates (expressed in the number of stems and basal area loss) from forest inventories (74 permanent plots of 1.56 ha) in undisturbed and logged forests. We demonstrate that repeated ALS overflights can effectively map possible variations in mortality rates, especially the rate of absolute basal area loss (R^2=0.60), which is better predicted when the analysis is restricted to the unlogged forest (R^2=0.72). These spatial patterns were related to local topography and canopy height (higher canopy forest at the site was more dynamic), demonstrating that mapping patterns of gap dynamics can help reveal environmental drivers of variability in forest demographic rates. However, a meaningful comparison of gap dynamics over time and space will require consistency in ALS acquisition characteristics. We recommend being cautious in the interpretation of canopy gap statistics in a landscape that includes mature stands recovering from recent disturbances with accelerated demographic rates. Indeed, we observed that in previously logged plots, intense self-thinning of smaller stems did not translate into detectable gaps, resulting in an underprediction of stem mortality from ALS, especially in those forests severely disturbed 30 years earlier.

In the second chapter **(Q2. Allometry and carbon stock)**, we aimed to establish the efficacy of fusing field inventories and ALS-derived canopy height models to fit local allometries (H-DBH) and improve the accuracy of individual tree height and AGB estimation. We considered two approaches. The first one relied on individual crown segmentation and manual stem-crown matching and field checking. The second one used automatic stem-crown matching without prior crown segmentation or field checking. Tree height was then modeled using Bayesian multilevel modeling. We first considered a single allometry for the entire site, then an allometry that included canopy height in a local neighborhood (LHC) or species identity as a co-variate, and finally, a full model combining both. We observed that the quadratic error in the prediction of mean height and AGB at the plot level was significantly reduced using the site-specific

allometries compared to the use of a pantropical allometry. About half of the quadratic error reduction was due to bias correction, not decreasing with sample size. The best Bayesian multilevel model (lowest WAIC) included LHC and species identity as covariates. The two approaches yielded similar AGB predictions, which were 12-13% superior to those obtained with a pantropical model.

Furthermore, the inclusion of species identity and LHC resolved the bias in height that occurred across forest types (Tall, short forest or different treatment intensities) and different types of hydromorphological units (habitats). We consider that to increase the robustness of the local models, and it is, however, necessary to include small DBH trees in the calibration data; the airborne LiDAR shows some limitations for the observation of these diametric classes, limitations that we observed previously in the mortality chapter (Chapter 1). The allometry calibration data can be enriched by considering TLS as an alternative.

The study on AGWNPP prediction from multitemporal ALS (**Q3 Influx productivity**) proved very insightful. The model developed to predict productivity from repeated ALS data was applied at the landscape scale, revealing a positive correlation between the Topographic Wetness index and AGWNPP. Plot level analysis showed that this relation at the site is expected to be either absent or moderately negative (depending on the allometric model considered). The reasons for such a spatial bias were analyzed and traced back to a disputable choice of the LiDAR metric (which did not effectively discriminate between different types of canopy dynamics) and not including the local drainage regime as a predictor in the model. Bottomlands (frequently waterlogged during the wet season) are underrepresented in permanent sample plots at the site and their specificity was overlooked when designing the model.

This analysis confirmed the strong negative correlation between plot-level mean wood density and median canopy height increase previously reported in multiple site analysis using a different LiDAR statistic (Sabatier et al., 2017). This indicates that multitemporal LiDAR can help reduce uncertainty in LiDAR-derived AGB at a large scale by providing maps of community weighted mean wood density, the lack of which remains a source of considerable uncertainty in remote sensing of AGB (Réjou-Méchain et al., 2019).

13.1.1. Strength of this study

As specified at the beginning of the synthesis, Paracou is a key site in tropical forest ecology studies and global forest carbon monitoring. An extensive ground inventory (118.75 ha) and historical records dating back to the mid 80’s) make it an extremely valuable site for testing/validating remote sensing approaches of carbon mapping. It encompasses a wide

variety of forest structures with plots with different treatment intensity histories, providing the opportunity to test the accuracy and sensitivity of models as a function of the degree of disturbance, a key aspect for establishing the robustness of carbon monitoring studies in degraded forests and secondary forests (Wright, 2010; Yang et al., 2010). Thirty years after logging, the increase in median canopy height (evaluated in Chapter 3) is still about twice as high as in control plots (Figure 25). There are also naturally occurring differences in forest structure and dynamics in the site with two categories of forests according to canopy height, TUF (tall undisturbed forest) and SUF (short undisturbed forest). Their differences are not only in canopy height and height-diameter allometry (Chapter 2) but go beyond that, such as in the distribution and dynamics of diameters (see Figure 7 and Appendix 6), and BA stem loss rates (Chapter 1). Despite the generally flat topography, a dense hydrographic network forms several valleys with a succession of seasonally flooded bottoms and a succession of small hills (elevation between 2 m and 40 m) with often steep slopes and flat tops (Schmitt, 1984) series of hydromorphic units or habitats that we present in the various chapters and which were defined in the studies of (Ferry et al., 2010; Morneau, 2007), proved to be a key factor in both understanding mortality patterns (Chapter 1) and effects on allometry H-DBH (Chapter 2) and decisive for understanding the limitations in productivity analyses (Chapter 3).

A high frequency of ALS data over the last ten years (6 different acquisition dates from 2004 until 2019), plus the support of additional LiDAR campaigns using lighter devices (TLS and UAV) and other remote sensing data (optical and hyperspectral imagery, and radar coverage), make it one of the most documented and suitable sites in the tropics for comparison and inter-calibration of various remote sensing approaches to carbon mapping. The CEOS Land Product Validation subgroup included Paracou among the Land Product Validation (LPV) Supersites from a list of 55 sites worldwide (8 in tropical and subtropical forests and the second along with Mata Seca in Brazil in Amazonia) (NASA, n.d.), whose selection parameters include super characterized sites at the level of forest structure and biogeophysical variables, well-established field measurement protocols, support of airborne LiDAR and/or hyperspectral acquisitions, and active long-term operations. As indicated by the CEOS protocol (NASA, 2020), to meet the objectives of the global change community, these sites are required to have well-tested validation approaches that are transparent and flexible for the generation of biomass products. Our study meets such needs for improved ground C estimates, especially by the new improved allometries (Chapter 2) that will allow improved estimation of carbon stocks and fluxes at the site.

13.1.2. Sources of uncertainty

When matching ground-based data and airborne LiDAR data through time, one must deal with a series of discrepancies. These include the change in LiDAR specifications over time, the continuously changing canopy and the fact that the remote sensing monitoring process is completed almost instantly while the ground monitoring of a large plot network will last for months.

One source of uncertainty affecting multitemporal analysis (Chapter 1 and chapter 3) is the effect of the difference in LiDAR sampling characteristics, such as the variation in aircraft attitude (170 - 800 m), acquisition mode (single or multiple returns), scan angle, flight strip overlaps, pulse repetition rate and unequal/uneven pulse densities between. During the development of this study, some differences (pulse density and scan angle) between the different periods were mitigated as much as possible; it would remain to evaluate the impact of the other characteristics on the temporal comparisons in the indicator calculations. So despite point density and scanning angle normalization, local calibration may be needed when applying any predictive model to a new acquisition (new site or new date) to reduce bias. Different LiDAR metrics (local maximum height - Hmax or local mean first return height – Hmean, for instance) will respond differently to changes in different parameters (e.g., pulse density or footprint size) and this response is likely to depend on local canopy properties such as ruggedness (surface geometry) and vegetation density.

Canopy height constantly changes on multiple time scales. At short time scales, lateral movement of tree canopies due to wind or tree fall (and gap creation) may occur. Slower changes include leaf exchange processes (with many species experiencing yearly transient leaflessness) as well as progressive senescence and death of standing trees. Even slower changes are due to canopy expansion of live trees: vertical growth of trees or the lateral expansion of the canopy. All these changes occur together and may translate into sources of uncertainty that affect the LiDAR indicators. For instance, it was observed (Chapter 1) that the yearly fraction of the canopy affected by gaps will decrease as the time between flights becomes longer. An artifact due to the constant regrowth after gap creation.

Another source of uncertainty is that ground measurements take 4 to 6 months to complete for the whole set of plots in Paracou, while ALS flights take only two hours. Therefore, the observation period inevitably differs between ground and aerial measurements, and this difference varies between periods, this error being more influential in short periods.

13.1.3. Future work

Limitations/recommendations

This work was conducted on a single site. Albeit particularly rich and with exceptional historical depth, replicating the work elsewhere is desirable. Similar studies could be expanded to a few Guyafor permanent sample plot network sites where multiple LiDAR has been collected by the French Forestry Services (ONF) and the labex CEBA (Nouragues site). The work could also be extended into the future to include climatic anomalies related to the ENSO cycle (El Niño Southern Oscillation), in particular, the severe dry season of 1995 in French Guiana or the extremely high precipitation recorded from August 2020 to April 2021 are related respectively to an El Niño or a La Niña episode. Anomalies in the Atlantic Ocean surface temperature at the equator further amplified the record high precipitations of 2021 (see https://meteofrance.gf/fr/actualites/linfluence-du-cycle-el-nino/la-nina-sur-le-climat-guyanais).

Nonetheless, expanding this kind of work will benefit from first establishing clearly what is the focus of such multitemporal studies. Detecting and mapping C raw fluxes (mortality and net primary productivity) can undoubtedly provide insights into how local forests respond to global climate change. However, monitoring stock changes with high accuracy over time may also provide useful information and may be more tractable. A stock monitoring approach could be complemented by specific canopy turnover maps (which will not necessarily distinguish between height increment and height loss components as done in the present work).

Estimating C stocks from LiDAR statistics is potentially easier than directly estimating net changes (and even more so than estimating separate components of change) for various reasons. The first and foremost reason is that single-date models will seamlessly incorporate the inter-campaign variation in LiDAR acquisition specifications and thus will be more robust to such inconsistencies. In addition, the SNR ratio will probably be higher in single date acquisitions as the signal originates from a single measurement (rather than the difference between two measurements each affected by noise). The signal itself (i.e., variation across space of AGB) may be smaller than a signal in temporal change at a very local scale (due to events such as tree fall), but this is also the scale at which noise is highest.

Of course, one may oppose that reducing uncertainty in C fluxes in tropical forests is important for a better understanding of the C cycle globally. Focusing on AGB stocks alone will not provide a complete picture. However, it may be argued that primary net woody productivity is a fairly indirect proxy of net primary productivity as 1/ the majority of above ground carbon influx goes to labile pools (foliage and twigs) rather than to the longer-lived woody component (Clark et al., 2001b) 2/ the carbon directed to the below ground compartment (roots) is ignored. It seems a little naïve to ignore spatial and temporal change occurring on C allocation

(wood/leaves/below-ground) in tropical forest systems in a context of changing climatic drivers. Changes in phenology may occur in response to changes in temperature and evaporative demand, likely affecting the balance between primary and secondary growth (Wagner et al., 2016). Changes in water availability can also affect the aboveground to belowground functional equilibrium. Pursuing an accurate mapping over time and space of Above-ground woody net primary productivity from ALS may be a misplaced effort. In any case, bridging our current knowledge gap regarding the phenology of tropical species will require specific efforts. High-frequency LiDAR can help in this respect and is currently being implemented in the PhenOBS project on the Paracou site (Barbier et al., 2021).

With regard to future studies to be conducted in Paracou, we believe that incorporating large expanses of seasonally flooded bottomlands into the set of plots regularly monitored (i.e., plots measured every year or every other year) would be a meaningful improvement of the current experimental set-up. The latter was historically designed to evaluate the impact of various sylvicultural treatments and therefore avoided waterlogged areas which are difficult to log with machinery and are typically poor in high-valued timber species. Now that Paracou is more and more considered and valued as an observatory of the impact of global change on Amazonian forests, it would probably make sense to consider including such underrepresented habitats into the core design.

While ALS proved capable of monitoring change in forest structure on a large scale, it also showed potential to improve local allometries and plot level AGB estimates significantly. In this respect, ALS would benefit from being used in combination with close-range LiDAR (TLS/ Mobile Laser Scanning (MLS)) operated below the canopy since ALS failed to detect and map lower canopy trees properly. Alternatively, this sampling bias might affect H-DBH allometries calibrated from data incorporating only upper canopy trees.

14. References

Aleixo, I., Norris, D., Hemerik, L., Barbosa, A., Prata, E., Costa, F., Poorter, L., 2019. Amazonian rainforest tree mortality driven by climate and functional traits. Nat. Clim. Change 9, 384–388. https://doi.org/10.1038/s41558-019-0458-0

Alexander, C., Korstjens, A.H., Hill, R.A., 2018. Influence of micro-topography and crown characteristics on tree height estimations in tropical forests based on LiDAR canopy height models. Int. J. Appl. Earth Obs. Geoinformation 65, 105–113. https://doi.org/10.1016/j.jag.2017.10.009

Alexander, C., Korstjens, A.H., Hill, R.A., 2017. Structural attributes of individual trees for identifying homogeneous patches in a tropical rainforest. Int. J. Appl. Earth Obs. Geoinformation 55, 68–72. https://doi.org/10.1016/j.jag.2016.11.004

Allen, C.D., Breshears, D.D., McDowell, N.G., 2015. On underestimation of global vulnerability to tree mortality and forest die-off from hotter drought in the Anthropocene. Ecosphere 6, art129. https://doi.org/10.1890/ES15-00203.1

Allié, E., Pélissier, R., Engel, J., Petronelli, P., Freycon, V., Deblauwe, V., Soucémarianadin, L., Weigel, J., Baraloto, C., 2015. Pervasive Local-Scale Tree-Soil Habitat Association in a Tropical Forest Community. PLOS ONE 10, e0141488. https://doi.org/10.1371/journal.pone.0141488

ALTOA, 2019. Levé topographique LIDAR - Photo Novembre 2019.

ALTOA, 2018. Plaquette de la présentation de la société ALTOA.

ALTOA, 2015. Rapport de mission d'acquisition ALTOA. Levé topographique LIDAR et multispectral – Octobre 2015 Zone d'étude : Paracou. Maitrise d'Ouvrage : Office National des Forêts.

ALTOA, 2013. Rapport de mission d'acquisition ALTOA.Levé topographique LIDAR – Septembre 2013. Zones d'étude : Paracou.

Asner, G.P., Alencar, A., 2010. Drought impacts on the Amazon forest: the remote sensing perspective: Research review. New Phytol. 187, 569–578. https://doi.org/10.1111/j.1469-8137.2010.03310.x

Asner, G.P., Kellner, J.R., Kennedy-Bowdoin, T., Knapp, D.E., Anderson, C., Martin, R.E., 2013. Forest Canopy Gap Distributions in the Southern Peruvian Amazon. PLoS ONE 8, e60875. https://doi.org/10.1371/journal.pone.0060875

Asner, G.P., Mascaro, J., 2014. Mapping tropical forest carbon: Calibrating plot estimates to a simple LiDAR metric. Remote Sens. Environ. 140, 614–624. https://doi.org/10.1016/j.rse.2013.09.023

Asner, G.P., Mascaro, J., Muller-Landau, H.C., Vieilledent, G., Vaudry, R., Rasamoelina, M., Hall, J.S., van Breugel, M., 2012. A universal airborne LiDAR approach for tropical forest carbon mapping. Oecologia 168, 1147–1160. https://doi.org/10.1007/s00442-011-2165-z

Aubry-Kientz, M., Dutrieux, R., Ferraz, A., Saatchi, S., Hamraz, H., Williams, J., Coomes, D., Piboule, A., Vincent, G., 2019. A Comparative Assessment of the Performance of Individual Tree Crowns Delineation Algorithms from ALS Data in Tropical Forests. Remote Sens. 11, 1086. https://doi.org/10.3390/rs11091086

Aubry-Kientz, M., Laybros, A., Weinstein, B., Ball, J., Jackson, T., Coomes, D., Vincent, G., 2021. Multisensor Data Fusion for Improved Segmentation of Individual Tree Crowns in Dense Tropical Forests. IEEE J. Sel. Top. Appl. Earth Obs. Remote Sens. 14, 3927–3936. https://doi.org/10.1109/JSTARS.2021.3069159

Ayrey, E., Hayes, D.J., Fraver, S., Kershaw, J.A., Weiskittel, A.R., 2019. Ecologically-Based Metrics for Assessing Structure in Developing Area-Based, Enhanced Forest Inventories from LiDAR. Can. J. Remote Sens. 45, 88–112. https://doi.org/10.1080/07038992.2019.1612738

Bachman, C.G., 1979. Laser radar systems and techniques.

Baker, T.R., Vicuña Miñano, E., Banda-R, K., Castillo Torres, D., Farfan-Rios, W., Lawson, I.T., Loja Alemán, E., Pallqui Camacho, N., Silman, M.R., Roucoux, K.H., Phillips, O.L., Honorio Coronado, E.N., Monteagudo Mendoza, A., Rojas Gonzáles, R., 2021. From plots to policy: How to ensure long-term forest plot data supports environmental management in intact tropical forest landscapes. PLANTS PEOPLE PLANET 3, 229–237. https://doi.org/10.1002/ppp3.10154

Banin, L., Feldpausch, T.R., Phillips, O.L., Baker, T.R., Lloyd, J., Affum-Baffoe, K., Arets, E.J.M.M., Berry, N.J., Bradford, M., Brienen, R.J.W., Davies, S., Drescher, M., Higuchi, N., Hilbert, D.W., Hladik, A., Iida, Y., Salim, K.A., Kassim, A.R., King, D.A., Lopez-Gonzalez, G., Metcalfe, D., Nilus, R., Peh, K.S.-H., Reitsma, J.M., Sonké, B., Taedoumg, H., Tan, S., White, L., Wöll, H., Lewis, S.L., 2012. What controls tropical forest architecture? Testing environmental, structural and floristic drivers. Glob. Ecol. Biogeogr. 21, 1179–1190. https://doi.org/10.1111/j.1466-8238.2012.00778.x

Barbier, N., Ball, J., Clocher, I., Poilvé, H., Verley, P., Vincent, G., 2021. Sensing Tropical Forest Phenology and Productivity from the Field to the Satellite, in: 2021 IEEE International

Geoscience and Remote Sensing Symposium IGARSS. Presented at the 2021 IEEE International Geoscience and Remote Sensing Symposium IGARSS, pp. 716–719. https://doi.org/10.1109/IGARSS47720.2021.9554372

Barlow, J., França, F., Gardner, T.A., Hicks, C.C., Lennox, G.D., Berenguer, E., Castello, L., Economo, E.P., Ferreira, J., Guénard, B., Gontijo Leal, C., Isaac, V., Lees, A.C., Parr, C.L., Wilson, S.K., Young, P.J., Graham, N.A.J., 2018. The future of hyperdiverse tropical ecosystems. Nature 559, 517–526. https://doi.org/10.1038/s41586-018-0301-1

Barthès, B., 1991. Caractérisation pédologique de parcelles du dispositif “forêt naturelle” du CTFT à Paracou (Sinnamary, Guyane). IRD.

Barthès, B., 1988. Où pousse cet arbre ? : premiers résultats à l’étude des relations sol-végétation en forêt de Paracou (Guyane) : cas du wapa et du gonfolo.

Baumgarten, G., 2010. Doppler Rayleigh/Mie/Raman lidar for wind and temperature measurements in the middle atmosphere up to 80 km. Atmospheric Meas. Tech. 3, 1509–1518. https://doi.org/10.5194/amt-3-1509-2010

Benoist, V., 2009. Étude de la mortalité des arbres en forêt tropicale humide par laser aéroporté.

Bivand, R.S., Pebesma, E.J., Gómez-Rubio, V., 2008. Applied Spatial Data Analysis with R, Use R.

Blanc, L., Echard, M., Herault, B., Bonal, D., Marcon, E., Chave, J., Baraloto, C., 2009. Dynamics of aboveground carbon stocks in a selectively logged tropical forest. Ecol. Appl. 19, 1397–1404. https://doi.org/10.1890/08-1572.1

Bonal, D., Bosc, A., Ponton, S., Goret, J.-Y., Burban, B., Gross, P., Bonnefond, J.-M., Elbers, J., Longdoz, B., Epron, D., Guehl, J.-M., Granier, A., 2008. Impact of severe dry season on net ecosystem exchange in the Neotropical rainforest of French Guiana: HIGHER NEP UNDER SEVERE DROUGHT. Glob. Change Biol. 14, 1917–1933. https://doi.org/10.1111/j.1365-2486.2008.01610.x

Bonan, G.B., 2008. Forests and Climate Change: Forcings, Feedbacks, and the Climate Benefits of Forests. Science 320, 1444–1449. https://doi.org/10.1126/science.1155121

Bossoukpe, M., 2020. Variation de la forme des arbres en fonction de la hauteur de canopée en forêt tropicale humide. Elaboration d’équations allométriques à partir de données lidar. Master Science et technologie de l’Agriculture, de l’alimentation et de l’Environnement (ST2AE) Parcours : Gestion Environnementale des Ecosystèmes et Forêts Tropicales (GEEFT)), France.

Boyd, D.S., Danson, F.M., 2005. Satellite remote sensing of forest resources: three decades of research development. Prog. Phys. Geogr. Earth Environ. 29, 1–26. https://doi.org/10.1191/0309133305pp432ra

Bretar, F., Pierrot-Deseilligny, M., Roux, M., 2004. Solving the strip adjustment problem of 3D airborne lidar data, in: IGARSS 2004. 2004 IEEE International Geoscience and Remote Sensing Symposium. Presented at the IGARSS 2004. 2004 IEEE International Geoscience and Remote Sensing Symposium, pp. 4734–4737 vol.7. https://doi.org/10.1109/IGARSS.2004.1370216

Brienen, R.J.W., Phillips, O.L., Feldpausch, T.R., Gloor, E., Baker, T.R., Lloyd, J., Lopez-Gonzalez, G., Monteagudo-Mendoza, A., Malhi, Y., Lewis, S.L., Vásquez Martinez, R., Alexiades, M., Álvarez Dávila, E., Alvarez-Loayza, P., Andrade, A., Aragão, L.E.O.C., Araujo-Murakami, A., Arets, E.J.M.M., Arroyo, L., Aymard C., G.A., Bánki, O.S., Baraloto, C., Barroso, J., Bonal, D., Boot, R.G.A., Camargo, J.L.C., Castilho, C.V., Chama, V., Chao, K.J., Chave, J., Comiskey, J.A., Cornejo Valverde, F., da Costa, L., de Oliveira, E.A., Di Fiore, A., Erwin, T.L., Fauset, S., Forsthofer, M., Galbraith, D.R., Grahame, E.S., Groot, N., Hérault, B., Higuchi, N., Honorio Coronado, E.N., Keeling, H., Killeen, T.J., Laurance, W.F., Laurance, S., Licona, J., Magnussen, W.E., Marimon, B.S., Marimon-Junior, B.H., Mendoza, C., Neill, D.A., Nogueira, E.M., Núñez, P., Pallqui Camacho, N.C., Parada, A., Pardo-Molina, G., Peacock, J., Peña-Claros, M., Pickavance, G.C., Pitman, N.C.A., Poorter, L., Prieto, A., Quesada, C.A., Ramírez, F., Ramírez-Angulo, H., Restrepo, Z., Roopsind, A., Rudas, A., Salomão, R.P., Schwarz, M., Silva, N., Silva-Espejo, J.E., Silveira, M., Stropp, J., Talbot, J., ter Steege, H., Teran-Aguilar, J., Terborgh, J., Thomas-Caesar, R., Toledo, M., Torello-Raventos, M., Umetsu, R.K., van der Heijden, G.M.F., van der Hout, P., Guimarães Vieira, I.C., Vieira, S.A., Vilanova, E., Vos, V.A., Zagt, R.J., 2015. Long-term decline of the Amazon carbon sink. Nature 519, 344–348. https://doi.org/10.1038/nature14283

Brokaw, N.V.L., 1985. Gap-Phase Regeneration in a Tropical Forest. Ecology 66, 682–687. https://doi.org/10.2307/1940529

Bürkner, P.-C., 2017. brms: An R Package for Bayesian Multilevel Models Using Stan. Journal of Statistical Software.

Burt, A., Calders, K., Cuni-Sanchez, A., Gómez-Dans, J., Lewis, P., Lewis, S.L., Malhi, Y., Phillips, O.L., Disney, M., 2020. Assessment of Bias in Pan-Tropical Biomass Predictions. Front. For. Glob. Change 3, 12. https://doi.org/10.3389/ffgc.2020.00012

Bustamante, M.M.C., Roitman, I., Aide, T.M., Alencar, A., Anderson, L.O., Aragão, L., Asner, G.P., Barlow, J., Berenguer, E., Chambers, J., Costa, M.H., Fanin, T., Ferreira, L.G., Ferreira,

J., Keller, M., Magnusson, W.E., Morales-Barquero, L., Morton, D., Ometto, J.P.H.B., Palace, M., Peres, C.A., Silvério, D., Trumbore, S., Vieira, I.C.G., 2016. Toward an integrated monitoring framework to assess the effects of tropical forest degradation and recovery on carbon stocks and biodiversity. Glob. Change Biol. 22, 92–109. https://doi.org/10.1111/gcb.13087

Campbell, M.J., Dennison, P.E., Tune, J.W., Kannenberg, S.A., Kerr, K.L., Codding, B.F., Anderegg, W.R.L., 2020. A multi-sensor, multi-scale approach to mapping tree mortality in woodland ecosystems. Remote Sens. Environ. 245, 111853. https://doi.org/10.1016/j.rse.2020.111853

Cao, L., Coops, N.C., Innes, J.L., Sheppard, S.R.J., Fu, L., Ruan, H., She, G., 2016. Estimation of forest biomass dynamics in subtropical forests using multi-temporal airborne LiDAR data. Remote Sens. Environ. 178, 158–171. https://doi.org/10.1016/j.rse.2016.03.012

Carreiras, J.M.B., Quegan, S., Le Toan, T., Ho Tong Minh, D., Saatchi, S.S., Carvalhais, N., Reichstein, M., Scipal, K., 2017. Coverage of high biomass forests by the ESA BIOMASS mission under defense restrictions. Remote Sens. Environ. 196, 154–162. https://doi.org/10.1016/j.rse.2017.05.003

Chambers, J.Q., Santos, J. dos, Ribeiro, R.J., Higuchi, N., 2001. Tree damage, allometric relationships, and above-ground net primary production in central Amazon forest. For. Ecol. Manag. 152, 73–84. https://doi.org/10.1016/S0378-1127(00)00591-0

Chao, K.-J., Phillips, O.L., Gloor, E., Monteagudo, A., Torres-Lezama, A., Martínez, R.V., 2008. Growth and wood density predict tree mortality in Amazon forests. J. Ecol. 96, 281–292. https://doi.org/10.1111/j.1365-2745.2007.01343.x

Chave, J., Andalo, C., Brown, S., Cairns, M.A., Chambers, J.Q., Eamus, D., Fölster, H., Fromard, F., Higuchi, N., Kira, T., Lescure, J.-P., Nelson, B.W., Ogawa, H., Puig, H., Riéra, B., Yamakura, T., 2005. Tree allometry and improved estimation of carbon stocks and balance in tropical forests. Oecologia 145, 87–99. https://doi.org/10.1007/s00442-005-0100-x

Chave, J., Condit, R., Lao, S., Caspersen, J.P., Foster, R.B., Hubbell, S.P., 2003. Spatial and temporal variation of biomass in a tropical forest: results from a large census plot in Panama. J. Ecol. 91, 240–252. https://doi.org/10.1046/j.1365-2745.2003.00757.x

Chave, J., Coomes, D., Jansen, S., Lewis, S.L., Swenson, N.G., Zanne, A.E., 2009. Towards a worldwide wood economics spectrum. Ecol. Lett. 12, 351–366. https://doi.org/10.1111/j.1461-0248.2009.01285.x

Chave, J., Davies, S.J., Phillips, O.L., Lewis, S.L., Sist, P., Schepaschenko, D., Armston, J., Baker, T.R., Coomes, D., Disney, M., Duncanson, L., Hérault, B., Labrière, N., Meyer, V., Réjou-Méchain, M., Scipal, K., Saatchi, S., 2019. Ground Data are Essential for Biomass Remote Sensing Missions. Surv. Geophys. 40, 863–880. https://doi.org/10.1007/s10712-019-09528-w

Chave, J., Piponiot, C., Maréchaux, I., Foresta, H., Larpin, D., Fischer, F.J., Derroire, G., Vincent, G., Hérault, B., 2020. Slow rate of secondary forest carbon accumulation in the Guianas compared with the rest of the Neotropics. Ecol. Appl. 30. https://doi.org/10.1002/eap.2004

Chave, J., Réjou-Méchain, M., Búrquez, A., Chidumayo, E., Colgan, M.S., Delitti, W.B.C., Duque, A., Eid, T., Fearnside, P.M., Goodman, R.C., Henry, M., Martínez-Yrízar, A., Mugasha, W.A., Muller-Landau, H.C., Mencuccini, M., Nelson, B.W., Ngomanda, A., Nogueira, E.M., Ortiz-Malavassi, E., Pélissier, R., Ploton, P., Ryan, C.M., Saldarriaga, J.G., Vieilledent, G., 2014. Improved allometric models to estimate the aboveground biomass of tropical trees. Glob. Change Biol. 20, 3177–3190. https://doi.org/10.1111/gcb.12629

Chust, G., Galparsoro, I., Borja, Á., Franco, J., Uriarte, A., 2008. Coastal and estuarine habitat mapping, using LIDAR height and intensity and multi-spectral imagery. Estuar. Coast. Shelf Sci. 78, 633–643. https://doi.org/10.1016/j.ecss.2008.02.003

CIRAD, 2016a. Experimental Design / Portal - Paracou research station, a large scale forest disturbance experiment in Amazonia [WWW Document]. URL https://paracou.cirad.fr/website/experimental-design (accessed 6.25.19).

CIRAD, 2016b. Disturbance experiment / Experimental Design - Paracou research station, a large scale forest disturbance experiment in Amazonia [WWW Document]. URL https://paracou.cirad.fr/website/experimental-design/disturbance-experiment (accessed 8.10.20).

Clark, D.A., Brown, S., Kicklighter, D.W., Chambers, J.Q., Thomlinson, J.R., Ni, J., 2001a. MEASURING NET PRIMARY PRODUCTION IN FORESTS: CONCEPTS AND FIELD METHODS. Ecol. Appl. 11, 356–370. https://doi.org/10.1890/1051-0761(2001)011[0356:MNPPIF]2.0.CO;2

Clark, D.A., Brown, S., Kicklighter, D.W., Chambers, J.Q., Thomlinson, J.R., Ni, J., Holland, E.A., 2001b. NET PRIMARY PRODUCTION IN TROPICAL FORESTS: AN EVALUATION AND SYNTHESIS OF EXISTING FIELD DATA. Ecol. Appl. 11, 371–384. https://doi.org/10.1890/1051-0761(2001)011[0371:NPPITF]2.0.CO;2

Cochrane, M.A., Barber, C.P., 2009. Climate change, human land use and future fires in the Amazon. Glob. Change Biol. 15, 601–612. https://doi.org/10.1111/j.1365-2486.2008.01786.x

Colgan, M.S., Asner, G.P., Swemmer, T., 2013. Harvesting tree biomass at the stand level to assess the accuracy of field and airborne biomass estimation in savannas. Ecol. Appl. 23, 1170–1184. https://doi.org/10.1890/12-0922.1

Collis, R.T.H., 1969. LIDAR.

Coomes, D., Disney, M., Burslem, D., Jackson, T., 2019. A 3D perspective on the effects of topography and wind on forest height and dynamics.

Corlett, R.T., 2016. The Impacts of Droughts in Tropical Forests. Trends Plant Sci. 21, 584–593. https://doi.org/10.1016/j.tplants.2016.02.003

Dalagnol, R., Wagner, F.H., Galvão, L.S., Streher, A.S., Phillips, O.L., Gloor, E., Pugh, T.A.M., Ometto, J.P.H.B., Aragão, L.E.O.C., 2021. Large-scale variations in the dynamics of Amazon forest canopy gaps from airborne lidar data and opportunities for tree mortality estimates. Sci. Rep. 11, 1388. https://doi.org/10.1038/s41598-020-80809-w

Dalponte, M., Jucker, T., Liu, S., Frizzera, L., Gianelle, D., 2019. Characterizing forest carbon dynamics using multi-temporal lidar data. Remote Sens. Environ. 224, 412–420. https://doi.org/10.1016/j.rse.2019.02.018

Dassot, M., Constant, T., Fournier, M., 2011. The use of terrestrial LiDAR technology in forest science: application fields, benefits and challenges. Ann. For. Sci. 68, 959–974. https://doi.org/10.1007/s13595-011-0102-2

de Toledo, J.J., Magnusson, W.E., Castilho, C.V., Nascimento, H.E.M., 2011. How much variation in tree mortality is predicted by soil and topography in Central Amazonia? For. Ecol. Manag. 262, 331–338. https://doi.org/10.1016/j.foreco.2011.03.039

Deems, J.S., Painter, T.H., Finnegan, D.C., 2013. Lidar measurement of snow depth: a review. J. Glaciol. 59, 467–479. https://doi.org/10.3189/2013JoG12J154

Detto, M., Muller-Landau, H.C., Mascaro, J., Asner, G.P., 2013. Hydrological Networks and Associated Topographic Variation as Templates for the Spatial Organization of Tropical Forest Vegetation. PLoS ONE 8, e76296. https://doi.org/10.1371/journal.pone.0076296

Di Vittorio, A.V., Negrón-Juárez, R.I., Higuchi, N., Chambers, J.Q., 2014. Tropical forest carbon balance: effects of field- and satellite-based mortality regimes on the dynamics and the spatial structure of Central Amazon forest biomass. Environ. Res. Lett. 9, 034010. https://doi.org/10.1088/1748-9326/9/3/034010

Dubayah, R.O., Sheldon, S.L., Clark, D.B., Hofton, M.A., Blair, J.B., Hurtt, G.C., Chazdon, R.L., 2010. Estimation of tropical forest height and biomass dynamics using lidar remote sensing at La Selva, Costa Rica: FOREST DYNAMICS USING LIDAR. J. Geophys. Res. Biogeosciences 115, n/a-n/a. https://doi.org/10.1029/2009JG000933

Duncanson, L., Armston, J., Disney, M., Avitabile, V., Barbier, N., Calders, K., Carter, S., Chave, J., Herold, M., Crowther, T.W., Falkowski, M., Kellner, J.R., Labrière, N., Lucas, R., MacBean, N., McRoberts, R.E., Meyer, V., Næsset, E., Nickeson, J.E., Paul, K.I., Phillips, O.L., Réjou-Méchain, M., Román, M., Roxburgh, S., Saatchi, S., Schepaschenko, D., Scipal, K., Siqueira, P.R., Whitehurst, A., Williams, M., 2019. The Importance of Consistent Global Forest Aboveground Biomass Product Validation. Surv. Geophys. 40, 979–999. https://doi.org/10.1007/s10712-019-09538-8

Duncanson, L., Armston, J., Disney, M., Avitabile, V., Barbier, N., Calders, K., Carter, S., Chave, J., Herold, M., MacBean, N., Mcroberts, R., Minor, D., Paul, K., Réjou-Méchain, M., Roxburgh, S., Williams, M., Albinet, C., Baker, T., Bartholomeus, H., Margolis, H., 2021. Aboveground Woody Biomass Product Validation Good Practices Protocol. https://doi.org/10.5067/doc/ceoswgcv/lpv/agb.001

Duncanson, L., Dubayah, R., 2018. Monitoring individual tree-based change with airborne lidar. Ecol. Evol. 8, 5079–5089. https://doi.org/10.1002/ece3.4075

Duncanson, L., Kellner, J.R., Armston, J., Dubayah, R., Minor, D.M., Hancock, S., Healey, S.P., Patterson, P.L., Saarela, S., Marselis, S., Silva, C.E., Bruening, J., Goetz, S.J., Tang, H., Hofton, M., Blair, B., Luthcke, S., Fatoyinbo, L., Abernethy, K., Alonso, A., Andersen, H.-E., Aplin, P., Baker, T.R., Barbier, N., Bastin, J.F., Biber, P., Boeckx, P., Bogaert, J., Boschetti, L., Boucher, P.B., Boyd, D.S., Burslem, D.F.R.P., Calvo-Rodriguez, S., Chave, J., Chazdon, R.L., Clark, D.B., Clark, D.A., Cohen, W.B., Coomes, D.A., Corona, P., Cushman, K.C., Cutler, M.E.J., Dalling, J.W., Dalponte, M., Dash, J., de-Miguel, S., Deng, S., Ellis, P.W., Erasmus, B., Fekety, P.A., Fernandez-Landa, A., Ferraz, A., Fischer, R., Fisher, A.G., García-Abril, A., Gobakken, T., Hacker, J.M., Heurich, M., Hill, R.A., Hopkinson, C., Huang, H., Hubbell, S.P., Hudak, A.T., Huth, A., Imbach, B., Jeffery, K.J., Katoh, M., Kearsley, E., Kenfack, D., Kljun, N., Knapp, N., Král, K., Krůček, M., Labrière, N., Lewis, S.L., Longo, M., Lucas, R.M., Main, R., Manzanera, J.A., Martínez, R.V., Mathieu, R., Memiaghe, H., Meyer, V., Mendoza, A.M., Monerris, A., Montesano, P., Morsdorf, F., Næsset, E., Naidoo, L., Nilus, R., O'Brien, M., Orwig, D.A., Papathanassiou, K., Parker, G., Philipson, C., Phillips, O.L., Pisek, J., Poulsen, J.R., Pretzsch, H., Rüdiger, C., Saatchi, S., Sanchez-Azofeifa, A., Sanchez-Lopez, N., Scholes, R., Silva, C.A., Simard, M., Skidmore, A., Stereńczak, K., Tanase, M., Torresan, C., Valbuena, R., Verbeeck, H., Vrska, T., Wessels, K., White, J.C., White, L.J.T., Zahabu, E.,

Zgraggen, C., 2022. Aboveground biomass density models for NASA's Global Ecosystem Dynamics Investigation (GEDI) lidar mission. Remote Sens. Environ. 270, 112845. https://doi.org/10.1016/j.rse.2021.112845

Duncanson, L., Neuenschwander, A., Hancock, S., Thomas, N., Fatoyinbo, T., Simard, M., Silva, C.A., Armston, J., Luthcke, S.B., Hofton, M., Kellner, J.R., Dubayah, R., 2020. Biomass estimation from simulated GEDI, ICESat-2 and NISAR across environmental gradients in Sonoma County, California. Remote Sens. Environ. 242, 111779. https://doi.org/10.1016/j.rse.2020.111779

Epron, D., Bosc, A., Bonal, D., Freycon, V., 2006. Spatial variation of soil respiration across a topographic gradient in a tropical rain forest in French Guiana. J. Trop. Ecol. 22, 565–574. https://doi.org/10.1017/S0266467406003415

Espírito-Santo, F.D.B., Gloor, M., Keller, M., Malhi, Y., Saatchi, S., Nelson, B., Junior, R.C.O., Pereira, C., Lloyd, J., Frolking, S., Palace, M., Shimabukuro, Y.E., Duarte, V., Mendoza, A.M., López-González, G., Baker, T.R., Feldpausch, T.R., Brienen, R.J.W., Asner, G.P., Boyd, D.S., Phillips, O.L., 2015. Size and frequency of natural forest disturbances and the Amazon forest carbon balance. Nat. Commun. 6. https://doi.org/10.1038/ncomms7638

FAO, 2020. The State of the World's Forests 2020. FAO and UNEP. https://doi.org/10.4060/ca8642en

Fatichi, S., Pappas, C., Zscheischler, J., Leuzinger, S., 2019. Modelling carbon sources and sinks in terrestrial vegetation. New Phytol. 221, 652–668. https://doi.org/10.1111/nph.15451

Fayolle, A., Doucet, J.-L., Gillet, J.-F., Bourland, N., Lejeune, P., 2013. Tree allometry in Central Africa: Testing the validity of pantropical multi-species allometric equations for estimating biomass and carbon stocks. For. Ecol. Manag. 305, 29–37. https://doi.org/10.1016/j.foreco.2013.05.036

Feldmann, E., Drößler, L., Hauck, M., Kucbel, S., Pichler, V., Leuschner, C., 2018. Canopy gap dynamics and tree understory release in a virgin beech forest, Slovakian Carpathians. For. Ecol. Manag. 415–416, 38–46. https://doi.org/10.1016/j.foreco.2018.02.022

Feldpausch, T.R., Banin, L., Phillips, O.L., Baker, T.R., Lewis, S.L., Quesada, C.A., Affum-Baffoe, K., Arets, E.J.M.M., Berry, N.J., Bird, M., Brondizio, E.S., de Camargo, P., Chave, J., Djagbletey, G., Domingues, T.F., Drescher, M., Fearnside, P.M., França, M.B., Fyllas, N.M., Lopez-Gonzalez, G., Hladik, A., Higuchi, N., Hunter, M.O., Iida, Y., Salim, K.A., Kassim, A.R., Keller, M., Kemp, J., King, D.A., Lovett, J.C., Marimon, B.S., Marimon-Junior, B.H., Lenza, E., Marshall, A.R., Metcalfe, D.J., Mitchard, E.T.A., Moran, E.F., Nelson, B.W., Nilus, R., Nogueira,

E.M., Palace, M., Patiño, S., Peh, K.S.-H., Raventos, M.T., Reitsma, J.M., Saiz, G., Schrodt, F., Sonké, B., Taedoumg, H.E., Tan, S., White, L., Wöll, H., Lloyd, J., 2011. Height-diameter allometry of tropical forest trees. Biogeosciences 8, 1081–1106. https://doi.org/10.5194/bg-8-1081-2011

Ferry, B., Morneau, F., Bontemps, J.-D., Blanc, L., Freycon, V., 2010. Higher treefall rates on slopes and waterlogged soils result in lower stand biomass and productivity in a tropical rain forest: Treefall and biomass in a tropical rain forest. J. Ecol. 98, 106–116. https://doi.org/10.1111/j.1365-2745.2009.01604.x

Fischer, F.J., Labrière, N., Vincent, G., Hérault, B., Alonso, A., Memiaghe, H., Bissiengou, P., Kenfack, D., Saatchi, S., Chave, J., 2020. A simulation method to infer tree allometry and forest structure from airborne laser scanning and forest inventories. Remote Sens. Environ. 251, 112056. https://doi.org/10.1016/j.rse.2020.112056

Fisher, J.I., Hurtt, G.C., Thomas, R.Q., Chambers, J.Q., 2008. Clustered disturbances lead to bias in large-scale estimates based on forest sample plots. Ecol. Lett. 11, 554–563. https://doi.org/10.1111/j.1461-0248.2008.01169.x

ForestPlots.net, Blundo, C., Carilla, J., Grau, R., Malizia, A., Malizia, L., Osinaga-Acosta, O., Bird, M., Bradford, M., Catchpole, D., Ford, A., Graham, A., Hilbert, D., Kemp, J., Laurance, S., Laurance, W., Ishida, F.Y., Marshall, A., Waite, C., Woell, H., Bastin, J.-F., Bauters, M., Beeckman, H., Boeckx, P., Bogaert, J., De Canniere, C., de Haulleville, T., Doucet, J.-L., Hardy, O., Hubau, W., Kearsley, E., Verbeeck, H., Vleminckx, J., Brewer, S.W., Alarcón, A., Araujo-Murakami, A., Arets, E., Arroyo, L., Chavez, E., Fredericksen, T., Villaroel, R.G., Sibauty, G.G., Killeen, T., Licona, J.C., Lleigue, J., Mendoza, C., Murakami, S., Gutierrez, A.P., Pardo, G., Peña-Claros, M., Poorter, L., Toledo, M., Cayo, J.V., Viscarra, L.J., Vos, V., Ahumada, J., Almeida, E., Almeida, J., de Oliveira, E.A., da Cruz, W.A., de Oliveira, A.A., Carvalho, Fabrício Alvim, Obermuller, F.A., Andrade, A., Carvalho, Fernanda Antunes, Vieira, S.A., Aquino, A.C., Aragão, L., Araújo, A.C., Assis, M.A., Gomes, J.A.M.A., Baccaro, F., de Camargo, P.B., Barni, P., Barroso, J., Bernacci, L.C., Bordin, K., de Medeiros, M.B., Broggio, I., Camargo, J.L., Cardoso, D., Carniello, M.A., Rochelle, A.L.C., Castilho, C., Castro, A.A.J.F., Castro, W., Ribeiro, S.C., Costa, F., de Oliveira, R.C., Coutinho, I., Cunha, J., da Costa, L., da Costa Ferreira, L., da Costa Silva, R., da Graça Zacarias Simbine, M., de Andrade Kamimura, V., de Lima, H.C., de Oliveira Melo, L., de Queiroz, L., de Sousa Lima, J.R., do Espírito Santo, M., Domingues, T., dos Santos Prestes, N.C., Carneiro, S.E.S., Elias, F., Eliseu, G., Emilio, T., Farrapo, C.L., Fernandes, L., Ferreira, G., Ferreira, J., Ferreira, L., Ferreira, S., Simon, M.F., Freitas, M.A., García, Q.S., Manzatto, A.G., Graça, P., Guilherme, F., Hase, E., Higuchi, N., Iguatemy, M., Barbosa, R.I., Jaramillo, M., Joly, C., Klipel, J., do Amaral, I.L., Levis, C.,

Lima, A.S., Dan, M.L., Lopes, A., Madeiros, H., Magnusson, W.E., dos Santos, R.M., Marimon, B., Junior, B.H.M., Grillo, R.M.M., Martinelli, L., Reis, S.M., Medeiros, S., Meira-Junior, M., Metzker, T., Morandi, P., do Nascimento, N.M., Moura, M., Müller, S.C., Nagy, L., Nascimento, H., Nascimento, M., Lima, A.N., de Araújo, R.O., Silva, J.O., Pansonato, M., Sabino, G.P., de Abreu, K.M.P., Rodrigues, P.J.F.P., Piedade, M., Rodrigues, D., Rodrigues Pinto, J.R., Quesada, C., Ramos, E., Ramos, R., Rodrigues, P., de Sousa, T.R., Salomão, R., Santana, F., Scaranello, M., Bergamin, R.S., Schietti, J., Schöngart, J., Schwartz, G., Silva, N., Silveira, M., Seixas, C.S., Simbine, M., Souza, A.C., Souza, P., Souza, R., Sposito, T., Junior, E.S., do Vale, J.D., Vieira, I.C.G., Villela, D., Vital, M., Xaud, H., Zanini, K., Zartman, C.E., Ideris, N.K.H., Metali, F. binti H., Salim, K.A., Saparudin, M.S., Serudin, R.M., Sukri, R.S., Begne, S., Chuyong, G., Djuikouo, M.N., Gonmadje, C., Simo-Droissart, M., Sonké, B., Taedoumg, H., Zemagho, L., Thomas, S., Baya, F., Saiz, G., Espejo, J.S., Chen, D., Hamilton, A., Li, Y., Luo, T., Niu, S., Xu, H., Zhou, Z., Álvarez-Dávila, E., Escobar, J.C.A., Arellano-Peña, H., Duarte, J.C., Calderón, J., Bravo, L.M.C., Cuadrado, B., Cuadros, H., Duque, A., Duque, L.F., Espinosa, S.M., Franke-Ante, R., García, H., Gómez, A., González-M., R., Idárraga-Piedrahíta, Á., Jimenez, E., Jurado, R., Oviedo, W.L., López-Camacho, R., Cruz, O.A.M., Polo, I.M., Paky, E., Pérez, K., Pijachi, A., Pizano, C., Prieto, A., Ramos, L., Correa, Z.R., Richardson, J., Rodríguez, E., Rodriguez M., G.M., Rudas, A., Stevenson, P., Chudomelová, M., Dancak, M., Hédl, R., Lhota, S., Svatek, M., Mukinzi, J., Ewango, C., Hart, T., Yakusu, E.K., Lisingo, J., Makana, J.-R., Mbayu, F., Toirambe, B., Mukendi, J.T., Kvist, L., Nebel, G., Báez, S., Céron, C., Griffith, D.M., Andino, J.E.G., Neill, D., Palacios, W., Peñuela-Mora, M.C., Rivas-Torres, G., Villa, G., Demissie, S., Gole, T., Gonfa, T., Ruokolainen, K., Baisie, M., Bénédet, F., Betian, W., Bezard, V., Bonal, D., Chave, J., Droissart, V., Gourlet-Fleury, S., Hladik, A., Labrière, N., Naisso, P., Réjou-Méchain, M., Sist, P., Blanc, L., Burban, B., Derroire, G., Dourdain, A., Stahl, C., Bengone, N.N., Chezeaux, E., Ondo, F.E., Medjibe, V., Mihindou, V., White, L., Culmsee, H., Rangel, C.D., Horna, V., Wittmann, F., Adu-Bredu, S., Affum-Baffoe, K., Foli, E., Balinga, M., Roopsind, A., Singh, J., Thomas, R., Zagt, R., Murthy, I.K., Kartawinata, K., Mirmanto, E., Priyadi, H., Samsoedin, I., Sunderland, T., Yassir, I., Rovero, F., Vinceti, B., Hérault, B., Aiba, S.-I., Kitayama, K., Daniels, A., Tuagben, D., Woods, J.T., Fitriadi, M., Karolus, A., Khoon, K.L., Majalap, N., Maycock, C., Nilus, R., Tan, S., Sitoe, A., Coronado G., I., Ojo, L., de Assis, R., Poulsen, A.D., Sheil, D., Pezo, K.A., Verde, H.B., Moscoso, V.C., Oroche, J.C.C., Valverde, F.C., Medina, M.C., Cardozo, N.D., de Rutte Corzo, J., del Aguila Pasquel, J., Llampazo, G.F., Freitas, L., Cabrera, D.G., Villacorta, R.G., Cabrera, K.G., Soria, D.G., Saboya, L.G., Rios, J.M.G., Pizango, G.H., Coronado, E.H., Huamantupa-Chuquimaco, I., Huasco, W.H., Aedo, Y.T.H., Peña, J.L.M., Mendoza, A.M., Rodriguez, V.M., Vargas, P.N., Ramos, S.C.P., Camacho, N.P., Cruz, A.P., Arevalo, F.R., Huaymacari, J.R., Rodriguez, C.R., Paredes, M.A.R., Bayona, L.R., del Pilar Rojas Gonzales, R., Peña, M.E.R.,

Revilla, N.S., Shareva, Y.C.S., Trujillo, R.T., Gamarra, L.V., Martinez, R.V., Arenas, J.V., Amani, C., Ifo, S.A., Bocko, Y., Boundja, P., Ekoungoulou, R., Hockemba, M., Nzala, D., Fofanah, A., Taylor, D., Bañares-de Dios, G., Cayuela, L., la Cerda, Í.G., Macía, M., Stropp, J., Playfair, M., Wortel, V., Gardner, T., Muscarella, R., Priyadi, H., Rutishauser, E., Chao, K.-J., Munishi, P., Bánki, O., Bongers, F., Boot, R., Fredriksson, G., Reitsma, J., ter Steege, H., van Andel, T., van de Meer, P., van der Hout, P., van Nieuwstadt, M., van Ulft, B., Veenendaal, E., Vernimmen, R., Zuidema, P., Zwerts, J., Akite, P., Bitariho, R., Chapman, C., Gerald, E., Leal, M., Mucunguzi, P., Abernethy, K., Alexiades, M., Baker, T.R., Banda, K., Banin, L., Barlow, J., Bennett, A., Berenguer, E., Berry, N., Bird, N.M., Blackburn, G.A., Brearley, F., Brienen, R., Burslem, D., Carvalho, L., Cho, P., Coelho, F., Collins, M., Coomes, D., Cuni-Sanchez, A., Dargie, G., Dexter, K., Disney, M., Draper, F., Duan, M., Esquivel-Muelbert, A., Ewers, R., Fadrique, B., Fauset, S., Feldpausch, T.R., França, F., Galbraith, D., Gilpin, M., Gloor, E., Grace, J., Hamer, K., Harris, D., Jeffery, K., Jucker, T., Kalamandeen, M., Klitgaard, B., Levesley, A., Lewis, S.L., Lindsell, J., Lopez-Gonzalez, G., Lovett, J., Malhi, Y., Marthews, T., McIntosh, E., Melgaço, K., Milliken, W., Mitchard, E., Moonlight, P., Moore, S., Morel, A., Peacock, J., Peh, K.S.-H., Pendry, C., Pennington, R.T., de Oliveira Pereira, L., Peres, C., Phillips, O.L., Pickavance, G., Pugh, T., Qie, L., Riutta, T., Roucoux, K., Ryan, C., Sarkinen, T., Valeria, C.S., Spracklen, D., Stas, S., Sullivan, M., Swaine, M., Talbot, J., Taplin, J., van der Heijden, G., Vedovato, L., Willcock, S., Williams, M., Alves, L., Loayza, P.A., Arellano, G., Asa, C., Ashton, P., Asner, G., Brncic, T., Brown, F., Burnham, R., Clark, C., Comiskey, J., Damasco, G., Davies, S., Di Fiore, T., Erwin, T., Farfan-Rios, W., Hall, J., Kenfack, D., Lovejoy, T., Martin, R., Montiel, O.M., Pipoly, J., Pitman, N., Poulsen, J., Primack, R., Silman, M., Steininger, M., Swamy, V., Terborgh, J., Thomas, D., Umunay, P., Uriarte, M., Torre, E.V., Wang, O., Young, K., Aymard C., G.A., Hernández, L., Fernández, R.H., Ramírez-Angulo, H., Salcedo, P., Sanoja, E., Serrano, J., Torres-Lezama, A., Le, T.C., Le, T.T., Tran, H.D., 2021. Taking the pulse of Earth's tropical forests using networks of highly distributed plots. Biol. Conserv. 260, 108849. https://doi.org/10.1016/j.biocon.2020.108849

Fradette, M.-S., Leboeuf, A., Riopel, M., Bégin, J., 2019. Method to Reduce the Bias on Digital Terrain Model and Canopy Height Model from LiDAR Data. Remote Sens. 11, 863. https://doi.org/10.3390/rs11070863

Freiberg, M., Winter, M., Gentile, A., Zizka, A., Muellner-Riehl, A.N., Weigelt, A., Wirth, C., 2020. LCVP, The Leipzig catalogue of vascular plants, a new taxonomic reference list for all known vascular plants. Sci. Data 7, 416. https://doi.org/10.1038/s41597-020-00702-z

Friedlingstein, P., Jones, M.W., O'Sullivan, M., Andrew, R.M., Bakker, D.C.E., Hauck, J., Le Quéré, C., Peters, G.P., Peters, W., Pongratz, J., Sitch, S., Canadell, J.G., Ciais, P., Jackson,

R.B., Alin, S.R., Anthoni, P., Bates, N.R., Becker, M., Bellouin, N., Bopp, L., Chau, T.T.T., Chevallier, F., Chini, L.P., Cronin, M., Currie, K.I., Decharme, B., Djeutchouang, L., Dou, X., Evans, W., Feely, R.A., Feng, L., Gasser, T., Gilfillan, D., Gkritzalis, T., Grassi, G., Gregor, L., Gruber, N., Gürses, Ö., Harris, I., Houghton, R.A., Hurtt, G.C., Iida, Y., Ilyina, T., Luijkx, I.T., Jain, A.K., Jones, S.D., Kato, E., Kennedy, D., Klein Goldewijk, K., Knauer, J., Korsbakken, J.I., Körtzinger, A., Landschützer, P., Lauvset, S.K., Lefèvre, N., Lienert, S., Liu, J., Marland, G., McGuire, P.C., Melton, J.R., Munro, D.R., Nabel, J.E.M.S., Nakaoka, S.-I., Niwa, Y., Ono, T., Pierrot, D., Poulter, B., Rehder, G., Resplandy, L., Robertson, E., Rödenbeck, C., Rosan, T.M., Schwinger, J., Schwingshackl, C., Séférian, R., Sutton, A.J., Sweeney, C., Tanhua, T., Tans, P.P., Tian, H., Tilbrook, B., Tubiello, F., van der Werf, G., Vuichard, N., Wada, C., Wanninkhof, R., Watson, A., Willis, D., Wiltshire, A.J., Yuan, W., Yue, C., Yue, X., Zaehle, S., Zeng, J., 2021. Global Carbon Budget 2021 (preprint). Antroposphere – Energy and Emissions. https://doi.org/10.5194/essd-2021-386

Frolking, S., Palace, M.W., Clark, D.B., Chambers, J.Q., Shugart, H.H., Hurtt, G.C., 2009. Forest disturbance and recovery: A general review in the context of spaceborne remote sensing of impacts on aboveground biomass and canopy structure: REMOTE SENSING OF FOREST DISTURBANCE. J. Geophys. Res. Biogeosciences 114, n/a-n/a. https://doi.org/10.1029/2008JG000911

Frost, C., Thompson, S.G., 2000. Correcting for Regression Dilution Bias: Comparison of Methods for a Single Predictor Variable. J. R. Stat. Soc. Ser. A Stat. Soc. 163, 173–189.

Gale, N., 2006. The Relationship between Canopy Gaps and Topography in a Western Ecuadorian Rain Forest1. Biotropica 32, 653–661. https://doi.org/10.1111/j.1744-7429.2000.tb00512.x

Gallay, M., 2013. GALLAY, M. (2013). Section 2.1.4: Direct Acquisition of Data:Airborne laser scanning. In: Clarke, L.E & Nield, J.M. (Eds.) Geomorphological Techniques (Online Edition). British Society for Geomorphology; London, UK. pp. 1–17.

Gaveau, D.L.A., Hill, R.A., 2003. Quantifying canopy height underestimation by laser pulse penetration in small-footprint airborne laser scanning data. Can. J. Remote Sens. 29, 650–657. https://doi.org/10.5589/m03-023

Gelman, A., Lee, D., Guo, J., 2015. Stan: A Probabilistic Programming Language for Bayesian Inference and Optimization. J. Educ. Behav. Stat. 40, 530–543. https://doi.org/10.3102/1076998615606113

Geo data, 2016. Aerial laser scanning (ALS) dataset, Crique Plomb and Montagne Plomb, French Guiana, acquired between 8 and 9 April 2009.

Gibson, L., Lee, T.M., Koh, L.P., Brook, B.W., Gardner, T.A., Barlow, J., Peres, C.A., Bradshaw, C.J.A., Laurance, W.F., Lovejoy, T.E., Sodhi, N.S., 2011. Primary forests are irreplaceable for sustaining tropical biodiversity. Nature 478, 378.

Goetz, S.J., Hansen, M., Houghton, R.A., Walker, W., Laporte, N., Busch, J., 2015. Measurement and monitoring needs, capabilities and potential for addressing reduced emissions from deforestation and forest degradation under REDD+. Environ. Res. Lett. 10, 123001. https://doi.org/10.1088/1748-9326/10/12/123001

Gonzalez de Tanago, J., Lau, A., Bartholomeus, H., Herold, M., Avitabile, V., Raumonen, P., Martius, C., Goodman, R.C., Disney, M., Manuri, S., Burt, A., Calders, K., 2018. Estimation of above-ground biomass of large tropical trees with terrestrial LiDAR. Methods Ecol. Evol. 9, 223–234. https://doi.org/10.1111/2041-210X.12904

Gourlet-Fleury, S. (ed), Guehl, J.-M. (ed), Laroussinie, O. (ed), 2004. Ecology and management of a neotropical rainforest : lessons drawn from Paracou, a long-term experimental research site in French Guiana. Elsevier.

GRASS Development Team, 2017. Geographic Resources Analysis Support System (GRASS GIS) Software, Version 7.2. Open Source Geospatial Foundation.

Guitet, S., Freycon, V., Brunaux, O., Pélissier, R., Sabatier, D., Couteron, P., 2016. Geomorphic control of rain-forest floristic composition in French Guiana: more than a soil filtering effect? J. Trop. Ecol. 32, 22–40. https://doi.org/10.1017/S0266467415000620

Guitet, S., Pélissier, R., Brunaux, O., Jaouen, G., Sabatier, D., 2015. Geomorphological landscape features explain floristic patterns in French Guiana rainforest. Biodivers. Conserv. 24, 1215–1237. https://doi.org/10.1007/s10531-014-0854-8

Harja, D., Vincent, G., Mulia, R., Noordwijk, M., 2012. Tree shape plasticity in relation to crown exposure. Trees 26, 1275–1285. https://doi.org/10.1007/s00468-012-0703-x

Harms, K.E., Condit, R., Hubbell, S.P., Foster, R.B., 2001. Habitat associations of trees and shrubs in a 50-ha neotropical forest plot: *Habitat associations of trees and shrubs*. J. Ecol. 89, 947–959. https://doi.org/10.1111/j.1365-2745.2001.00615.x

Hickman, G.D., Hogg, J.E., 1969. Application of an airborne pulsed laser for near shore bathymetric measurements. Remote Sens. Environ. 1, 47–58. https://doi.org/10.1016/S0034-4257(69)90088-1

Hijmans, R.J., 2020. raster: Geographic Data Analysis and Modeling.

Houghton, R.A., House, J.I., Pongratz, J., van der Werf, G.R., DeFries, R.S., Hansen, M.C., Le Quéré, C., Ramankutty, N., 2012. Carbon emissions from land use and land-cover change. Biogeosciences 9, 5125–5142. https://doi.org/10.5194/bg-9-5125-2012

Hubau, W., Lewis, S.L., Phillips, O.L., Affum-Baffoe, K., Beeckman, H., Cuní-Sanchez, A., Daniels, A.K., Ewango, C.E.N., Fauset, S., Mukinzi, J.M., Sheil, D., Sonké, B., Sullivan, M.J.P., Sunderland, T.C.H., Taedoumg, H., Thomas, S.C., White, L.J.T., Abernethy, K.A., Adu-Bredu, S., Amani, C.A., Baker, T.R., Banin, L.F., Baya, F., Begne, S.K., Bennett, A.C., Benedet, F., Bitariho, R., Bocko, Y.E., Boeckx, P., Boundja, P., Brienen, R.J.W., Brncic, T., Chezeaux, E., Chuyong, G.B., Clark, C.J., Collins, M., Comiskey, J.A., Coomes, D.A., Dargie, G.C., de Haulleville, T., Kamdem, M.N.D., Doucet, J.-L., Esquivel-Muelbert, A., Feldpausch, T.R., Fofanah, A., Foli, E.G., Gilpin, M., Gloor, E., Gonmadje, C., Gourlet-Fleury, S., Hall, J.S., Hamilton, A.C., Harris, D.J., Hart, T.B., Hockemba, M.B.N., Hladik, A., Ifo, S.A., Jeffery, K.J., Jucker, T., Yakusu, E.K., Kearsley, E., Kenfack, D., Koch, A., Leal, M.E., Levesley, A., Lindsell, J.A., Lisingo, J., Lopez-Gonzalez, G., Lovett, J.C., Makana, J.-R., Malhi, Y., Marshall, A.R., Martin, J., Martin, E.H., Mbayu, F.M., Medjibe, V.P., Mihindou, V., Mitchard, E.T.A., Moore, S., Munishi, P.K.T., Bengone, N.N., Ojo, L., Ondo, F.E., Peh, K.S.-H., Pickavance, G.C., Poulsen, A.D., Poulsen, J.R., Qie, L., Reitsma, J., Rovero, F., Swaine, M.D., Talbot, J., Taplin, J., Taylor, D.M., Thomas, D.W., Toirambe, B., Mukendi, J.T., Tuagben, D., Umunay, P.M., van der Heijden, G.M.F., Verbeeck, H., Vleminckx, J., Willcock, S., Wöll, H., Woods, J.T., Zemagho, L., 2020. Asynchronous carbon sink saturation in African and Amazonian tropical forests. Nature 579, 80–87. https://doi.org/10.1038/s41586-020-2035-0

Huertas, C., Sabatier, D., Derroire, G., Ferry, B., Jackson, Toby.D., Pélissier, R., Vincent, G., 2022. Mapping tree mortality rate in a tropical moist forest using multi-temporal LiDAR. Int. J. Appl. Earth Obs. Geoinformation 109, 102780. https://doi.org/10.1016/j.jag.2022.102780

Hunter, M.O., Keller, M., Morton, D., Cook, B., Lefsky, M., Ducey, M., Saleska, S., de Oliveira, R.C., Schietti, J., 2015. Structural Dynamics of Tropical Moist Forest Gaps. PLOS ONE 10, e0132144. https://doi.org/10.1371/journal.pone.0132144

Hunter, M.O., Keller, M., Victoria, D., Morton, D.C., 2013. Tree height and tropical forest biomass estimation. Biogeosciences 10, 8385–8399. https://doi.org/10.5194/bg-10-8385-2013

Ichii, K., Hashimoto, H., Nemani, R., White, M., 2005. Modeling the interannual variability and trends in gross and net primary productivity of tropical forests from 1982 to 1999. Glob. Planet. Change 48, 274–286. https://doi.org/10.1016/j.gloplacha.2005.02.005

IPCC, 2021. Summary for Policymakers. In: Climate Change 2021: The Physical Science Basis. Contribution of Working Group I to the Sixth Assessment Report of the Intergovernmental Panel on Climate Change.

Irish, J.L., White, T.E., 1998. Coastal engineering applications of high-resolution lidar bathymetry. Coast. Eng. 35, 47–71. https://doi.org/10.1016/S0378-3839(98)00022-2

Joetzjer, E., Douville, H., Delire, C., Ciais, P., 2013. Present-day and future Amazonian precipitation in global climate models: CMIP5 versus CMIP3. Clim. Dyn. 41, 2921–2936. https://doi.org/10.1007/s00382-012-1644-1

Jucker, T., 2022. Deciphering the fingerprint of disturbance on the three-dimensional structure of the world's forests. New Phytol. 233, 612–617. https://doi.org/10.1111/nph.17729

Keeling, H.C., Phillips, O.L., 2007. The global relationship between forest productivity and biomass. Glob. Ecol. Biogeogr. 16, 618–631. https://doi.org/10.1111/j.1466-8238.2007.00314.x

Kellner, J.R., Asner, G.P., 2009. Convergent structural responses of tropical forests to diverse disturbance regimes. Ecol. Lett. 12, 887–897. https://doi.org/10.1111/j.1461-0248.2009.01345.x

Kellner, J.R., Asner, G.P., Vitousek, P.M., Tweiten, M.A., Hotchkiss, S., Chadwick, O.A., 2011. Dependence of Forest Structure and Dynamics on Substrate Age and Ecosystem Development. Ecosystems 14, 1156–1167. https://doi.org/10.1007/s10021-011-9472-4

Knapp, N., Huth, A., Fischer, R., 2021. Tree Crowns Cause Border Effects in Area-Based Biomass Estimations from Remote Sensing. Remote Sens. 13, 1592. https://doi.org/10.3390/rs13081592

Kohyama, T.S., Kohyama, T.I., Sheil, D., 2018. Definition and estimation of vital rates from repeated censuses: Choices, comparisons and bias corrections focusing on trees. Methods Ecol. Evol. 9, 809–821. https://doi.org/10.1111/2041-210X.12929

Larjavaara, M., Muller-Landau, H.C., 2013. Measuring tree height: a quantitative comparison of two common field methods in a moist tropical forest. Methods Ecol. Evol. 4, 793–801. https://doi.org/10.1111/2041-210X.12071

Laurance, W.F., Williamson, G.B., 2001. Positive Feedbacks among Forest Fragmentation, Drought, and Climate Change in the Amazon. Conserv. Biol. 15, 1529–1535. https://doi.org/10.1046/j.1523-1739.2001.01093.x

Ledo, A., Cornulier, T., Illian, J.B., Iida, Y., Kassim, A.R., Burslem, D.F.R.P., 2016. Re-evaluation of individual diameter : height allometric models to improve biomass estimation of tropical trees. Ecol. Appl. 26, 2376–2382. https://doi.org/10.1002/eap.1450

Lefsky, M.A., Cohen, W.B., Acker, S.A., Spies, T.A., Parker, G.G., Harding, D., 1998. Lidar remote sensing of forest canopy structure and related biophysical parameters at H.J. Andrews Experimental Forest, Oregon, USA, in: IGARSS '98. Sensing and Managing the Environment. 1998 IEEE International Geoscience and Remote Sensing. Symposium Proceedings. (Cat. No.98CH36174). Presented at the IGARSS '98. Sensing and Managing the Environment. 1998 IEEE International Geoscience and Remote Sensing. Symposium Proceedings. (Cat. No.98CH36174), IEEE, Seattle, WA, USA, pp. 1252–1254 vol.3. https://doi.org/10.1109/IGARSS.1998.691367

Lefsky, M.A., Cohen, W.B., Parker, G.G., Harding, D.J., 2002. Lidar Remote Sensing for Ecosystem Studies. BioScience 52, 19. https://doi.org/10.1641/0006-3568(2002)052[0019:LRSFES]2.0.CO;2

Leitold, V., Morton, D.C., Longo, M., dos-Santos, M.N., Keller, M., Scaranello, M., 2018. El Niño drought increased canopy turnover in Amazon forests. New Phytol. 219, 959–971. https://doi.org/10.1111/nph.15110

Lim, K., Treitz, P., Wulder, M., St-Onge, B., Flood, M., 2003. LiDAR remote sensing of forest structure. Prog. Phys. Geogr. Earth Environ. 27, 88–106. https://doi.org/10.1191/0309133303pp360ra

Lima, R.B. de, Görgens, E.B., Elias, F., de Abreu, J.C., Baia, A.L., de Oliveira, C.P., Silva da Silva, D.A., Batista, A.P.B., Lima, R.C., Sotta, E.D., Caraciolo Ferreira, R.L., Aleixo da Silva, J.A., Carneiro Guedes, M., 2021. Height-diameter allometry for tropical forest in northern Amazonia. PLOS ONE 16, e0255197. https://doi.org/10.1371/journal.pone.0255197

Lohani, B., Ghosh, S., 2017. Airborne LiDAR Technology: A Review of Data Collection and Processing Systems. Proc. Natl. Acad. Sci. India Sect. Phys. Sci. 87, 567–579. https://doi.org/10.1007/s40010-017-0435-9

Longo, M., Saatchi, S., Keller, M., Bowman, K., Ferraz, A., Moorcroft, P.R., Morton, D.C., Bonal, D., Brando, P., Burban, B., Derroire, G., dos-Santos, M.N., Meyer, V., Saleska, S., Trumbore, S., Vincent, G., 2020. Impacts of Degradation on Water, Energy, and Carbon Cycling of the Amazon Tropical Forests. J. Geophys. Res. Biogeosciences 125. https://doi.org/10.1029/2020JG005677

Loubry, D., 1994. La phénologie des arbres caducifoliés en forêt guyanaise (5° de latitude nord) : illustration d'un déterminisme à composantes endogène et exogène. Can. J. Bot. 72, 1843–1857. https://doi.org/10.1139/b94-226

Lovenduski, N.S., Bonan, G.B., 2017. Reducing uncertainty in projections of terrestrial carbon uptake. Environ. Res. Lett. 12, 044020. https://doi.org/10.1088/1748-9326/aa66b8

Malhi, Y., Phillips, O.L., Lloyd, J., Baker, T., Wright, J., Almeida, S., Arroyo, L., Frederiksen, T., Grace, J., Higuchi, N., Killeen, T., Laurance, W.F., Leaño, C., Lewis, S., Meir, P., Monteagudo, A., Neill, D., Núñez Vargas, P., Panfil, S.N., Patiño, S., Pitman, N., Quesada, C.A., Rudas-Ll., A., Salomão, R., Saleska, S., Silva, N., Silveira, M., Sombroek, W.G., Valencia, R., Vásquez Martínez, R., Vieira, I.C.G., Vinceti, B., 2002. An international network to monitor the structure, composition and dynamics of Amazonian forests (RAINFOR). J. Veg. Sci. 13, 439–450. https://doi.org/10.1111/j.1654-1103.2002.tb02068.x

Malhi, Y., Roberts, J.T., Betts, R.A., Killeen, T.J., Li, W., Nobre, C.A., 2008. Climate Change, Deforestation, and the Fate of the Amazon. Science 319, 169–172. https://doi.org/10.1126/science.1146961

Maltamo, M., 2014. Forestry applications of airborne laser scanning: concepts and case studies. Springer, New York.

Maréchaux, I., Chave, J., 2017. An individual-based forest model to jointly simulate carbon and tree diversity in Amazonia: description and applications. Ecol. Monogr. 87, 632–664. https://doi.org/10.1002/ecm.1271

Marvin, D.C., Asner, G.P., Knapp, D.E., Anderson, C.B., Martin, R.E., Sinca, F., Tupayachi, R., 2014. Amazonian landscapes and the bias in field studies of forest structure and biomass. Proc. Natl. Acad. Sci. 111, E5224–E5232. https://doi.org/10.1073/pnas.1412999111

Mascaro, J., Detto, M., Asner, G.P., Muller-Landau, H.C., 2011. Evaluating uncertainty in mapping forest carbon with airborne LiDAR. Remote Sens. Environ. 115, 3770–3774. https://doi.org/10.1016/j.rse.2011.07.019

Mattivi, P., Franci, F., Lambertini, A., Bitelli, G., 2019. TWI computation: a comparison of different open source GISs. Open Geospatial Data Softw. Stand. 4, 6. https://doi.org/10.1186/s40965-019-0066-y

McDowell, N., Allen, C.D., Anderson-Teixeira, K., Brando, P., Brienen, R., Chambers, J., Christoffersen, B., Davies, S., Doughty, C., Duque, A., Espirito-Santo, F., Fisher, R., Fontes, C.G., Galbraith, D., Goodsman, D., Grossiord, C., Hartmann, H., Holm, J., Johnson, D.J., Kassim, Abd.R., Keller, M., Koven, C., Kueppers, L., Kumagai, T., Malhi, Y., McMahon, S.M.,

Mencuccini, M., Meir, P., Moorcroft, P., Muller-Landau, H.C., Phillips, O.L., Powell, T., Sierra, C.A., Sperry, J., Warren, J., Xu, C., Xu, X., 2018. Drivers and mechanisms of tree mortality in moist tropical forests. New Phytol. 219, 851–869. https://doi.org/10.1111/nph.15027

Mesas-Carrascosa, F.J., Castillejo-González, I.L., de la Orden, M.S., Porras, A.G.-F., 2012. Combining LiDAR intensity with aerial camera data to discriminate agricultural land uses. Comput. Electron. Agric. 84, 36–46. https://doi.org/10.1016/j.compag.2012.02.020

METEO France, 2020. Les climats en outre-mer | Météo-France [WWW Document]. URL https://meteofrance.com/comprendre-climat/france/les-climats-en-outre-mer (accessed 5.5.22).

Meyer, V., Saatchi, S.S., Chave, J., Dalling, J.W., Bohlman, S., Fricker, G.A., Robinson, C., Neumann, M., Hubbell, S., 2013. Detecting tropical forest biomass dynamics from repeated airborne lidar measurements. Biogeosciences 10, 5421–5438. https://doi.org/10.5194/bg-10-5421-2013

Middleton, W.E.K., Spilhaus., A.F., 1954. Meteorological Instruments. Q. J. R. Meteorol. Soc., University of Toronto Press. 3rd 80, 484–484. https://doi.org/10.1002/qj.49708034532

Miranda, D.L.C. de, Sanquetta, C.R., Costa, L.G. da S., Corte, A.P.D., 2012. Biomassa e carbono em Euterpe oleracea Mart. na ilha do Marajó - PA. Floresta E Ambiente 19, 336–343. https://doi.org/10.4322/floram.2012.039

Molto, Q., Hérault, B., Boreux, J.-J., Daullet, M., Rousteau, A., Rossi, V., 2014. Predicting tree heights for biomass estimates in tropical forests – a test from French Guiana. Biogeosciences 11, 3121–3130. https://doi.org/10.5194/bg-11-3121-2014

Molto, Q., Rossi, V., Blanc, L., 2013. Error propagation in biomass estimation in tropical forests. Methods Ecol. Evol. 4, 175–183. https://doi.org/10.1111/j.2041-210x.2012.00266.x

Momo Takoudjou, S., Ploton, P., Sonké, B., Hackenberg, J., Griffon, S., Coligny, F., Kamdem, N.G., Libalah, M., Mofack, G.I., Le Moguédec, G., Pélissier, R., Barbier, N., 2018. Using terrestrial laser scanning data to estimate large tropical trees biomass and calibrate allometric models: A comparison with traditional destructive approach. Methods Ecol. Evol. 9, 905–916. https://doi.org/10.1111/2041-210X.12933

Montealegre, A.L., Lamelas, M.T., de la Riva, J., García-Martín, A., Escribano, F., 2016. Use of low point density ALS data to estimate stand-level structural variables in Mediterranean Aleppo pine forest. Forestry 89, 373–382. https://doi.org/10.1093/forestry/cpw008

Morneau, F., 2007. Effets d'un gradient d'engorgement sur la structure et la dynamique d'une forêt tropicale humide (Paracou, Guyane française) (PhD). ENGREF AgroParis Tech, PARIS.

NASA, 2020. CEOS land validation sites.

NASA, n.d. CEOS Land Product Validation Subgroup [WWW Document]. URL https://lpvs.gsfc.nasa.gov/LPV_Supersites/LPVsites.html (accessed 4.29.22).

Nascimento, H.E.M., Laurance, W.F., Condit, R., Laurance, S.G., D'Angelo, S., Andrade, A.C., 2005. Demographic and life-history correlates for Amazonian trees. J. Veg. Sci. 16, 625–634. https://doi.org/10.1111/j.1654-1103.2005.tb02405.x

NOAA, 2012. Lidar 101: An Introduction to Lidar Technology, Data, and Applications., Revised. Charleston, SC: NOAA Coastal Services Center. ed.

Osunkoya, O.O., Omar-Ali, K., Amit, N., Dayan, J., Daud, D.S., Sheng, T.K., 2007. Comparative height crown allometry and mechanical design in 22 tree species of Kuala Belalong rainforest, Brunei, Borneo. Am J Bot 94, 1951–1962. https://doi.org/10.3732/ajb.94.12.1951

Pan, Y., Birdsey, R.A., Fang, J., Houghton, R., Kauppi, P.E., Kurz, W.A., Phillips, O.L., Shvidenko, A., Lewis, S.L., Canadell, J.G., Ciais, P., Jackson, R.B., Pacala, S.W., McGuire, A.D., Piao, S., Rautiainen, A., Sitch, S., Hayes, D., 2011. A Large and Persistent Carbon Sink in the World's Forests. Science 333, 988–993. https://doi.org/10.1126/science.1201609

Parent, C., Nicolas, C., Audrey, B., Crevècoeur, M., Dat, J., 2008. An overview of plant responses to soil waterlogging. Plant Stress 20–27.

Pélissier, R., Dray, S., Sabatier, D., 2002. Within-plot relationships between tree species occurrences and hydrological soil constraints: an example in French Guiana investigated through canonical correlation analysis. Plant Ecol. 162, 143–156. https://doi.org/10.1023/A:1020399603500

Phillips, O.L., Lewis, S.L., Baker, T.R., Chao, K.-J., Higuchi, N., 2008. The changing Amazon forest. Philos. Trans. R. Soc. B Biol. Sci. 363, 1819–1827. https://doi.org/10.1098/rstb.2007.0033

Phillips, O.L., Lewis, S.L., Higuchi, N., Baker, T., 2016. Recent Changes in Amazon Forest Biomass and Dynamics, in: Nagy, L., Forsberg, B.R., Artaxo, P. (Eds.), Interactions Between Biosphere, Atmosphere and Human Land Use in the Amazon Basin, Ecological Studies. Springer Berlin Heidelberg, Berlin, Heidelberg, pp. 191–224. https://doi.org/10.1007/978-3-662-49902-3_10

Popescu, S.C., Wynne, R.H., Nelson, R.F., 2003. Measuring individual tree crown diameter with lidar and assessing its influence on estimating forest volume and biomass. Can. J. Remote Sens. 29, 564–577. https://doi.org/10.5589/m03-027

Réjou-Méchain, M., Barbier, N., Couteron, P., Ploton, P., Vincent, G., Herold, M., Mermoz, S., Saatchi, S., Chave, J., de Boissieu, F., Féret, J.-B., Takoudjou, S.M., Pélissier, R., 2019. Upscaling Forest Biomass from Field to Satellite Measurements: Sources of Errors and Ways to Reduce Them. Surv. Geophys. 40, 881–911. https://doi.org/10.1007/s10712-019-09532-0

Réjou-Méchain, M., Tymen, B., Blanc, L., Fauset, S., Feldpausch, T.R., Monteagudo, A., Phillips, O.L., Richard, H., Chave, J., 2015. Using repeated small-footprint LiDAR acquisitions to infer spatial and temporal variations of a high-biomass Neotropical forest. Remote Sens. Environ. 169, 93–101. https://doi.org/10.1016/j.rse.2015.08.001

Rex, F.E., Corte, A.P.D., Silva, C.A., Machado, S.A., Sanquetta, C.R., 2020. Dynamics of Above-Ground Biomass in the Brazilian Amazon Using LiDAR Data. Anuário Inst. Geociências - UFRJ 43, 228–238. https://doi.org/10.11137/2020_1_228_238

RIEGL, 2013. LiDAR Magazine 3.

RIEGL, 2010. Airborne Laser ScanningAirborne Laser Scanner for Full Waveform Analysis LMS-Q560.

RIEGL, 2004. LASER MIRROR SCANNERLMS Q280iTECHNICAL DOCUMENTATION AND USER'S INSTRUCTIONS.

Robson, J., Sutton, R., Lohmann, K., Smith, D., Palmer, M.D., 2012. Causes of the Rapid Warming of the North Atlantic Ocean in the Mid-1990s. J. Clim. 25, 4116–4134. https://doi.org/10.1175/JCLI-D-11-00443.1

Rocha de Souza Pereira, F., Kampel, M., Gomes Soares, M., Estrada, G., Bentz, C., Vincent, G., 2018. Reducing Uncertainty in Mapping of Mangrove Aboveground Biomass Using Airborne Discrete Return Lidar Data. Remote Sens. 10, 637. https://doi.org/10.3390/rs10040637

Roth, B.E., Slatton, K.C., Cohen, M.J., 2007. On the potential for high-resolution lidar to improve rainfall interception estimates in forest ecosystems. Front. Ecol. Environ. 5, 421–428. https://doi.org/10.1890/060119.1

Roussel, J.-R., Auty, D., 2020. lidR: Airborne LiDAR Data Manipulation and Visualization for Forestry Applications.

Roussel, J.-R., Caspersen, J., Béland, M., Thomas, S., Achim, A., 2017. Removing bias from LiDAR-based estimates of canopy height: Accounting for the effects of pulse density and footprint size. Remote Sens. Environ. 198, 1–16. https://doi.org/10.1016/j.rse.2017.05.032

Rutishauser, E., Hérault, B., Baraloto, C., Blanc, L., Descroix, L., Sotta, E.D., Ferreira, J., Kanashiro, M., Mazzei, L., d'Oliveira, M.V.N., de Oliveira, L.C., Peña-Claros, M., Putz, F.E., Ruschel, A.R., Rodney, K., Roopsind, A., Shenkin, A., da Silva, K.E., de Souza, C.R., Toledo, M., Vidal, E., West, T.A.P., Wortel, V., Sist, P., 2015. Rapid tree carbon stock recovery in managed Amazonian forests. Curr. Biol. 25, R787–R788. https://doi.org/10.1016/j.cub.2015.07.034

Rutishauser, E., Hérault, B., Petronelli, P., Sist, P., 2016. Tree Height Reduction After Selective Logging in a Tropical Forest. Biotropica 48, 285–289. https://doi.org/10.1111/btp.12326

Sabatier, D., Grimaldi, M., Prévost, M.-F., Guillaume, J., Godron, M., Dosso, M., Sabatier, D., 1997. The influence of soil cover organization on the floristic and structural heterogeneity of a Guianan rain forest. Plant Ecol. Former. Veg. 131, 81–108. https://doi.org/10.1023/A:1009775025850

Sabatier, D., Guitet, S., Vincent, G., 2017. Forçages environnementaux et anthropiques du turnover forestier, conséquences sur la diversité des communautés d'arbres en forêt tropicale.

Salovaara, K.J., Thessler, S., Malik, R.N., Tuomisto, H., 2005. Classification of Amazonian primary rain forest vegetation using Landsat ETM+ satellite imagery. Remote Sens. Environ. 97, 39–51. https://doi.org/10.1016/j.rse.2005.04.013

Schmitt, L., 1984. Recherches sylvicoles sur les peuplements naturels en forêt dense guyanaise. Phase préliminaire : localisation du dispositif principal. Nogent-sur-Marne, GERDAT-CTFT. ed.

Schuur, E.A.G., 2003. PRODUCTIVITY AND GLOBAL CLIMATE REVISITED: THE SENSITIVITY OF TROPICAL FOREST GROWTH TO PRECIPITATION. Ecology 84, 1165–1170. https://doi.org/10.1890/0012-9658(2003)084[1165:PAGCRT]2.0.CO;2

Seidel, D., Annighöfer, P., Ammer, C., Ehbrecht, M., Willim, K., Bannister, J., Soto, D.P., 2021. Quantifying Understory Complexity in Unmanaged Forests Using TLS and Identifying Some of Its Major Drivers. Remote Sens. 13, 1513. https://doi.org/10.3390/rs13081513

Senécal, J.-F., Doyon, F., Messier, C., 2018. Tree Death Not Resulting in Gap Creation: An Investigation of Canopy Dynamics of Northern Temperate Deciduous Forests. Remote Sens. 10, 121. https://doi.org/10.3390/rs10010121

Shan, J., Toth, C.K. (Eds.), 2009. Topographic laser ranging and scanning: principles and processing. CRC Press/Taylor & Francis Group, Boca Raton.

Shao, G., Stark, S.C., de Almeida, D.R.A., Smith, M.N., 2019. Towards high throughput assessment of canopy dynamics: The estimation of leaf area structure in Amazonian forests

with multitemporal multi-sensor airborne lidar. Remote Sens. Environ. 221, 1–13. https://doi.org/10.1016/j.rse.2018.10.035

Smearcheck, M., 2008. Investigation of Dual Airborne Laser Scanners for Detection and State Estimation of Mobile Obstacles in an Aircraft External Hazard Monitor. (Electronic Thesis or Dissertation).

Sousa, T.R., Schietti, J., Coelho de Souza, F., Esquivel-Muelbert, A., Ribeiro, I.O., Emílio, T., Pequeno, P.A.C.L., Phillips, O., Costa, F.R.C., 2020. Palms and trees resist extreme drought in Amazon forests with shallow water tables. J. Ecol. 108, 2070–2082. https://doi.org/10.1111/1365-2745.13377

Sullivan, M.J.P., Lewis, S.L., Affum-Baffoe, K., Castilho, C., Costa, F., Sanchez, A.C., Ewango, C.E.N., Hubau, W., Marimon, B., Monteagudo-Mendoza, A., Qie, L., Sonké, B., Martinez, R.V., Baker, T.R., Brienen, R.J.W., Feldpausch, T.R., Galbraith, D., Gloor, M., Malhi, Y., Aiba, S.-I., Alexiades, M.N., Almeida, E.C., de Oliveira, E.A., Dávila, E.Á., Loayza, P.A., Andrade, A., Vieira, S.A., Aragão, L.E.O.C., Araujo-Murakami, A., Arets, E.J.M.M., Arroyo, L., Ashton, P., Aymard C., G., Baccaro, F.B., Banin, L.F., Baraloto, C., Camargo, P.B., Barlow, J., Barroso, J., Bastin, J.-F., Batterman, S.A., Beeckman, H., Begne, S.K., Bennett, A.C., Berenguer, E., Berry, N., Blanc, L., Boeckx, P., Bogaert, J., Bonal, D., Bongers, F., Bradford, M., Brearley, F.Q., Brncic, T., Brown, F., Burban, B., Camargo, J.L., Castro, W., Céron, C., Ribeiro, S.C., Moscoso, V.C., Chave, J., Chezeaux, E., Clark, C.J., de Souza, F.C., Collins, M., Comiskey, J.A., Valverde, F.C., Medina, M.C., da Costa, L., Dančák, M., Dargie, G.C., Davies, S., Cardozo, N.D., de Haulleville, T., de Medeiros, M.B., del Aguila Pasquel, J., Derroire, G., Di Fiore, A., Doucet, J.-L., Dourdain, A., Droissant, V., Duque, L.F., Ekoungoulou, R., Elias, F., Erwin, T., Esquivel-Muelbert, A., Fauset, S., Ferreira, J., Llampazo, G.F., Foli, E., Ford, A., Gilpin, M., Hall, J.S., Hamer, K.C., Hamilton, A.C., Harris, D.J., Hart, T.B., Hédl, R., Herault, B., Herrera, R., Higuchi, N., Hladik, A., Coronado, E.H., Huamantupa-Chuquimaco, I., Huasco, W.H., Jeffery, K.J., Jimenez-Rojas, E., Kalamandeen, M., Djuikouo, M.N.K., Kearsley, E., Umetsu, R.K., Kho, L.K., Killeen, T., Kitayama, K., Klitgaard, B., Koch, A., Labrière, N., Laurance, W., Laurance, S., Leal, M.E., Levesley, A., Lima, A.J.N., Lisingo, J., Lopes, A.P., Lopez-Gonzalez, G., Lovejoy, T., Lovett, J.C., Lowe, R., Magnusson, W.E., Malumbres-Olarte, J., Manzatto, Â.G., Marimon, B.H., Marshall, A.R., Marthews, T., de Almeida Reis, S.M., Maycock, C., Melgaço, K., Mendoza, C., Metali, F., Mihindou, V., Milliken, W., Mitchard, E.T.A., Morandi, P.S., Mossman, H.L., Nagy, L., Nascimento, H., Neill, D., Nilus, R., Vargas, P.N., Palacios, W., Camacho, N.P., Peacock, J., Pendry, C., Peñuela Mora, M.C., Pickavance, G.C., Pipoly, J., Pitman, N., Playfair, M., Poorter, L., Poulsen, J.R., Poulsen, A.D., Preziosi, R., Prieto, A., Primack, R.B., Ramírez-Angulo, H., Reitsma, J., Réjou-Méchain, M., Correa, Z.R.,

de Sousa, T.R., Bayona, L.R., Roopsind, A., Rudas, A., Rutishauser, E., Abu Salim, K., Salomão, R.P., Schietti, J., Sheil, D., Silva, R.C., Espejo, J.S., Valeria, C.S., Silveira, M., Simo-Droissart, M., Simon, M.F., Singh, J., Soto Shareva, Y.C., Stahl, C., Stropp, J., Sukri, R., Sunderland, T., Svátek, M., Swaine, M.D., Swamy, V., Taedoumg, H., Talbot, J., Taplin, J., Taylor, D., ter Steege, H., Terborgh, J., Thomas, R., Thomas, S.C., Torres-Lezama, A., Umunay, P., Gamarra, L.V., van der Heijden, G., van der Hout, P., van der Meer, P., van Nieuwstadt, M., Verbeeck, H., Vernimmen, R., Vicentini, A., Vieira, I.C.G., Torre, E.V., Vleminckx, J., Vos, V., Wang, O., White, L.J.T., Willcock, S., Woods, J.T., Wortel, V., Young, K., Zagt, R., Zemagho, L., Zuidema, P.A., Zwerts, J.A., Phillips, O.L., 2020. Long-term thermal sensitivity of Earth's tropical forests. Science 368, 869–874. https://doi.org/10.1126/science.aaw7578

Sullivan, M.J.P., Lewis, S.L., Hubau, W., Qie, L., Baker, T.R., Banin, L.F., Chave, J., Cuni-Sanchez, A., Feldpausch, T.R., Lopez-Gonzalez, G., Arets, E., Ashton, P., Bastin, J., Berry, N.J., Bogaert, J., Boot, R., Brearley, F.Q., Brienen, R., Burslem, D.F.R.P., Canniere, C., Chudomelová, M., Dančák, M., Ewango, C., Hédl, R., Lloyd, J., Makana, J., Malhi, Y., Marimon, B.S., Junior, B.H.M., Metali, F., Moore, S., Nagy, L., Vargas, P.N., Pendry, C.A., Ramírez-Angulo, H., Reitsma, J., Rutishauser, E., Salim, K.A., Sonké, B., Sukri, R.S., Sunderland, T., Svátek, M., Umunay, P.M., Martinez, R.V., Vernimmen, R.R.E., Torre, E.V., Vleminckx, J., Vos, V., Phillips, O.L., 2018. Field methods for sampling tree height for tropical forest biomass estimation. Methods Ecol. Evol. 9, 1179–1189. https://doi.org/10.1111/2041-210X.12962

Sullivan, M.J.P., Talbot, J., Lewis, S.L., Phillips, O.L., Qie, L., Begne, S.K., Chave, J., Cuni-Sanchez, A., Hubau, W., Lopez-Gonzalez, G., Miles, L., Monteagudo-Mendoza, A., Sonké, B., Sunderland, T., ter Steege, H., White, L.J.T., Affum-Baffoe, K., Aiba, S., de Almeida, E.C., de Oliveira, E.A., Alvarez-Loayza, P., Dávila, E.Á., Andrade, A., Aragão, L.E.O.C., Ashton, P., Aymard C., G.A., Baker, T.R., Balinga, M., Banin, L.F., Baraloto, C., Bastin, J.-F., Berry, N., Bogaert, J., Bonal, D., Bongers, F., Brienen, R., Camargo, J.L.C., Cerón, C., Moscoso, V.C., Chezeaux, E., Clark, C.J., Pacheco, Á.C., Comiskey, J.A., Valverde, F.C., Coronado, E.N.H., Dargie, G., Davies, S.J., De Canniere, C., Djuikouo K., M.N., Doucet, J.-L., Erwin, T.L., Espejo, J.S., Ewango, C.E.N., Fauset, S., Feldpausch, T.R., Herrera, R., Gilpin, M., Gloor, E., Hall, J.S., Harris, D.J., Hart, T.B., Kartawinata, K., Kho, L.K., Kitayama, K., Laurance, S.G.W., Laurance, W.F., Leal, M.E., Lovejoy, T., Lovett, J.C., Lukasu, F.M., Makana, J.-R., Malhi, Y., Maracahipes, L., Marimon, B.S., Junior, B.H.M., Marshall, A.R., Morandi, P.S., Mukendi, J.T., Mukinzi, J., Nilus, R., Vargas, P.N., Camacho, N.C.P., Pardo, G., Peña-Claros, M., Pétronelli, P., Pickavance, G.C., Poulsen, A.D., Poulsen, J.R., Primack, R.B., Priyadi, H., Quesada, C.A., Reitsma, J., Réjou-Méchain, M., Restrepo, Z., Rutishauser, E., Salim, K.A., Salomão, R.P.,

Samsoedin, I., Sheil, D., Sierra, R., Silveira, M., Slik, J.W.F., Steel, L., Taedoumg, H., Tan, S., Terborgh, J.W., Thomas, S.C., Toledo, M., Umunay, P.M., Gamarra, L.V., Vieira, I.C.G., Vos, V.A., Wang, O., Willcock, S., Zemagho, L., 2017. Diversity and carbon storage across the tropical forest biome. Sci. Rep. 7. https://doi.org/10.1038/srep39102

Taylor, P., Asner, G., Dahlin, K., Anderson, C., Knapp, D., Martin, R., Mascaro, J., Chazdon, R., Cole, R., Wanek, W., Hofhansl, F., Malavassi, E., Vilchez-Alvarado, B., Townsend, A., 2015. Landscape-Scale Controls on Aboveground Forest Carbon Stocks on the Osa Peninsula, Costa Rica. PLOS ONE 10, e0126748. https://doi.org/10.1371/journal.pone.0126748

Thomas, R.Q., Kellner, J.R., Clark, D.B., Peart, D.R., 2013. Low mortality in tall tropical trees. Ecology 94, 920–929. https://doi.org/10.1890/12-0939.1

van der Heijden, G.M.F., Phillips, O.L., 2008. What controls liana success in Neotropical forests? Glob. Ecol. Biogeogr. 17, 372–383. https://doi.org/10.1111/j.1466-8238.2007.00376.x

van der Laan-Luijkx, I.T., van der Velde, I.R., Krol, M.C., Gatti, L.V., Domingues, L.G., Correia, C.S.C., Miller, J.B., Gloor, M., van Leeuwen, T.T., Kaiser, J.W., Wiedinmyer, C., Basu, S., Clerbaux, C., Peters, W., 2015. Response of the Amazon carbon balance to the 2010 drought derived with CarbonTracker South America: AMAZON CARBON CYCLE DURING 2010 DROUGHT. Glob. Biogeochem. Cycles 29, 1092–1108. https://doi.org/10.1002/2014GB005082

van der Meer, P.J., Bongers, F., 1996. Patterns of Tree-Fall and Branch-Fall in a Tropical Rain Forest in French Guiana. J. Ecol. 84, 19. https://doi.org/10.2307/2261696

Vanclay, J., K., 2009. Tree diameter, height and stocking in even-aged forests. Ann Sci 66, 702.

Vanclay, J.K., Henry, N., 1988. Assessing site productivity of indigenous cypress pine forest in southern Queensland. Commonw. For. Rev. 67, 53–64.

Vieira, S., de Camargo, P.B., Selhorst, D., da Silva, R., Hutyra, L., Chambers, J.Q., Brown, I.F., Higuchi, N., dos Santos, J., Wofsy, S.C., Trumbore, S.E., Martinelli, L.A., 2004. Forest structure and carbon dynamics in Amazonian tropical rain forests. Oecologia 140, 468–479. https://doi.org/10.1007/s00442-004-1598-z

Villikka, M., Maltamo, M., Packalén, P., Vehmas, M., Hyyppä, J., n.d. Alternatives for predicting tree-level stem volume of norway spruce using airborne laser scanner data 10.

Vincent, G., Antin, C., Laurans, M., Heurtebize, J., Durrieu, S., Lavalley, C., Dauzat, J., 2017. Mapping plant area index of tropical evergreen forest by airborne laser scanning. A cross-

validation study using LAI2200 optical sensor. Remote Sens. Environ. 198, 254–266. https://doi.org/10.1016/j.rse.2017.05.034

Vincent, G., Caron, F., Sabatier, D., Blanc, L., 2012a. LiDAR shows that higher forests have more slender trees. Bois Forets Trop. 314.

Vincent, G., Harja Asmara, D., 2008. Exploring ecological significance of tree crown plasticity through three-dimensional modelling. Ann. Bot. 101, 1221–1231. https://doi.org/10.1093/aob/mcm189

Vincent, G., Molino, J.-F., Marescot, L., Barkaoui, K., Sabatier, D., Freycon, V., Roelens, J.B., 2011a. The relative importance of dispersal limitation and habitat preference in shaping spatial distribution of saplings in a tropical moist forest: a case study along a combination of hydromorphic and canopy disturbance gradients. Ann. For. Sci. 68, 357–370. https://doi.org/10.1007/s13595-011-0024-z

Vincent, G., Sabatier, D., Blanc, L., Chave, J., Weissenbacher, E., Pélissier, R., Fonty, E., Molino, J.-F., Couteron, P., 2012b. Accuracy of small footprint airborne LiDAR in its predictions of tropical moist forest stand structure. Remote Sens. Environ. 125, 23–33. https://doi.org/10.1016/j.rse.2012.06.019

Vincent, G., Sabatier, D., Caron, F., Deng, N., Véga, C., 2011b. Multitemporal LiDAR applications to tropical forest dynamics studies. A few examples from French Guiana.

Vincent, G., Sabatier, D., Rutishauser, E., 2014. Revisiting a universal airborne light detection and ranging approach for tropical forest carbon mapping: scaling-up from tree to stand to landscape. Oecologia 175, 439–443. https://doi.org/10.1007/s00442-014-2913-y

Vincent, G., Weissenbacher, E., Sabatier, D., Blanc, L., Proisy, C., Couteron, P., 2010. Détection des variations de structure de peuplements en forêt dense tropicale humide par Lidar aéroporté. Rev. Francaise Photogramm. Teledetection.

Wagner, F.H., Hérault, B., Bonal, D., Stahl, C., Anderson, L.O., Baker, T.R., Becker, G.S., Beeckman, H., Boanerges Souza, D., Botosso, P.C., Bowman, D.M.J.S., Bräuning, A., Brede, B., Brown, F.I., Camarero, J.J., Camargo, P.B., Cardoso, F.C.G., Carvalho, F.A., Castro, W., Chagas, R.K., Chave, J., Chidumayo, E.N., Clark, D.A., Costa, F.R.C., Couralet, C., da Silva Mauricio, P.H., Dalitz, H., de Castro, V.R., de Freitas Milani, J.E., de Oliveira, E.C., de Souza Arruda, L., Devineau, J.-L., Drew, D.M., Dünisch, O., Durigan, G., Elifuraha, E., Fedele, M., Ferreira Fedele, L., Figueiredo Filho, A., Finger, C.A.G., Franco, A.C., Freitas Júnior, J.L., Galvão, F., Gebrekirstos, A., Gliniars, R., Graça, P.M.L.D.A., Griffiths, A.D., Grogan, J., Guan, K., Homeier, J., Kanieski, M.R., Kho, L.K., Koenig, J., Kohler, S.V., Krepkowski, J., Lemos-

Filho, J.P., Lieberman, D., Lieberman, M.E., Lisi, C.S., Longhi Santos, T., López Ayala, J.L., Maeda, E.E., Malhi, Y., Maria, V.R.B., Marques, M.C.M., Marques, R., Maza Chamba, H., Mbwambo, L., Melgaço, K.L.L., Mendivelso, H.A., Murphy, B.P., O'Brien, J.J., Oberbauer, S.F., Okada, N., Pélissier, R., Prior, L.D., Roig, F.A., Ross, M., Rossatto, D.R., Rossi, V., Rowland, L., Rutishauser, E., Santana, H., Schulze, M., Selhorst, D., Silva, W.R., Silveira, M., Spannl, S., Swaine, M.D., Toledo, J.J., Toledo, M.M., Toledo, M., Toma, T., Tomazello Filho, M., Valdez Hernández, J.I., Verbesselt, J., Vieira, S.A., Vincent, G., Volkmer de Castilho, C., Volland, F., Worbes, M., Zanon, M.L.B., Aragão, L.E.O.C., 2016. Climate seasonality limits leaf carbon assimilation and wood productivity in tropical forests. Biogeosciences 13, 2537–2562. https://doi.org/10.5194/bg-13-2537-2016

Wang, Y., Titus, S.J., LeMay, V.M., 1998. Relationships between tree slenderness coefficients and tree or stand characteristics for major species in boreal mixedwood forests. Can. J. For. Res. 28, 1171–1183. https://doi.org/10.1139/x98-092

Wehr, A., 2018. LiDAR Systems and Calibration, in: Shan, J., Toth, C.K. (Eds.), Topographic Laser Ranging and Scanning. CRC Press, Second edition. | Boca Raton : Taylor & Francis, CRC Press, 2018., pp. 159–200. https://doi.org/10.1201/9781315154381-4

Wilkes, P., Lau, A., Disney, M., Calders, K., Burt, A., Gonzalez de Tanago, J., Bartholomeus, H., Brede, B., Herold, M., 2017. Data acquisition considerations for Terrestrial Laser Scanning of forest plots. Remote Sens. Environ. 196, 140–153. https://doi.org/10.1016/j.rse.2017.04.030

Wright, S.J., 2010. The future of tropical forests: Future tropical forests. Ann. N. Y. Acad. Sci. 1195, 1–27. https://doi.org/10.1111/j.1749-6632.2010.05455.x

Xiao, J., Chevallier, F., Gomez, C., Guanter, L., Hicke, J.A., Huete, A.R., Ichii, K., Ni, W., Pang, Y., Rahman, A.F., Sun, G., Yuan, W., Zhang, L., Zhang, X., 2019. Remote sensing of the terrestrial carbon cycle: A review of advances over 50 years. Remote Sens. Environ. 233, 111383. https://doi.org/10.1016/j.rse.2019.111383

Xu, Q., Man, A., Fredrickson, M., Hou, Z., Pitkänen, J., Wing, B., Ramirez, C., Li, B., Greenberg, J.A., 2018. Quantification of uncertainty in aboveground biomass estimates derived from small-footprint airborne LiDAR. Remote Sens. Environ. 216, 514–528. https://doi.org/10.1016/j.rse.2018.07.022

Yang, X., Richardson, T.K., Jain, A.K., 2010. Contributions of secondary forest and nitrogen dynamics to terrestrial carbon uptake. Biogeosciences 7, 3041–3050. https://doi.org/10.5194/bg-7-3041-2010

Yao, Y., Vehtari, A., Simpson, D., Gelman, A., 2017. Using stacking to average Bayesian predictive distributions. Bayesian Anal. https://doi.org/10.1214/17-BA1091

Zeide, B., Vanderschaaf, C., 2002. The Effect of Density on the Height-Diameter Relationship., Gen. Tech. Rep SRS-48. U.S. Department of Agriculture, Forest Service, Southern Research Station, Asheville, NC.

Zhao, K., Suarez, J.C., Garcia, M., Hu, T., Wang, C., Londo, A., 2018. Utility of multitemporal lidar for forest and carbon monitoring: Tree growth, biomass dynamics, and carbon flux. Remote Sens. Environ. 204, 883–897. https://doi.org/10.1016/j.rse.2017.09.007

15. Appendix

Appendix 1. Silvicultural treatments were implemented on the plots in Paracou. The number of individuals dead under the "silviculture" heading includes dead trees following forest treatment (timber, fuelwood, and thinning) and trees destroyed by forest works. Adapted from: [72]

Intensity	Plots	Treatments implemented	Trees dead						Canopy height increase* ($m\ ha^{-1}\ yr^{-1}$)
		Timber	Fuelwood	Thinning	Felled	Logging	Poison-girdling	Silviculture	
T0: SUF	1,6,11,13,14,15				0	0	0	0	0.15
T1: Low intensity	2,7,9	DBH $\geq$ 50 or 60 cm			3.3	2.3	0	5.6	0.19
T2: Medium intensity	3,5,10	DBH $\geq$ 50 or 60 cm		DBH $\geq$ 40 cm	3.8	2.6	5.2	11.6	0.23
T3: Heavy intensity	4,8,12	DBH $\geq$ 50 or 60 cm	40 cm $\leq$ DBH $\leq$ 50 cm	DBH $\geq$ 50 cm	6.3	4.2	3.6	14.1	0.24
P16: 25 ha plot – TUF	16				0	0	0	0	

* Measured from 2009 and 2019 canopy models.

Appendix 2. Characteristics of ALS acquisitions for the different overflights chapter mortality.

Year	2009	2015	2019
Acquisition time	April, September, October 2009	20th October 2015	November 2019
Vehicle	Helicopter	Airplane	Airplane
Sensor model	Riegl LMS-280i / LMS6Q140i-60	LMS-Q780 RIEGL (12% power)	LMS-Q780 RIEGL (25% power)
Laser beam divergence (mrad)	≤0.5 mrad/≤3.0 mrad	≤ 0.25	≤ 0.25
Average point density (pulses m^{-2})	10	10 (25*)	10 (27*)
Maximum scan angle	15°	20°	20°
Average flying altitude (m)	170	800	800
Mean footprint size (cm)	10 / 40	20	20
Penetration**	0.009	0.020	0.024

*Initial pulse density (before thinning)

** ground last return divided by all last returns; calculated after excluding shots outside $\pm$15° angular range

Appendix 3. Mean stem density (stems.ha^{-1}, left) and basal area (BA in m^2 ha^{-1}, right) of lowland forest plots in the different habitat units. The line shows the trend, in black the habitats, the total value and labeled the calculated rate of change between 1999 and 2017.

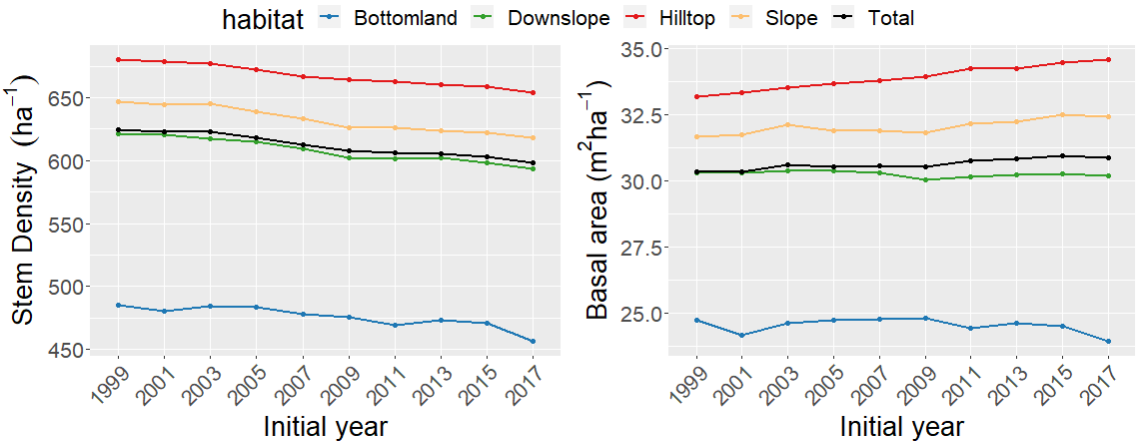

Appendix 4. Comparison of the GDI indicator calculated, i.e., using 2009 and 2019 as inputs and the composite as the sum of GDI 2009-2015 and 2015-2019 for all plots (75 subplots).

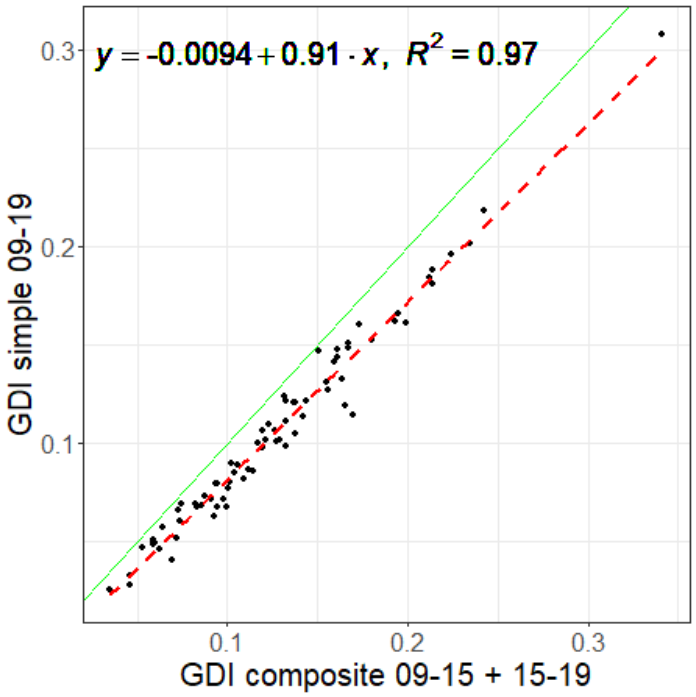

Note: Gaps detected in 2015-2019, also detected in 2009-2015 represented 3.6% of the total gap areas formed between 2009 and 2019.

Appendix 5. Visual comparison of the different methodologies used for the detection of mortality from gap dynamics analysis. (Benoist, 2009; Brokaw, 1985; Leitold et al., 2018; Senécal et al., 2018).

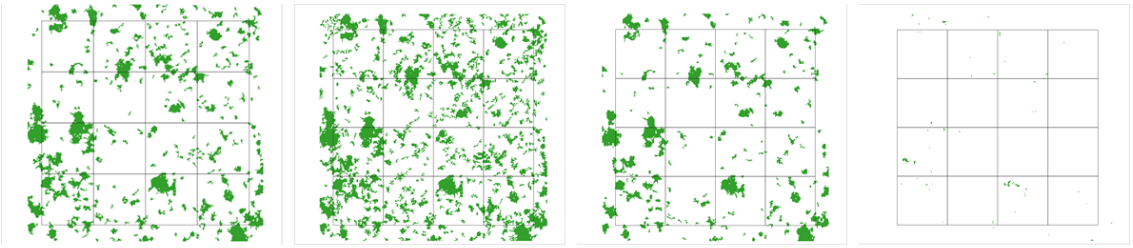

Senecal hra , 2009 – 2019, Plot 1 | Benoist, 2009 - 2019, Plot 1 | Leitold, 2009 - 2019, Plot 1 | Brokaw, 2009 - 2019, Plot 1

- Brokaw (1985) Aperture extending at all levels up to an average height of 2 meters above the ground.
- Benoist (2009) Developed an algorithm to detect and delimit gaps. "The threshold of 5m² minimum makes it possible to exclude low points that are too isolated and that correspond to old gaps that are in the process of aggradation. On the other hand, the 10m height criterion restores their shape well, and it is reasonable to accept a high point in the middle of a hole."
- Senécal et al. (2018). Height reduction areas (HRA) groups of pixels in which a reduction of at minimum 1 m in height and a minimum size of 5 m^2 were observed (six years). Within the HRA, new gap pixels were detected as CHM year1 pixels in the HRA of height 3 m or less, and for year0 heights above 3 m, while canopy height erosion pixels were detected as CHM year1 pixels of height above 3 m after the height loss.
- Leitold et al., (2018), threshold >= 4 m² and height losses >= 3 m.

Appendix 6. Dynamic characteristics per forest type during 2009-2019 (2010-2020) (a) Diameter distribution of trees that died; bins of 10 cm starting at 10cm DBH. (b) Mean value of wood density for surviving, dying and recruited trees (c) Demographic rates were calculated as instantaneous rates in SUF plots, logged plots (T1 to T3) between 1999 and 2019 and TUF between 2010 and 2020 for individuals with DBH>=10 cm. Circles for medians, vertical bars for 95% highest posterior distribution intervals, and horizontal axis dotted for y=0.

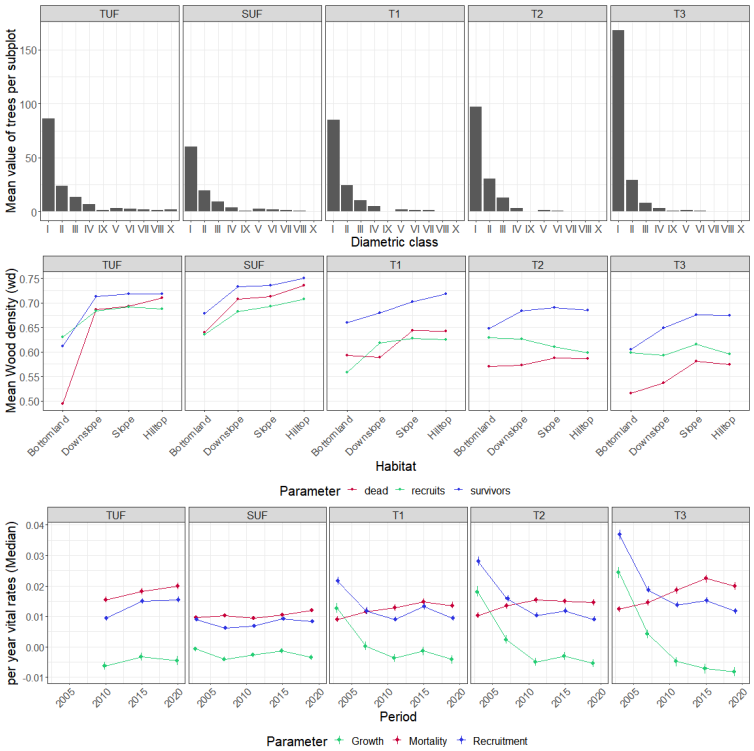

Appendix 7. Pseudo change (noise) in canopy height evaluated at one m resolution from two flights (05/102015 and 20/10/2015) in Paracou. The scan angle was limited to +/- 20 deg. Pulse density was 10 pulses.m^2.

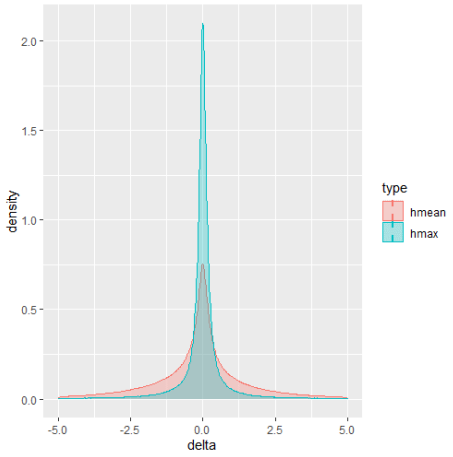

Appendix 8. Impact of change in leaf density (phenology) on Canopy Height Model occurring over two weeks (05/10/2015 and 20/10/2015, Paracou - French Guiana).

In the upper left corner: a crop of the 20/10/2015 Canopy Height Model based on mean first return height (CHM_hmean). In the lower-left corner: the Canopy Height model based on maximum first return height (CHM_hmax, used in the present study), for the same area, same date exact resolution. In the center: raster of change between the two dates. Two crowns (green and red boxes) are highlighted. A significant increase in CHM_hmean is perceptible for those crowns. On the right: Pictures (20/10/2015) of those crowns show that they were re-foliating on the second date. CHM_hmax is not sensitive to such phenology-related changes in the canopy. In addition, CHM_hmean seems spatially more variable, with significant contrasts often associated with gaps.

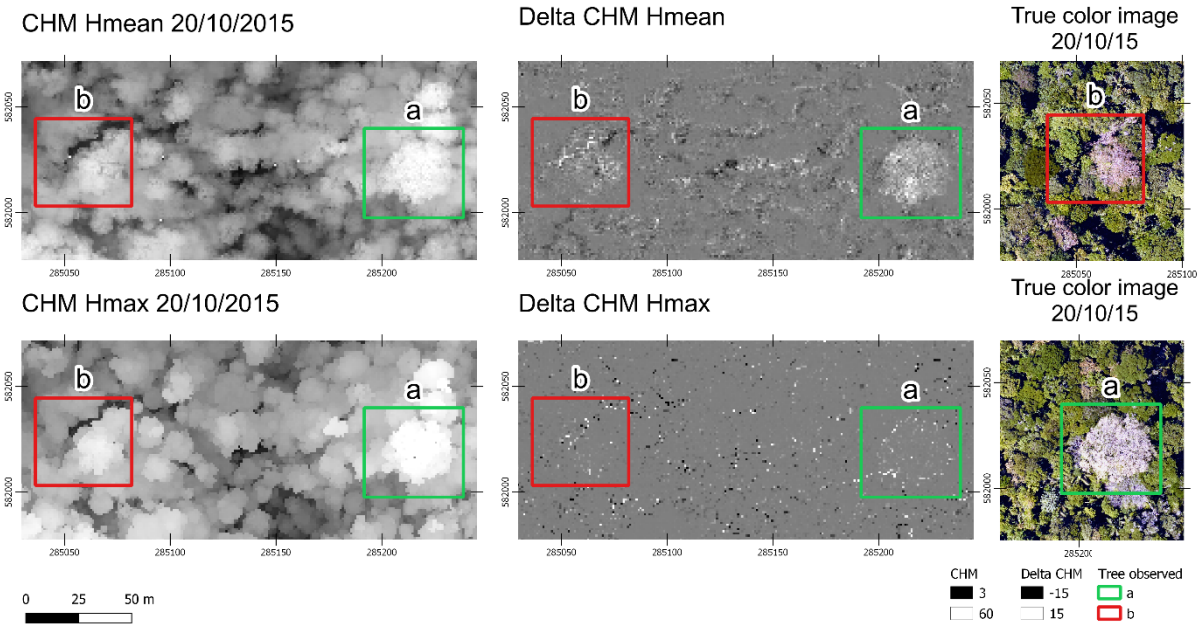

Appendix 9. Sensitivity of Gap fraction to unbalanced pulse density between dates

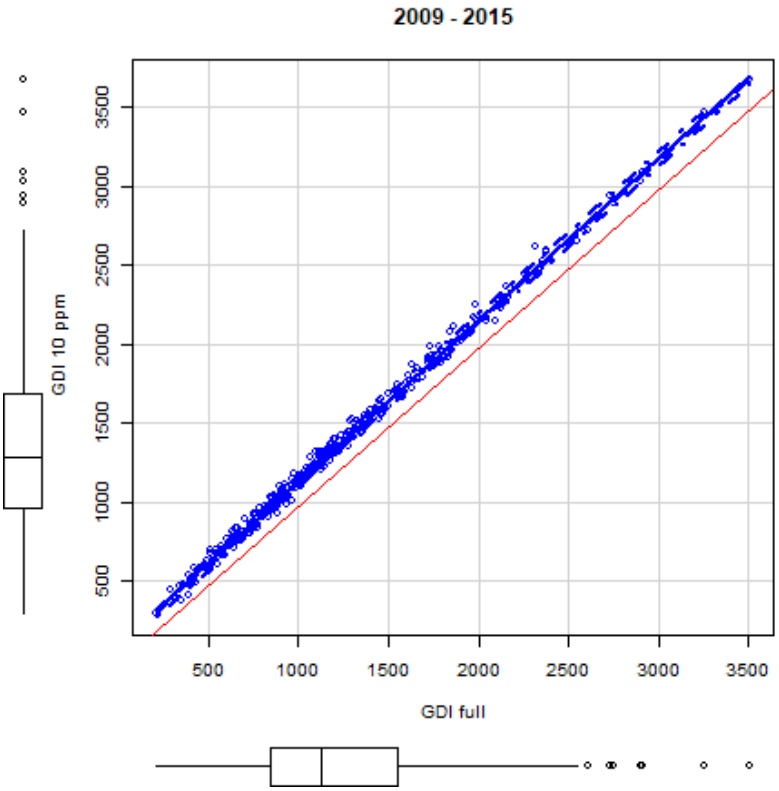

Area in gaps detected using Leitold gap definition (nobs=321) per 125x125 m cell. Mean difference in gap area is 134 m^2.

Appendix 10. Quadratic Mean Diameter (QMD in cm) per Habitat and Forest Type. The vertical bars represent the standard error of the mean per subplot.

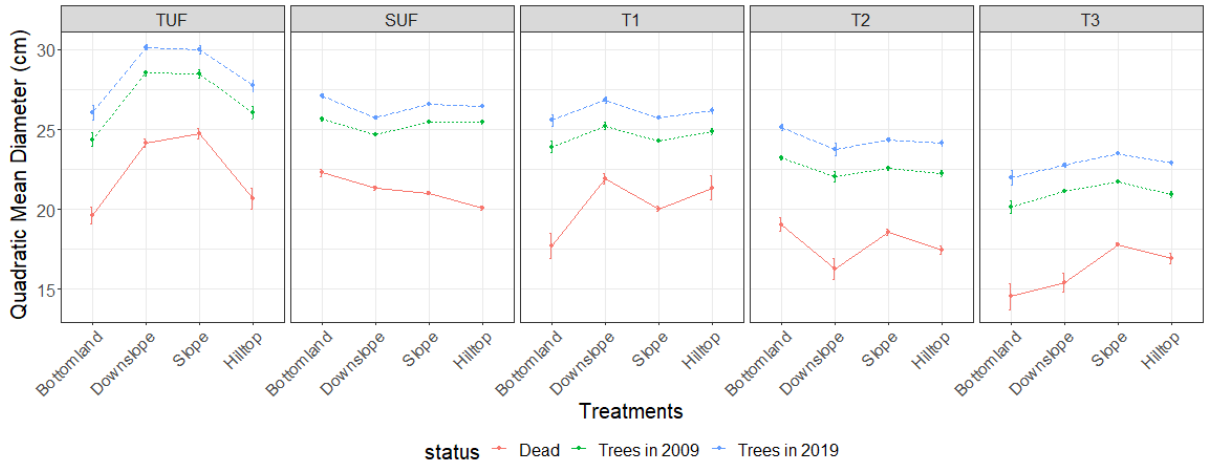

Appendix 11. The number of individuals sampled per plot. T1 to T3 refers to the plots harvested 36 years ago, with T1 being the least harvested and T3 the most intensively. In the case of INRA plots, some individuals were segmented outside the PSP. The plot boundary on the map has been adjusted to include all sampled trees.

Network	Measuring area (ha)	Units	Plot	Treatment				
				Control	T1	T2		T3
CIRAD	16.3	SUF	1	26				
		T1	2		129			
		T2	3			74		
		T3	4					357
		T1	7		304			
		T3	8					316
		T1	9		275			
		T2	10			96		
		SUF	11	287				
		T3	12					71
		SUF	15	391				
	3.9	TUF	16	269				
CNES	0.5		17	52				
INRA	6.8		19	77				
			20	116				
			21	74				
			22	119				
			23	163				
			24	108				
	Total			1682	708	170	0	744

Appendix 12. Local allometric equations adjusted to predict mean height (H; in m) as a function of DBH (in cm), using the three functions: power, Michaelis Menten and Weibull simplified (2 params) n=3304. A gamma distribution for both alpha and beta of gamma (1.5, 0.01) was used as a prior.

Model	Function	Equation	Predictors	Parameters	WAIC	RMSE	BIAS
model 1	Power	$\widehat{H}$=a x DBH^b	----	Two param	18501.02	3.97	0.0011
model 1	Michaelis Menten	$\widehat{H}$=a x DBH/(b+DBH)	----	Two param	18574.06	4.02	0.0123
model 1	Weibull	$\widehat{H}$= a x (1-exp(-DBH/b)	----	Two param	18724.38	4.11	0.033
model 2	Power	$\widehat{H}$= (a x LHC + b) x DBH^c	LHC	Three param	17761.67	3.55	-0.004
model 2	Michaelis Menten	$\widehat{H}$=(a x LHC + b) DBH/(c+DBH)	LHC	Three param	17781.97	3.56	0.0044
model 2	Weibull	$\widehat{H}$= (a x LHC + b) x (1-exp(-DBH/c)	LHC	Three param	17914.96	3.64	0.0211
model 2b	Power	$\widehat{H}$=a x DBH^b	species (random effect)	Two param	17440.21	3.55	-0.004
model 2b	Michaelis Menten	$\widehat{H}$=a x DBH/(b+DBH)	species (random effect)	Two param	17485.29	3.56	0.0044
model 2b	Weibull	$\widehat{H}$= (a x LHC + b) x (1-exp(-DBH/c)	species (random effect)	Two param	17560.33	3.64	0.0211
model 3	Power	$\widehat{H}$= (a x LHC + b) x DBH^c	LHC + species (random effect)	Three param	16634.38	2.8	-0.0023
model 3	Michaelis Menten	$\widehat{H}$= (a x LHC + b) DBH/(c+DBH)	LHC + species (random effect)	Three param	16627.92	2.78	0.0024
model 3	Weibull	$\widehat{H}$= (a x LHC + b) x (1-exp(-DBH/c))	LHC + species (random effect)	Three param	16673.77	2.77	0.0107

Appendix 13. Scatterplot compares observed H individuals corresponding to the ALS segmented data (Dataset 1) to the pantropical model, CC and model 3 in the height of the different functions.

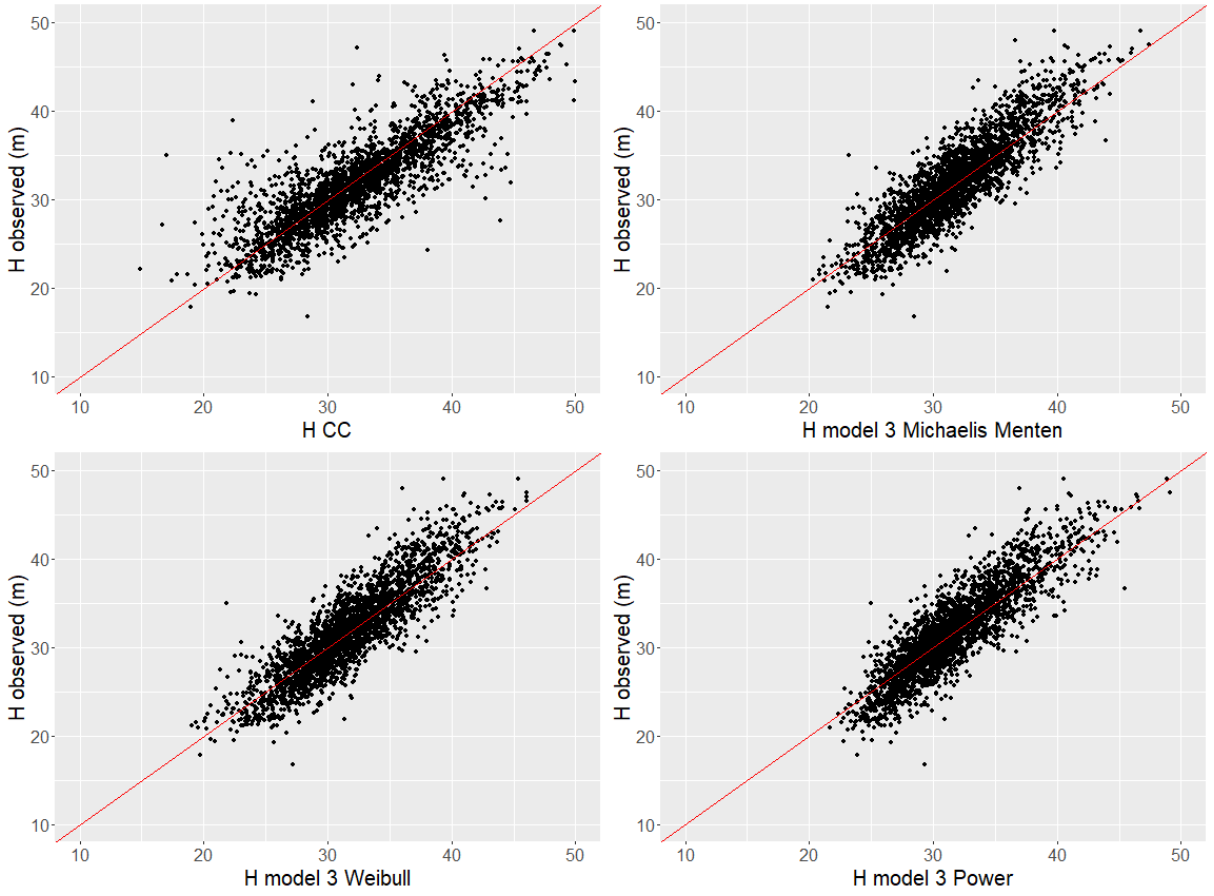

Appendix 14. Comparison between observed vs. predicted height (Dataset 1) for the three functions (MM, Weibull and power) and CC model. The gamma method was employed for the smooth lines using the formula 'y ~ s(x, bs = "cs").'

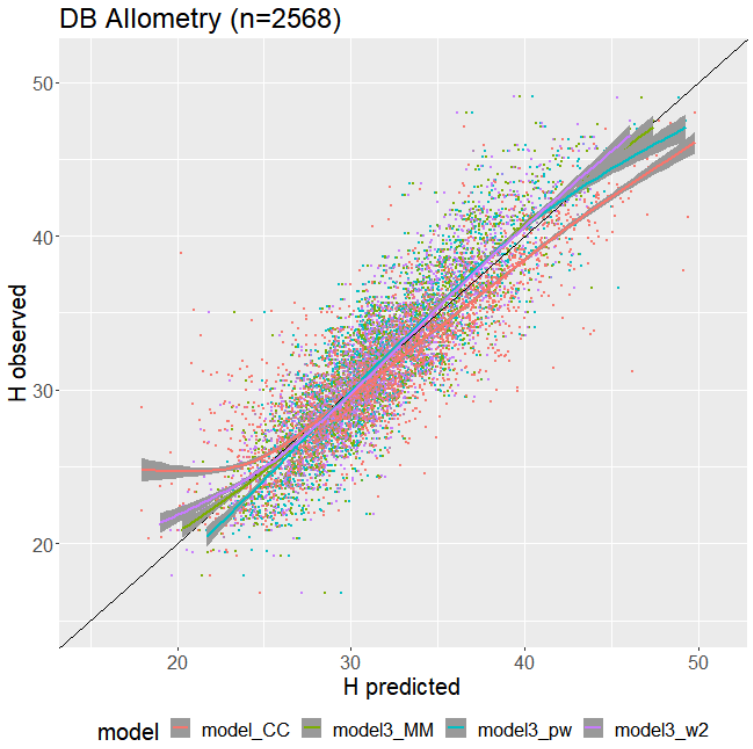

The residuals (H observed - H predicted) of the canopy model builder on the subset of observations (Dataset1), on the left scatterplot of residues vs. DBH in smooth gray line, using the loess model, on the right boxplot of residuals vs. diametric classes defined in intervals of 10

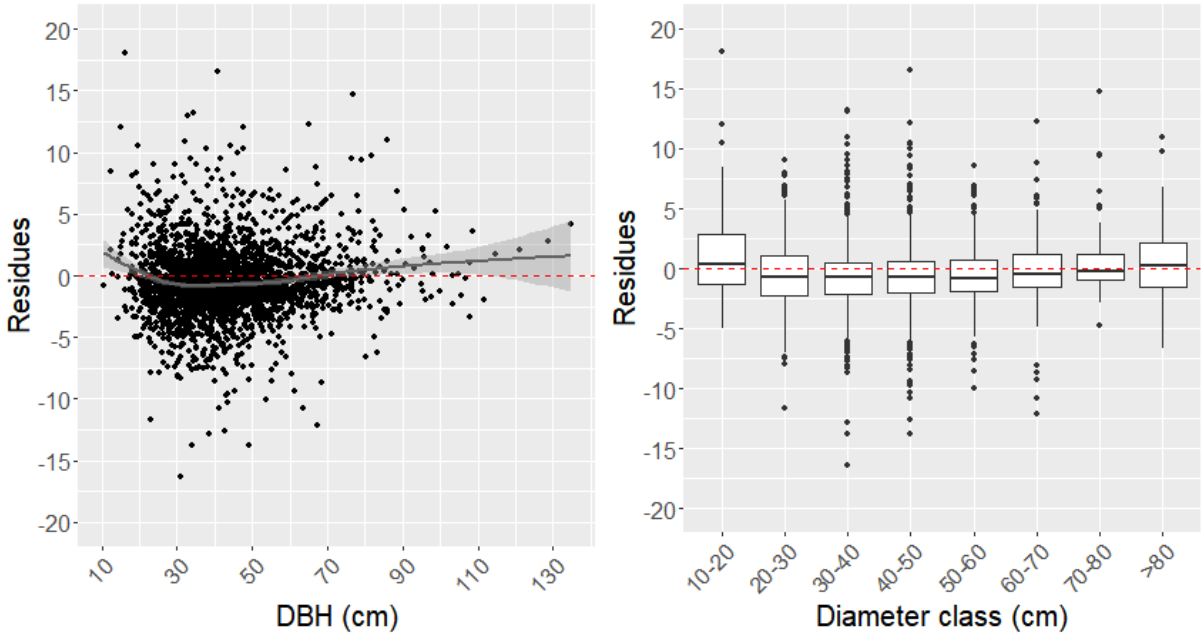

Appendix 15. Scatter plot between the predicted heights of the three functions (MM, Weibull and power) and the CC model versus the diameter of dataset 2 of the Paracou database. The modeled heights were fitted to the entire (CC) Dataset2 database. The latter two models were applied to stems larger than 20 cm DBH. Predictions are compared using smooth_geom with gam in ggplot; the gray band around the regression line is the confidence interval.

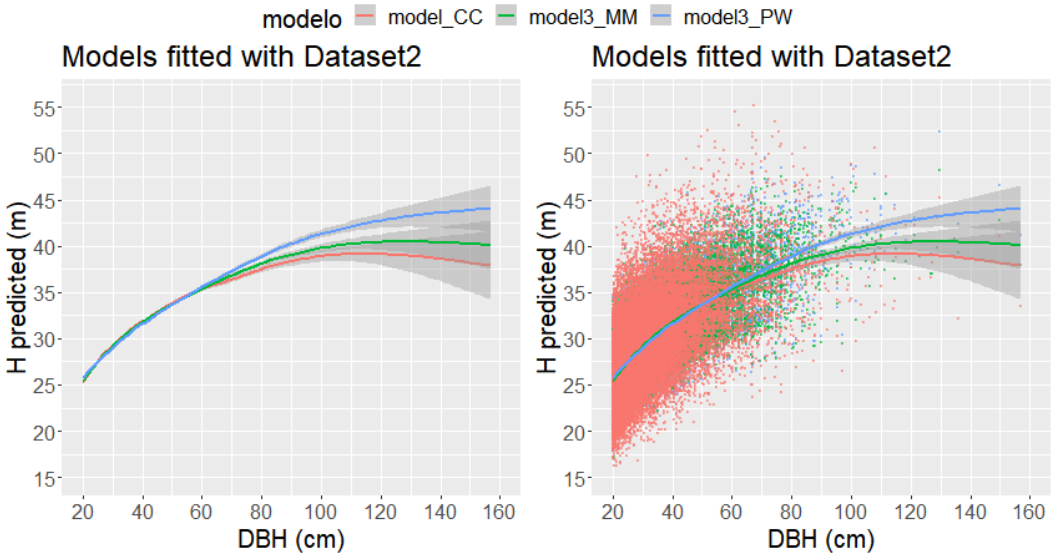

Appendix 16. Scatterplot between the predicted heights of the three functions (MM, Weibull and power) and the CC model vs. diameter of the Paracou database. The modeled heights above were adjusted either on the entire database (CC) or a subset of observations (model3 MM_allo and model3 PW_allo). The latter two models have then applied to stems >20cm DBH. Predictions are compared using smooth_geom with gam in ggplot; the grey band around the regression line is the confidence interval.

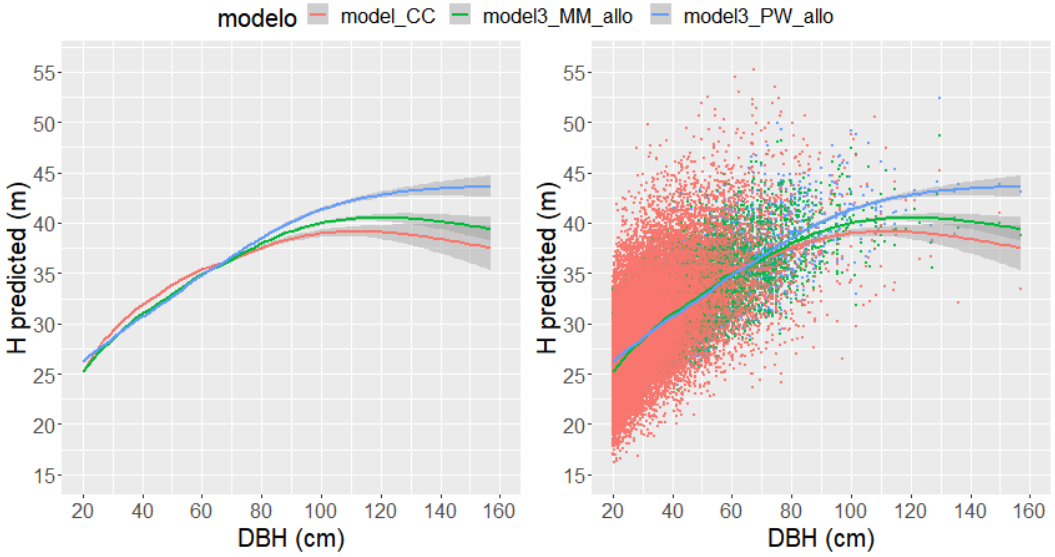

Appendix 17. Comparison of individual tree height measurements by TLS and ALS. The TLS height data was previously extracted by Bossoukpe (2020). The green line corresponds to the reference line with slope = 1, intercept =0. The blue line corresponds to the fitted line of a given linear regression model.

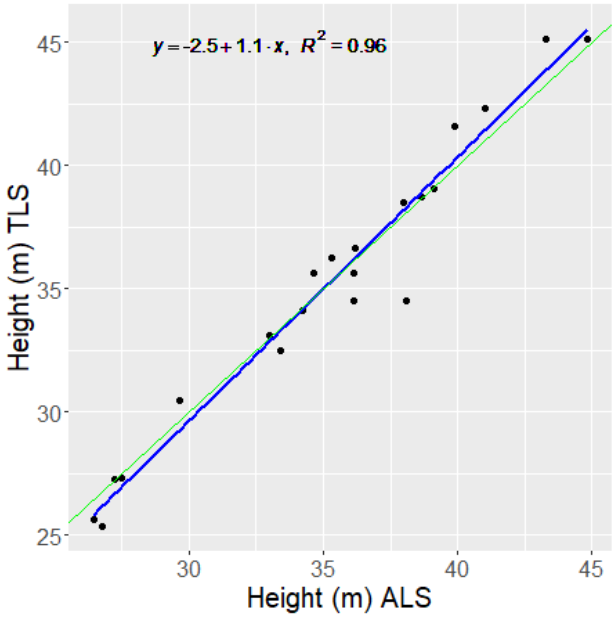

Appendix 18. Residuals of power-law and MM equation models compared with the habitat/ drainage units defined by Ferry et al. (2010). The data entry only considers individuals larger than 20 cm DBH (n=28845). The label under each box corresponds to the median value of the residue. The label under each box corresponds to the mean value of the residue.

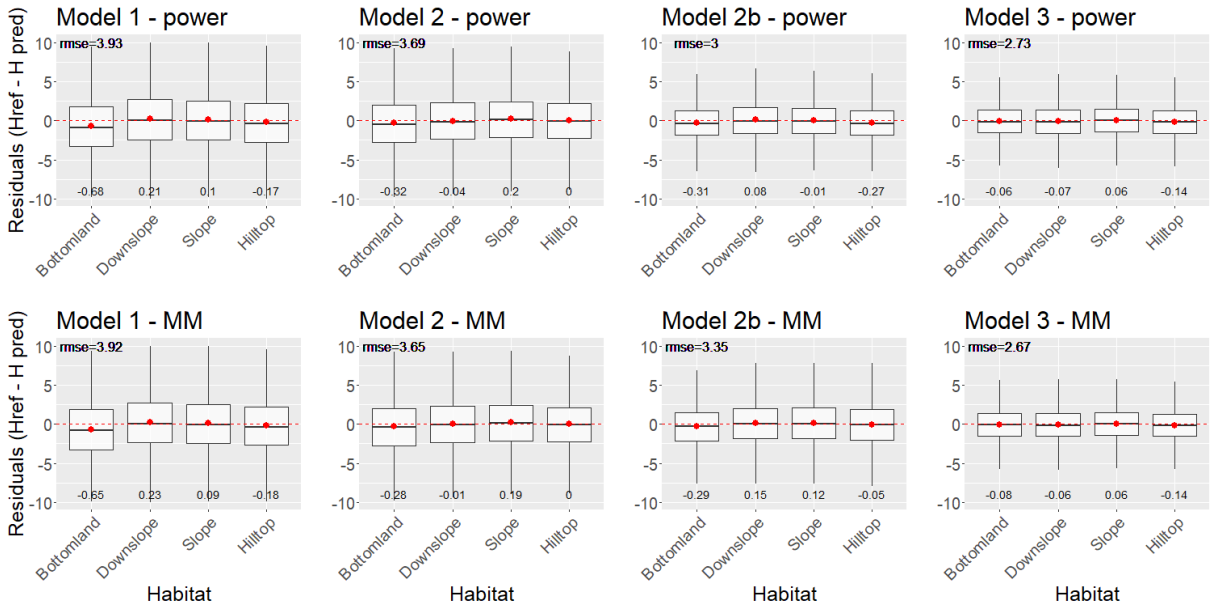

Appendix 19. Residuals from power-law equation models and MM 1 and 2 compared to habitat/drainage units defined by Ferry et al. (2010). Model data input only considers individuals classified with 25% or greater perc_exposure (n= 29965). Applied for the CC convex hull crown data. The label under each box corresponds to the mean value of the residue.

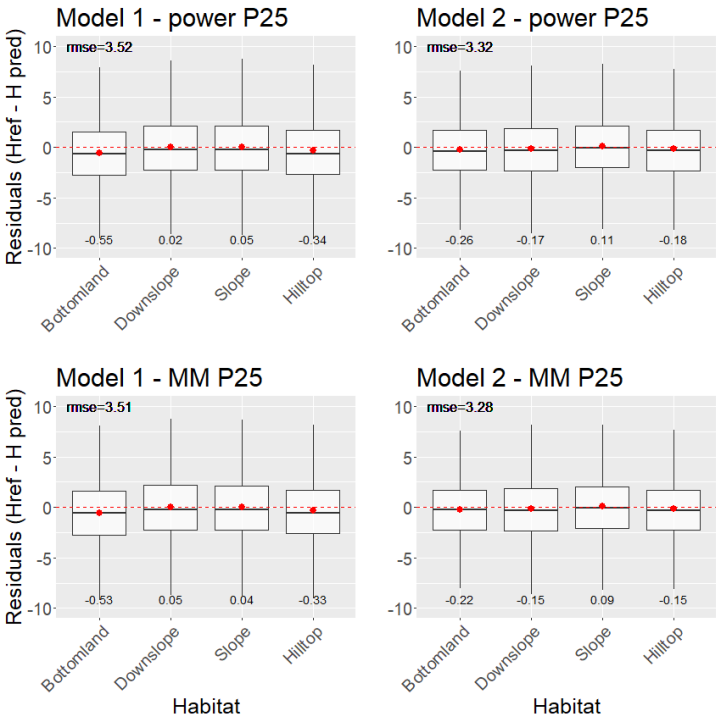

Appendix 20. Residuals of power-law and MM equation models are compared in the top section with the habitat units defined by Ferry et al. (2010) and in the bottom section with the different treatments (T1-T3) and plots of low forest (SUF) and high forest (TUF) (Dataset 2). The data entry only considers individuals larger than 20 cm DBH (n=28845). The label under each box corresponds to the mean value of the residue.

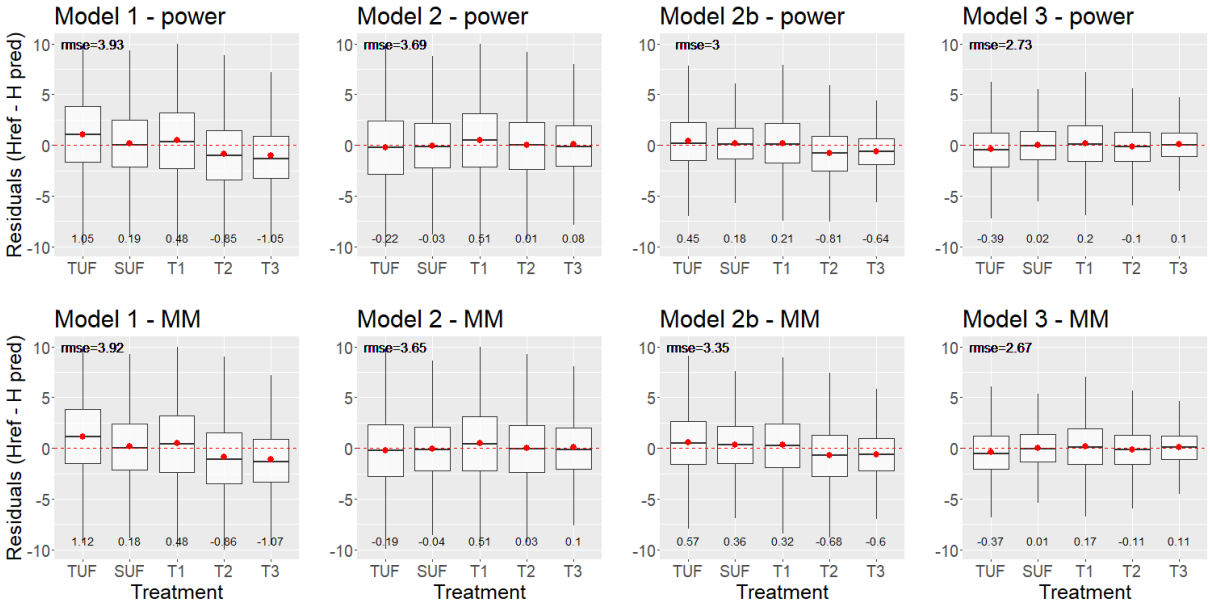

Appendix 21. Residuals of power-law and MM equation models are compared in the top section with the habitat units defined by Ferry et al. (2010) and in the bottom section with the different treatments (T1-T3) and plots of low forest (SUF) and high forest (TUF) (Dataset 2). The model data input only considers individuals classified with 25% or more of perc_exposed (n= 29965), applied for the CC convex hull crown data. The label under each box corresponds to the mean value of the residue.

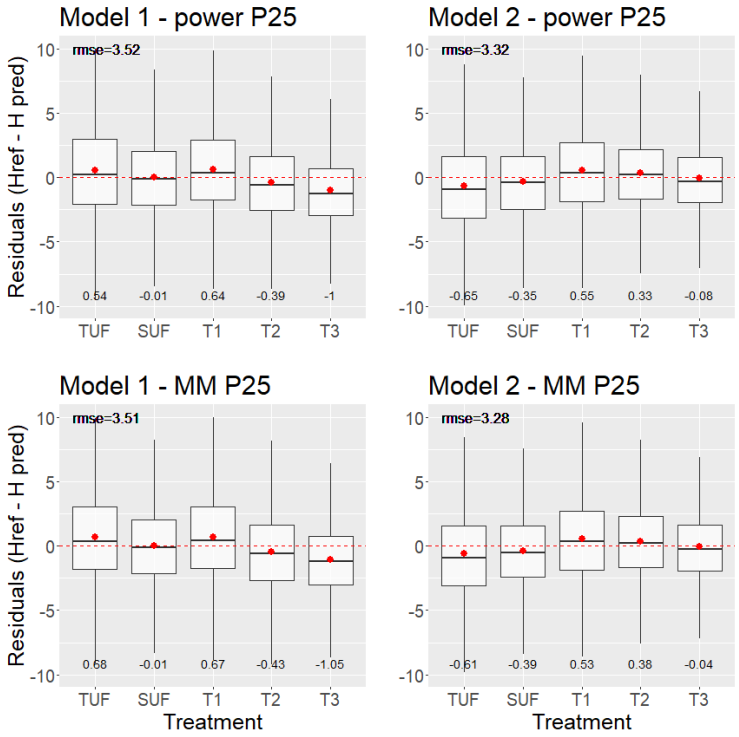

Appendix 22. *Scatterplot of residuals Model MM (model 3 and model 2b) applied to cc (H observed - H predicted) in a 125 X 125 square (square level).*

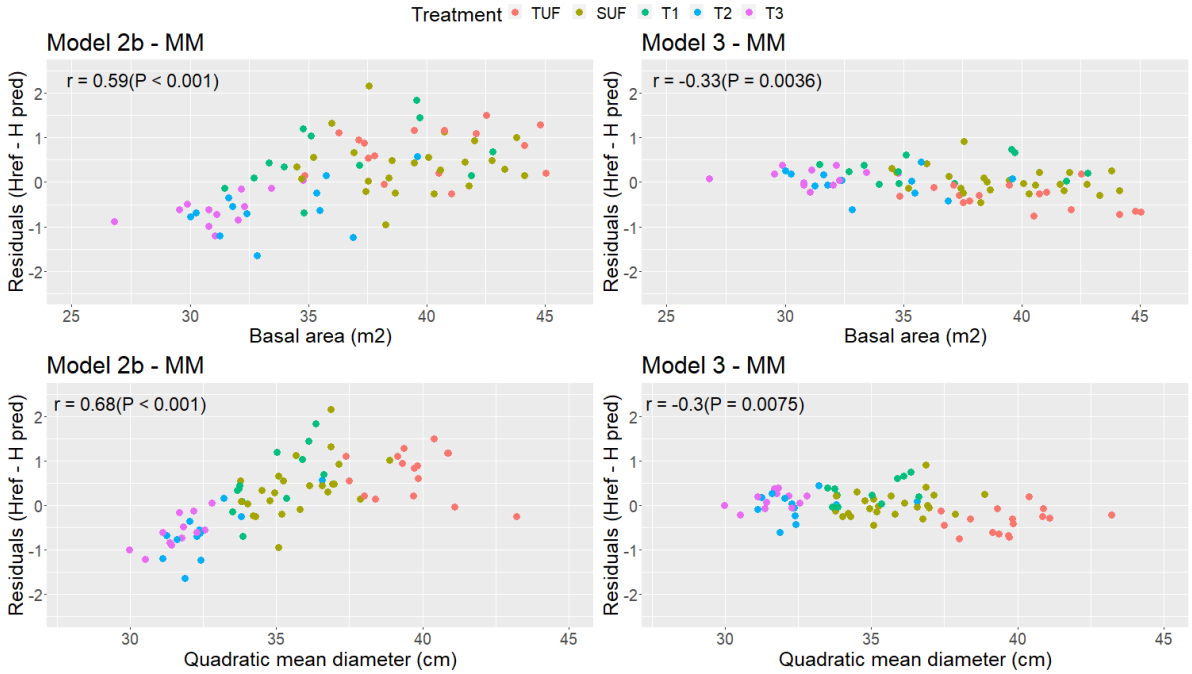

Appendix 23. Residuals of the power-law equation models and MM 1 and 2 are compared in section A with the habitat units and section B with the different treatments (T1-T3) and plots of low unlogged forest (SUF) and high unlogged forest (TUF). In each section, we present on the superior side the model trained with data greater than DBH >=20 (n= 28845) and in the inferior section, trained with all the data of the CIRAD database (n=72200) and applied for the CC convex hull crown data. For calculating the graphs and RMSE, a subselection of only individuals equal to or larger than 20 cm was made for comparison. The label under each box corresponds to the mean value of the residue.

Section A

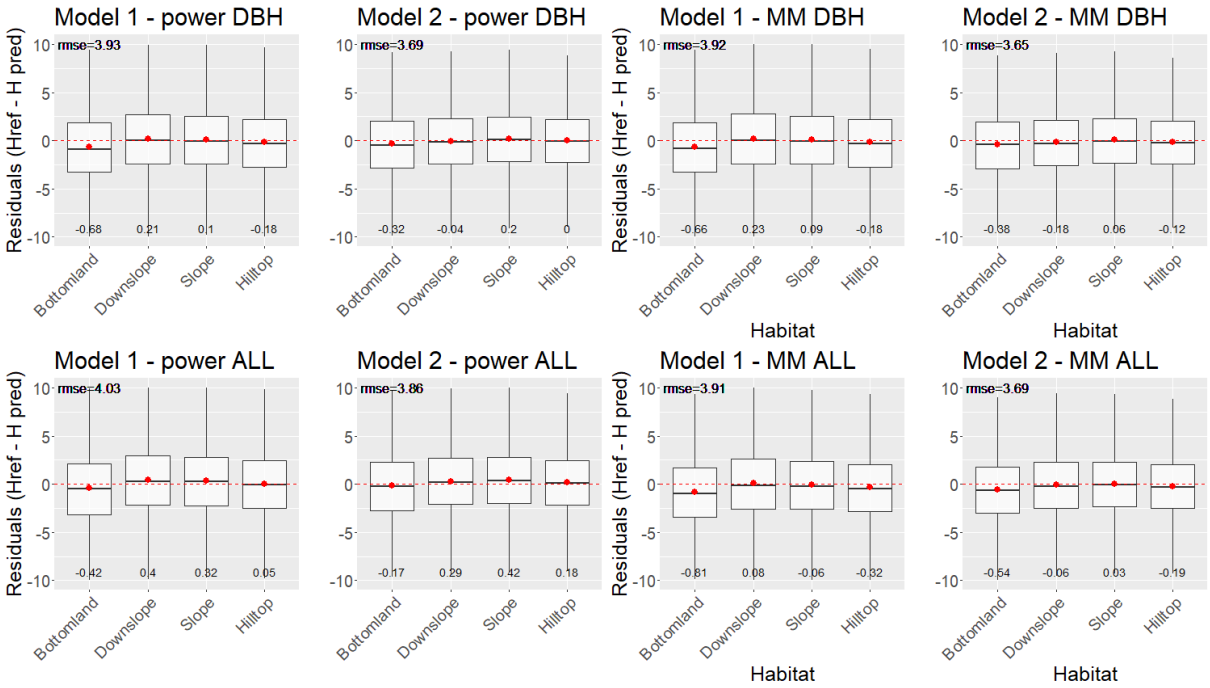

Section B

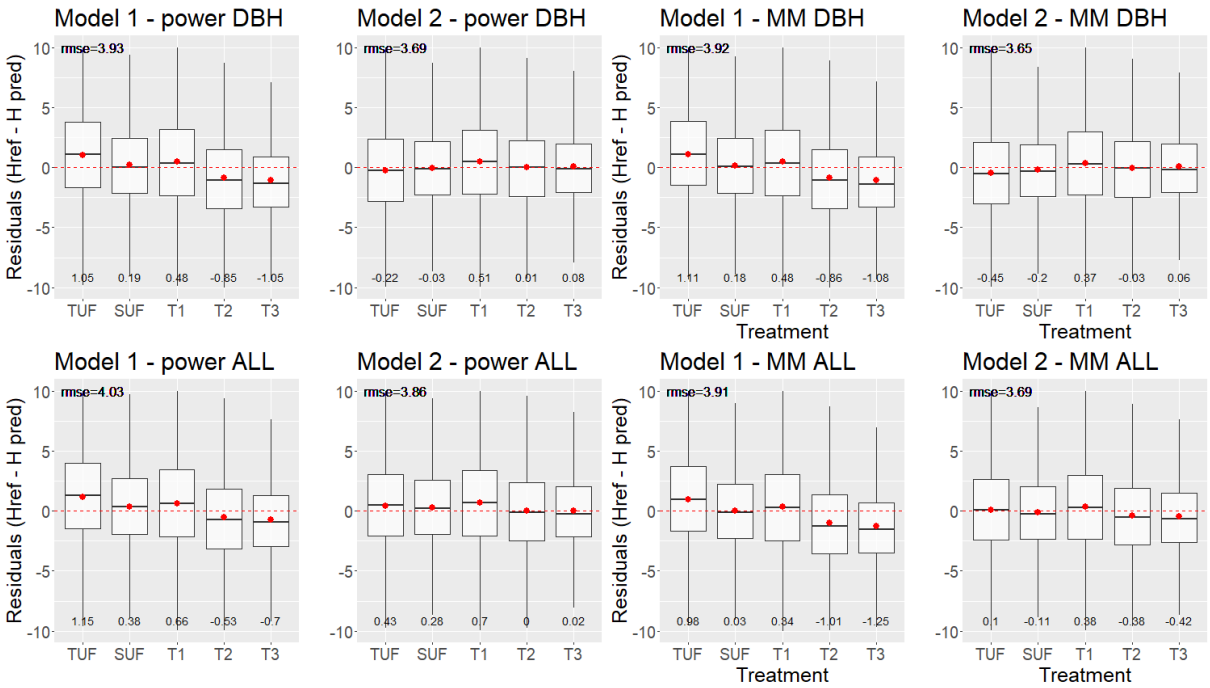

Appendix 24. Scatter plot between the predicted heights of the two functions (MM and power) models 1 and 2 and the CC model versus the diameter of the Paracou database. The heights modeled above were fitted on the whole database (CC) Dataset2. These models have been applied to the whole data (n=72200). Predictions are compared using smooth_geom with gam in ggplot; the gray band around the regression line is the confidence interval.

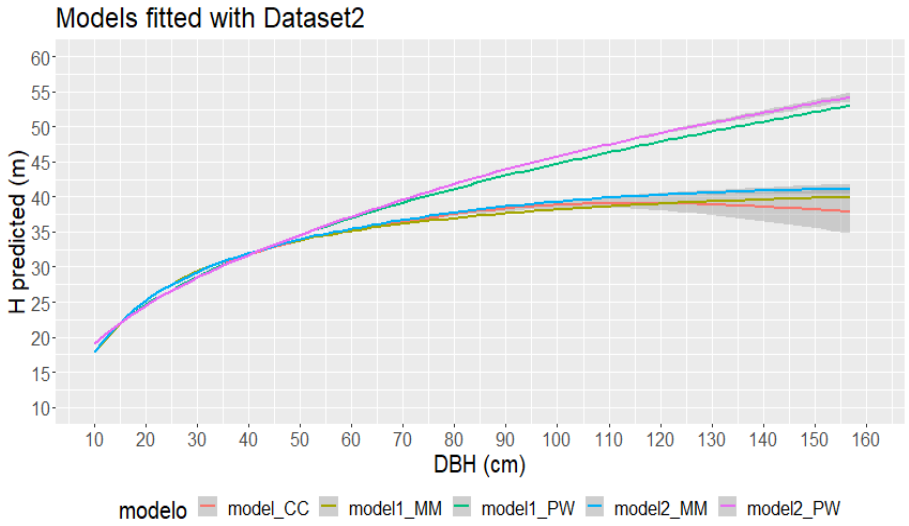

Appendix 25. BRMS R. code used to fit final model (MM3) to observed tree heights (full code available on GitHub https://github.com/chuertas18/public/blob/main/Paracou_allometry_models.R)

```
model3_MM = brm(
  bf(height~(alpha*dbh)/(beta+dbh),
     alpha ~ HC + 1|species_noSing,
     beta ~ 1|species_noSing,
     nl = TRUE),
  data = data,
  family = "gaussian",
  prior = c(
    prior(gamma(1.5, 0.01), lb = 0, nlpar = alpha),
    prior(gamma(1.5, 0.01), lb = 0, nlpar = beta)
  ),
  iter = 3000,
  warmup = 1500,
  chains = 4,
  control = list(adapt_delta = 0.95,
                 max_treedepth = 12), # adapt_delta can be set to 0.99 and max_treedepth = 12,
  seed = 25,
  silent = FALSE
)
```

16. List of figures and tables

Figures

Figure 1. Left. The general principle of an Airborne LiDAR acquisition. Extracted and modified from Presentation of the International Conference on Tropical Silviculture. (Vincent et al., 2011b). Right. Conceptual differences between waveform and discrete return LiDAR recording (Adapted and modified from Lefsky et al.,(2002)). 33
Figure 2. Diagram detailing the organization of research questions that characterize tropical forest carbon fluxes and stocks from LiDAR 35
Figure 3. Map of the study area showing the individual plots and sub-plots division (125 X 125 m) considered in the analyses, with the respective habitat units according to Ferry et al. (2010) classification. The top profile corresponds to a trace (white line) on plot P13. The drainages shown are extracted from the LiDAR terrain model and calculated in GRASS GIS (GRASS Development Team, 2017) using the (r. watershed) function. 38
Figure 4. Climatological description of the Paracou site. On the left. Annual rainfall records CSG, Sinnamary, Savane Combi (source MétéoFrance and CNES). Right. Records of average daily mean temperature (TM), minimum temperature (TN) and maximum temperature (TX) at Savane Combi (source MétéoFrance). 39
Figure 5. Treatment-estimated mean values of the dendrometric variables: stem density (N in stems. ha^{-1}), basal area (BA in m^2 ha^{-1}), and mean square diameter (in cm). The vertical bars represent the standard deviation of the mean per subplot (125 X 125 m). In the case of plot 16, the inventories correspond to the years 2010, 2015, and 2020. 41
Figure 6. Left. Map of the study area, showing the different plots and the soil hydrological classes (Habitats; see text). Plot numbers refer to Forest type characteristics summarized in Table 4. Right. Boxplot showing the consistency between Habitat classification and Topographic Wetness Index (TWI) computed over the entire landscape based on the digital terrain model derived from Airborne LiDAR Scanning data (see text). 50
Figure 7. Mean stem density (stems.ha^{-1}, left) and basal area (BA in m^2 .ha^{-1}, right) over 20 years in the different forest types. TUF: Tall Undisturbed Forest; SUF: Short Undisturbed Forest; T1-3: Logged forests of increasing intensity (see ha^{-1} for details). 52
Figure 8. Adjusted R-squared of the linear regression between GDI and BA or stem loss rates according to different periods. Absolute loss rates in red and relative loos rates in blue. Upper graphs include all plots, and lower graphs include only undisturbed plots.....55
Figure 9. Absolute basal area loss (m^2.ha^{-1}.yr^{-1}) versus GDI (annual rate of canopy subsidence) for 2009 -2019 per 125 x 125 m subplot for all types of forests. Regression lines (solid) with a

95% confidence level. TUF: Tall Undisturbed Forest; SUF: Short Undisturbed Forest. T1 to T3: Sylvicultural treatments of increasing intensity (see Table 4 for more details). 56
Figure 10. Effect of Habitat and Forest type (TUF = Tall Undisturbed Forest, SUF = Short Undisturbed Forest, T1-T3 = increasing level of logging intensity) on annual basal and stem loss rates predicted for the period 2009-2019 per hectare. Error bars represent 95% confidence limits. 56
Figure 11. a) GDI per pixel of 1 m. b) TWI (calculated at 60 m, resampled at 10 m. c) and canopy height (HC) taken as the 90th percentile (p90) of 1-m CHM 2009 values in a 125 m radius neighborhood. 58
Figure 12. Map of a Gap Dynamics Index derived from repeated Airborne LiDAR Scanning data in two successive periods: 2009-2015 and 2015-2019, showing a persistent spatial pattern. 58
Figure 13. Mortality (BA and stem loss rates) and gap dynamics index GDI (annual rate of canopy subsidence) derived from repeated Airborne LiDAR Scanning data for different study periods (unlogged plots only). The red dots correspond to the mean value. 59
Figure 14. Distribution of the trees segmented and sampled for the allometric models (n=3304). The background represents the canopy height smoothed in 2015 with a resolution of 30 m. The individuals are located inside the permanent CIRAD plots (dotted white line) and outside (the northeast of the images). 68
Figure 15. Schematic diagram showing the processes for modeling the heights, including the procedure of the two Datasets used and the allometric equations. 69
Figure 16. (a) Scatterplot of the trees presented in Figure 14 in X the diameters and in Y the heights measured with the ALS (dataset 1). The marginal distribution shows the boxplot of the two variables for the population. (b). Scatterplots of trees from the global fit of CC predictions to the CIRAD database for individuals with DBH>=10 cm diameters are extracted from permanent plot monitoring and height predicted with the CC modeling (dataset 2). The marginal distribution shows the boxplot of the two variables for the population. 71
Figure 17. Boxplot of individual tree height estimation error in meters per plot using Chave's pantropical equation, reference model and the canopy constructor predictions. The dotted line represents the 0 error. 75
Figure 18. Curves of the H-DBH relationships of the value simulated by CC (H_{CC}) and the observed value (Dataset 1), for the most abundant species (n>=30), in solid line the curve (gam method) of the CC model, in dashed line the curve of the data observed in the field. The analysis is limited to individuals over 20 cm DBH, excluding intensely logged plots (T1 and T2). 76

Figure 19. Curves of the H-DBH relationships were obtained from the prediction of the 3-MM model, taking as reference the extracted heights adjusted by CC of the trees with DBH > 20 cm (Dataset 2).....77
Figure 20. Estimates of above-ground biomass in Mg.ha^{-1} per plot of 1.56 ha. The colors indicate the different treatments. Right comparison between the reference model (model 3) and the pantropical model. The comparison between the local and CC models is on the left. We consider the CC estimates as a reference (Dataset 2). 77
Figure 21. Residuals of models MM equation compared in the top section with the habitat units and in the bottom section with the different treatments (T1-T3) and plots of unlogged low forest (SUF) and unlogged high forest (TUF). 78
Figure 22. Mean stem density (stems.ha^{-1}, left) and above-ground biomass per treatment (AGB in Mg.ha^{-1}, right) per treatment; vertical bars represent +/- the standard error of the mean per plot of 1.56 ha.....88
Figure 23. Mean AGWNPP over the six years for plots of 1.56 ha. The dotted line shows the trend as a simple linear regression. The vertical bars represent +/- the standard error of the plot mean. 89
Figure 24. AGWNPP (Left) and BA gain (Right) regression for the different plot sizes (0.39, 1.56 and 6.25 ha) over the period 2013 -2019. The solid lines correspond to the regression line, and the filling shows the confidence interval. 92
Figure 25 Left - AGWNPP regression model. Right – Basal area model for the period 2013 - 2019. Each point represents one 125 x 125 m plot. Different forest types are color-coded (T0: undisturbed forests, T1 to T3: logged over plots ordered by increasing disturbance). The solid lines correspond to the regression line and 0.95 confidence interval in shaded tones. 93
Figure 26 Linear regression of canopy height gain and AGWNPP (Left) or Basal area gain (Right) for different time intervals (color-coded). Each point represents one 125 x 125 m plot. 93
Figure 27 Left: AGWNPP (Mg C.ha^{-1}.yr^{-1}) prediction map calculated from the canopy gain map from 2015 to 2019 at the grid cell size of 60m; the shapefile of the plots is overlaid with the treatment label. Right: TWI for a resolution of 60 m. The two maps were smoothed with a 3x3 kernel–centered mean filter 94
Figure 28 Left: the map with the representation of the landscape grid of 125x125m cells. Right: the boxplots of the median canopy gain for the years 2013 - 2019 per cell. The control and treatment plots are in different colors and the landscape areas outside the T0-T3 plots are gray. Right: boxplot showing the general decrease in AGWNPP over time.....95

Tables

Table 1. Treatments were applied to the Paracou plots. The number of dead individuals in silvicultural treatments includes trees that died after forest treatment (logging, firewood, and thinning) and trees destroyed by forestry work. Adapted from:(CIRAD, 2016b; Gourlet-Fleury et al., 2004) 40
Table 2. LiDAR acquisition characteristics and parameters, in their raw form and delivered by ALTOA, discriminated for each date for the periods 2009 to 2015. This information was adapted from (ALTOA, 2019; Geo data, 2016; Vincent et al., 2012a, 2012b) 43
Table 3. Detailed technical specifications of ALS used in the 2009, 2013, and 2015 intakes. Information was adapted from technical reports: (ALTOA, 2019, 2015, 2013; Maltamo, 2014; RIEGL, 2013, 2010, 2004; Shan and Toth, 2009; Smearcheck, 2008; Vincent et al., 2012a) 44
Table 4. Forest Types definition combining silvicultural treatments of increasing intensity (T1 to T3) and canopy height (HC) for undisturbed plots. Plot numbers refer to Fig. 1. Forest stature was defined from the 2009 Canopy Height Model (CHM) derived from Airborne LiDAR Scanning data as the 90th percentile of pixel-wise CHM values in a 125 m radius (see text). Biomass loss corresponds to the total woody biomass loss attributed to silvicultural treatments (see for details Appendix 1 and (Gourlet-Fleury et al., 2004)).....51
Table 5. Median values of statistics of nested models of gap dynamic index computed at 1m pixel for 100 random pixel selections.....57
Table 6. Local allometric equations fitted to predict mean height (H; in m) as DBH function (in cm). Results for each of the models and functions are presented in Appendix 12. Data input corresponds to Dataset 1 74
Table 7. Table of individual tree height estimation error for the different models, including the pantropical, model 3 (reference model) and CC simulation. The data used here correspond to the 16 CIRAD plots in 2015. * single arbitrarily chosen simulation output 75
Table 8. Above-ground biomass per treatment (AGB in $Mg.ha^{-1}$) is calculated as the mean per plot of 1.56 ha. (Number of trees=72200) 78
Table 9. Pearson correlation test between model residues and the structure variables (basal area and quadratic diameter) for plots of 125 m X 125 m and the residuals of models 1 to 3 of the power and MM equations. Total observations 76.....79
Table 10. Characteristics of LiDAR acquisitions for the different overflights.....89
Table 11. Relative Root Mean Squared Deviation in canopy height gain predictors for different spatial scales estimated from split sub-sampling (period 2015-2019). 91
Table 12. Adjusted R-squared (R^2), root mean square error (RMSE) and relative root mean square error (rRMSE), calculated as the ratio of RMSE over the mean of the values of the dependent variable, fit statistics of the linear regression between the median canopy height

increase versus AGWNPP and Basal Area increment per plot between 2013 - 2019. RMSE is expressed in the following units: (AGWNPP) $Mg.ha^{-1}.yr^{-1}$, (BA) $m^2.ha^{-1}.yr^{-1}$ 91
Table 13. Effect of spatial resolution on intercept and slope model parameters for the 2013-2019 analysis period. The estimated value of interception and slope. The 95% confidence interval is presented between parentheses; the intervals were calculated using the bias-corrected and accelerated (BCa) bootstrap percentile method based on 1000 replications. .92
Table 14. Impact of period length on the prediction of AGWNPP and BA increase (T0, T1, T2, T3) Estimated intercept and slope value. A 95% confidence interval is given in brackets; the intervals are calculated using the bias-corrected and accelerated bootstrap percentile (BCa) based on 1000 replications. 94
Table 15. Total annualized AGWNPP by habitat unit and forest type, calculated using 2013-2019 data. 99